Quantitative Impurities Effects on Temperatures of Tin and Aluminium Fixed-Point Cells

A thesis submitted for the degree of Doctor of Philosophy

by

Patchariya Petchpong

School of Engineering and Design, Brunel University

May 2009

ABSTRACT

The International Temperature Scale of 1990 (ITS-90) defines the present S.I. ("System International") means of measuring temperature. The ITS-90 uses the freezing points of metals to define temperature fixed points. It also uses long-stem platinum resistance thermometers to interpolate between the fixed points from 660 °C down to 84 K (if one includes the Argon triple point). Impurities are a major source of uncertainty in the fixed point temperature (of the order of 1 mK). And a better understanding of the impurity effect is required to improve top-level metrological thermometry. Most historical experiments with impurities have worked at a much higher levels of impurities – say of the order of 100ppm - and in arrangements that are not used on a day-to-day basis in a metrology laboratory.

This thesis describes the deliberate doping of tin and aluminium, each with three different impurities and the effects of these on the temperature of the tin and aluminium liquid-solid phase transitions. The impurities, of the order of 1-30 ppm, were Co, Pb and Sb in the tin and Cu, Si and Ti in the aluminium.

The tin and aluminium samples were in the form of ~0.3 kg ingots that would normally be used to realise an ITS-90 fixed point. Measurements were made using equipment normally available in a metrological thermometry laboratory, rather than using specially prepared samples.

The samples were chemically analysed (by Glow Discharge Mass Spectrometry (GD-MS)) before and after the doping. Using the amount of dopants introduced, and/or the chemical analysis data, the measured temperature changes were compared with those interpolated from the standard text. The experimental undoped liquid-solid transition curves were also compared against theoretical curves (calculated from a theoretical model MTDATA).

The results obtained did not disagree with the Hansen interpolated values (though there was considerable uncertainty in some of the measurements (e.g. a factor of 2 or more) due to the measurement of small changes. Within these uncertainties it indicates that the Sum of Individual Estimates (SIE) method of correcting for, at least, metal

impurities in otherwise high purity metals remain valid. However the results also showed considerable discrepancies between the initial measured and calculated temperature shifts (based on the pre-existing impurities prior to doping) suggesting that there may be impurities that are not (separately) detected by the GD-MS method.

There was evidence that the thermal history of the metal phase transitions can cause considerable segregation of some impurities, particularly those likely to increase the phase transition temperature through a peritectic ("positive" impurities), and that the effects of this segregation can be clearly seen on the shape of the melting curves of the tin doped with Sb.

Some of the aluminium doped with Ti freezing curves may also show evidence of a "concave up" shape at the start of the freezing curve, as previously calculated by MTDATA, though the effect is not as pronounced.

All individual phase transition measurements - made over tens of hours – were repeated at least three times and found to be reproducible, hence providing a real data set that can be used for comparison with theoretical models still under development.

Acknowledgements

The work presented in this thesis would not have been possible without the support and encouragement of many people. First, I am deeply grateful to my PhD supervisor, Dr. Y H Joe Au, Lecturer in the School Engineering and Design at Brunel University, for his personal guidance and important support throughout the course of this work. He has provided assistance in numerous ways in his excellent supervision. I must also thank him for his valuable comments, support, and motivation in the completion of the thesis.

This thesis would not have been completed without the unwavering support from Dr David I Head who gave me the opportunity and permission to start my research at the UK National Physical Laboratory and guided me through every stage of the work. Dr David I Head is my other PhD supervisor, who was the Project Leader of Temperature Section of the UK National Physical Laboratory (NPL). With his enthusiasm, inspiration, and patience to explain things clearly and simply, he makes temperature metrology fun for me. Throughout the writing up of my thesis, he has provided great encouragement, sound advice, good company, and lots of good ideas. His knowledge and experience have had a remarkable influence on how I see my future career in the field of thermal metrology research. I am indeed most indebted to him for his guidance.

I wish to thank Dr. Richard Rusby who was Head of Temperature Standards at NPL from 1981-2001 and the NPL's representative on the Consultative Committee for Thermometry (CCT). He is now a consultant in temperature measurement specialising in contact methods. He gave me the opportunity to start the research in the Temperature Section of NPL. His excellent advice and valuable guidance have been of great value for me to improve my background knowledge of the thermal metrology. I would also like to thank him for his significance assistance in my review of the literature in the fixed-point temperature of this study.

This research work was financially supported by the UK Department for Innovation, Universities, and Skills (DIUS). I am also grateful to the Ministry of Science and Technology in the Royal Thai Government for awarding me a full PhD scholarship.

I wish to thank the School of Engineering and Design at Brunel University for funding me to attend and present a paper at the Condensed Matter and Materials Physics (CMMP) Conference, 26th – 28th April 2008, at Royal Holloway University of London, UK. I would also like to thank Brunel Graduate School, Brunel University for the award of Vice-Chancellor's Travel Prizes and School of Engineering and Design funding for their financial support to enable me to present my paper to the SICE Annual Conference 2008: International Conference on Instrumentation, Control and Information Technology, 20th – 22nd August 2008, Univ. of Electro-Communication, Chofu City, Tokyo, Japan. In addition, my gratitude extends to the UK, DIUS for their funding to allow me to present two papers at the International Conference on Temperature and Thermal Measurement, 20th -23rd October 2008, held in Beijing, China.

I would like to give my special thanks to the Temperature Section of the NPL for providing all the equipment and the Mass Section of the NPL for supplying the mass measurements of both the tin and aluminium metal ingots and the impurity dopants. I also gratefully acknowledge the Temperature Division of Centro Espanñol De Metrología (CEM), Spain, and the company Isothermal Technology for the donation of the standard tin fixed-point cells. During this work I have collaborated with many colleagues for whom I have great regard, and I wish to extend my warmest thanks to all those who have helped me with my work in the Temperature Section at the UK NPL.

Last but not the least, I owe my loving thanks to my parents for motivating and encouraging me in all my academic pursuits.

Patchariya Petchpong

Publications and Conferences concerning this work

1. Patchariya Petchpong, David I. Head (2007) Argon pressure is maintained in an aluminium thermometric fixed-point cell, *Metrologia* **44**, L73-L75.

2. P Petchpong, D I. Head and Au Y. H. Joe (2008) The influence of cobalt doping on the melting point temperature of tin, Condensed Matter and Materials Physics (CMMP), 26th – 28th April 2008, Royal Holloway University of London, UK [Conference]

3. P Petchpong, D I. Head and Au Y. H. Joe (2008) Thermal Analysis and Calorimetry (TAC 2008) Ensuring Accuracy and Relevance, 1st – 2nd April 2008, National Physical Laboratory, Teddington, UK [Conference]

4. P Petchpong, D I. Head and Au Y. H. Joe (2008) The influence of cobalt doping on the melting point temperature of tin, Graduate School Research Poster Conference, 30th April - 1st May 2008, Brunel University, Uxbridge, UK [Conference]

5. P Petchpong, D I. Head and Au Y. H. Joe (2008) Effect of Low-level Cobalt, Lead and Antimony Impurities on the Temperature of the Tin Fixed-Point, **EURAMET 732 workshop: Towards more accurate fixed points,** 3rd - 4th June 2008, National Physical Laboratory, Teddington, UK.

6. P Petchpong, D I. Head and Au Y. H. Joe (2008) Effect of Low-level Copper, Silicon and Titanium Impurities on the Temperature of the Aluminium Fixed-Point, **EURAMET 732 workshop: Towards more accurate fixed points,** 3rd - 4th June 2008, National Physical Laboratory, Teddington, UK.

7. Patchariya Petchpong, David I. Head, Au Y. H. Joe (2008) Influence of a Trace Impurity on Tin Fixed Point Plateaus, SICE Annual Conference 2008: International Conference on Instrumentation, Control and Information Technology, 20th – 22nd August 2008, Univ. of Electro-Communication, Chofu City, Tokyo, Japan.

8. Patchariya Petchpong, David I. Head, Au Y. H. Joe (2008) Influence of a Trace Impurity on Tin Fixed Point Plateaus, Proceedings of SICE Annual Conference 2008 , pp. 3155 – 3158.

9. Patchariya Petchpong, David I. Head, Au Y. H. Joe (2008) Effects of Impurities on the Melting Curve of the Aluminium Fixed Point, Tempbeijing 2008: The International Conference on Temperature and Thermal Measurement, 20th -23rd October 2008, Beijing, China (To be published in Acta Metrologica Sinica V.29 No. 4A).

10. Patchariya Petchpong, David I. Head, Au Y. H. Joe (2008) Impurity Effects on the Tin Fixed-Point Temperature, Tempbeijing 2008: The International Conference on Temperature and Thermal Measurement, 20th -23rd October 2008, Beijing, China (To be published in Acta Metrologica Sinica V.29 No. 4A).

Contents

LIST OF FIGURES

LIST OF FIGURES (Cont.)

LIST OF FIGURES (Cont.)

LIST OF FIGURES (Cont.)

LIST OF FIGURES (Cont.)

LIST OF FIGURES (Cont.)

LIST OF FIGURES (Cont.)

LIST OF TABLES

LIST OF TABLES (Cont.)

LIST OF TABLES (Cont.)

LIST OF TABLES (Cont.)

LIST OF TABLES (Cont.)

.

LIST OF ABBREVIATIONS

ASL	Automatic Systems Laboratories
BIPM	Bureau International des Poids et Mesures
CCT	Consultative Committee for Thermometry
CEM	Centro Espanñol De Metrología, Spain
CGPM	General Conference on Weights and Measures
CIPM	International Committee for Weights and Measures
EPT-76	Echelle Provisoire de Température de 1976 (Provisional 0.5 K to 30 K Temperature Scale)
ERC	Estimate based on Representative Comparisons
EURAMET	European Association of National Metrology Institutes
FP	Freezing Curve
GD-MS	Glow Discharge Mass Spectrometry
IPTS-68	International Practical Temperature Scale of 1968
ISO	International Organization for Standardization
ITS-90	International Temperature Scale of 1990
MP	Melting Curve
NIST	National Institute of Standards and Technology, USA
NMIs	National Measurement Standards
NPL	National Physical Laboratory, United Kingdom
NRC	National Research Council of Canada
OME	Overall Maximum Estimate
ppm	Mass fraction in parts per million
ppmw	Mass fraction in parts per million by weight
PRT	Platinum Resistance Thermometer
PTB	Physikalisch-Technische Bundesanstalt, Germany
R_{Al}	Resistance Values at the Aluminium Fixed-Point Temperature
R_{TWP}	Resistance Values at the Triple Point of Water
RMO	Regional Metrology Organisation
SI	International System of Units
SIE	Sum of Individual Estimates
SPRT	Standard Platinum Resistance Thermometer
TBTs	Technical Barriers to Trade

LIST OF ABBREVIATIONS (Cont.)

T_{90}	International Kelvin Temperature
t_{90}	International Celsius Temperature
UKAS	United Kingdom Accreditation Service
W(T_{90})	Ratio of the Resistance R(T_{90}) at a Temperature T_{90} and the Resistance R(273.16 K) at the Triple Point of Water
W_{ref} (T_{90})	Polynomial Reference Functions as given in the Definition of the ITS-90
$\Delta W(T_{90})$	Deviation Functions: $W(T_{90}) - W_{ref}(T_{90})$

Chapter 1
Introduction

Thermal metrology is the study of the accurate measurement of temperature, which is one of the most basic parameters in key sectors of industry, significantly affecting the ability and efficiency of processes, and the environmental impact of industrial manufacturing processes. It can therefore be said that metrology enables quality measurements to be made in industry, and it is a guide to improve the accuracy of the production process. Metrology has a very significant role to play in sustaining industrial growth and competitiveness and enables industry to carry out accurate measurements for the statutory requirements of domestic and international trade agreements. It also facilitates economic activities in the international market by providing the same measurement standard throughout the world. The use of the same standard, which is internationally agreed, allows customers to accurately specify products and also to enhance reliability of the production process anywhere in the world. This reduces and eliminates technical trade barriers and enables trade liberalisation, which maximises economic efficiency and produces overall productivity gains. Precise measurement and/or control of temperature is an essential part of most operations in any processes, such as manufacturing industries; meteorology; medical services; aerospace; power generation; automotive industries; food and drink; these often affect the health and safety, all of which affect our daily life. An improved measurement system should help enhance the quality of life for the world's population.

The general meaning of the word metrology is the study of measurement but it has come to mean the study of improvement of measurement. The **Bureau International des Poids et Mesures** (BIPM) is a standards organisation, which has the responsibility to ensure the global consistency and regularity of measurements and their traceability to the International System of the Units (SI), which has been recognized and accepted by the worldwide community. The definition of metrology specified by the **International Bureau of Weights and Measures**, which is the English translation of BIPM is "the science of measurement, embracing both experimental and theoretical determinations at any level of uncertainty in any field of

science and technology" [BIPM, 2004a]. This organisation is controlled and obtains its authority under an intergovernmental treaty called **the Convention of the Metre (*Convention du Mètre*),** which was signed in 1875 in Paris [BIPM, 2004b]**.** The purpose of this treaty is "to act in matters of world metrology, particularly concerning the demand for measurement standards of ever increasing accuracy, range, and diversity, and the need to demonstrate equivalence between national measurement standards." [BIPM, 2004b]. The Convention of the Metre established three main organisations, namely the General Conference on Weights and Measures (CGPM), the International Committee for Weights and Measures (CIPM) and the International Bureau of Weights and Measures (BIPM) to maintain the metric standards and to provide the worldwide measurement system used around the world. Nowadays, there are 51 signatory Member States- including all the major industrialised countries- they are represented by the national metrology institutes (NMIs) who participate in the activities under the Metre Convention [BIPM, 2004b]. In 1999, the Convention of the Metre set up the **Mutual Recognition Agreement** (CIPM MRA) to demonstrate the level of accuracy that each national measurement standards is at and to enable calibration and measurement certificates issued by NMIs [BIPM, 2008] to be used in other countries. It provides benefits to participants by eliminating the technical barriers to trade (TBTs) and securing the technical basis for wider understandings between governments and other parties associated with international trade, commerce, and regulatory affairs.

The national metrology institutes (NMIs) are established to maintain the quality of their national measurement standards in their own countries in line with the CIPM MRA. In addition, the NMIs are responsible for disseminating the national measurement standard units to their users as well as developing a wide range of standards for research, calibration and testing. Moreover, the NMIs provide calibration services for the manufacturers, which enable them to have confidence in their measurements and products.

It can, therefore, be concluded that the job of metrology is to ensure that measurements are accurate and the obtained results are reliable and acceptable for use in the society. In brief, metrology plays in a significant role in three main fields.

1. In the scientific field, metrology provides an internationally agreed system of units (the SI), the means to realise these units practically and an ongoing means for the

development of the new improved measurement methods. This assures the traceability of measurement results from the standards provider to users in society.

2. In the applied or industrial fields, metrology can guarantee the suitability of measurement equipment and maintains the quality control standards of measurements, used for manufacturing and other processes calibration.

3. In the field of regulatory measurement requirements, i.e. in legal metrology, it provides the necessary protection to humans and the environments.

1.1 Essential Role of Fixed-Point Cells in Temperature Calibration

Generally, temperature is an indicator of hotness or coldness of a body or environment, which is measured from the average of the heat or thermal energy of the particles in a substance. It has a direct effect on daily life of everybody through the weather temperature. Temperature can be correctly measured with thermometers designed and calibrated for use in the temperature range of interest and if used by a person with appropriate "know-how". In the International System of Units (SI), the unit of temperature is the kelvin (K), which is named after the British scientist, William Thomson, Lord Kelvin. It was defined as the fraction 1/273.16 of the thermodynamic temperature of the triple point of water in 1960 [Nicholas and White, 2001a]. Nowadays, temperature can be measured using the latest scientific thermometers but if one goes as far back as the early sixteenth century a crude thermometer-like device appeared, which was referred to as a "thermoscope" [Middleton, 1966]. It was invented by Santorio Santorio, an Italian physicist. Galileo mentioned [Helden, 1995] that Santorio Santorio was the first inventor who applied a numerical scale to the instrument, which later evolved into a thermometer. In 1641, the first sealed thermometer using wine spirit as the thermometric medium was invented by Ferdinand II, Grand Duke of Tuscany [Nicholas and White, 2001a]. It was the first device referred to as a thermometer. However, one of the most important things for the thermometer is an accurate scale. Occasionally, the results of the measurement do not need to be the numeric that is it can be the suitable context, for example cat (kind of animals), grade B, and black colour. These are the symbolic representation, which the symbols are used to make predictions and measurements. The symbolic representation of measurement scales or nominal scales were the

fundamental systems, which were constructed in the sixteenth and seventeenth centuries that are still in use today. However, the nominal scales need to have its own definition or standard in each classification or naming, which is the one of the principal aspects [Nicholas and White, 2001b]. The scales of temperature measurement include kelvin (K), Celsius (^{o}C), Fahrenheit (^{o}F), and Rankin (^{o}Ra). The Celsius, Fahrenheit, and Rankin are based on an arbitrary scale must now be compared and derived from the Kelvin scale. These scales can be related by the expression of the relationships as follows: T_K K = (T_K - 273.15) °C = [1.80 x (T_K - 273.15) + 32] °F = 1.80 T_K °R, where T_K is Kelvin temperature. However, the kelvin is based on physics and universal properties of nature, i.e. it is a thermodynamic scale.

The thermodynamic or Kelvin scale is the absolute measurement of temperature scale. This scale is based on two points, which are absolute zero of the zero point of the ideal gas temperature scale and the triple point of water. In theory, the volume of the most gas would directly proportional to the temperature and the pressure, therefore, the volume of the ideal gas at absolute zero would be zero and the motion of all molecular would stop. But in the actual conditions, all gases cannot be at the absolute zero state and the solid and liquid states would be above from this point. Absolute zero can be referred to the coldest possible temperature. Therefore, at 0 degrees of the Kelvin temperature scale equals to -273.15 ^{o}C and at 273.16 K (the triple point of water) is equivalent to 0.01 °C.

However, it is very difficult to perform calibrations and measurements directly in terms of thermodynamic temperature due to the lack of thermodynamic thermometers with adequate supply of repeatability and accuracy for both commercial and research uses [Nicholas and White, 2001c]. As a result, the first International Temperature Scale (ITS), which was then a “wire scale”, was created in 1927 [Preston-Thomas, 1990] and was adopted by the seventh General Conference of Weights and Measures. It was introduced to eliminate the practical difficulties of direct measurement of thermodynamic temperatures based purely on a gas thermometer. It was also proposed as a substitute for unrelated, individual national temperature scales and enabled an agreed worldwide temperature scale. This ITS scale is an ordinal scale to an interval scale where is estimated the interpolating temperature between the defined point by using the phase transitions (melting, freezing and triple points) and physical properties (e.g. vapour pressure) of pure materials, called fixed points. Cells of these fixed-point materials were used to calibrate interpolating

thermometers, i.e. thermometers that enabled one to measure temperature between the reference fixed points. Over the years subsequent, ITS scales have been improved in such a way that the temperature value is a close numerical approximation to thermodynamic temperature. Moreover, the ITS scale was more precise, repeatable and practical to realise than the thermodynamic scale. Nowadays, the International Temperature Scale of 1990 (ITS-90) has been constructed and adopted internationally since 1 January 1990 [Preston-Thomas, 1990]. The ITS-90 defines a precise calibration procedure using thermometers, measured at the reference temperatures of the fixed points, to define an agreed temperature scale more reproducible than 1 mK. The interpolating thermometers specified in ITS-90 use interpolating equations to enable measurement over the full range of the scale. This scale extends from 0.65K (defined in terms of the helium vapour pressures) up to the copper fixed-point temperature (1084.62 ^{o}C) and then extrapolated in terms of the Planck radiation law to higher temperatures. The full details of the ITS-90 definition are mentioned in Chapter 2.

In this thesis, the freezing point temperatures of high purity tin (231.928 ^{o}C) and aluminium (660.323 ^{o}C), which form part of a fixed-point series specified for use in the definition of the ITS-90, are studied in order to understand the effects of trace impurities on the melting and freezing transitions. Standard platinum resistance thermometers (SPRTs) are used for measurements on these temperature fixed points.

1.2 Reasons for Doping the Impurities into the Fixed-Point Cell

The temperature value, of a metallic fixed-point in the ITS-90, is based on the behaviour of high purity substances. However, it is difficult to produce the metallic elements at 100% purity. Therefore, as stated in CCT report [Ripple *et al.*, 2005], the ideal pure metal can be replaced by the use of 6N (99.9999%) nominal purity metal with an estimated standard uncertainty due to the impurities. The precision of the fixed-point temperature is influenced by the purity of the metal used. At the level of 1 mK a purity of nominally 99.9999% has a noticeable effect on the temperature realised. The influence of chemical impurities on the fixed-point is one of the most important contributions in the uncertainty budgets of the metal fixed-point realisations. If the impurity content and their specific affects on the pure fixed-point

metals were identified, the total correction to the temperature of the metal fixed-point would be more precise and reliable.

The effect of impurity metal elements may either decrease or increase the equilibrium temperature plateaus depending on the behaviour of each impurity in the high purity sample. Each impurity can be considered as part of a binary alloy system between the impurity and host metal at the low impurity levels of impurities fixed-point metals. It is presumed that the influence of each impurity in the host material remains independent of each other at low concentrations. The magnitude of each temperature effect depends on both the species type and the amount of that particular species and the total temperature change is the sum of the individual effects, taking into account of any sign.

The investigation of this work is focused on the effects of low level doping on, the melting and freezing curves of tin and aluminium in order to improve the measurement of the temperature change caused by increasing the low level concentration of metal dopants. This will also test the interpolation of previous data [Hansen, 1958]; all of which were obtained from relatively high impurity concentrations. The reason why tin and aluminium fixed points have been selected for studying is because NPL responsible for tin and aluminium fixed points of "The European Association of National Metrology Institutes" (Euramet) 732 project. The aim of this project is toward more accurate temperature fixed points, (see more information in Chapter 3). An improved understanding of low-level impurities affects to reduce the uncertainty budget component for the realisation of tin and/or aluminium temperature fixed-points in the long term benefit. The shifts and shapes of equilibrium melting and freezing plateaus of tin and aluminium fixed points are determined by doping with small concentrations (mass fraction in parts per million by weight (ppmw). These experiments have been carried out using the normal conditions available in most national measurement institutes around the world, which is important in ensuring the applicability of these temperature measurements around the world.

Finally, the tin and aluminium samples will be analysed by Glow Discharge Mass Spectrometry (GD-MS) after doping to detect the type and amount of impurity elements. This analysis will be compared with GD-MS results before doping, to confirm the increased dopant in the originally "pure" tin and aluminium cells. The "state-of-the-art" GD-MS analysis is a technique used to check the impurities contents

of the pure metal fixed-point cells with its low limit of detection down to ppb level, therefore, the sum of individual estimates (SIE) method [Ripple *et al.*, 2005] (to be described in Chapter 3) can be used to estimate the uncertainty from all relevant impurities concentrations. This method allows the fixed-point temperature to be corrected for the influence of impurities. By applying the SIE method, the uncertainty budgets for temperature measurements at the tin and aluminium fixed points can be reduced from the overall uncertainty of measurement, which is referred to as an "Overall Maximum Estimate (OME) method [Ripple *et al.*, 2005] used in the general uncertainty contribution. Furthermore, the GD-MS results will be used to calculate the theoretical temperature offset predicted by a special thermodynamic impurity model, i.e. "MTDATA" programme developed by the materials-science department of NPL. From the MTDATA analysis, the theoretical and actual measured melting curve shapes of the tin and aluminium fixed points, before doping, will be compared (there is sufficient background impurities in the samples (due to their age) to enable this prior to their specific doping).

In this thesis, the originally pure tin samples were doped with three types of impurities; cobalt, lead and antimony. Also, three types of impurities; copper, silicon and titanium were put into the originally pure aluminium samples, increasing the concentrations in order to study the influence of a trace impurity on tin and aluminium fixed point plateaus.

1.3 Aims and Objectives

The primary aim of this work is to study the quantitative effect of low level impurities on the freezing and melting temperatures provided by the tin and aluminium thermometric fixed-point cells. This will be complemented by a couple of further aims.

The second aim: an improved understanding of low level impurities would provide the benefit of reducing the uncertainty budget of the realisation of the tin and aluminium temperatures fixed-point through the correction for impurities effect. It is a part of present development in thermal metrology.

The third aim: to improve the accuracy of the standard temperature realisations based on the International Temperature Scale 1990 (ITS-90). It provides the potential

for better production process and the reliability of the products, which is important in terms of economic development.

In order to achieve the key aims; the following research objectives have been specified:

- To investigate the offsets and shape changes of the melting/freezing curves of high purity (99.9999%) tin and aluminium fixed-point cells caused by a variety of impurities at low levels of concentration.
- To test the interpolation of previous data [Hansen, 1958] on Sn-X and Al-X binary alloy systems, all of which were obtained from relatively high impurity concentrations.
- To complete a literature review of previous work/information on the effects of low levels impurities or dopants in binary alloy systems. This is needed due to the lack of reliable results on very low level impurity concentrations in existing databases [Hansen, 1958].
- To reproduce such measurements within standard conditions by using normal NPL equipment, as available in most other national measurement institutes (NMIs) worldwide. This is important in ensuring the application of temperature-impurity measurements around the world.
- To use a state-of-the-art chemical analysis technique, i.e. Glow Discharge Mass Spectrometry (GD-MS), to detect the distribution, and measure the concentration of any background elements within "pure" tin and aluminium fixed-point ingots before deliberately doping and re-analysing the impurity content after doping to confirm the increase in dopants within their ingots.
- To compare the effect of the background trace impurities on the tin and aluminium temperature fixed-point both theoretically (i.e. MTDATA program) and experimentally.
- To establish, implement and improve suitable impurity mixing techniques within the fixed-point cells. It is an important process to confirm that each impurity dopant is sufficiently well mixed throughout the fixed-point cells (see Chapter 4).

The accomplishment of the overall objective will lead to an improvement of the realisation of standard temperatures provided by tin and aluminium metallic fixed-

points based on the definition of the ITS-90 when using 99.9999% metal. Additionally, the effect of low-level impurities on temperature fixed-point will provide the relevant information for the database of the Sn-X and Al-X binary alloy systems. The improved data will be used to reduce the uncertainty of temperature realisation, which is a part of ongoing thermal metrology development.

Research on the estimation of uncertainty of measurement evinces the reliability of measurement results and provides confidence to customers. Moreover, a thermodynamic model will be used to predict the temperature offsets, which will then compared with actual measured experimental offsets. In chapters 2 and 3 the general and specific backgrounds to this work are reviewed. The experimental design and method details will be explained in Chapter 4 and 5. Then the measurement results for tin and aluminium are presented in chapters 6 and 7 respectively. Conclusions of this work are presented in Chapter 8, including a recommendation for future work.

Chapter 2

Background of Temperature Measurement and Calibration

In this chapter, the primary background of temperature measurement and calibration realised by the International Temperature Scale 1990 (ITS-90) is reviewed. The chapter begins with an overview of the fundamentals of thermometry, followed by a description of the principle and the definition of the International Temperature Scale of 1990 (ITS-90), which is an approximation to the thermodynamic temperature scale. The fixed-points, which are the essential reference point of the ITS-90, for calibration of standard platinum resistance thermometers (SPRTs) are described.

Platinum resistance thermometers are used for temperature measurement. Its characteristics in terms of the resistance values of pure platinum and their use as resistance ratios in temperature measurement are explained. The chapter ends with a discussion of the concepts of calibration and traceability, and the types of uncertainty.

2.1 Fundamentals of Thermometry

As the James Clerk Maxwell mentioned, "the temperature of a body is its thermal state, regarded as a measure of its ability to transfer heat to other bodies [Michalski *et al.*, 2001a]. Temperature can be obtained with a thermometer that may be calibrated to a variety of standard temperature scales, for example, the kelvin, the Celsius, the Fahrenheit and the Rankine scales. It is a valid question how those numbers on the scales can give people the confidence that they are accurate.

For this reason, the definition of temperature in what is known as fundamental thermometry is used as the basis to explain the temperature scales. The following two sections explain the concept of thermodynamic temperature and the units used for temperature measurement.

2.1.1 Thermodynamic Temperature

The study of thermodynamics concerns a spontaneous process related to the changes of heat, work, temperature, and energy in a physical system as it approaches an equilibrium state. Thermodynamic temperature, by definition, is the absolute

measure of temperature and is one of the principal parameters of thermodynamics. Moreover, thermodynamic temperature is an "absolute" scale because it is the measure of the fundamental property underlying temperature: its *null* or zero point, absolute zero, is the lowest possible temperature where nothing could be colder. Absolute zero is defined as a temperature of precisely 0 kelvins (−273.15 °C), at which the motion of particles in the matter is minimal. [Thermodynamics temperature, 2008]

The standard temperature scale based on the laws of thermodynamics and thermodynamic systems is used to indicate the hotness or coldness of objects expressed in terms of numerical values. Certain numerical values on the scale correspond to the temperature fixed points defined by the freezing or melting of thermometric substances. Other temperature values are obtained by interpolation between these fixed points. Evidently, the temperature fixed points depend on the physical property of each thermometric substance.

An ideal gas is the substance, which most closely approximate to the corresponding thermodynamic temperature value. The thermodynamic properties of an ideal gas are governed by the "ideal gas law", derived from a combination of the experimental Boyle's law, Charles' law and Avogadro's law. The ideal gas law is written in an equation form as [Michalski *et al.*, 2001b]:

$$pV = nkT \tag{2.1}$$

where p is the pressure, V the volume, n the number of the moles, k the Boltzmann's constant (1.3807×10^{-23} J/K) and T the absolute temperature.

The thermodynamics laws and thermodynamic systems are used to measure the values of temperature on the scale. In the given temperature range on the scales, repeatability and reproducibility of the substance's property are required. However, it still had the problem of the limitation of some finite range determined by the chosen thermometric substance's thermal behaviour even though it may be applied in principle. Therefore, any temperature range and the thermometric substance have to be completely independent working for proposing suitable temperature scale. For more details of previous experiments, see Temperature Measurement Book [Michalski *et al*, 2001b] and Tracelable Temperatures [Nicholas and White, 2001d]. The thermodynamic temperature scale is defined by choosing the values of two points, namely absolute zero, and the triple point of water (temperature at which ice, water

and water vapour exist in thermal equilibrium) as accepted by international agreement. For standard temperature measurements, the values of practical thermometers are closely approximating the corresponding thermodynamic temperature value. Since it is very difficult to accomplish the real thermodynamic temperature, a series of fixed points specified in the International Temperature Scale (ITS-90) are used to measure the temperature values on the scale in practice.

The international scales have been revised in 1948, 1960), 1968, 1976 and 1990. Nicholas and White [2001d] commented that "these revisions have provided improvements in respect of closer approximation of the thermodynamic temperature, improved interpolating equations, extensions to lower temperatures, and greater accessibility for users." The ITS-90 is an approximation to the thermodynamic temperature scale. Standard thermometers such as the standard platinum resistance thermometer, SPRT, can be calibrated at the fixed points with the necessary high precision and reproducibility, and used for the comparison and dissemination of the scale, with uncertainties ranging from 0.1 mK to 1 mK.

2.1.2 Units of Temperature Measurement

Thermodynamic temperature, denoted as *T,* is one of seven base quantities in the International System of Units (SI units). The unit of thermodynamic temperature is called the kelvin and is denoted by the symbol K. The unit of thermodynamic temperature is defined as "the fraction 1/273.16 of the thermodynamic temperature of the triple point of water." [Michalski *et al.*, 2001b]

This definition was introduced in 1967 at the Thirteenth General Conference on Weights and Measures (CGPM). A Celsius temperature (denoted by the symbol *t*) had been generated to replace the old centigrade scale since 1948, and it is expressed as the difference from the ice point (273.15 K). The degree Celsius (^{o}C) is the unit of Celsius temperature. Thus, the degree Celsius *t* can be obtained from the thermodynamic temperature *T* from [Preston-Thomas, 1990]

$$t/°C = T/K - 273.15 \qquad (2.2)$$

The International Kelvin Temperature (T_{90}) and the International Celsius Temperature (t_{90}) as defined in the ITS-90 are now used to be the units of temperature. The conversion equation between T_{90} and t_{90} is

$$t_{90}/^{o}C = T_{90}/K - 273.15 \qquad (2.3)$$

2.2 International Temperature Scale of 1990 (ITS-90)

According to Mangum et al [1997], the purpose of ITS-90 is to specify internationally agreed procedures and practical thermometers that will enable laboratories to realise the scale independently and/or interdependently to determine highly reproducible values of temperature.

Although the temperature values as defined in ITS-90 are only an approximation to the thermodynamic temperatures, they are actually a very good approximation and can be more easily evaluated than their thermodynamic counterparts.

ITS-90 has been accepted in 1989 by the International Committee for the Weights and Measures [Preston-Thomas, 1990; Rusby, 1987] and took effect from 1 January 1990. Its adoption supplanted the International Practical Temperature Scale of 1968, its revised edition of 1975 (IPTS-68(75)) and the 1976 Provisional 0.5 K to 30 K Temperature Scale (EPT-76) [Preston-Thomas, 1990].

The values of temperature as defined in ITS-90 were revised to be in nearer agreement with thermodynamic values. Figure 2.1 shows the numerical differences between the values of T_{90} and the corresponding values of T_{68} measured on the International Practical Temperature Scale of 1968 (IPTS-68). For more detailed information, see "Supplementary Information for the ITS-90" [Preston-Thomas *et al.*, 1990].

The ITS-90 is based on a number of defining fixed-points. Also, interpolation methods would be used for linking among the fixed points. The ITS-90 uses either of the two types of international unit temperature scales, namely kelvin (symbol T_{90}) and Celsius (symbol t_{90}). The principles and the definition of the International Temperature Scale of 1990 are described in Section 2.2.1.

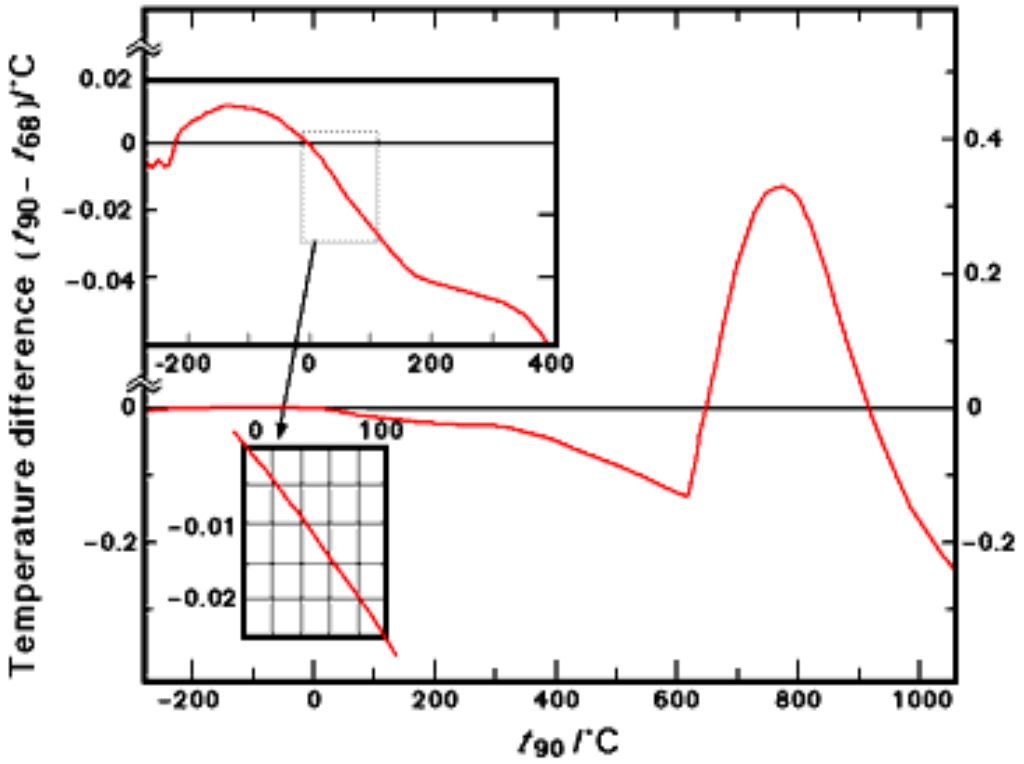

Figure 2.1 The relation of the Temperature differences (t_{90} – t_{68}) and the Celsius temperature (t_{90}/°C) [Preston-Thomas, 1990].

2.2.1 Principles of the International Temperature Scale of 1990

ITS-90 is subdivided into overlapping temperature (T_{90}) ranges and sub-ranges from 0.65 K to above 961.78 °C; at the overlapping sub-ranges, differing definitions of T_{90} exist. The temperature values are identified in terms of the equilibrium states of the pure substances as a given set of defining fixed-points. Different types of thermometers are used for temperature measurement within the different ranges.

According to Preston-Thomas [1990], "for measurements of the very highest precision there may be detectable numerical differences between measurements made at the same temperature but in accordance with differing definitions. Similarly, even using one definition, at a temperature between defining fixed points two acceptable thermometers may differ; of these differences are of negligible practical importance and are at minimum level consistent with a scale of no more than reasonable complexity."

In ITS-90, there are three interpolation instruments used in establishing the scale:

1. Fixed points (melting, freezing, boiling, and triple points of the high purity materials);
2. Interpolating thermometers; and
3. Interpolating equations.

The temperatures are realised at each of the fixed points using the equation of a specified form that passes through each of the fixed point. The range and sub-ranges of the interpolation instruments as defined on the ITS-90 are as shown in Figure 2.2. For further details about the principles of the ITS-90 and the interpolation techniques, see "The ITS-90" [Preston-Thomas, 1990] and "Supplementary Information for the ITS-90" [Preston-Thomas *et al.*, 1990].

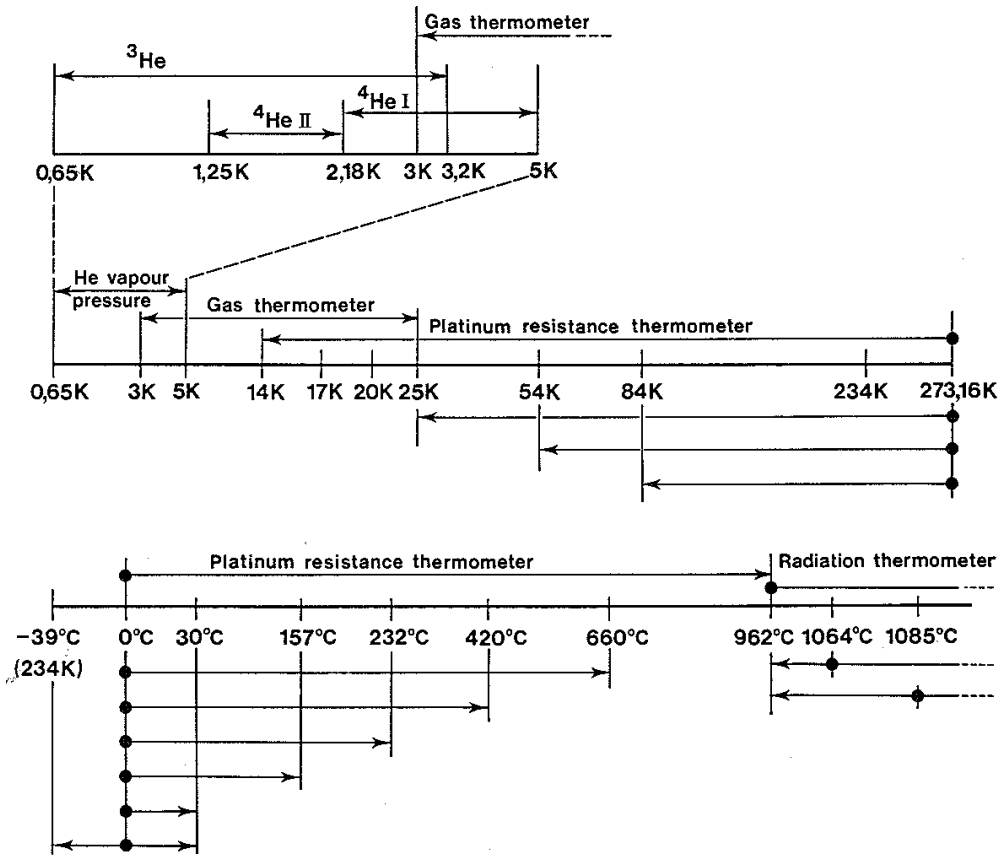

Figure 2.2 Diagram of the ranges, sub-ranges and the interpolation of instruments as defined on the ITS-90. The temperatures on the diagram are only approximate [Preston-Thomas *et al.*, 1990].

2.2.2 Definition of the International Temperature Scale of 1990

The interpolation instruments used for the ITS-90 are divided into four different ranges as follows [Preston-Thomas, 1990]:

Temperature range	*How is T_{90} defined?*
0.65 K to 5.0 K	Using the vapour-pressure temperature relations of ^{3}He and ^{4}He.
3.0 K to 24.5561 K (the triple point of neon)	By calibrating a helium gas thermometer using interpolation techniques to realise three numerical (defining fixed points) temperature values.
13.8033 K (the triple point of equilibrium hydrogen) to 961.78 °C (the freezing point of silver)	With the platinum resistance thermometer calibrated at the appropriate set of defining fixed points using defined interpolation procedures.
Above 961.78 °C	With the radiation thermometer calibrated at a defining fixed point referring to the Plank radiation law.

There are 17 defining fixed points of ITS-90 throughout the ranges on the scale. These fixed points are listed in Table 2.1 [Preston-Thomas *et al.*, 1990]. Each fixed point is highly reproducible, which means that the measured temperature is close to the thermodynamic temperature of the point. The defined functions information for interpolation at intermediate temperatures in each range can be found in the "Supplementary Information for the ITS-90" [Preston-Thomas *et al.*, 1990] and the text in Preston-Thomas's publication [Preston-Thomas, 1990].

Table 2.1 Defining fixed point of the ITS-90 [Preston-Thomas, 1990].

Number	Temperature		Substance [a]	State [b]	$W_r(T_{90})$ [c]
	T_{90}/K	t_{90}/°C			
1	3 to 5	-270.15 to -268.15	He	V	
2	13.8033	-259.3467	e-H_2	T	0.001 190 07
3	~17	~-256.15	e-H_2 (or He)	V (or G)	
4	~20.3	-252.85	e-H_2 (or He)	V (or G)	
5	24.5561	-248.5939	Ne	T	0.008 449 74
6	54.3584	-218.7916	O_2	T	0.091 718 04
7	83.8058	-189.3442	Ar	T	0.215 859 75
8	234.3156	-38.8344	Hg	T	0.844 142 11
9	273.16	0.01	H_20	T	1.000 000 00
10	302.9146	29.7646	Ga	M	1.118 138 89
11	429.7485	156.5985	In	F	1.609 801 85
12	505.078	231.928	Sn	F	1.892 797 68
13	692.677	419.527	Zn	F	2.568 917 30
14	933.473	660.323	Al	F	3.376 008 60
15	1234.93	961.78	Ag	F	4.286 420 53
16	1337.33	1064.18	Au	F	
17	1357.77	1084.62	Cu	F	

[a] All substances except ^{3}He are of natural isotopic composition, e-H_2 is hydrogen at the equilibrium concentration of the ortho- and para-molecular forms.

[b] For complete definitions and advice on the realization of these various states, see "Supplementary Information for the ITS-90". The symbols have the following meanings: V: vapour pressure point; T: Triple Point (temperature at which the solid, liquid and vapour phases are in equilibrium); G: gas thermometer point; M,F melting point, freezing point (temperature, at a pressure of 101 325 Pa, at which the solid and liquid phases are in equilibrium)

[c] $W_r(T_{90})$ is the polynomial reference functions as given in the definition of the ITS-90

Additionally, the depth to which a thermometer sensor is inserted into the fixed point cell affects the equilibrium temperature because of the hydrostatic pressure. The pressure below the liquid surface is called the hydrostatic head. The effect of pressure on the temperature in each of fixed point is given on Table 2.2 [Preston-Thomas, 1990]. The constant values for ^{3}He and ^{4}He vapour pressure temperature equation, which is used to find the T_{90} is given in Table 2.3.

Table 2.2 Effect of pressure on the temperatures of some defining fixed points[#] [Preston-Thomas, 1990].

Substance	Assigned Value of equilibrium temperature T_{90}/K	Temperature with pressure, p, $(dT/dp)/10^{-8}$K.Pa$^{-1})^{*}$	Variation with depth, *l*, $(dT/dl)/10^{-3}$ K.m$^{-1})^{**}$
e-Hydrogen (T)	13.8033	34	0.25
Neon (T)	24.5561	16	1.9
Oxygen (T)	54.3584	12	1.5
Argon (T)	83.8058	25	3.3
Mercury (T)	234.3156	5.4	7.1
Water (T)	273.16	-7.5	-0.73
Gallium	302.9146	-2.0	-1.2
Indium	429.7485	4.9	3.3
Tin	505.078	3.3	2.2
Zinc	692.677	4.3	2.7
Aluminium	933.473	7.0	1.6
Silver	1234.93	6.0	5.4
Gold	1337.33	6.1	10
Copper	1357.77	3.3	2.6

[*] Equivalent to millikelvins per standard atmosphere

[**] Equivalent to millikelvins per metre of liquid

[#] The Reference Pressure for melting and freezing points is the standard atmosphere (p_0 = 101 325 Pa). For triple points (T) the pressure effect is a consequence only of the hydrostatic head of liquid in the cell

Table 2.3 Values of the constants for the helium vapour-pressure equations and the temperature range for which each equation, specified by its set of constants, is valid [Preston-Thomas, 1990].

	^{3}He 0.65 K to 3.2 K	^{4}He 1.25 K to 2.1768 K	^{4}He 2.1768 K to 5.0 K
A_0	1.053 447	1.392 408	3.146 631
A_1	0.980 106	0.527 153	1.357 655
A_2	0.676 380	0.166 756	0.413 923
A_3	0.327 692	0.050 988	0.091 159
A_4	0.151 656	0.026 514	0.016 349
A_5	-0.002 263	0.001 975	0.001 826
A_6	0.006 596	-0.017 976	-0.004 325
A_7	0.088 966	0.005 409	-0.004 973
A_8	-0.004 770	0.013 259	0
A_9	-0.054 943	0	0
B	7.3	5.6	10.3
C	4.3	2.9	1.9

2.3 Defining Fixed-Points of ITS-90 for Resistance Thermometers

Standard platinum resistance thermometers (SPRTs) are used as the interpolating instrument for temperatures between the fixed points in the range of 13.8033 K to 961.78 ^{o}C. There are three types of SPRTs in general use for calibration. For an explanation on PRTs see Section 2.4. This section introduces the definition and the methods of the realisation of the fixed points as the ITS-90 for the calibrations of long stem thermometers, which were used in the experiments reported in this thesis. Thus, the fixed-points are focused on the temperature ranges at the triple point of water, the freezing points of tin and aluminium respectively.

2.3.1 Triple Point of Water

When liquid water, ice and water vapour are in thermal equilibrium, it is called "the triple point of water". By the definition of ITS-90, the temperature value of the triple point of water on the scale equals 273.16 K or 0.01°C. This fixed-point temperature plays an important role in measuring and defining the unit of the kelvin thermodynamic temperatures and also it is the most significant defining point on the ITS-90 scale. In practice, sealed glass cells, like the one shown in Figure 2.3, containing high purity water are used as accurate temperature references. By definition, the isotopic composition of ocean water is used to make the cell. The assorted isotopic composition in the water can affect the temperature at the triple point of water. It depends on the distillation method, water sources, and freezing technique. For more details on the construction and preparation of the triple point of water, see Barber *et al.* (1994) and "Supplementary Information for the ITS-90" [Preston-Thomas *et al.*, 1990]. The long-stem thermometers will be used for measurements. The water triple point cell, with proper control of the impurity level can attain a reproducibility of better than 0.1 mK [Furukawa and Bigge, 1982].

The water triple point cell is made of a cylinder of sealed glass, with a re-entrant thermometer well for measurements with long-stem thermometers, filled with high-purity, gas-free water. After an ice mantle – item (4) in Figure 2.3 - is frozen around the well and a thin layer of this ice mantle is melted next to the well by inserting a metal rod into the well, the triple point of water temperature can be measured in the well with the thermometer. The triple point of water also provides the stability check of the thermometers used for the highest accuracy application.

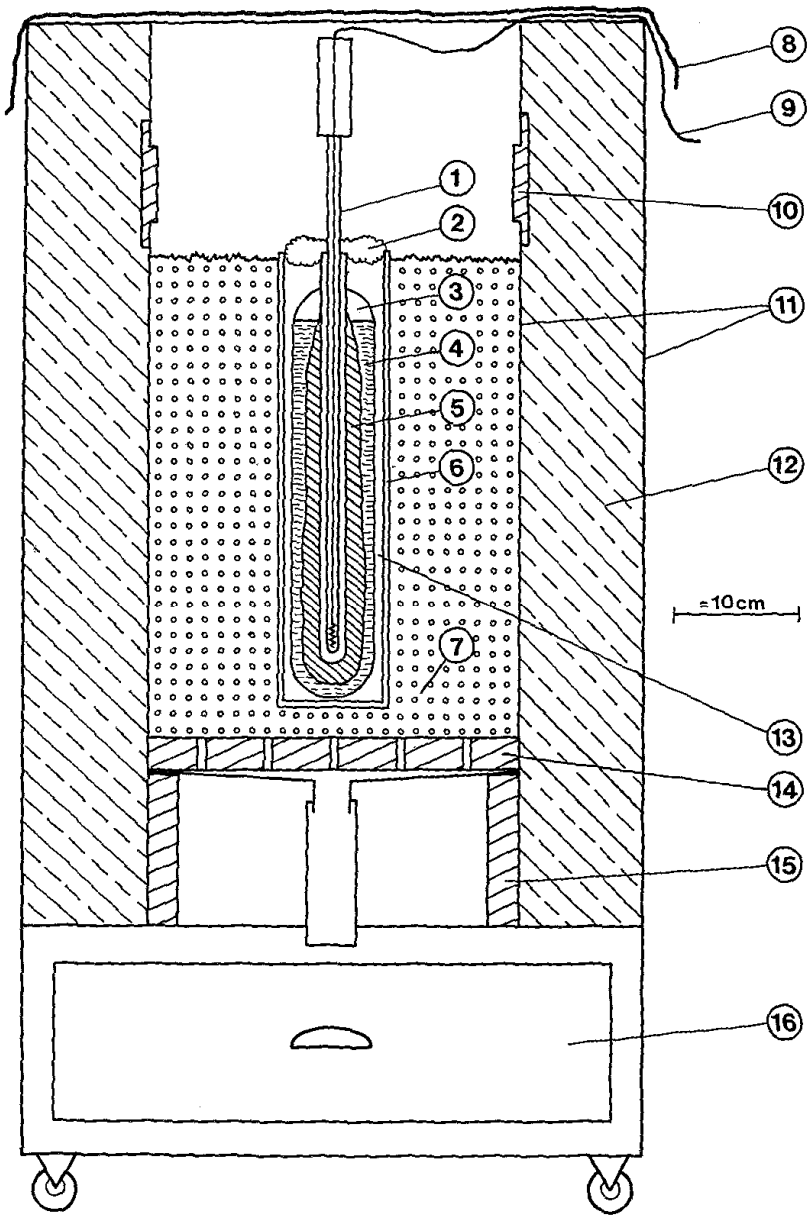

Figure 2.3 Schematic diagram of water triple point cell, which was contained in an ice bath. (1) PRT; (2) plug of glass wool; (3) water vapour in cell; (4) high purity water; (5) ice sheath; (6) plastic container; (7) crushed ice; (8) opaque cover; (9) thermometer leads; (10) insulation break in stainless-steel container wall; (11) stainless-steel container; (12) polystyrene-form insulation; (13) air gap; (14) base containing drain holes; (15) supports and (16) water container [Preston-Thomas *et al.*, 1990].

2.3.2 Metal Fixed Points

The metal fixed points are defined to extend the areas of reproducible temperature on the ITS-90 scale. The liquid-solid phase transition of metal is used to realise and reproduce the uniform temperature, which is directly measured from the fixed points of metal. On the ITS-90 scale, PRTs are placed into the thermometer well in the fixed point cells to measure and realise the temperature for all defining fixed points of the ITS-90. There are two types of fixed point cells, the sealed cell and the opened cell as shown in Figure 2.4 and 2.5 respectively. For this research, the metal fixed points specified for the calibration of the freezing points of tin and aluminium will be explained. For the realisation details for other metal fixed points, see "Supplementary Information for the ITS-90" [Preston-Thomas *et al.*, 1990].

(a) Freezing point of tin (231.98 ^{o}C)

As discussed in the "Supplementary Information for the ITS-90" [Preston-Thomas *et al.*, 1990], a freezing point (liquid to solid direction) is the most accurate realisation of a liquid-solid phase transition in metal. The pressure of the inert gas, which also affects the fixed-point temperature, needs to be at 1 atmosphere (101.325 kPa) inside the cell while the temperature is set at the tin fixed point as defined in ITS-90.

The freezing curve of tin is obtained when the temperature slowly cools down and approaches the freezing temperature of the tin. Because the tin metal has a dip of supercooling at the beginning of the freeze, the extremely small crystals of tin thus formed are unstable and compact together rather than grow unless they are beyond a critical size. To avoid this, the following nucleation technique is used to encourage external shell formation of uniform thickness at the outer walls of the crucible:.

1. The furnace temperature is first lowered to 10 ^{o}C below the freezing point.
2. The tin ingot is lifted out of the furnace when the temperature of the monitoring thermometer indicates the recalescence point.
3. The tin ingot is re-inserted immediately back into the furnace block.
4. The temperature of the furnace is increased to the tin freezing temperature.

To start the inner nucleation, a cold rod is put into the thermometer well. A mantle of solid tin then begins to grow rapidly on the wall of the thermometer well. What the thermometer records is the freezing temperature of tin at the inner interface

on the well. For more information, see "Supplementary Information for the ITS-90" [Preston-Thomas *et al.*, 1990].

The reproducibility of the temperature realisation can be better than 1 mK if the tin metal is very pure (typically better than 99.9999% pure) [Nicholas and White, 2001e].

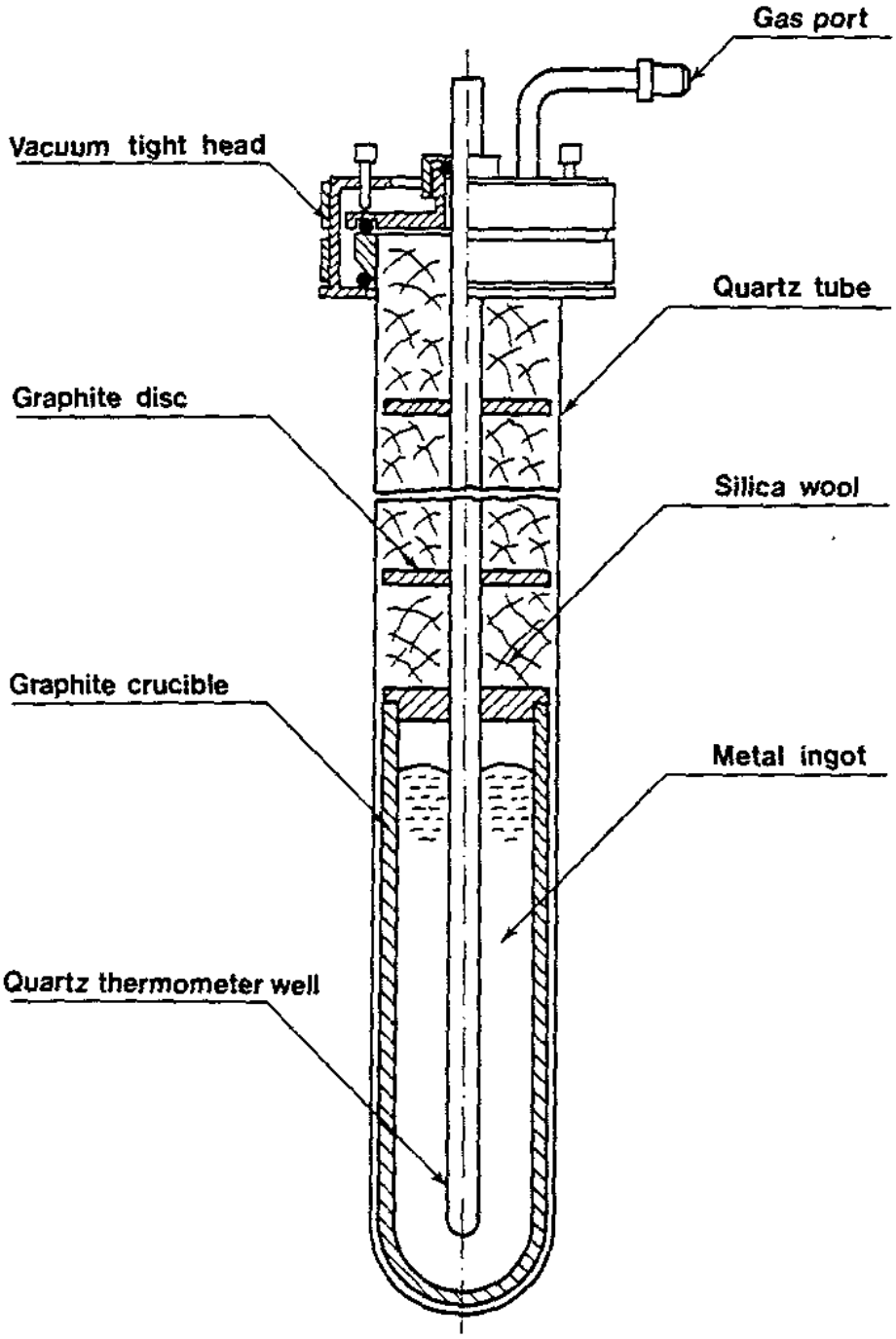

Figure 2.4 An example of the opened metal fixed point cell for resistance thermometry [Preston-Thomas *et al.*, 1990].

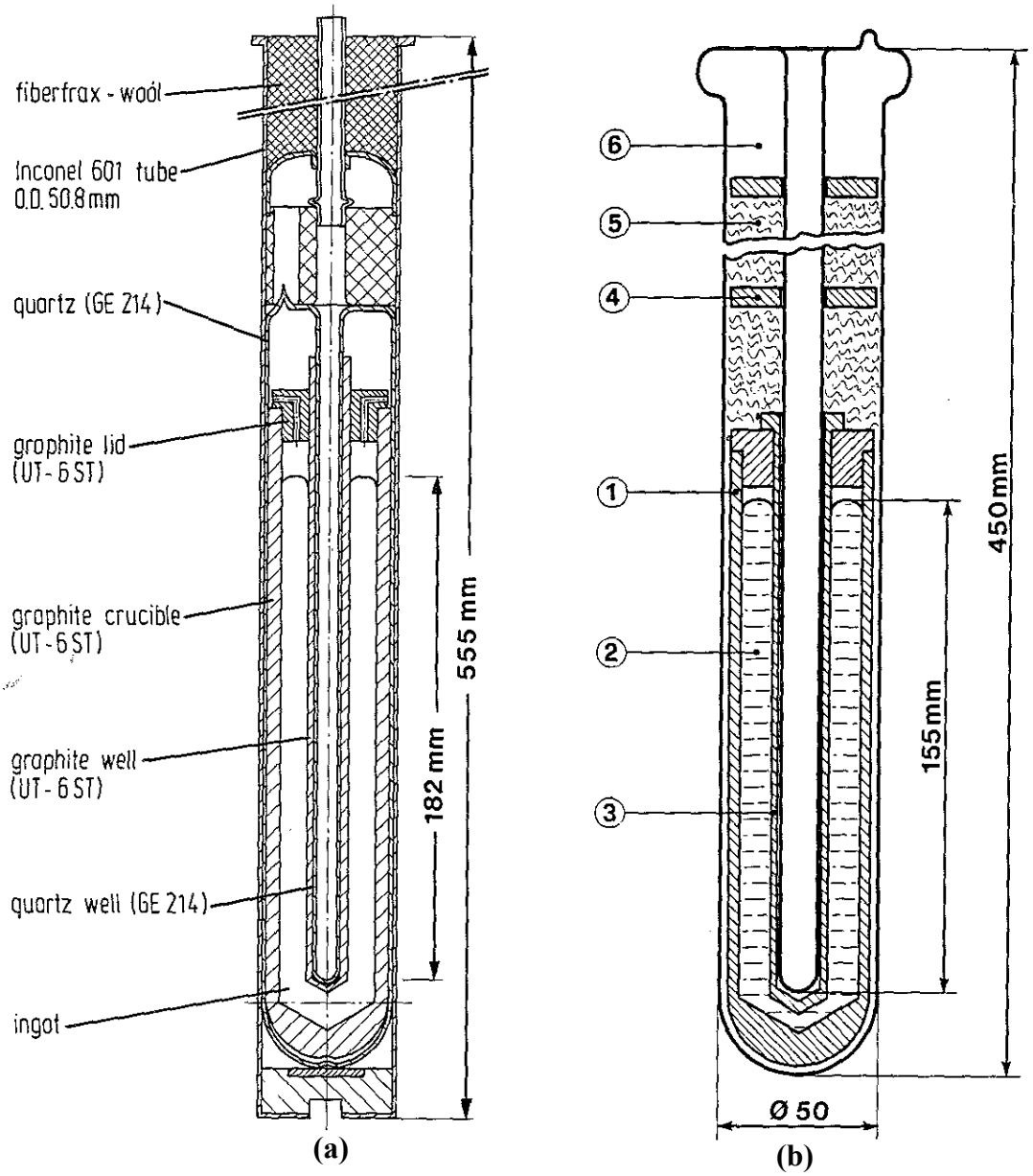

Figure 2.5 Schematic diagram of sealed metal fixed point cell. (a) Sealed cell in an inconel container for the indium, tin, zinc, aluminium, and silver fixed-point cells. Stainless steel can be used for tin and zinc. (b) Sealed cell in silica container; (1) graphite crucible, (2) metal ingot, (3) silica re-entrant well, (4) graphite disk shields, (5) pure silica wool, (6) argon atmosphere, and (7) graphite well [Preston-Thomas *et al.*, 1990].

(b) Freezing point of aluminium (660.323 °C)

The freezing point of aluminium (660.323 °C) is one of the metallic fixed-points specified for use in the definition of the ITS-90 [Preston-Thomas, 1990]. First of all, the aluminium ingot is completely molten at the temperature at 10 °C above the freezing point. To make sure the aluminium metal is well mixed, the temperature should be left at least 2 hours at the high temperature. Then, the ingot is cooled down by setting the temperature of the furnace at 0.5 °C below the aluminium freezing point. The supercooling of aluminium is generally about 0.4 to 0.6 °C. When the recalescence is recognised, a fused-silica or an alumina rod is inserted into the well in order to induce an inner-solid aluminium mantle on the well. Then, thermometer is replaced into the cell and the freezing curves could be recorded.

The reproducibility of the aluminium temperature realisation is approximate 1 mK [Preston-Thomas, 1990]. However, the stability of the thermometers used is the limitation of the measurements.

2.4 Platinum Resistance Thermometry

One of the instruments, which are used to approximate the temperature in the ITS-90 definition, is the interpolating thermometers. There are four types of highly reproducible thermometers, i.e. helium vapour-pressure thermometer, helium or hydrogen gas thermometer, platinum resistance thermometer, and radiation thermometer [Nicholas and White, 2001d]. In this work, only the platinum resistance thermometer is used as the interpolation device, which covers the temperature range of freezing point of tin and aluminium. The platinum resistance thermometer (PRT) is a remarkable device, measuring temperatures accurately on the ITS-90 scale. The PRTs can realise the temperature over the range 13.8 K to 960 °C, with accuracies approaching 1 mK. The PRTs can be divided into 3 kinds as follows [Preston-Thomas *et al.*, 1990]:

- Capsule PRTs, as shown in Figure 2.6, are designed for use at low temperature between 13.8 K and 156 °C. They have resistances of 25.5 Ω at the triple point of water.

- Long-stem PRTs are intended to cover the range 84 K to 660 ^{o}C. The long glass or quartz tubes (8 mm diameter and 450 mm long), as presented in Figure 2.7, are mounted and filled with dry air at a pressure of approximately 30 KPa at room temperature. They also have triple point of water resistance of 25.5 Ω.

- High temperature PRTs are used to cover the temperature range between 0.01 ^{o}C and the freezing point of silver (961.78 ^{o}C). In these thermometers, the resistances are from 0.25 Ω to 2.5 Ω, which is lower than the capsule and long-stem PRTs, to minimise the electrical leakage problem. Figure 2.8 shows the high temperature PRT.

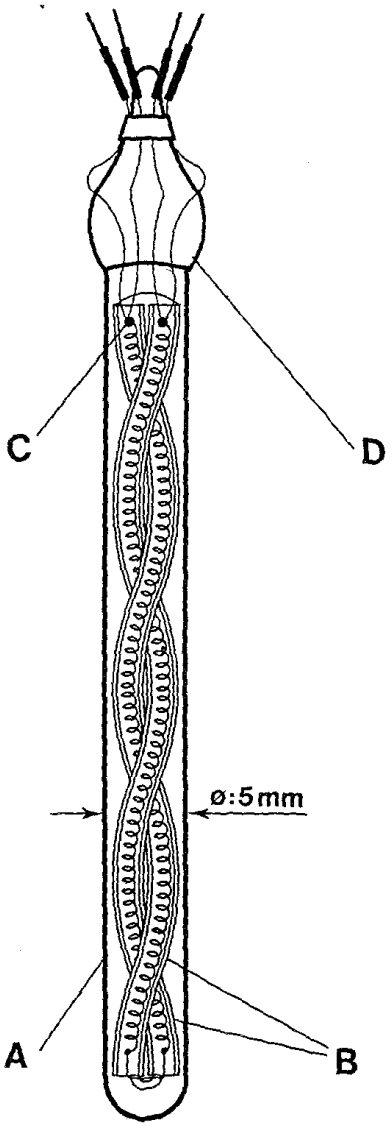

Figure 2.6 A 25 Ω capsule-type PRT: (A) platinum sheath 5 mm in diameter and 50 mm long, (B) the two glass tubes containing the 0.07 mm diameter coiled platinum wire, (C) flame welds to platinum leads, and (D) glass/platinum seal [Preston-Thomas *et al.*, 1990].

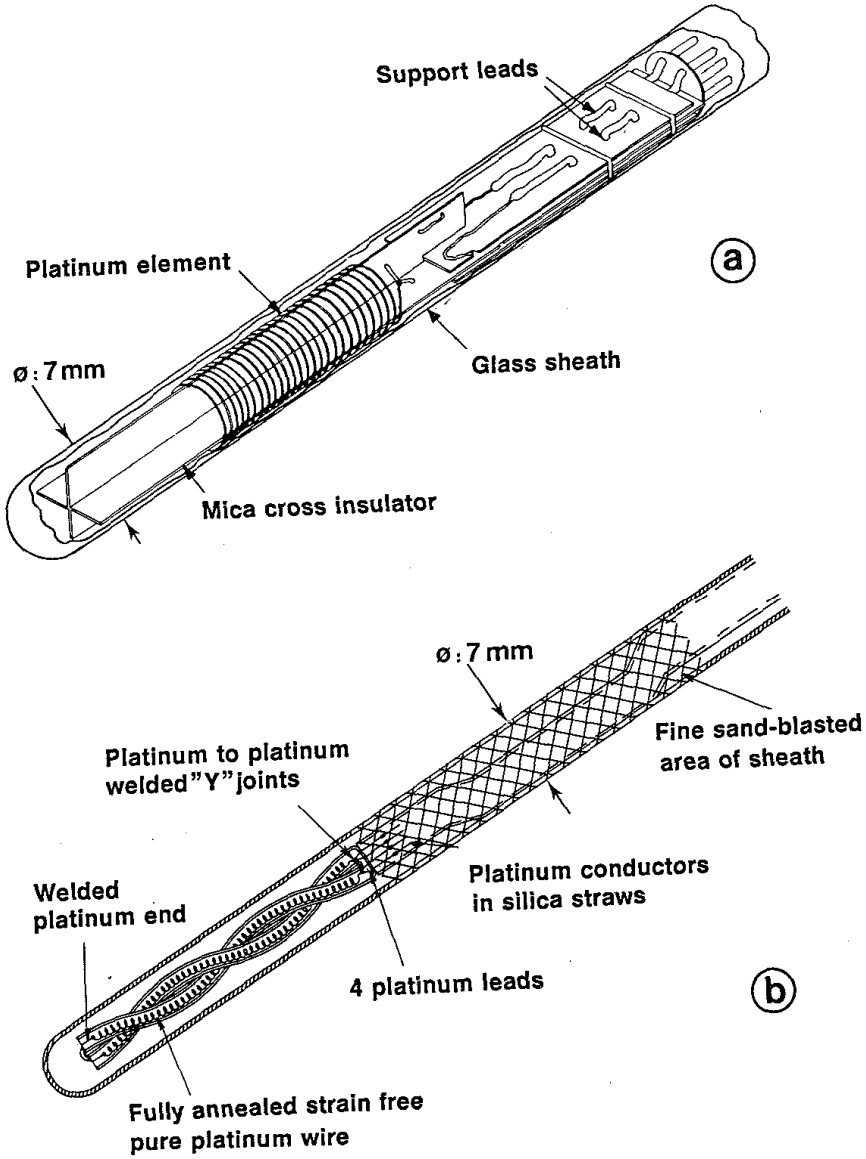

Figure 2.7 Schematic diagram of 25 Ω long-stem type PRTs [Preston-Thomas *et al.*, 1990].

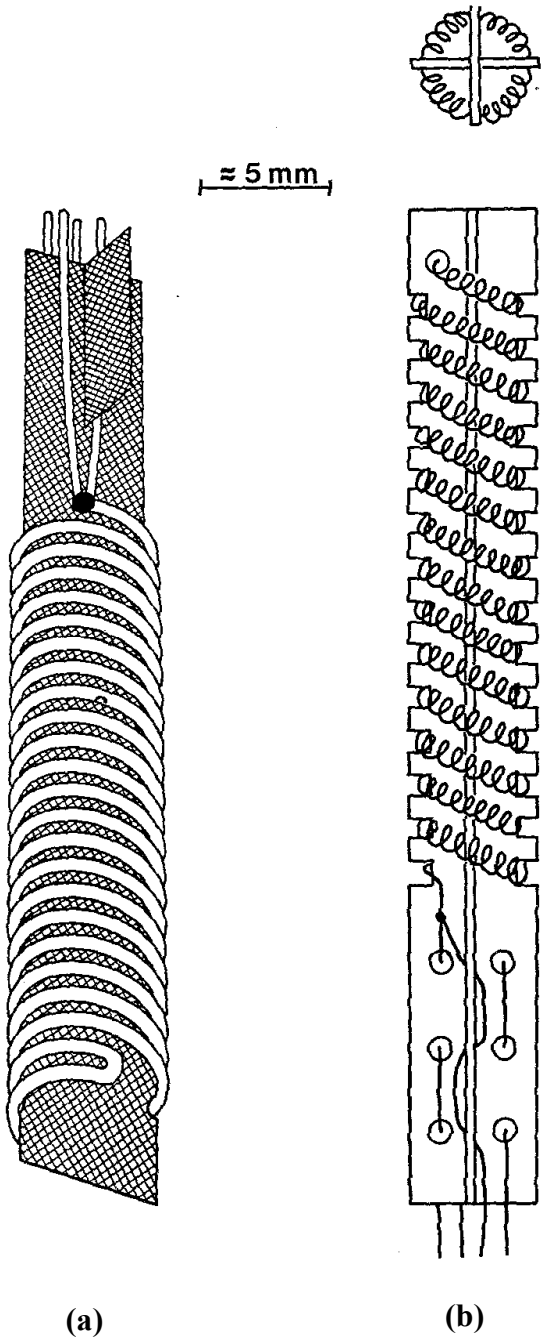

Figure 2.8 Schematic diagram of typical designs of high temperature platinum resistance thermometers; (a) resistance at the triple point of water 0.25 Ω and (b) resistance at the triple point of water 2.5 Ω [Preston-Thomas *et al.*, 1990].

All three kinds of PRTs have high purity platinum as the sensing resistor. For their construction details, see "Traceable Temperatures" [Nicholas and White, 2001f] and "Supplementary Information for the ITS-90" [Preston-Thomas *et al.*, 1990].

The temperature is measured according to the ITS-90 requirements by means of the resistance ratio $W(T_{90})$ defined as:

$$W(T_{90}) = R(T_{90})/R(273.16\ \mathrm{K}) \tag{2.4}$$

where $R(T_{90})$ is the resistance at T_{90}

$R(273.16\ \mathrm{K})$ is the resistance at the triple point of water

The pure platinum used in the PRT must satisfy [Preston-Thomas *et al.*, 1990]:

$$W(29.7646\ ^{o}\mathrm{C}) \geq 1.11807, \tag{2.5a}$$

$$W(-38.8344\ ^{o}\mathrm{C}) \leq 0.844235 \tag{2.5b}$$

For PRTs that measure up to the freezing point of silver, the resistance ratio must also satisfy:

$$W(961.78\ ^{o}\mathrm{C}) \geq 4.2844 \tag{2.6}$$

For each thermometer calibration, the resistance ratio is determined by the interpolation formula:

$$W(T_{90}) = W_{ref}(T_{90}) + \Delta W(T_{90}) \tag{2.7}$$

where $W_{ref}(T_{90})$ is the polynomial reference functions (shown in Table 2.1).

and $\Delta W(T_{90})$ is the deviation functions.

Precision measurements of the PRTs rely on accurate resistance values. The sources of errors may be due to mechanical shock and vibration (generating strains), self-heating, insulation resistance, thermometer immersion (hydrostatic pressure) and radiation effects. For further sources of errors information, see "Temperature Measurement and Calibration" [NPL, 2003b].

2.5 Calibration

Calibration expresses the relations and the comparisons of the values of the scale between the definition of SI and a measurement of instrument to ensure a precisely qualitatively determination and correspond to the international standards temperature scale, which is the ITS-90. Additionally, the uncertainty measurement and the reliability of the instrument are estimated in the calibration. The calibration is also a process transferring the values on the scale of ITS-90 from primary standard to

secondary instruments. By definition, Calibration is defined that "the set of operations which establish, under specified conditions, the relationship between values indicated by a thermometer and the corresponding known values of temperature" [NPL, 2003c]. This definition is applied to temperature measurement. For temperature measurement, the calibration comprises two main procedures as follows:

2.5.1 Calibration using fixed points

There are 4 kinds of realisation using the fixed points: freezing, melting, boiling, and triple point. As previously discussed about the fixed point, the phase change and equilibrium state of the substance are used as highly reproducible reference points on the temperature scale. For more information, see the section 2.2.2 on the definition and fixed points of the ITS-90. The thermometer to be calibrated is measured at the equilibrium temperature and measurement of its thermometric parameter (e.g. resistance) is produced.

To complete the calibration of the thermometer, it needs the measurement at several temperatures with the interpolation technique. Using the specified fixed points as defined in the ITS-90 in the calibration is the most accurate method for the calibration [NPL, 2003d]. But the temperature ranges for calibrating are restricted only in the number of available fixed points. See more detailed realisation, see "Temperature Measurement and Calibration" [NPL, 2003e].

2.5.2 Calibration by comparison

As described in "Temperature Measurement and Calibration" [NPL, 2003c], in calibration by comparison technique, the thermometer to be calibrated is inserted into an environment together with a standard thermometer and measurements are made on both. The environment may be a bath or furnace whose temperature can be controlled manually or electrically.

Compared with the fixed points, the advantages of calibration by comparison are: the technique is easier, faster, and cheaper; several thermometers can be calibrated simultaneously; and use of high purity substance is not essential.

2.6 Uncertainty and Traceability of Measurement

In this section, the concept of uncertainty and traceability of measurements will be described. The accreditation of measurement in science and commerce can be accepted with both quantities (i.e. uncertainty and traceability), which are important requirements for calibration.

2.6.1 Uncertainty

The ISO Guide to the Expression of Uncertainty in Measurement [GUM, 1993] gives the general principles for expressing and estimating uncertainty in measurement including the interpretation of uncertainties as:

Uncertainty of Measurement

"The parameter associated with the result of a measurement that characterises the dispersion of the values that could reasonably be attributed to the measurand."

The uncertainty measurement of the result can show the accuracy of a measurement. There are two categories of uncertainty: Type A and Type B. Type A uncertainty is evaluated by statistical methods whilst Type B uncertainty is evaluated by other methods. These are explained further in the following two sections.

2.6.1.1 Evaluation of Type A uncertainty

This method of the uncertainty estimation uses both the actual measurements and the statistical analysis of a series of observations. The statistic calculation of the standard deviation of repeated measurements follows well-established practice. As an example of a Type A evaluation [NPL, 2003f], consider an input quantity (q) whose value is estimated from n independent observations q_k of q obtained under the same conditions of measurement. In this case the input estimate q is simply the average value $\overline{q}$ where

$$\overline{q} = \frac{1}{n}\sum_{k=1}^{n} q_k \tag{2.8}$$

and the standard uncertainty $u(x_i)$ to be associated with q is the estimated **standard deviation of the mean** (s);

$$s = \left(\frac{1}{(n-1)} \sum_{k=1}^{n} \left(q_k - \bar{q} \right)^2 \right)^{1/2}$$

The standard deviation (s) is likely to be a safer estimate of the Type A standard uncertainty, unless a very large number of measurements are made. This type corresponds with the normal distribution, which indicates the probability of attaining a result. See more information in the National Physical Laboratory book [NPL, 2003f].

2.6.1.2 Evaluation of Type B uncertainty

Type B uncertainties can be estimated from the physical theory of the measurement, prior data from handbook or other experiments, calibration certificates, the general knowledge of the action and properties of the materials and equipment including the intuition and experience. For further information, see "Traceable Temperatures" [Nicholas and White, 2001g].

For each measurement, all the components of uncertainty must be evaluated and then combined, by summing in quadrature or similarly adding the variances linearly ($u^2 = u_1^2 + u_2^2 + u_3^2 + \ldots$), into one standard uncertainty. The uncertainty (u) is taken and multiplied by the suitable coverage factor to show the total uncertainty for the measurement at the required level of confidence [Nicholas and White, 2001g]. This value is called the combined uncertainty.

2.6.2 Traceability

The International Vocabulary of Basic and General Terms in Metrology (ISO 1993) defines the traceability [NPL, 2003g] as;

"The property of the results of a measurement or the value of a standard whereby it can be related to stated references, usually national or international standards through an unbroken chain of comparisons having stated uncertainties."

Traceability is, therefore, the ability to exhibit the precision of measurement result by means of proper national and international standards – for example, the SI Kelvin that is defined on the temperature scale. The traceability chain for the primary standard measurement links in terms of international comparisons of calibration with the ITS-90. "The purpose of traceability is to enable different users, potentially on opposite sides of the world, to compare measurement results meaningfully." (Nicholas

and White [2003h]). An example of the traceability chain in temperature measurement in the UK is explained in Figure 2.9, which links the final end user's measurement with the ITS-90, through the calibration chain. For more detailed traceability information, see "Traceable Temperatures" [Nicholas and White, 2001h] and "Temperature measurement and calibration" [NPL, 2003g].

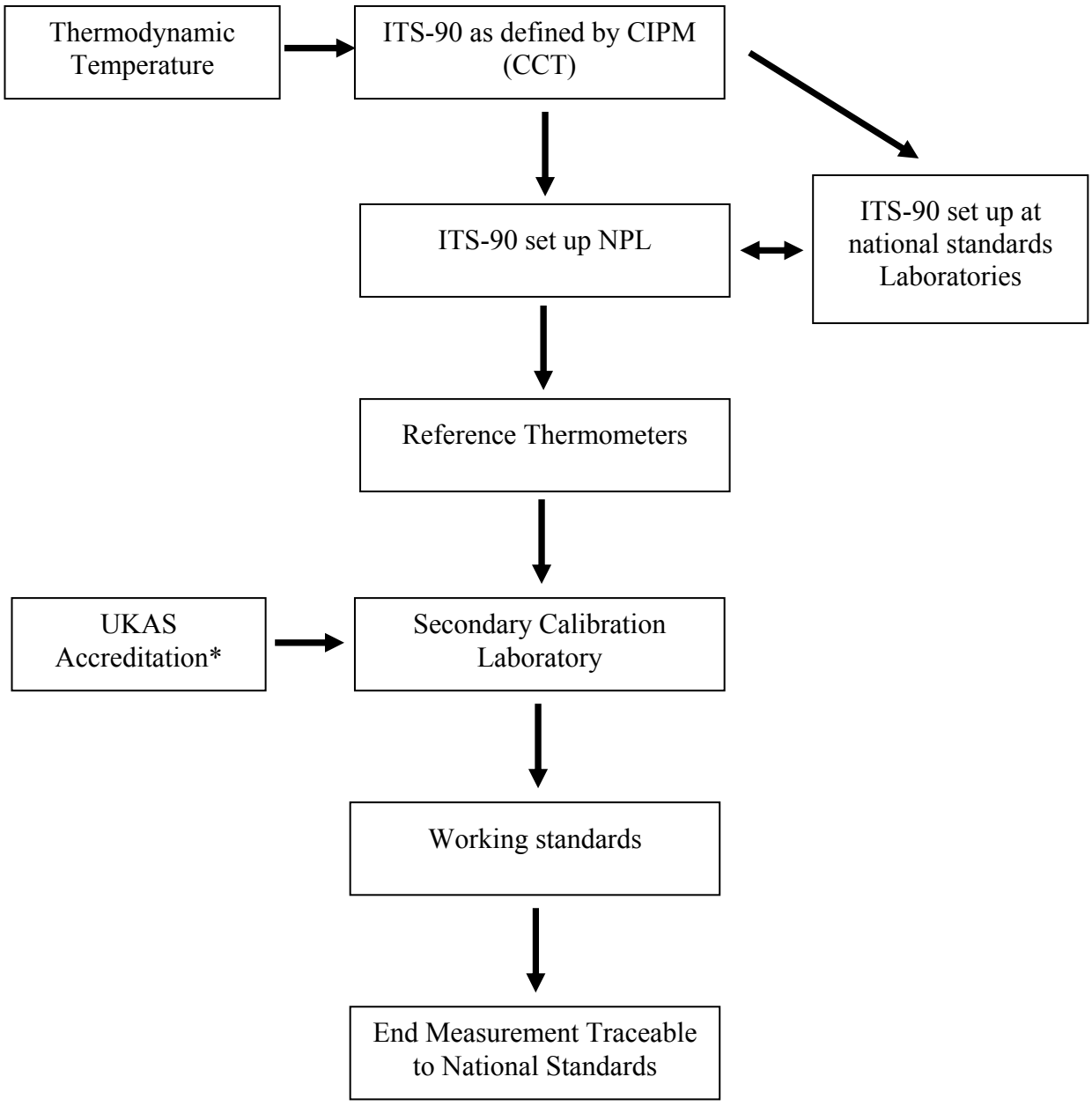

* UKAS Accreditation = the UK accreditation is managed by the United Kingdom Accreditation Service

Figure 2.9 Chain of traceability in temperature measurement in UK [NPL, 2003h].

Chapter 3

Literature Review

An overview of the previous research to improve the temperature realisation at two types of metallic fixed-points; namely tin (231.928 ^{o}C) and aluminium (660.323 ^{o}C) is presented in this chapter. The study emphasises the influence of trace impurity concentrations on the shapes of the melting, and offsets of freezing, curves of high purity tin, and aluminium fixed-point cells. A better understanding of low-level impurities will provide the benefit of reducing the uncertainty budget of the temperature fixed-point realisation, where impurities are the biggest contribution to the fixed-point temperature uncertainty. This will be revealed for the advantage of the temperature measurement community. Unlike the previous work, which was often carried out by using specially designed equipment, such measurements in this work will be produced by using standard NPL equipment, under standard conditions, as used in most national measurement institutes around the world.

This chapter is separated into three parts. The first part introduces the impurity distribution and segregation behaviour in the solution of substances, which affects the fixed-point temperature. The second part describes the influence of chemical impurities on the uncertainty budgets. The third part investigates the temperature offsets and the shape change as various types of impurities affected the "pure" tin and aluminium fixed points.

3.1 The Influence of Impurities on the Fixed-Point Temperature

For the metallic fixed points in the definition of the International Temperature Scale of 1990 (ITS-90), the temperature realisations are measured from the solid-liquid phase transitions (freezing, melting, or triple points). In spite of the fact that the temperature realisation is based on the behaviour of the highest purity substances available, trace impurities always exist in the pure metal. Working Group 1 of the Consultative Committee for Thermometry has made recommendations about how to estimate uncertainties due to impurities, based on the information available [Ripple *et al.*, 2005]. Where the information is lacking or the analysis is incomplete, they recommend that the nominal purity, e.g. 'six nines' (99.9999%) or 1 ppm impurity, is

used to estimate the standard uncertainty. They also calculate the effect of a total of 1 ppm of impurity on the freezing point temperatures, assuming that Raoult's law is obeyed.

In general, the pre-existing trace impurities in the sample cause a change (depression or elevation) to the 100% pure metal phase transition curve at the fixed-point temperature. This temperature deviation makes the uncertainty of the fixed-point temperature realisation difficult to estimate. Uncertainty budgets of fixed points realised according to ITS-90 are influenced by many factors such as chemical impurities and isotopic effect, hydrostatic head correction, error in gas pressure, etc. One of the most important contributions to the uncertainty is the chemical impurities effect. Impurity elements, at the level of parts per million, in the metals at nominally six nines purity level is already enough to generate a major contribution to the overall uncertainty of the temperature realised. Due to such strong effect, the analysis of the content of impurities and their effects on the temperature fixed-point is essential so that a corresponding correction can later be applied. This will lead to a reduction of the uncertainty budgets and eventually benefit the temperature metrology overall as more precise measurement can be attained.

Consider the presence of trace impurities in the metal fixed-point: these solutions act like a binary solute-solvent system. In order to evaluate the quantity of phase transition temperature departure from the high purity fixed-point curves due to the impurity effect, the influence of the solute concentrations (impurities) on the base metal solvents must be analysed. This influence is explained by using the basic behaviour of the crystallisation of the dilute solutions, which also determines the shape of the curves. Furthermore, the segregation of the solute in the solution during the freezing and melting, which can be likened to "*Zone Refining*", will be provided. The effects of impurity on the initial temperature have traditionally been approached by following Raoult's law [Fellmuth, 2003]. It can be formulated to show the change of temperature (ΔT) of the 100% pure fixed-point material (T_{pure}) and the observed sample temperatures (T_{obs}), using the following equation [Fellmuth, 2003]:

$$\Delta T = T_{pure} - T_{obs} = c_l / A \tag{3.1}$$

where c_l is the mole fraction impurity concentration in the liquid, the subscript is '*l*' for 'liquid' and A is the first cryoscopic constant. A is specified as:

$$A = \frac{L}{R \cdot T^2} \tag{3.2}$$

where L is the heat fusion of the fixed-point material, R is the gas constant and T is the melting temperature of the pure fixed-point substance. The first cryoscopic constants and the latent heats of fusion for the fixed-point materials specified in the ITS-90 are expressed in Table 3.1.

Table 3.1 First cryoscopic constants (A) and latent heat of fusion (L) of the ITS-90 defining fixed-point materials [Ripple *et al.*, 2005].

Substance	T_{90} (K)	L (KJ/mol)	$A\,(K^{-1})$	Purity for $T_{pure} - T_{obs}(F=1) \le 0.5\,\text{mK}$
e-H_2	13.8033	0.117	0.0739	99.996
Ne	24.5561	0.335	0.0668	99.997
O_2	54.3584	0.444	0.0181	99.9991
Ar	83.8058	1.188	0.0203	99.9990
Hg	234.3156	2.292	0.00502	99.9997
H_2O	273.16	6.008	0.00968	99.9995
Ga	302.9146	5.585	0.00732	99.9996
In	429.7485	3.264	0.00213	99.99989
Sn	505.078	6.987	0.00329	99.9998
Zn	692.677	7.385	0.00185	99.99991
Al	933.473	10.79	0.00149	99.99993
Ag	1234.93	11.3	0.000891	99.99996
Au	1337.33	12.364	0.000831	99.99996
Cu	1357.77	13.14	0.000857	99.99996

However, equation (3.1), representing Raoult's law, is only valid when all impurities are insoluble in the solid phase of the host material. In this case the impurity concentration c_l is inversely proportional to the fraction F of the sample which is liquid and in equilibrium with the pure solid phase. That is to say

$$c_l = c_{l1} / F \tag{3.3}$$

where c_{l1} is the overall impurity concentration when the material is completely melted ($F = 1$), F is the fraction of sample melted.

Corresponding to equation (3.1), the temperature difference is given by the expression

$$\Delta T(F) = T_{pure} - T_{obs}(F) = \frac{c_{l1}}{F \cdot A} \tag{3.4}$$

Basically, Raoult's law works for ideal mixtures of two liquids [Clark, 2005]. For the mixing solution, when solute is added to the solvent then almost always the freezing point of the solution is decreased from the pure solvent. As stated in the ideal solution law, the decrease of freezing point occurred because of the different sizes of the crystal lattice between the solute and solvent particles. That is, the solute particles that fundamentally remain in solution prohibit other solvent particles from crystallising during the freezing process. Thus, in the ideal case the solution in the solid state, after the freezing process, is almost pure solvent.

Nevertheless, the approach based on Raoult's law applies only for all impurities that are insoluble in the solid state of the fixed-point material, as several reports in recent years [Fellmuth, 2003; Ripple *et al.*, 2005; Fellmuth and Hill, 2006]. If this ideal law is used in the case that the impurities are still in the liquid solution when the solution freezes, it presumes that there are no concentration gradients in the liquid as the slow freeze process occurs. The shift in the freezing temperature of the solution relative to the freezing temperature of the pure substance (ΔT), is estimated directly using equation (3.4). Furthermore, the effect of the total impurity concentration (c_{l1}) is proportional to the factor ($1/F$). At the 100% fraction of sample melted or liquidus point (F = 1), the depression of the freezing temperature caused by

the impurities is shown approximately as: $\Delta T = c_{l1} / A$. This is not reliable and valid for most of the fixed-point substances used in the ITS-90. This is because there is some solubility of impurities in the solid state. Therefore, the use of Raoult's law could lead to the errors.

For the impurities which are soluble in the solid state, the basic facts of crystallography phase diagram and the segregation of impurities in the freezing process is considered. First of all, "zone refining" is used to explain impurity segregation and the fixed-point temperature change. In fact, deliberate zone refining is a technique used to control the soluble impurities distribution in any solute-solvent systems including metals, alloys, semiconductors, and other materials [Pfann, 1958a]. The significant object of zone refining is to prepare high purity materials by use of zone melting methods. It aims to decrease the level of impurities in materials, which is a purification process. The movement of the impurities distribution in the solution depends on the effect they have on the melting point of the pure solvent substances. They move along the zone when impurities increase the melting point of the solvent substances and to the opposite direction when they decrease, which was reported in 1958 by Pfann [1958b]. The impurities are more concentrated at one side, or one end of the substances, after such operations, thereby purifying the other end. From the reason previously mentioned, it can be applied to concentrate required impurities as well as to remove unrequired ones. Furthermore, zone refining technique can be applied, in conjunction with conventional methods, as a particular analytical device to detect unknown or unobservable impurities in the substances.

An essential parameter of the material, which describes the zone refining procedure, is the equilibrium distribution coefficient, designated k_0 [Pfann, 1958c]. It is defined as the ratio of impurity concentrations in solid and liquid equilibrium phases of the solutions, which is given by the relation

$$k_0 = \frac{c_s}{c_l} \tag{3.5}$$

In equation (3.5), c_s and c_l are the mole fraction concentration of impurity in the solid and liquid equilibrium phases of the sample, respectively. Values of k_0 can

be either smaller or larger than unity, and their significance can be explained from the phase diagram of a binary system as shown in Figure 3.1 [Fellmuth, 2001]. The value of k_0 virtually designates the solubility or the segregation of the impurity in the solid and liquid phases of the solvent material. Also, it is a characteristic of a particular impurity.

Consider Figure 3.1(a), the k_0 value is smaller than 1 ($k_0 < 1$). It shows the melting point of the solvent, which is decreased due to the effect of the solute. At temperatures above the upper curve (liquidus), the entire solution is completely melted. Therefore, the solute concentration contained in the solution is in the liquid phase (c_l). When the temperature is slowly reduced to the liquidus temperature (T), the freezing process of the solution starts. The atoms of solvent in liquid phase, such as melted metal, will come together at nucleation points and start to form crystals, which separate out from the solute. The rejected solute will be concentrated in the liquid just ahead of the advancing solid front. However, the crystals of solvent still contain the solute concentration in the solid phase (c_s). At the c_s point on the phase diagram in Figure 3.1(a), it is at the intersection point of the temperature horizontal and the lower curve (solidus), where $c_s = k_0 c_l$. This relationship remains valid when the solution is under equilibrium freezing. As freezing continues, the concentrations in the liquid and freezing solid constantly increase, following the solidus and liquidus lines until the whole sample is frozen. Of course, both c_l and c_s vary during the freeze, but the relationship $c_s = k_0 c_l$ always applies at the interface. If the impurities diffuse in the solid phase (so the concentration is uniform in the shaded part of Figure 3.2), i.e. the whole solid (not just new solid) is always on the solidus line, and the freezing is complete when the solidus line reaches the initial value of c_l (because that is the overall concentration of the sample). In fact diffusion is too slow and the solid supports a concentration gradient (starting from the initial low value of c_s) and freezing is not complete until some point further down the solidus line (lower temperature, higher concentration) to accommodate all the impurities.

Given the distribution coefficient k_0>1 as shown in the system of Figure 3.1(b), the melting point temperature of the mixture solution is higher than the pure

solvent resulting from the solute concentrations. The solidification procedure is the same as Figure 3.1(a), but both the slopes of solidus and liquidus are upward. The end of the freezing process will be reached when the solute concentration is c_l/k_0. Again, if diffusion is too slow, the freezing range is wider.

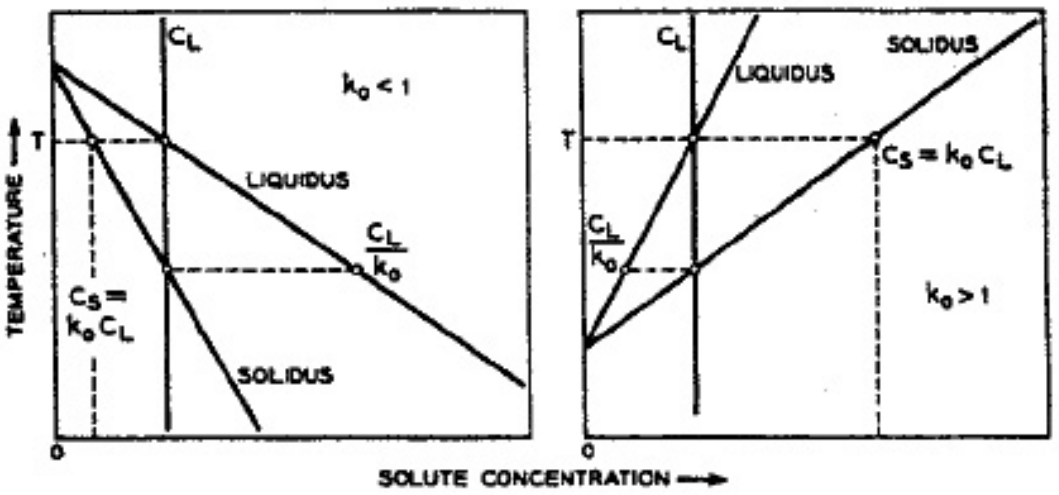

(a) **(b)**

Figure 3.1 Parts of phase diagrams in which the freezing point and melting point of the pure solvent is (a) lowered (k_0 < 1), (b) raised (k_0 > 1), by the solute [Fellmuth, 2001].

Additionally, the solution solidification processes, which are referred to as normal freezing operations, can be described schematically as in Figure 3.2 [Pfann, 1958d]. This method is usually used for preparing monocrystals, which is mentioned by Gilman [1963]. It leads to segregation along the solid sample, which is called "normal segregation". The impurity is commonly (for k_0 < 1) accumulated in the last-to-freeze region of the substance. The impurities are re-distributed or segregated since the atoms at the liquid-solid interface prefer the liquid phase to the solid phase. Besides the value of k_0, another important factor affecting the impurity distribution in the solution during freezing is the experimental conditions, especially the freezing rates and the degree of mixing in the liquid [Pfann, 1958e]. The freezing rate affecting the coefficient has been reported by Thurmond [1959]; that is, the effective distribution coefficient value would fall with an increasing freezing rate.

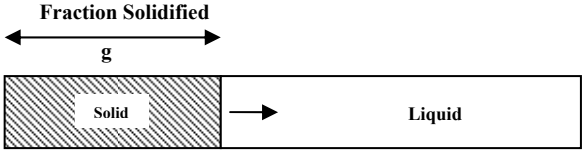

Figure 3.2 Schematic representation of normal freezing [Pfann, 1958d].

Different conditions of a normal freezing process affect the impurity segregation. The crystallographic behaviour of impurities under various experimental conditions is reviewed. There are four distinguishable conditions to the degree of impurity segregation when solid solutions of a fixed-point substance and its impurities are produced (solid solution/liquid solution) as explained in Figure 3.3 [Gilman**,** 1963].

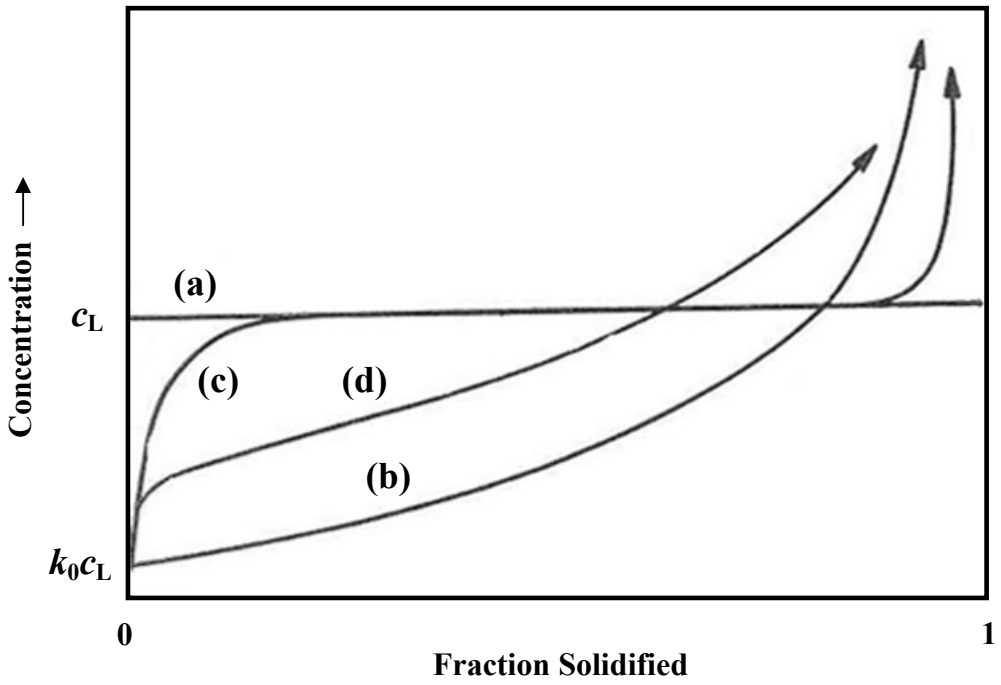

Figure 3.3 Four distinct conditions of solute distributions in a solid frozen from liquid of the initial concentration c_L [Gilman**,** 1963]. (a) equilibrium freezing, (b) complete mixing, (c) no mixing, and (d) partial mixing.

These conditions can exist in dependence on the impurity distribution in the liquid as Pfann and document CCT/99-11 reported [Pfann, 1958; Mangum *et al.*, 2000]. Four conditions of segregation are as follows:

1. Equilibrium freezing
2. Complete equilibrium mixing in the liquid
3. Partial mixing in the liquid
4. No mixing in the liquid

The impurity segregation, which has an influence on the freezing curves in the case of these four conditions, is described in more detail.

1. Equilibrium freezing

It has been explained by Gilman [1963] that *"equilibrium freezing"* exists if the temperature and the concentration gradients are infinitesimal or insignificant. It is because diffusion processes in the liquid and solid of the sample are completed. This case occurs when the rate of freezing of the sample is extremely slow, slow enough to eliminate all concentration gradients. Therefore, there is no segregation in this case. However, in practice, diffusion rates in the solid phase would have to be very slow, which is almost impossible, thus, the reason the theory rarely applies in the real world.

2. Complete equilibrium mixing in the liquid

For this condition, as illustrated by Gilman and in document CCT/99-11 [Gilman**,** 1963; Mangum *et al.*, 2000], the rate of freezing needs to be slow, i.e. sufficiently slow to allow complete and uniform mixing in the liquid. The convection can prevail over the tendency for impurity concentration gradients to diffuse in the liquid phase. At the same time, the freezing rate has to be fast enough to produce negligible diffusion in the solid. As a result of convection and diffusion effects, all concentration gradients are erased. This leads to the highest possible degree of impurity segregation. Dependence of the observed liquidus temperature (T_{obs}) on the liquid fraction F of the sample is given by equation 3.6 below [Mangum *et al.*, 2000];

$$T_{pure} - T_{obs} = -\sum_i c_{11}^i (\partial T_1 / \partial c_1^i) / F^{1-k_0^i} \qquad (3.6)$$

Where c_{11}^i is the total concentration of the impurity *i* at the liquidus point, c_1^i is the mole fraction concentration of the impurity *i* in the liquid equilibrium phase, k_0^i is

the equilibrium distribution coefficient of impurity *i* and $\partial T_1 / \partial c_1^i$ is the derivative m_1^i of the liquidus temperature line (T_1) with regard to the concentration of impurity *i* in the phase diagram. The derivative m_1^i is expressed from the following relation:

$$m_1^i = \partial T_1 / \partial c_1^i = -(1 - k_0^i) / A \tag{3.7}$$

This equation (3.7) is applied at low impurity concentrations [Mangum *et al.*, 2000]. If it has no solid solution ($c_s = 0$ in the solid phase i.e. $k_0^i = 0$), the equation (3.4) is used to estimate for all impurities, with ΔT dependent on $1/F$. However, if $k_0 \neq 0$ that means the solid solutions are formed and therefore the impurity concentrations in the liquid/solid interface are not homogeneous. This is the reason for the impurity concentration to change as freezing occurs. It yields a more complex dependence on the temperature difference or ΔT versus F.

Considering at $k_0^i = 1$, the observed temperature does not depend on the liquid fraction F of the sample. Furthermore, it has no segregation in the solution and ΔT is constant. Therefore, the impurity effect cannot be determined by defining the melting or freezing curves for this condition. The relationship between ΔT and $1/F$, which is affected from equation (3.6) at various $k^i{}_0$ values are shown in Figure 3.4.

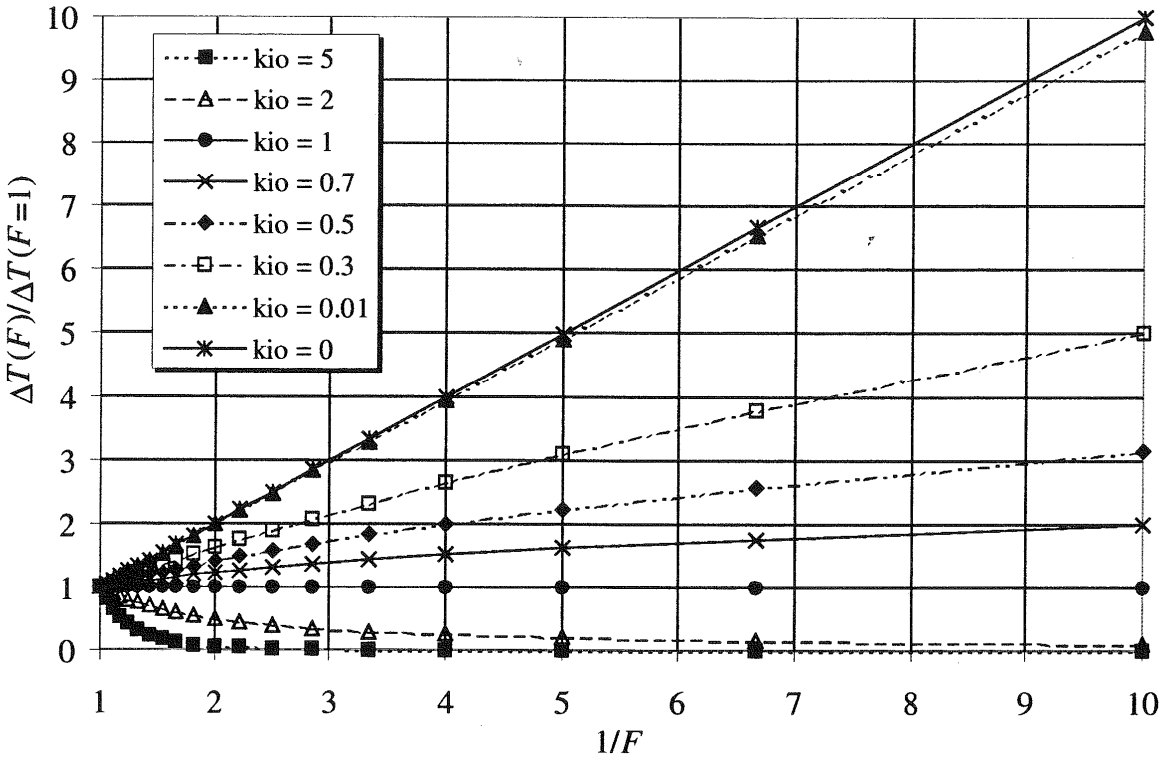

Figure 3.4 Relationship between $\Delta T(F)/\Delta T(F=1) = (T_{pure} - T_{obs}(F))/(T_{pure} - T_{obs}(F=1))$ and $1/F$ range from for the complete mixing in the liquid resulting from equation (3.6) for different k_0^i values [Mangum *et al.*, 2000].

For k_0^i>1, ΔT has a negative value and its absolute value becomes less as freezing increases. For this situation, the value of T_{obs} clearly deviates from T_{pure} when $1/F$ gets close to 1, which is at small liquid fraction of the sample. For k_0^i<1, the temperature difference ΔT is the positive and the line gradually rises as more and more increased solid fraction of the sample.

In Figure 3.4, an application of Raoult's law as expressed in equation (3.4) is considered to estimate the influence of impurities on T_{obs}. Raoult's law is valid if k_0^i = 0 (no impurities in the solid phase) at the liquidus point ($F = 1$). Therefore, if $k_0^i \neq 0$, then the application of Raoult's law to estimate the freezing temperature change caused by impurities is not valid. For the case when impurities are soluble in the solid phase (k_0^i > 0.01), the curves of the relationship between ΔT and $1/F$ are not straight lines and hence the application of Raoult's law cannot estimate and determine the

influence of impurities on T_{obs}. For an example for this under-reckoning as described in document CCT/99-11 [Mangum *et al.*, 2000] is specified: "For instance, the influence is underestimated by a factor of nearly 5 if equation (4) is used to approximate $\Delta T(F)/\Delta T(F=1)$ versus $1/F$ in the $1/F$ range from 1.1 ($F=0.9$) to 10 ($F=0.1$) for impurities having an equilibrium distribution coefficient k_0^i of 0.5.". (In CCT/99-11, equation (4) refers to Raoult's law, which is equation (3.4) in this Chapter).

The errors resulting from a misapplication of Raoult's law are clarified in Document CCT/03-12 [Fellmuth, 2003]. It is described in Figure 3.5. This is the simple case, which is considered at one dominant impurity *i*. From equation (3.6), the temperature change of the freezing curve at the liquidus point ($F=1$) is expressed by the relation

$$\Delta T_{liquidus} = \Delta T_{obs}(F=1) = -c_{11}^i m_1^i \tag{3.8}$$

Equation 3.8 would be the slope of the freezing curve, corresponded as the relationship between $-T_{obs}$ and $1/F$ if Raoult's law is valid ($k_0^i = 0$).

The misapplication of Raoult's law to calculate the freezing curve i.e. applied when $k_0^i \neq 0$ will lead to an inaccurate estimation of change in the freezing temperature. The estimation will be lower than the actual temperature value.

The misapplication of Raoult's law is given as the procedure of which a straight line is fitted to the freezing curve $T_{obs}(1/F)$ by choosing two different F ranges (represented by F_1 and F_2, respectively). Fellmuth [2003] has reported that we can estimate the freezing curve from the slope of this straight line, which is given by $c_{11}^i m_1^i (1/F_1^{1-k_0^i} - 1/F_2^{1-k_0^i})/(1/F_1 - 1/F_2)$. This slope line will give the inaccurate estimate (ΔT_{wrong}) when the slope of the freezing curve is considered at $k_0^i = 0$. Therefore, $\Delta T_{liquidus}$ (as referred in equation 3.8) is underestimated by the factor

$$E_R = \Delta T_{liquidus}/\Delta T_{wrong} = (1/F_1 - 1/F_2)/(1/F_1^{1-k_0^i} - 1/F_2^{1-k_0^i}) \tag{3.9}$$

In Figure 3.5, the factor E_R depends on the distribution coefficient k_0 in two selected F ranges ($F_1 = 0.1, F_2 = 0.9$ and $F_1 = 0.5, F_2 = 0.9$, respectively). The freezing curve estimations normally use the closer range because different effects may alter in their shape at lower F values. The factor E_R of the estimated change in the liquidus temperature can be applied by Raoult's law when the distribution coefficient is very small ($k_0^i << 1$), i.e. it approaches 1. At k_0^i=0.5, the factor E_R is increased to about 2.5. However, the value of E_R becomes very large when k_0^i comes near one, for example $E_R \approx 15$ for $k_0^i = 0.9$ and $F_1 = 0.5, F_2 = 0.9$.

Fellmuth [2003] also reviewed that the evaluation of the freezing curves cannot determine the effect of impurities at $k_0^i \approx 1$. Considering $k_0^i > 1$, the application of Raoult's law will give an incorrect direction for the liquidus temperature change in spite of the temperature is increased compared with T_{pure}. The factor E_R value shows the negative number as seen in Figure 3.5 (two lower lines). Moreover, at F = 0 (completely solid phase), the difference $T_{pure} - T_{obs}$ has its smallest absolute value. The reason for the wrong direction of the factor E_R is described by Fellmuth and Hill [2006], which it is specified: "Impurities with $k_0^i > 1$ are especially troublesome because their influence can reduce the apparent width of the freezing curve compared with that which would result from the remainder impurities (with $k_0^i < 1$) in their absence."

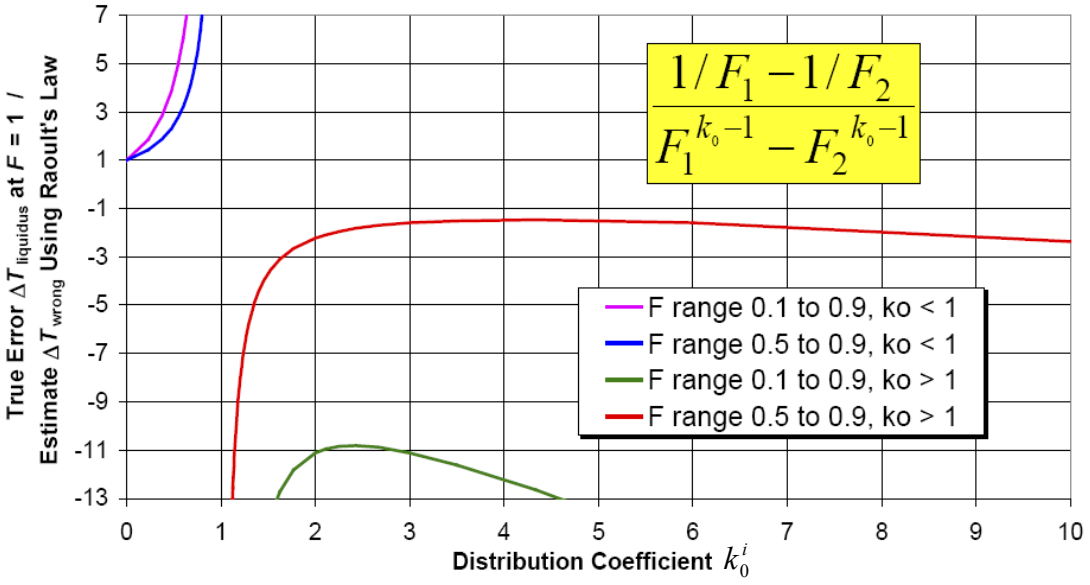

Figure 3.5 Relationship between distribution coefficient k_0^i and the underestimate factor of the influence of impurities when Raoult's law is inappropriately used [Fellmuth, 2003].

3. Partial mixing in the liquid

In document CCT/99-11 [Mangum *et al.*, 2000], diffusion and convection are two effects resulting in the movement of impurities in the liquid phase. This condition causes intermediate segregation [Gilman**,** 1963]. The freezing conditions mainly affect the segregation of impurities. It is controlled by an effective distribution coefficient k_{eff}^i [Brice, 1965; Fellmuth, 2001]. The definition of the k_{eff}^i value is the ratio of the solute concentration in the solid to that in the bulk liquid. This is illustrated by the information obtained by Brice [1965]. The value of k_{eff}^i is given by

$$k_{eff}^i = c_s^i / c_{1\infty}^i = k_0^i / (k_0^i + (1 - k_0^i) \exp(-\nu \delta_c / D^i)) \qquad (3.9)$$

Where δ_c is the thickness of the boundary layer in the freezing direction, $c_{1\infty}^i$ is the impurity concentration i outside the layer, υ is the velocity of the interface and D^i is the diffusion coefficient in the liquid metal. As equation (3.9), the k_{eff}^i value depends on a function of the layer thickness and it can be determined by considering the velocity of solute at the growing interface.

There are two limiting cases for applying equation (3.9), which are as follows;

1. If $v\delta_c / D^i << 1$, the condition becomes complete mixing case due to the growth-freezing rate is very small: $k^i_{eff} = k^i_0$

2. If $v\delta_c / D^i >> 1$, the condition becomes no mixing, which will be explained in the following section, as the velocity of distribution in the liquid/solid interface is high, and accordingly, the k^i_{eff} value comes close to 1.

The accumulated impurity concentration exists just ahead of the advancing solid-liquid interface or the diffusion boundary layer. k^i_{eff} has a value in the range that of the limits $k^i_0 \le k^i_{eff} \le 1$. A significant condition for the impurities analysis in the partial mixing case, the k^i_{eff} value has closely the same as the k^i_0 value. The partial mixing is the usual case in practice [Gilman**,** 1963].

4. No mixing in the liquid

In this condition, only liquid diffusion produces an effect on the distribution of impurity at the solid/liquid interface. It results from a rapid freezing rate. Consequently, diffusion is not strong enough to mix the impurities through the whole of the liquid during the typical time of a temperature fixed-point realisation. Then only slight segregation will occur which is frequently realised in practice [Gilman**,** 1963]. The segregation will reduce when the freezing process increases. Consider progressive freezing, the amount of solute concentration in the liquid (c_l) in the boundary layer is dependent on the value of k_0. If the impurities are rejected by the freezing solid ($k_0 < 1$), then c_l increases. On the other hand, c_l decreases as the amount of the accumulated impurities ($k_0 > 1$). The solute concentration in the boundary layer continually increases until the concentration of impurities in the liquid will be c^i_{11}/k^i_0 and the impurity concentration segregation of freezing into the solid is c^i_{11}. It is under the steady state conditions. As a result, there is no further impurities segregation and the influence of impurities analysis cannot be determined from the freezing or melting curves. In the case of no mixing in the liquid can be described by the equation, which is given by Tiller *et al.* [1953]. This equation shows the impurity distribution in the solid that is written as

$$c_s^i = c_{11}^i (1 - (1 - k_0^i) \exp(-k_0^i \upsilon x / D^i)) \quad (3.10)$$

where x is the distance of the liquid-solid interface from the location where freezing started.

From four different conditions of segregation, it can be concluded that the impurity effects are efficiently analysed if the mixing in the liquid is complete. As already explained above, it is because the maximum possible segregation in the solution, which is provided by equation (3.6).

There are usually several impurity components in the metal fixed-points, even through materials of high purity (99.9999%) are used. Accordingly, there can be different equilibrium distribution coefficient (k_0^i) values in a substance as seen in Figure 3.6. The k_0^i value not only impacts on the temperature change of observed freezing curves, but also the shapes of curves. The shapes of the curves containing the concentration of impurities are mainly controlled under the different experimental conditions, particularly the freezing rate, or the time length in the liquid state before freezing process [Mangum *et al.*, 2000]. The variations in the impurity segregation occur in slowly and rapidly frozen metals affects the shape of the subsequent melting curve in the fixed-point cell [Ancsin, 2007; Nicholas and White, 2001i]. Bongiovanni *et al*. [1975] reported that the oxygen content, which dissolved in the silver fixed-point, might affect the shape change of the silver-melting curve.

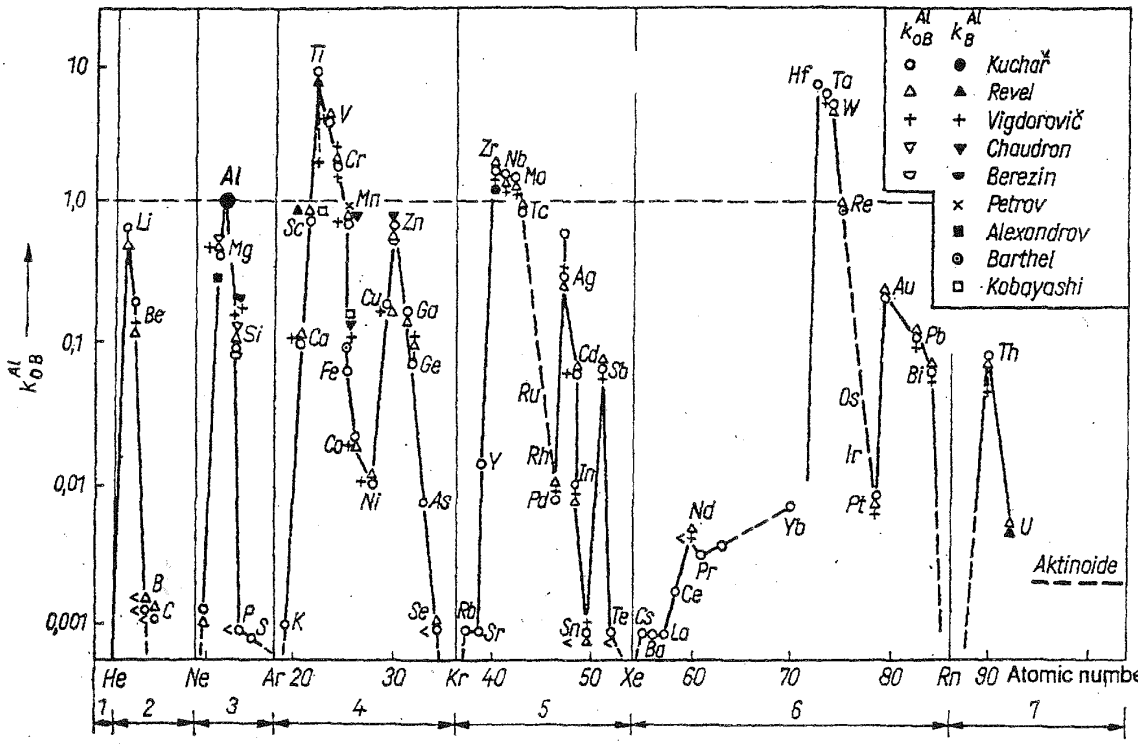

Figure 3.6 Periodic dependence of equilibrium distribution coefficients k_0^i on the atomic number of the solutes B in Al [Fellmuth, 2001].

An example of the fixed-point Al material as illustrated in 3.6 shows the equilibrium distribution coefficient of solutes (impurities), which remain in pure aluminium fixed point (one of fixed point materials of interest). It indicates that the majority of impurities have $k_0^i < 1$ causing a decrease in the temperature of the freezing curve of this Al. This is the generally happening case for realising the metal fixed-point materials.

It can be briefly summarised that the behaviour of impurities at low concentrations in the host material may result in the change of the freezing temperature, although the metals, which are used to realise the fixed point temperatures, are normally produced from very high purity grade metal. The freezing process based on the elemental physics enables to comprehend the impurity behaviour on the freezing and melting curves. The freezing process is not able to reliably estimate temperature changes or to investigate the amount of the impurity concentrations. Therefore, more reliable methods are needed as tools to estimate the uncertainty in the correction for the effect of impurities applied to metal fixed-point materials. These methods will be mentioned in more detail in the next section.

3.2 Methods for Evaluation of Uncertainty Budgets and Correction of Fixed-Point Temperatures ascribable to the Influence of the Chemical Impurities

Accurate temperature measurement relies on accurate measurement techniques and high stability temperature equipment, and also an evaluation of the uncertainty. The uncertainty assessment generally comprises many components, which are grouped into two categories, namely type A and type B, according to the method used to estimate the numerical value. Type A is calculated by statistical means and type B is evaluated by all other means (e.g. Hydrostatic-head correction, Bridge-measurement errors, Self-heating of the SPRT errors and Standard resistor etc). The impurity effect is one of components in the standard uncertainty of type B.

As presented in the reported CCT Key Comparisons (CCT-K3 and CCT-K4) [Mangum *et al.*, 2002; Nubbemeyer *et al.*, 2002], one of the agreements is the evaluation of uncertainties and the correction of the fixed-point temperatures that are resulted from chemical impurity effects. The accurate realisation of the temperature, which plays an important role in the provision and dissemination of standard temperature values in the definition of the ITS-90, strongly depends on the purity level of the material used. It has been already reviewed on the previous section that the impurities remaining in the high purity fixed-point materials cause the temperature shifts and the shapes of melting and freezing curves during phase transformation.

An improved understanding of the effects of low-level impurities would allow one to reduce the magnitude of the “impurity” component, which is a significant part of the budget. It is supported by Rudtsch that the impurity effect is the biggest contribution to the uncertainty budgets of the temperature realisation [Rudtsch *et al.*, 2008]. The uncertainty of the best fixed-point realisations for the fixed-point materials is importantly affected by the natural variability of impurities of the available samples. If the impurities content and their specific effects of the pure fixed-point metals are identified, the correction temperature of metal fixed-point could be more precise and reliable.

Therefore, the evaluation of uncertainties attributed to chemical impurity effects in a variety of approaches and the fixed-point temperature correction are revealed in this section.

Uncertainties of the temperature measurements, as mentioned in Chapter 2, are used to estimate for the achievement of high-accuracy temperature measurements. At the present time, the uncertainty procedure of measurement for chemical analyses is published by the International Organization for Standardization (ISO) in the "Guide to the Expression of Uncertainty in Measurement", which referred as GUM [ISO/IEC Guide 98, 1995]. The influence of impurities on the fixed-point temperature is one of the main important component uncertainties. The uncertainty budgets of the temperature realisation can be reduced if this component can be estimated very carefully considering the base crystallographic behaviour as previous mentioned.

The component uncertainties of the temperature realisation attributable to the impurity effect can be estimated from three different significant methods. These methods are discussed in CCT/01-02 and CCT/05-08 document reports [Fellmuth, 2001; Ripple *et al.*, 2005]. Their methods comprise the "Sum of Individual Estimates" (SIE), the "Overall Maximum Estimate" (OME) and the "Estimate based on Representative Comparisons" (ERC). Additionally, the combined SIE/OME method will be provided.

3.2.1 Sum of Individual Estimates (SIE)

This method is applied to estimate the uncertainty component and the temperature change correction when the concentrations of all impurities are determined and also the knowledge of the concentration dependence of the fixed-point temperature for the different impurities is revealed. The suitable analytical techniques are used to detect the impurities inside the "pure" metal fixed-point ingot. For instance, the Glow Discharge Mass Spectrometer (GD-MS) is the most comprehensive and sensitive technique available for the analysis of solids, which is used to detect the impurities element. Therefore, the change of freezing temperature at the liquidus point, which is corrected for the influence of impurities as the SIE method, can be evaluated from the equation 3.11 as follows [Ripple *et al.*, 2005]:

$$\Delta T_{SIE} = T_{pure} - T_{liquidus} = -\sum_i c_{11}^i m_1^i = -\sum_i c_{11}^i (\partial T_1 / \partial c_1^i) \qquad (3.11)$$

where c_{11}^i is the concentration of the impurity *i* at liquidus point and m_1^i is the first derivative, which is explained in the equation 3.7.

The uncertainty of the ΔT_{SIE} estimation, which is calculated from the uncertainties of the chemical analysis results $u(c_{11}^i)$ and the concentration dependences $u(m_1^i)$, is given by the relation [Ripple *et al.*, 2005]:

$$u^2(\Delta T_{SIE}) = \sum_i [u(c_{11}^i) m_1^i]^2 + [c_{11}^i u(m_1^i)]^2 \tag{3.12}$$

Therefore, the SIE method is used to estimate of the uncertainty from all relevant impurities concentrations, whereupon the fixed-point temperatures are corrected for the influence of impurities. However, if the metal material is less pure than 99.999% then the use the SIE method may not be suitable for estimation the uncertainty due to "the assumptions of independent influence appropriate to the dilute limit may no longer apply" [Ripple *et al.*, 2005].

3.2.2 Overall Maximum Estimate (OME)

The OME method can be applied for the uncertainty estimation if the individual impurity concentrations or their effect on the liquidus temperature are not determined. The expected temperature change at liquidus point is estimated by [Fellmuth and Hill, 2006; White *et al.*, 2007]

$$\left| T_{liq} - T_{pure} \right| < \Delta T_{OME,\max} = c_{11} / A \tag{3.13}$$

This temperature estimation is based on equation (3.4). From equation 3.13, the estimation for the bound of the impurity effect yields from the overall impurity content and the first cryoscopic constant. The uncertainty estimation as the OME method is written as [Fellmuth and Hill, 2006; White *et al.*, 2007]

$$u^2(\Delta T_{OME}) = [\Delta T_{OME}]^2 / 3 = [c_{11} / A]^2 / 3 \tag{3.14}$$

However, the uncertainty of the OME method, $u(\Delta T_{OME})$, is usually larger than other estimates. It provides a maximum estimate provided that the overall impurity content is estimated reliably, because impurities having high equilibrium distribution coefficients are very efficiently removed by zone refining.

3.2.3 Estimate based on Representative Comparisons (ERC)

The Estimate based on Representative Comparisons (ERC) method is applied if the overall impurity content cannot be estimated reliably. It is a crude estimate, which can be inferred indirectly from the comparison of different fixed-point materials. The valuable data for the application of the ERC method result from the CIPM Key Comparisons in the field of thermometry, (see more details in CCT/01-02 [Fellmuth *et al.*, 2001]). Therefore in the absence of other information, the data for estimate the chemical impurities in the uncertainty budgets type B can be found from 2 types of the uncertainty, i.e. the "normal category of uncertainty" and the PTB uncertainty budgets, as described in document CCT/01-02 [Fellmuth *et al.*, 2001]. The normal category of uncertainty is used as an alternative, which is obtained from the national metrology institutes. CCT/01-02 also gives an example from the PTB uncertainty budgets, belong to the commonly called "best category of uncertainty" [Jung, 1977], i.e. they can be obtained only with considerable effort by a small number of leading workers in the field. The uncertainty budgets, which are composed the individual uncertainty contributions, for the calibration defining fixed-points of the ITS-90 of PTB and the normal category of uncertainty are presented in Appendix B. The influence of impurities is the largest contribution to the uncertainty budgets of temperature fixed points as shown in the uncertainty budgets (Appendix B).

Table 3.2 Data for influence of impurities in the uncertainty budgets type B of the PTB uncertainty budgets and the "normal category of uncertainty" for the calibration of SPRTs at the defining fixed points of the ITS-90 [CCT/01-02]. (Temperature equivalents in mK)

Type B uncertainty components (mK)												
Chemical impurities, isotopes												
Fixed-Point	**e-H_2**	**Ne**	**O_2**	**Ar**	**Hg**	**H_2O**	**Ga**	**In**	**Sn**	**Zn**	**Al**	**Ag**
PTB	0.17	0.16	0.19	0.14	0.06	0.031	0.06	0.25	0.31	0.54	0.40	0.65
Normal Category	0.42	0.20	0.20	0.29	0.25	0.10	0.20	0.78	0.52	0.71	1.50	3.60

All three methods, as mentioned above, can be used to estimate the uncertainty component caused by the change of the liquidus point temperature of the fixed-point sample due to the effect of impurities.

From the information in the CCT/01-02 document report [Fellmuth, 2001], the uncertainty estimation cannot be corrected for the fixed-point temperature with respect to the influence of impurities from Methods 2 and 3. Only Method 1 can be used for that case. However, "Method 1 does not allow calculating corrections because the uncertainty of the analysis results is comparable with the results themselves (this uncertainty may be as large as a factor of three)".

Therefore, Method 4 has been produced for estimate the uncertainty. This method is combined from the first two methods. It is called **"SIE/Modified OME Combined Method".**

3.2.4 SIE/Modified OME Combined Method

Both SIE and OME methods are combined to estimate uncertainty. The application of SIE method is used for the dominant impurities and the OME method is used for the rest of the impurities as demonstrated in the CCT/05-08 document [CCT/05-08, 2005]. If the equilibrium distribution coefficients (k_0^i) of all relevant impurities are comprehended, then it will make a simpler case for estimation by use the modified OME method. The SIE method would be used for only the dominant impurities with $k_0^i < 0.1$. The rest of impurities with $k_0^i \geq 0.1$ are evaluated by applying Raoult's law, which is approached by the OME method [Fellmuth and Hill, 2006]. The uncertainty estimation of SIE/Modified OME Combined Method would be calculated by use of two equations, which combine the result from equation (3.12)-SIE method with that from equation (3.14)-OME method.

All four methods are produced to estimate the uncertainty component of fixed-point temperatures resulting from the influence of impurities. The Sum of Individual Estimates (SIE) method is recommended for estimating the uncertainty after correcting the influence of impurities. However, the chemical analysis of the fixed-point metal needs to be determined and also the information of concentrations and influences of the individual impurities on its fixed-point temperature must be known.

If the information of individual impurities for SIE method is deficient, then the OME method would be an alternative estimate to consider. This method yields a maximum estimate if overall impurity content is dependable with the equilibrium distribution coefficient bigger than two can be removed by zone-refining and disregarded.

The SIE/Modified OME combined method is applied to estimate the uncertainty when the equilibrium distribution coefficients are known. This is approached from the SIE method for only most impurities with $k_0^i < 0.1$ and from the OME method for the influence of impurities with $k_0^i \geq 0.1$.

3.3 The influence of impurities on the metal fixed-point temperatures

The nominally 99.9999% high purity metals are normally sufficiently pure to be used in new fixed-point cells. In 2003, National Institute of Standards and Technology of the United State of America (NIST) reported the minimum purity level (wt%) requirement of each fixed-point material used in the NIST PRT Laboratory for producing the fixed-point cells [Strouse, 2003]. The requirement of each fixed-point is listed in Table 3.3.

Table 3.3 The minimum sample purity requirement of each fixed-point material, which are used by NIST PRT Laboratory in order to make the fixed-point cells as specified in the ITS-90 [Strouse, 2003].

ITS-90 fixed-point sample	Minimum purity, wt %	ITS-90 fixed-point sample	Minimum purity, wt %
Ar	99.9999	Sn	99.9999
Hg	99.999 999	Zn	99.9999
Ga	99.999 995	Al	99.9999
In	99.999 99	Ag	99.9999

However, the best available high purity for the various metal fixed points (e.g. 99.99999% In, 99.99999% Zn, and 99.99995% Al) are produced and expected to make certain that the influence of impurities is not a significant factor for the uncertainty budget [Hill and Rudtsch, 2005].

Although the materials of high purity are produced, the amount of impurities that are present in the materials is still a problem. This is because the low level

concentration of impurities (in terms of part per millions by weight, ppmw) can affect the high purity metal phase transition curve at fixed-point temperatures after various processes of intensive refining. This agrees with the report of Renaot, *et al.*, [2008]. In this report, a new aluminium open cell was fabricated with 99.99995% purity of aluminium, which is the purest available aluminium sample. This sample was determined the chemical analysis by Glow Discharge Mass Spectrometry (GD-MS) technique. The GD-MS result indicated that trace impurity concentrations were still contained in the aluminium sample even though this sample is the best high purity of aluminium at present. Furthermore, increasing the purity of the material would also increase the cost and hence make the project unnecessarily expensive. As shown in the reasons above, the studies of the impurity effects have been interested with small amount of impurity additives into the purity metal fixed points. After correcting the temperature with the influence of impurities, the higher level of the confidence in the uncertainty budget would be produced due to the value of the uncertainty component is reduced by use of the SIE method. This yields the accuracy and the reliability of the realised fixed-point temperature.

The data relating to the effect of all impurities existing in the fixed-point material would be obtained from the phase diagrams of the mixtures of materials. The alloy of two or more component materials is considered to be the base system in order to evaluate the departure of temperatures from the high purity fixed-point curves. The constitution of binary alloys book is one of existing information [Hansen, 1958], which is used to study the phase diagrams. The improved data of the phase diagrams are also available in "the American Society for Metals (ASM) Handbook Volume 3" [Baker *et al.*, 1992], "Binary Alloy Phase Diagrams" [Massalski *et al.*, 1990] and "Handbook of Ternary Alloy Phase Diagrams" [Villars *et al.*, 1995].

First of all, the research of a series of dilute binary alloys would be stated to show the example of the impurity behaviours and their effects in the based materials. In 1963, the base alloys of zinc (Zn) and lead (Pb) were studied with solute additions of silver (Ag), gold (Au), antimony (Sb), thallium (Tl), tin (Sn) and Zn [Weinberg and McLaren, 1963]. Considering in example case of a Zn-Tl system, Tl was chosen for doping due to it has a low distribution coefficient (0.01), which is good to study the solute distribution in the base metal alloy, and also the phase diagram information at the very low Tl concentrations is available [Weinberg and McLaren, 1961]. The

previous phase diagram information of the Zn-Tl alloys would help to predict how much the fixed-point temperature after adding Tl will be changed.

This Zn-Tl alloy system was investigated after using a slow induced freeze technique. This was commenced with the normal slow freeze (< 1 ^{o}C below the equilibrium temperature was set at the furnace) until the initiate solidification (or nucleation) appeared, then the cold rod was inserted into the thermometer well to induce the thin solid mantel from inside of the ingot. From this experimental stage, it was discovered that the influence of induced freeze time significant affected on the shapes of the pure Zn curves, as illustrated in Figure 3.7. The proper selection of the induced time leads to obtain a flatter the freezing curve.

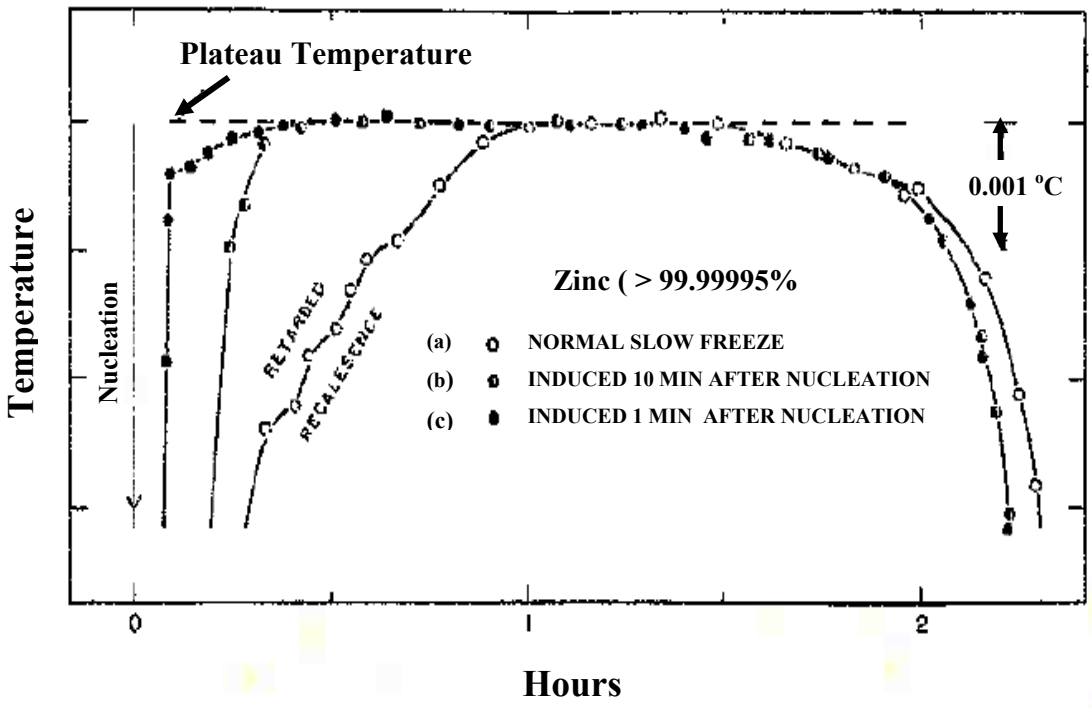

Figure 3.7 Effect of Induced time on the slow freezing curves in high purity Zn [Weinberg and McLaren, 1963].

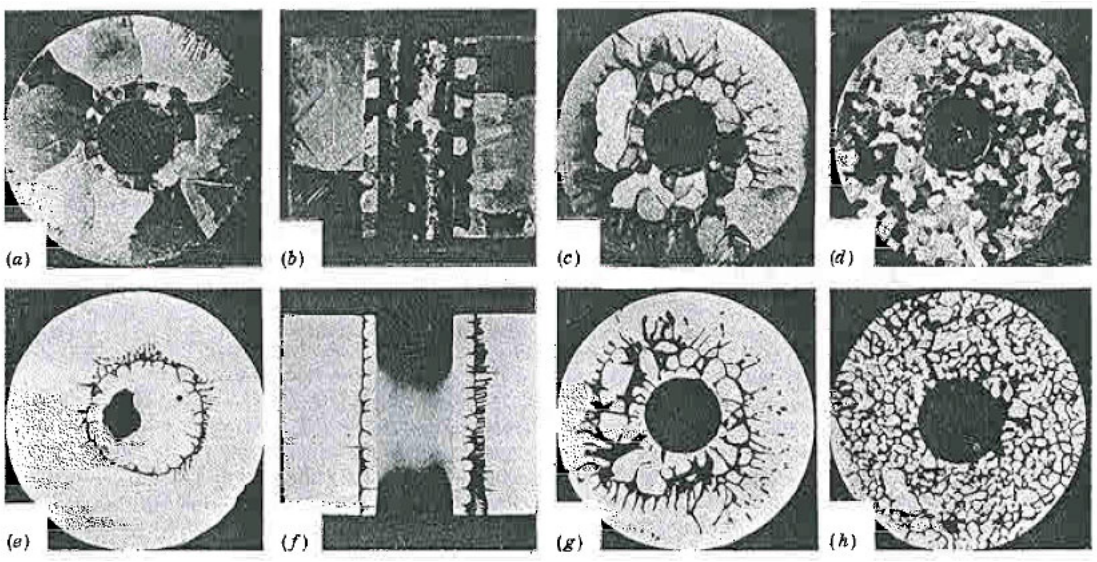

Figure 3.8 Photographs (*a,b,c,d*) and autoradiographs (*e,f,g,h*) of sectioned on the surfaces of Zn-Tl [Weinberg and McLaren, 1963]. (*a*),(*b*),(*e*),(*f*) 8 ppmw of Tl; (*c*), (*g*) 59 ppmw of Tl; and (*d*),(*h*) 567 ppmw of Tl.

The segregations of Tl, as increased the concentrations of 8 ppmw, 59 ppmw and 567 ppmw, respectively), within the pure Zn ingots and the morphology of the solidified ingots were shown via the autoradiograph techniques, as shown in Figure 3.8. The photographs on the surface and autoradiographs of the sectioned parallel and perpendicular of 8 ppmw Tl in Zn ingot were shown in Figure 3.8 (*a*), (*b*), (*e*) and (*f*), respectively. A layer of small grains appear at the middle of the Zn ingot after slow inducing freezing techniques, as seen on both sectioned parallel and perpendicular photographs of the ingot in (*a*) and (*b*). The following grains, which are the main residual grains of the ingot, are rather large. Autoradiographs in (*e*) and (*f*) also indicate the corresponding results, which can see the small gap separating the two different sizes of the grains. Weinberg and McLaren [1963] explained the reason for this evidence is that "all the Tl has pushed into a narrow band separating the large grains from the small grains (i.e. the final portion of the ingot to freeze) either along the grain boundaries or forming a segregation substructure near the boundaries". At 8 ppmw Tl, the micro segregation of Tl only distributes in the centre of the ingot. It does not have any signs to show the micro segregation or the substructure of the additional nucleation in the large grains after solidification started at the outside area of the ingot.

The photograph and autoradiograph of 59 ppmw Tl are shown in Figure 3.8 (*c*) and (*g*) [Weinberg and McLaren, 1963]. The Tl segregation in Zn ingot exhibits the resembling distribution when is compared with 8 ppmw case; that is the most small grains layer is around the middle of the ingot at the grains boundaries. However, the segregation at the further area from the middle has much smaller grains when likened to the large grains of 8 ppmw Tl. It may be because the amount of Tl concentrations is increased in the ingot; therefore the Tl was pushed in more spread area. In addition, the large grains in the outer edge could be observed that it has no solute concentrations. Weinberg and McLaren [1963] also gave the complementary explanation that "some large grains were nucleated in the liquid at the later stage in the freezing process after which the solid-liquid interface could no longer be considered approximately cylindrical. They appear essentially free of solute and are surrounded by a layer of alloy that is high in solute concentration".

The structure of 567 ppmw of Tl in Zn-Tl alloy is shown in Figure 3.8 (*d*) and (*h*). A big number of small grains evenly distribute in the ingot. The most impurity concentrations are at the grain boundaries and just some impurities are in the grains. This indicates the amount of solute (impurity) concentrations is very important to the impurity segregation and distribution in the ingot. Also, in this case, the formation of the solid Zn-Tl alloy in the ingot was conducted by the nucleation and the growth of a large number of crystals process throughout the bulk of the liquid.

Figure 3.9 indicates that the Tl is separated to the area close to the mantle which was the last portion to freeze, which is agreed with their autoradiographs.

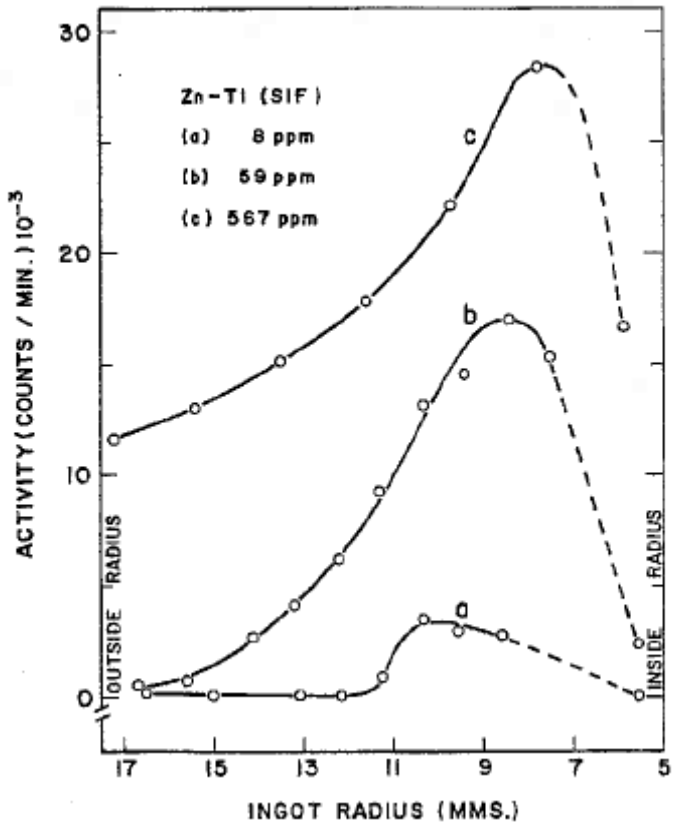

Figure 3.9 Average solute distribution of Zn-Tl alloys as a function of the increased solute concentrations [Weinberg and McLaren, 1963].

Moreover, Weinberg and McLaren's article [1963] displays the effect of freezing rate on the solute distribution in the Zn-Tl system, as shown in Figure 3.10. The fast freeze of Zn-Tl reveals the extensive solute segregation throughout the ingot.

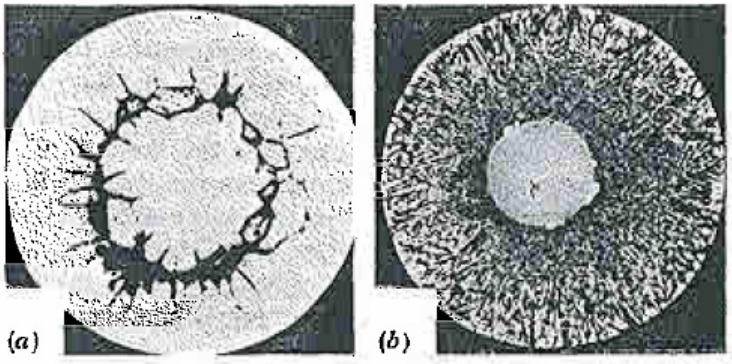

Figure 3.10 Autoradiographs of Zn-Tl alloy, (a) very slow induced freeze (18 hrs) 71 ppm; (b) very rapidly freeze (8 mins) 20 ppm [Weinberg and McLaren, 1963].

Considering at high metal fixed-point temperature, i.e. silver (Ag), six pure Ag samples were deliberately doped in the adiabatic system with the various amounts of Pd, Fe, Au, In, An, Pb, Zn, Sb, Cu, Ni and Al, one at a time, as referred in the experiment of Ancsin's work [Ancsin, 2001a]. A reason why this research was started is two of three nominally 99.9999% purity Ag samples of the earlier research by Ancsin [2001b] were noticed that their liquidus temperatures was different about 5 mK. That was caused by the contamination of trace impurities (about 5 ppmw in total) in the samples. Therefore, the effect of impurities was considered and investigated in the high purity fixed-point samples. The impurity elements, except Al and Pb, were the dominant impurities of the Ag pure samples, which were detected using GD-MS analysis before doping [Ancsin, 2001a]. From the experimental results, each of these impurities caused the melting temperature curves to shift. The corresponding changes of liquidus temperature as increased amounts of impurities were introduced (with the exception of Al); the rates are as follows: Pd +0.97; Fe +0.13; Au +0.09; In -0.49; Sn -0.60; Pb -0.48; Zn -1.10; Sb -0.73; Cu -0.69; and Ni -0.74 in units of mK/ppmw. Some curve examples of the melting temperature shifts after doping with the various impurities in the Ag samples as a function of increased impurity concentrations are shown in Figure 3.11 and 3.12. Figure 3.11 illustrates the corresponding shifts of liquidus temperature of silver samples as increased amounts of various impurities.

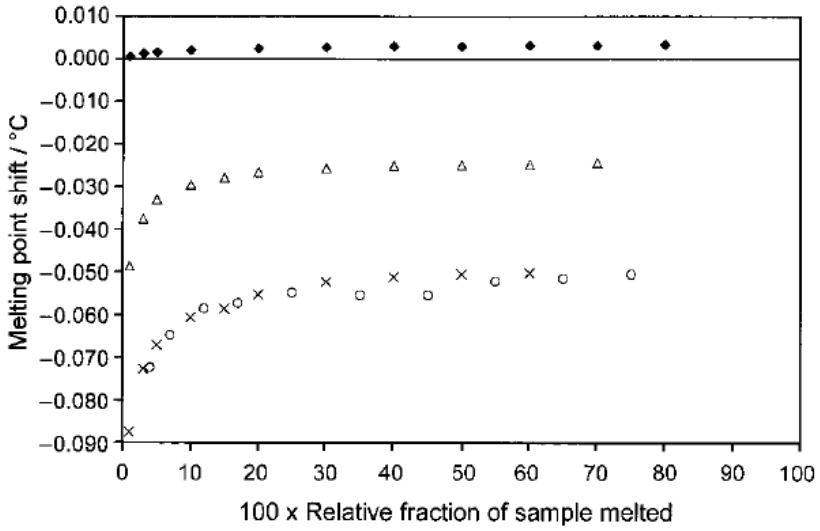

Figure 3.11 Effect of adding trace amounts of impurities to pure sample; ♦ 20 June, 99.9999 % Ag; Δ 26 June, 25 ppmw Zn; × 26 June, 25 ppmw Zn + 38.5 ppmw Sn; ○ 27 June, 25 ppmw Zn + 38.5 ppmw Sn [Ancsin, 2001b].

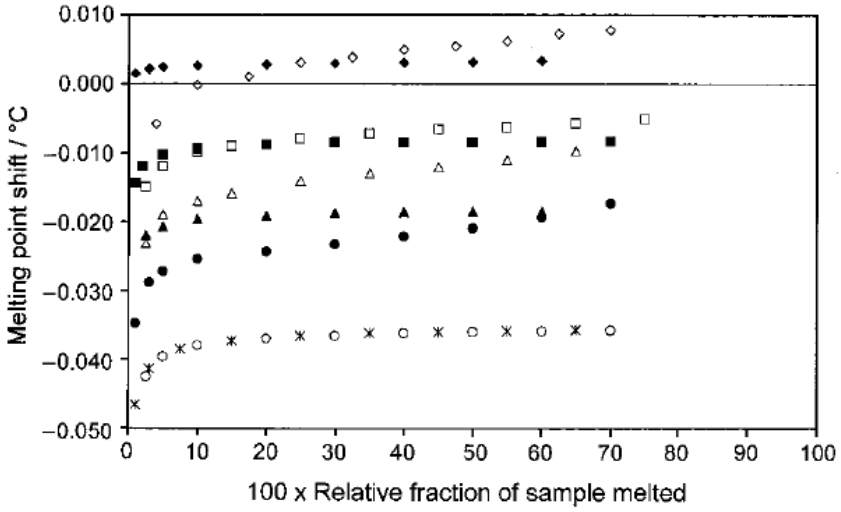

Figure 3.12 Effect of adding trace amounts of impurities to pure sample; ♦ 6 July, fresh 99.9999 % Ag; ■ 6 July, 16.3 Ni; ▲7 July, 29 Ni; ○ 7 July, 53 Ni; ✶ 8 July, 53 Ni; ● 9 July, 53 Ni + 19.5 Pd; Δ 10 July, 53 Ni + 32.2 Pd; □ N 10 July, 53 Ni + 45.7 Pd; ◇ 11 July, 53 Ni + 45.7 Pd [Ancsin, 2001b].

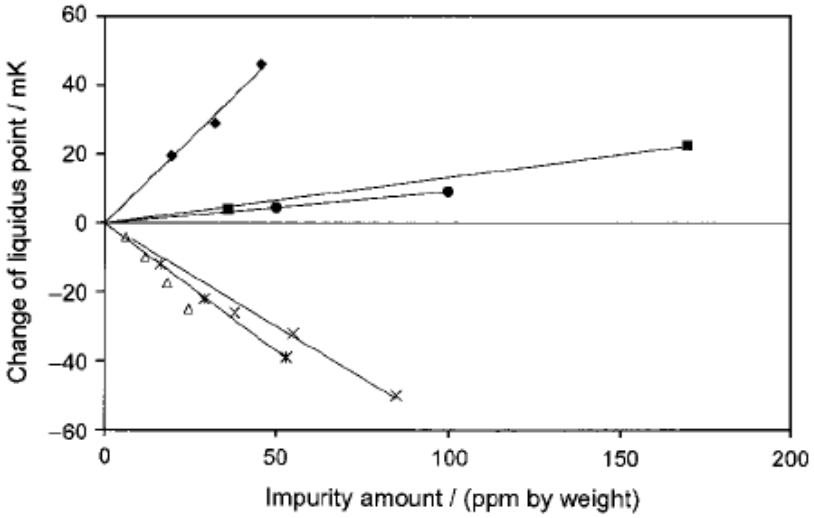

Figure 3.13 The corresponding changes of liquidus temperature of silver samples as increased amounts of various impurities: ♦ Pd; ■ Fe; Δ Cu; × Sn; ✶ Ni; ● Au [Ancsin, 2001b].

Consider two curves of the 53 Ni + 45.7 Pd, as measured at the different date, in Figure 3.12, the shifts of the curves indicate that Pd was demanding much time to be dissolved in the silver liquid and the curve took many hours to stabilise. It was

supposed by Ancsin that it possibly was because of its low solubility. In addition, Ancsin suggested that Al did not have any effect on the temperature Ag curve. Maybe it is because the liquid phase of trace Al could not dissolve in the liquid silver or it possibly the liquid Al, being lighter than Ag, floats on top of liquid silver. This was proved by GD-MS analysis that it had no detection of any amount of Al in the Ag sample after doping with Al several times [Ancsin, 2001a]. From above-described information, we can conclude that the influence of each impurity in the host material remains independent of each other at low concentrations. The magnitude of each effect on the temperature depends on both the species type and the amount of that particular species and the total temperature change is the sum of the individual effects, taking account of any sign. Moreover, the solubility of the impurity, which affects the segregation in the host, is also a significant factor on the accurate fixed-point temperature.

Considering at low temperature, Gallium fixed-point cells were added with different amounts of impurities [Bonnier *et al.*, 2001].

Furthermore, the freezing curves themselves can be considered to show the content of impurity, as confirmed in Mendez-Lango's article [2001]. The fixed-point ingots with larger curvature and lower temperature can be explained that they are contaminated with the impurities. Also, the freezing temperature curve near the liquidus point is higher means the purer and the curvature is flatter means the purer.

Moreover, the shift of the freezing point caused by the impurities present in the fixed-point ingot agreed with the research of Widiatmo *et al.* [2004] as well. It was also discovered that the rate of solidification influences the shift of the measured metal freezing curves. This research was investigated on the Sn, Zn, Al, and Ag metal fixed points with the variety of the solidification rate in terms of the different furnace setting. This work can be explained by use the theory of impurity segregation in the base metal. That is, an effective distribution coefficient (k_{eff}) value would be near the equilibrium distribution coefficient (k_0) when the solidification rate is high [Widiatmo *et al.*, 2004]. Therefore, it can be concluded that the change of the freezing temperature is smaller if the rate of solidification is higher.

In a subsequent experimental research, the Zn fixed-point samples were of interest to study the influence of impurities on their melting point temperatures. This work was determined by Ancsin [2007]. The Zn samples were added with an

assortment of impurities, which already exist in the 99.9999% purity Zn. These impurities were Fe, Pb, Cd, In, Cu, Ag and Au, which the original sample was detected by GD-MS technique. In particular, the shift of the melting curves caused by these impurities would be investigated under the adiabatic condition. In this condition, the furnace temperature needs to set as close as possible to the sample temperature in order to decrease the heat exchange between sample and its surroundings. The aim of the adiabatic furnace is to maintain the stable temperature along the furnace, in which the vertical heat losses are insignificant, as described in the Ancsin and Mendez-Lango's research [1999]. This adiabatic furnace was specially designed, and the diagram of the furnace components is shown in Figure 3.14 [Ancsin, 2007].

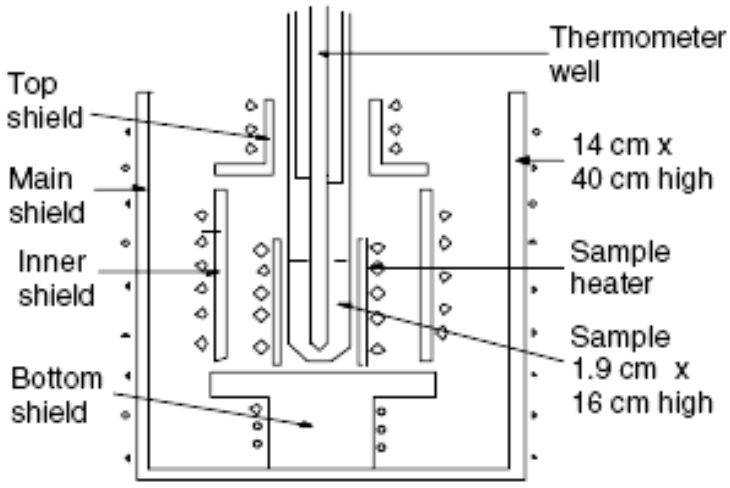

Figure 3.14 Adiabatic furnace components designed by Ancsin [2007].

After experiment, the Fe, Pb, Cd, In, Cu, Ag and Au impurities shifted the Zn melting points by -0.51, -0.27, -0.33, -0.39, +0.23, +0.26 and +0.078 mK/ppmw, respectively. Some examples of both elevation and depression shifts of the Zn melting curves after doping impurities are illustrated in Figures 3.15 and 3.16 (One vertical division is about 1 mK) [Ancsin, 2007]. Figure 3.17 shows the summary of the shifts of the melting Zn temperature after doping with assortment impurities as a function of impurity content.

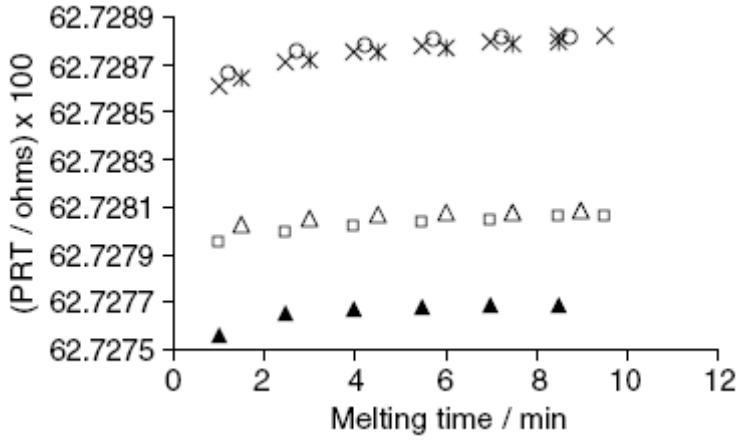

Figure 3.15 Melting curves of high purity Zn fixed-point and the elevation of these curves after doping with increasing concentration of Cu, plotted as a function of melting time. ▲ undoped Zn sample, □ and Δ 20 ppmw of Cu, × and ○ 59 ppmw of Cu [Ancsin, 2007].

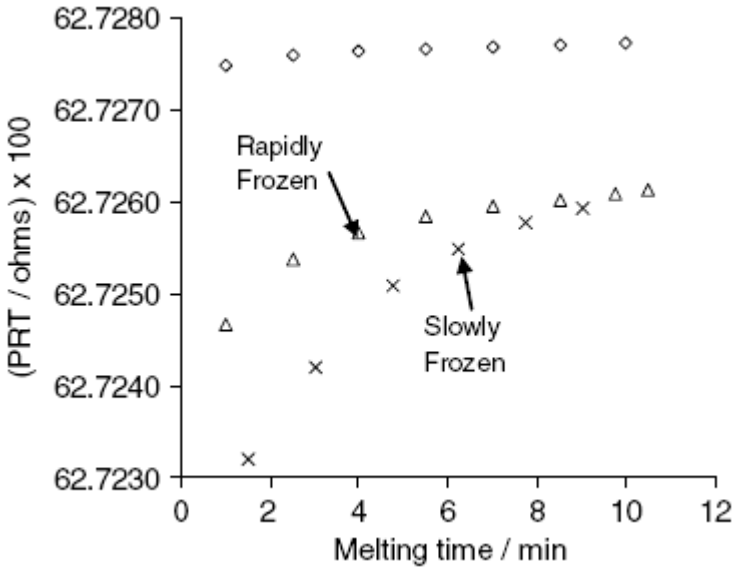

Figure 3.16 Melting curves of high purity Zn fixed-point and the depression of these curves after doping with Fe, plotted as a function of melting time. ◇ undoped Zn sample, △ and × are melts with 35.6 ppmw Fe after freezing at different rates, namely rapidly and slowly, respectively [Ancsin, 2007].

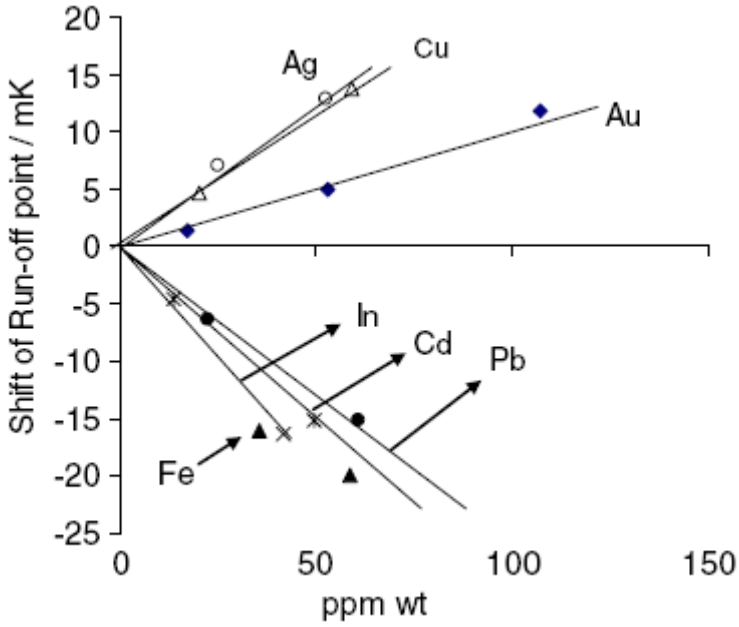

Figure 3.17 Elevation and depression shifts of the Zn melting curves after doping with increasing amounts of various impurities [Ancsin, 2007].

At Figure 3.16, two differences of the freezing rate before melting, i.e. rapidly and slowly frozen, were considerably determined at the same Zn sample. In general, the "rapidly (or quench) frozen" method is done by lifting the whole sample out of the furnace until about 20 ^{o}C - 30 ^{o}C below its melting point or by turning the temperature of the furnace down about 5 ^{o}C - 10 ^{o}C below its normal melting point to freeze it very quickly from the outside, then insert the cold rod for a few minutes into the thermometer well to freeze from the inside. The other frozen method is "slowly frozen". It is carried out the slow freezing overnight by lowering the temperature of the furnace about 1 ^{o}C below the melting range of that sample. The result as shown in Figure 3.16 shows the totally different effect at the beginning of shapes of those two melting curves even though the material was from the same Zn doped with Fe. This indicates that the rate of the preceding freeze of the melting curve influences to the impurity distribution in the solid metal ingot, which then would also affect the shape of the melting curve. The influence of freezing rate on the melting curves of this work is in agreement with respect to the other researchers [Ancsin, 2001a; 2001b; and Zhang, 2008]. Ancsin [2007] suggested in the article that the solubility level of the impurity in base metal fixed point is significant to the scatter in the shift of run-off point, as shown in Figure 3.17. In actual fact, this scatter would appear if some remaining concentration gradients in the samples exist. The very low solubility of Fe in Zn would affect the deviation from linearity in its shift due to the Fe concentration

may be because the saturation value is approached, which is “the most extreme case” (no line is drawn for Fe impurity in Figure 3.17). Also, the experimental results from all different impurity effects showed the reproducibility of the curves if they were investigated by the same techniques and the same metal impurity.

Generally, the higher solubility impurity shows the smaller scatter, which appears with the other impurities in Figure 3.17. The other impurities which were added to the Zn sample were also more homogeneous, as seen in the straight lines plotted through the points.

In recent research on the fixed-point temperature [Rudtsch *et al.*, 2008], the work of PTB revealed the influence of impurity behaviour at different materials on melting and freezing curves of the metal fixed-point temperatures. It helps to understand the impurity distributions in the metal ingot to receive more precise information on the binary phase diagrams at low level impurity contents. Various impurities were added to the PTB fixed-point cells. Also, this work indicates the importance of the thermal effects.

As above described, they are the examples of the study of the impurity effects on the freezing and melting curves fixed-point cells.

The traceable analysis of impurity contents on tin and aluminium fixed-point temperature is the focus of this thesis, and the previous research activities will be reviewed in the next section.

3.4 Reasons for studying tin and aluminium fixed-point temperatures

Two metallic fixed points, i.e. tin and aluminium, were selected to study the influence of trace impurities in their pure metal fixed points. The reason why these two freezing points were chosen is because this activity is a joint project of NPL contact thermometry, under the European Association of National Metrology Institutes (EURAMET) project 732. The EURAMET, formerly EUROMET, is the Regional Metrology Organisation (RMO) of Europe, which was founded by the concurrence of National Metrology Institutes (NMIs) within the European countries. The objective of this organisation is to study and research in metrology, which included traceability of measurements to the SI units, international recognition of national measurement standards, and enables a higher degree of consolidation and coordination of metrology research. Further, it is aimed that the joint efforts can

obtain an improved understanding of the difficulties and eventually lead to the possibility of attaining a better accuracy of the ITS-90 realisation in Europe.

For EURAMET 732 project, "Toward more accurate temperature fixed points" is the title of this project [EURAMET Technical Committee Projects, 2008]. The main purpose of this project is to improve the fixed-point realisation as defined in the ITS-90. The principal work is restricted within the temperature fixed points linked with Long Stem Platinum Resistance Thermometers (argon triple point to silver freezing point). In EUROMET 732 project, there are many research areas, in which each activity is distributed among the 16 participating laboratories [Renaot *et al.*, 2008].

For NPL (UK), the improvement in the study of the fixed-point cells of tin (231.928 °C) and aluminium (660.323 °C) is the main activity**.** Also, the application of MTDATA is planned to correct for impurities so as to enable a reduction in the uncertainty using the SIE (Sum of Individual Estimates). This would play a significant role in the improvement of the temperature standards and to reduce the uncertainties of the fixed-point temperature realisation. It would enhance the confidence in the uncertainty budget and lead to developments in the temperature scale in the future.

3.5 The influence of impurities on the melting and freezing curves of the tin fixed point

The eutectic alloy is used to explain the reaction or phenomenon of the equilibrium phase diagram of the fixed-point cell when is doped with the impurities. In general, this mixture system composes of two components, which is a simple binary system.

The reports of influence of impurities on the melting/freezing curves of tin fixed-point temperature have been reviewed in many previous investigations. In 1980 Connolly and McAllan [1980] reported the sensitivity of the temperature measurement of metal fixed points, which was limited by the effect of very small amounts of impurities. In this article the freezing point of tin temperature was studied by adding from low concentrations up to 56 ppmw of Fe and 36.5 ppmw of Sb. Considering the antimony results; it appeared that the melting and freezing tin temperatures were raised by an amount proportional to concentrations of Sb impurity at low concentrations from 0.7 up to 36.5 ppmw. It was because the peritectic system of Sn-Sb. However, the melting curve at 36.5 ppmw of Sb showed the increased melt but it

had become broad near the end of the liquidus point. Furthermore, the additions of Sb caused a peak in the freeze curve at around 10% - 20% fraction frozen, followed by the temperature falling less than that of pure tin.

In 1999, Stolen and Gronvold studied the effects of trace impurities of Sb and Bi on tin fixed points both theoretically and experimentally [Stolen and Gronvold, 1999]. In this paper, the results indicated that the behaviour of the Sn-Bi system represented a eutectic type and the Sn-Sb system a peritectic type.

Several more recent investigations have been accomplished on the effect of impurity on the melting/freezing curves of tin temperature fixed-point. There has been considerable experiment to study the influence of Sb impurity on the tin point substances by Zhang *et al.* [2008]. The Sb impurity is only one metal, which increases the tin temperature fixed point. It is because the solubility of antimony in the solid is more than in the liquid phase. The influence of Sb on tin was studied from 0.41 up to 11.4 ppmw concentrations under different conditions. The results confirmed that the freezing/melting temperatures were elevated with increasing Sb content. Also, the depth of tin supercooling was decreased with increasing amounts of Sb. This publication showed that the prior freezing process affected the impurity distribution in the tin ingot, which we can see the effect on the melting curves. The peak of the melting curves with a second inner interface after accounting for the overheated liquid around the re-entrant well was due to the accumulated antimony. The size of the peak relies on the history of the freezing conditions.

In the same year, the tin fixed-point measurement focused on the impurity dependence of Sn and the properties of the Sn-Fe eutectic [Ancsin, 2008]. The high purity Sn fixed-point samples were doped with small concentrations of Fe, Sb, Pb, In and Al, which were chosen from the impurities present in the Sn samples. The results showed the shift of the melting curves of the initially “pure” Sn by -0.75 mK/ppmw of Fe, +0.23 mK/ppmw of Sb, -0.16 mK/ppmw of Pb, -0.21 mK/ppmw of In and -2.3 mK/ppmw of Al. Ancsin [2008] revealed the interesting point that the precipitate of Fe and Al impurity metals were found in the liquid tin samples. This is because of the supersaturation of Fe and Al at concentrations at 1654 and 12.2 ppmw, respectively. Furthermore, this work presented the effect of impurities by using the adiabatic furnace, as shown in Figure 3.18 [Ancsin, 2007]. Some examples of melting curves of tin samples after doping with introduced impurities are indicated in Figure 3.19. Moreover, Ancsin [2008] showed the influence of the freezing rate from

a partially molten state, as illustrated in Figure 3.19. The different rate of prior freezing of melting curves showed the different shape at the beginning of the curves.

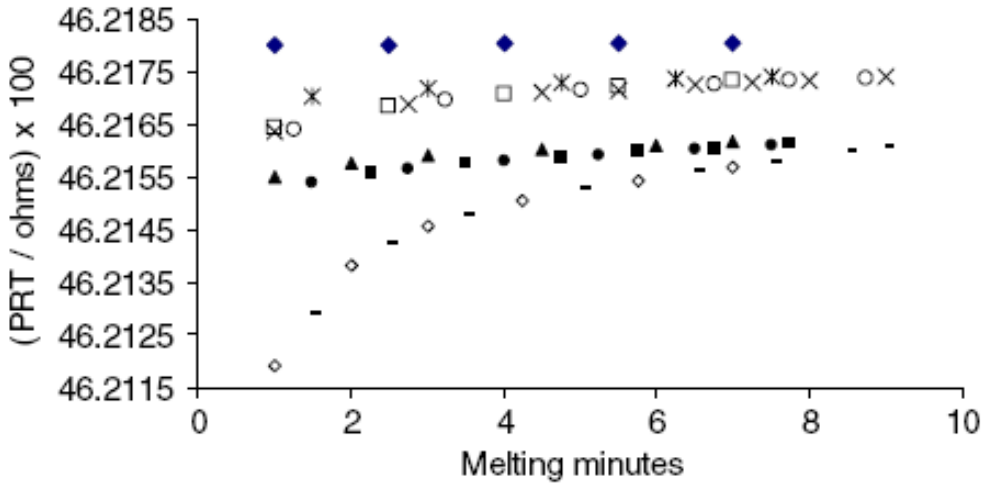

Figure 3.18 Melting curves of a "pure" Sn sample and the shift of these curves after doping the tin with increasing concentrations of Pb. ♦ equilibrium melting curves of rapidly frozen high purity Sn (the liquid sample was lifted out of the furnace for 3.5 min). The lower curves are 39.7 ppmw Pb and 119.5 ppmw Pb doped samples, respectively. The bottom curve is the equilibrium melting curve of the 119.5 ppmw sample that was slowly frozen (about 8 h) from the partially molten state [Ancsin, 2007].

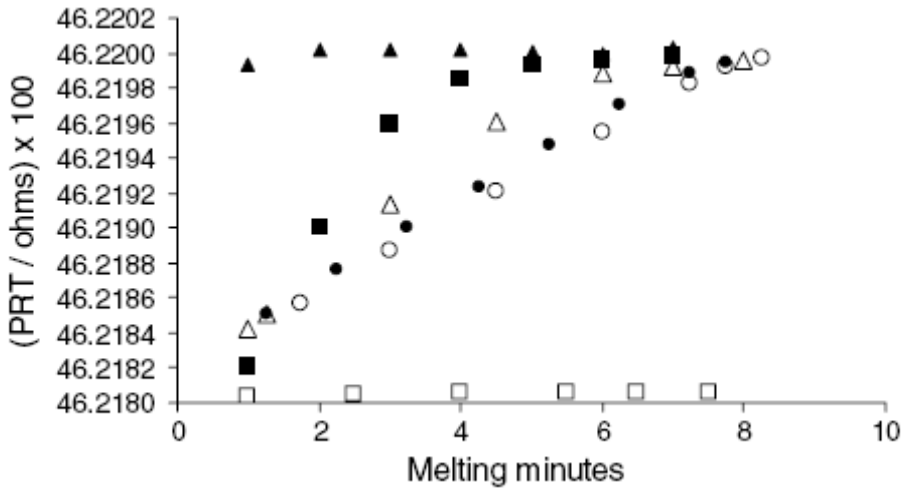

Figure 3.19 Melting curves of a "pure" Sn sample and the shift of these curves after doping the tin with 88.8 ppmw of Sb. □ high purity Sn, ▲ Sn with 88.8 ppmw of Sb rapidly frozen by lifting out of the furnace for 3.5 min. The other curves are those of samples slowly frozen (8 h to 12 h) after the following melting minutes: ■ 2.5 mins, Δ 5.5 mins, ● 7.5 mins and ○ 7.75 mins [Ancsin, 2008].

3.6 The influence of impurities on the melting and freezing curves of aluminium fixed point

The aluminium freezing point (660.323 ^{o}C) is one of a series metallic fixed point, adopted by the ITS-90. This fixed point plays an important role in providing and dissemination of high temperature standard values. The handling of the high purity metal used has a strong influence on the accurate temperature realisation at aluminium fixed point.

Recent research studies have investigated the influence of impurities on the aluminium fixed point e.g. Widiatmo *et al.* [2003]; Widiatmo *et al.* [2006] and Renaot *et al.* [2008].

In this thesis, the work of Ancsin [2003] on the influence of impurity on aluminium e.g. Ti in Al has given us an inspiration for our work. In Ancsin's work, Aluminium ingots (99.9999%) had been doped using 13 metal impurities in different concentrations (i.e. Ag, Zn, Cu, Fe, In, Quartz, Si, Ti, Mn, Cd, Sb, Ca, and Ni) under adiabatic conditions. It found that the run-off point of pure Al melting temperatures was decreased with all impurities except Ti, which increased it. The shift of run-off temperatures caused by those impurities is as follows (in mK/ppmw); Ag -0.12; Zn -

0.16; Cu; -0.29; Fe -0.35; In -0.21; Quartz -0.33; Si -0.66; Ti +3.30; Mn -0.063; Cd -0.10; Sb -0.19; and Ni -0.43 [Ancsin, 2003]. Considering Calcium at "low level" concentrations (138.8 ppmw), the run-off point of the melting curves had no change for all experimental works. In Anscin's work [2003], he gave the reason why the run-off was used to determine instead of the liquidus point that "an accurate determination of the liquidus point requires an accurate determination of the total melting time, whereas an accurate determination of the run-off temperature does not."

Later, the aluminium fixed point curves of Ancsin were studied by use of the application of a thermodynamic model, embodied in NPL's MTDATA software [Head *et al.*, 2008]. That work was to investigate "the initial drop in the freezing temperature and the temperature fall during the freezing using both equilibrium and "Scheil" approaches". This work compared the theoretical curves with the previous published experimental data on impurity-doped aluminium, which was Ancsin's work [2003]. The equilibrium simulations were in close agreements with Ancsin's work for doping with Ag and Si but not the Ti impurity. The Ti doped Al simulation gave the wrong curvature as seen in Figure 3.20, which still remains to be explained.

It is this "contradiction" curvature that suggested to us that one of the binary substances that we should study in this work is pure aluminium doped with titanium. The results of our work on this binary are described in chapter 7.

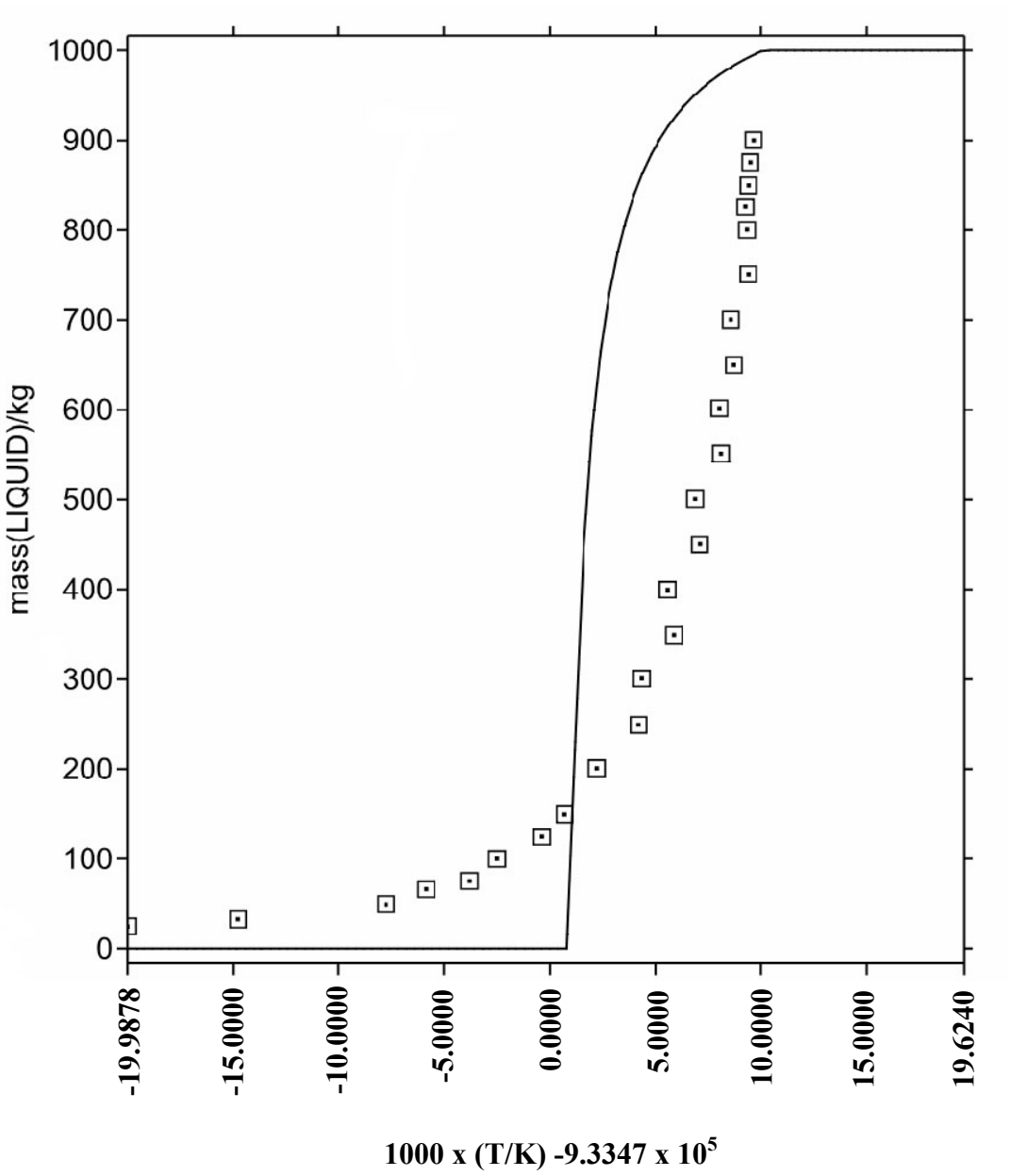

Figure 3.20 2.8 ppm Ti impurity in the aluminium point – MTDATA theory (line) compared to experimental points of Ancsin [2003]. Temperature scale range is 933.450 to 933.490 K. Note how the experimental data shows the "contradiction" curvature [Head *et al.*, 2008].

Chapter 4
Experimental Design

This chapter describes in detail the experimental plans and strategies that were designed to improve the principles of the temperature realisation and the calibration techniques reported in this thesis. The freezing points of tin (231.928 °C) and aluminium (660.323 °C) are two of the metallic fixed-points specified for use in the definition of the International Temperature Scale of 1990 (ITS-90), which were selected for study. The effects of very low levels of impurities on the tin and aluminium transition temperatures would be investigated in order to check the offset values interpolated from the experiments using relatively high levels of impurities. The aim of the experimental design is to evaluate the capability and the limitations of the experimental procedures and to predict the likelihood that the appropriate experimental conditions to accomplish the objective of this research have been achieved. A better understanding of low-level impurities would help reduce the uncertainty budget of the tin fixed-point realisation, where impurities are the biggest contribution to the uncertainty budget. However, demands for reduced uncertainties persist and techniques evolve to other factors. Also, the purpose of this research is to include the improvements of thermal conditions and heating method, furnace design, and control.

Three stages of experimental designs studied in tin and aluminium fixed-point temperatures will be presented. Firstly, the issue of choice of suitable measurement instruments will be explored in the context of extracting meaningful information from the measurement process. It leads to obtaining the reproducibility of the results in both tin and aluminium fixed-point when the appropriate apparatus settings are constructed. In this work we try to reproduce such measurements using standard NPL equipment, which provides standard controlled condition, as used by national measurement institutes (NMIs) worldwide. This is important in ensuring the inter changeability of temperature measurements around the world. Secondly, the appropriate temperature realisation method, and doping/mixing techniques will be investigated and performed to achieve the plateaux stability and homogeneity inside the cells. The actual freezing and melting plateaux will be obtained at this stage. Finally, the chemical analysis, i.e. glow discharge mass spectrometer (GD-MS) characteristic technique, will be used to

determine the distribution of the impurity elements within the metal ingot, before and after deliberate doping. Also, both theoretical (using the NPL's MTDATA software) and experimental results will be compared before doping in order to determine the initial drop of the high purity freezing temperature and temperature decrease during freezing.

4.1 Tin Fixed Point

For tin fixed-point experiment, two standard purity tin fixed-point cells were used to study the influence of trace impurities on the equilibrium tin temperature. Both standard tin cells were named after their donors as "Spanish tin" and "Mini Isotech tin"; these tin ingots were donated by Centro Espanñol De Metrología (CEM), Spain, and the Isothermal Technology Company, respectively. The experiment procedures of both tin cells are similar as explained in Figure 4.1.

4.1.1 Spanish tin fixed-point

For the Spanish tin cell, it was originally of the sealed-fixed point type which had been opened up and re-assembled into an "open cell" by means of the addition of a thin quartz tube, which had been special addition made by Isothermal Technology Ltd (Isotech). Pictures of the 'opened sealed cell' can be seen at Figures 5.2, 5.3, and 5.4. The original sealed cell looks very similar except that it has no projecting silica tube - in fact the silica shroud is totally sealed on itself. (The cell was later converted to a traditional open cell similar to the diagram at Figure 5.6). Its original purity (based on Isotech information) was nominally 99.9999%. This tin fixed-point cell was purchased in 1993, but it has been out of use since 1998. The problem with the cell was that, at ambient temperature, the quartz envelope had broken due to a shock. Therefore, this tin cell was donated to our studies to measure the effect of adding impurities to a tin fixed point.

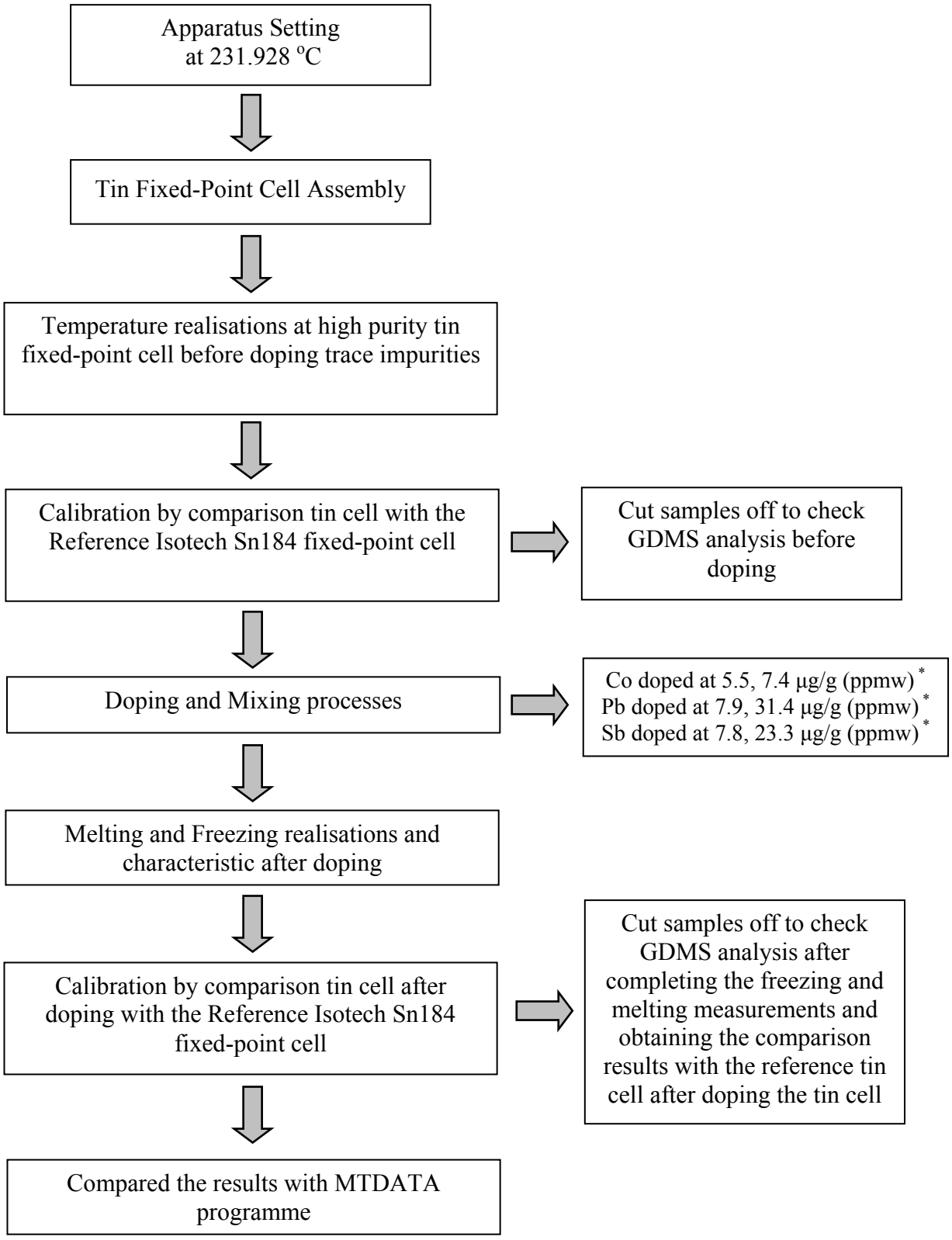

Figure 4.1 Diagram of experimental procedure for studying the effect of trace impurities on the tin fixed-point cells. *The impurity concentrations are presented in ppm unit, whereas the present work is carried out on weight basis, hence ppmw (parts per million by weight), i.e. µg/g unit is used.

More details will be presented in Chapter 5 of the experimental procedures of each step studied on the Spanish tin fixed-point, i.e. the apparatus setting, the cell re-assembly, the size, and weight of the tin ingot, the temperature realisation, and characteristic, doping process and so on. A three-zone Elite furnace was used to maintain the uniform temperature around the Spanish tin cell. The three-zone furnace has the top, the middle, and the bottom heater zones. An example of the three zone furnace diagram is shown in Appendix C. The top and the bottom zones are the protection zones, isolating the influence of the ambient temperature on the temperature of the freezing point. The middle zone provides the temperature uniformity over the length of the metal ingot. Each heater zone is operated individually; therefore the optimum set-up for the Spanish tin cell was investigated.

At the stage of temperature realisation, the outside nucleation followed by an internal induced freeze technique were used for both the Spanish and Mini Isotech tin cells to induce both outer and inner liquid-solid interfaces. This process produces flat and long freezing curves for the temperature realisation process. Details of both techniques will be explained in Chapter 5. In fact, the internal nucleation helps produces a flat shape to the initial part of the freezing curve, whereas outside nucleation alone, which normally occurs at the crucible walls for the high purity materials, shows a slow rising slope on the freeze curve due to the temperature gradient between the outside shell and the thermometer. For tin, which has a large supercooling, the nucleation can also be started on the thermowell, this is one of the techniques reported by Weinberg and McLaren [1963] though the different techniques will affect the shape of the subsequent freezing plateau. Before the impurities were doped in the Spanish tin cell, the glow discharge mass spectrometry (GD-MS) technique was used for chemical analysis in order to investigate the quantity and distribution (or uniformity) of the impurity elements within the “pure” tin. Also the impurity levels in the tin samples, after doping, would be re-measured using the GD-MS again. Analysis results are expected to be within a factor of two of the values obtained, at a confidence level of 95%. This is the state-of-the-art technique for checking impurities in a “pure” metal fixed-point cell. The lower limit of detection is down to the ppb level. However, Ancsin’s research into the equilibrium melting curves of pure and doped silver ingots [Ancsin, 2001a] indicates that the GD-MS analysis results detected at National Research Council of Canada (NRC) are significantly better than what the stated uncertainty would introduce.

Each element, which interacts with tin, was added into the high purity Spanish tin fixed-point cell. Information for selected trace impurities will be discussed in Section 4.1.3. Then, the experimental procedure as explained in the pre-doped Spanish tin cell was repeated at this stage to determine the offsets of their freezing temperatures and changes in the shape of the melting curve due to those impurities. The thermodynamic modelling in particular with MTDATA was used to calculate the equilibrium thermodynamic curves and to estimate the shift in the initial freezing temperature compared with the experimental results before doping.

4.1.2 Mini Isotech Tin Fixed-Point

For the second cell, named "Mini Isotech tin", the ingot was smaller than normal, being 110 mm in length, 26 mm in outer diameter, and 16 mm in inner diameter. The total mass of the tin sample put in this cell was approximately 240 g. The main experimental procedure for Mini Isotech tin is similar to Spanish tin fixed point. However, the three-zone Carbolite furnace was mainly used for this cell. It provides a uniform temperature along the length of the ingot achieved by controlling the temperature in the three zones. Also, the best setting for the three-zone furnace was determined for realisation of equilibrium phase states of pure tin substance. The measured value for the vertical gradient needed for the proper realisation of phase transition is less than 30 mK over the length of the tin ingot. More details regarding the cell assembly and the apparatus setting can be found in Chapter 5.

Platinum resistance thermometers (PRTs) were used to measure and calibrate the equilibrium temperature at the freezing value of the tin fixed-point. The resistance value of the PRT was recorded from which the temperature could be calculated. The experimental procedure for the Mini Isotech tin is the same as that for the Spanish tin cell including the GD-MS technique used for chemical analysis on Mini Isotech tin before and after doping. Also, the experimental melt/freeze curve(s), before doping, will be compared with those predicted by MTDATA, (using the GD-MS chemical analysis as an input and the MTDATA data base of the effects of individual impurity elements on the phase transition temperature). MTDATA assumes the system is in thermodynamic equilibrium (we approximate this by using long experimental times for the melt and freeze.

4.1.3 Types and Concentration of Impurities for Doping in Tin Fixed- Point Cells

Trace impurities of cobalt (Co) and lead (Pb) were added to the high purity Spanish tin in parts per million by weight (ppmw). Hansen's work [Hansen, 1958] shows that the tin temperature is depressed by 0.60 mK/ppmw and 0.133 mK/ppmw for cobalt and lead impurities, respectively. The binary alloy phase diagram for the eutectic system of Sn-Co and Sn-Pb has the equilibrium distribution coefficient (k_0^i) much less than 1 for Co (very small solubility in solid tin) and less than 1 for Pb [Fellmuth and Hill, 2006]. Adding these two impurities to tin decreases the initial pure tin fixed-point. Also, we believe these two metals have never been studied experimentally on their effects as trace impurities on tin fixed-point temperature at this low level of concentration. For the doping process, a normal NPL apparatus had been used under standard conditions, as is the case in most national measurement institutes around the world.

Amongst trace impurities in the Mini Isotech tin cell, only antimony (Sb) is known to increase the initial temperature of tin due to the equilibrium distribution coefficient (k_0^i) being greater than 1, as defined for peritectic system Sn-Sb [Fellmuth and Hill, 2006]. The tin transition plateau was raised by 0.128 mK/ppmw for antimony impurity according to the work by Hansen [1958]. From the behaviour of the impurities used for doping in the two tin cells, it suggests that both the increase and decrease in temperature can be investigated. This is the reason why these impurities were selected.

Our measurements uses lower concentrations (in terms of part per million) of dopants than those of other researchers; this will verify the interpolation used by them. For pure Co and Pb metal impurities doping, their total concentrations in the Spanish tin cell are (in ppmw): Co 5.5 and 7.4, Pb 7.9 and 31.4. As for the metal impurity Sb, 7.8 and 23.2 ppmw were added into the Mini Isotech tin cell. For each metal impurity, it was added to the top, middle and bottom sections of the tin ingots. Then it was mixed within the tin in the manner as described in Chapter 5.

4.2 Aluminium Fixed Point

The freezing point of aluminium (660.323 ^{o}C) as a metal fixed-point has been adopted by the ITS-90. Results indicate that impurities affect the melting curves of the aluminium fixed point. Some impurity metals can depress the melting temperature while others can increase it.

Two originally nominally 99.9999% pure aluminium point cells, constructed according to the NPL design, were used in this study to realise as test cells to measure before and after doping and compare against a reference cell. These two cells were designated after the year they were fabricated in 1974 (Al 174) and 1998 (Al 298). Figure 4.2 shows a block diagram of the experimental procedure adopted for the aluminium fixed-point cell.

First of all, a systematic study of an assortment of impurities effect on the equilibrium melting curves of Al fixed point, which was already carried out by Ancsin [2003], was investigated to be an example idea before the studies of the quantitative effect of impurities on the temperature of tin fixed-point cells were carried out. Therefore, the experiment by realising and doping on the aluminium fixed-point temperature as Ancsin's report was repeated to improve techniques and method.

However, the furnace system as used in Ancsin's work was totally different from our technique by using a special adiabatic furnace and a specialized cells design as seen in Figure 1 of Ancsin's work [Ancsin, 2001b]. In this work we try to produce such measurements using standard NPL equipment, under standard conditions, used in most national measurement institutes around the world.

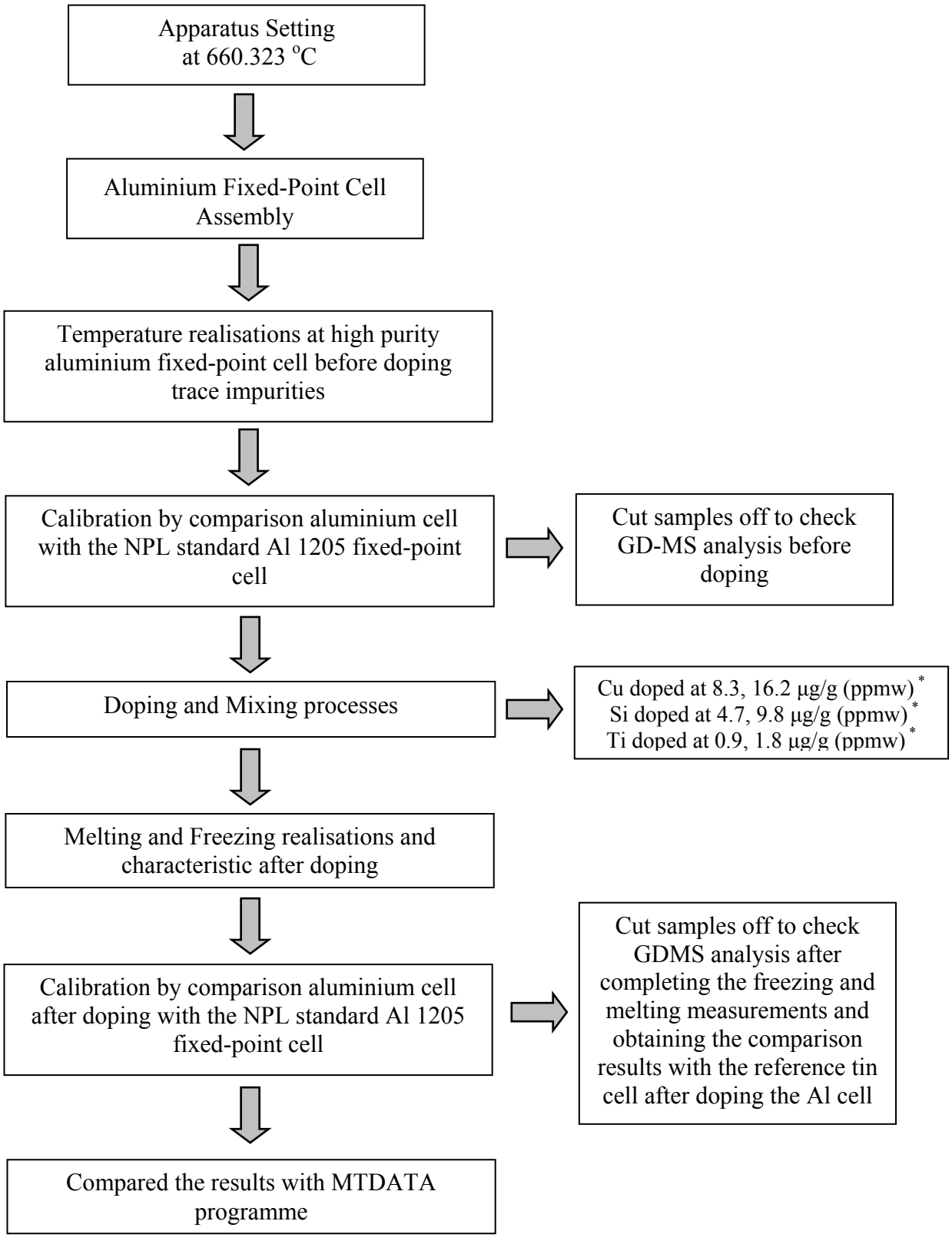

Figure 4.2 Diagram of experimental procedure for studying the effect of trace impurities on the aluminium fixed-point cells. *The impurity concentrations are presented in ppm unit, whereas the present work is carried out on weight basis, hence ppmw (parts per million by weight), i.e. µg/g unit is used.

In the work of Ancsin [2003], high purity (99.9999%) aluminium fixed-point cells were doped with 13 impurities in different concentrations as guided by the results of chemical analysis of the samples. Three impurity metals were selected from the results, which clearly showed a shift in the liquidus point of Al temperature. Three of the impurities were copper (Cu), silicon (Si), and titanium (Ti). The reasons why Cu and Si impurities were chosen were that they caused a depression of the transition temperature of Al. Moreover, Cu is easy to get hold of in a pure usable (wire) form and it is a potential subsequent impurity in a cell due to its presence in a laboratory environment. Both elements have also been often found in the impurity analysis of real "pure" aluminium samples. Therefore, Cu and Si were doped in the Al 174 cell to study the temperature decrease due to these trace impurity metals. From previous work [Head *et al.*, 2008], the Al-Si experiment result was compared with the MTDATA theory. It could be seen that the equilibrium simulation was in close agreement with Ancsin's experimental result [Ancsin, 2003].

On the other hand, the Ti impurity metal causes an elevation of the Al transition temperature. Also, it was selected for doping in Al 298 because the curvature obtained from Ancsin's experimental result was different from that calculated by MTDATA [Head *et al.*, 2008], unlike the Si in Al as explained in section 3.4. The Ancsin experimental data show the "contradiction" curvature in the melt/freeze curve compared to that calculated from MTDATA as reproduced in Figure 3.20 of this thesis. Therefore, the Ti doped Al fixed point was studied to repeat the experiment. However, the amount of concentrations for doping used in this work was smaller than those used in Ancsin's work, which should give an improved understanding of the effects of low-level impurities on the Al transition temperature. It is in order to check the temperature offset values interpolated from the experiments using relatively high levels of impurities.

For calibration by comparison of our cells with the reference Al cell, an aluminium sealed fixed-point cell (Al 1205) was designated as a reference cell, which was related to NPL national standard Al cell, for Al 174 and Al 298 fixed-point cells. This aluminium fixed-point cell was designed and built by NPL.

4.2.1 Aluminium (Al 174) Fixed Point

A single zone Carbolite furnace was used in conjunction with a potassium heat pipe for maintaining a uniform temperature above or below the equilibrium temperature of Al 174 cell. This means that the conditions are only quasi-adiabatic, but this was the desired way to carry out the tests, as these are the "normal" conditions for the realisation of fixed-points. Details of cell assembly and the temperature realisation technique can be found in Chapter 5. Measurement values were recorded using the thermometric parameter, which for this work, is the resistance value of the PRT. Then, the Al 174 cell was calibrated by comparing its reading against the standard NPL Al (Al 1205) cell in order to see how good this Al 174 was before adding any impurities into the cell. Then, some samples were removed from the ingot for the GD-MS analysis before further doping and mixing with impurities. The type and amount of metal impurities for doping of Al 174 will be mentioned in Section 4.2.3. More details of the experiment procedure performed with the Al 174 fixed-point cell will be discussed in Chapter 5. Then, the same procedure would be repeated with the doped ingot. Thermodynamic modelling with MTDATA was carried out to calculate the equilibrium thermodynamic curves and to estimate the shift in the initial freezing temperature compared with the experimental results before doping.

4.2.2 Aluminium (Al 298) Fixed Point

The Al 298 cell assembly, details of which are given in Chapter 5, was heated inside a three-zone Hart furnace that maintained an even, but offset, temperature distribution for the realisation of the fixed point. The best setting of the top and bottom zones of the furnace was checked to ensure an even temperature over the length of the ingot for realisation of the equilibrium phase states of Al. This step of the experimental procedure of the Al 298 fixed point was similar to that of the Al 174 except for the type of impurity doping. More details regarding the realisation and doping/mixing technique including the GD-MS technique and MTDATA can be found in Chapter 5.

4.2.3 Types and Concentration of Impurities for Doping in Aluminium Fixed- Point Cells

The temperature offsets and shapes of melting and freezing plateaus of high purity aluminium in this work were investigated to determine how they were affected by the added impurities (concentrations of order ~1-20 ppmw) of copper, silicon, and titanium pure metals.

In Ancsin's paper [Ancsin, 2003], the shift in temperature was considered from the run-off points of the sample. The run-off point as defined by Ancsin is the temperature of the fixed-point metal when the trace breaks away from the melting curve and then rapidly starts to rise, which is occurs at different sample molten fractions. When melting an ingot, the melt will often occur along grain boundaries, so it is believe that melted material penetrates the cell more quickly than freezing dendrites. Consequently melts more quickly expose the thermometer to outside thermal influences – particularly in the second half of the melt. This causes the thermometer to rise in temperature, apparently signifying the end of the melt, when in fact a large amount of the ingot is still solid – albeit heavily penetrated with liquid filaments. This apparent end of the melt is sometimes referred to as the run off, while the true liquidus should occur only when all the metal has melted, as there may be different concentrations of impurities in the liquid and solid. The need for the run off concept is a sign that thermometerists are still not able to produce ideal thermal conditions.

In Ancsin's work, the shifts in the run-off temperatures due to the three impurities added to the originally 99.9999% pure Al are (mK/ppmw): Cu -0.29, Si -0.66 and Ti +3.30.

Moreover, in previous experiments on these binary alloy systems, using higher levels of impurities [Hansen, 1958], the fixed-point temperature of aluminium was interpolated using the knowledge that copper depressed the temperature by 0.37 mK/ppmw and silicon, by 0.71 mK/ppmw whereas titanium elevated the temperature by 3.31 mK/ppmw. From the results of the Ancsin's work, the shift of the run-off points was in agreement with the calculated results obtained from the estimated melting point shifts of Hansen's book.

In the present work, the normal techniques using standard NPL equipment, under standard conditions, i.e. the furnace and doping/mixing impurities, were

performed to confirm that the national measurement institutes around the world can use our techniques to realise the temperature shift caused by the impurities. Also, the amount of concentrations of each impurity doped in our Al cells was much less than that used in Ancsin's work. The work by the author is to study the effects of very low levels of impurities on the aluminium transition temperature and to compare them with the temperature offset values interpolated from the experiments using relatively high levels of impurities.

After the equilibrium curves of "initial" Al 174 and Al 298 cells were measured, three types of impurities; namely copper, silicon and titanium were used for doping. Each impurity was dropped into the top, the middle, and the bottom of the originally pure Al samples. Having completed the measurements using one impurity, the sample was doped with another impurity and the resulting shift in the transition temperature curve was again investigated. Considering Cu and Si metals doped in Al 174 cell, the concentrations of the impurity metals were increased as follows (in ppmw); Cu 8.3 and 16.2, Si 4.7 and 9.8, respectively. For Ti metal doped in Al 298 cell, the concentrations of Ti was increased as follows; 0.9 and 1.8 ppmw, respectively. Then, the mixing process was carried out in the next step, where the normal method and condition were applied. For more specific information about how to do the mixing process see Chapter 5. The temperature changes during freezing and melting of the aluminium after each doping were measured and compared with the original curves to find out how much each of the trace impurities affected the equilibrium temperatures of the aluminium fixed point.

4.3 Elemental Analysis by Glow Discharge Mass Spectrometry

One of the most potent elemental analytical techniques is the glow discharge mass spectrometry (GD-MS) [Betti *et al.*, 2003]. GD-MS is a comprehensive and versatile technique for use in the direct analysis and determination of traces impurities at the parts-per-billion level in an assortment of solid-state substances. Additionally, GD-MS is an analytical method able to provide the data on the chemical composition of a substance [King *et al.*, 1995]. The advantages of this technique are high accuracy, low detection limits, and bulk/depth profile.

King and co-workers [King *et al.*, 2005] have given the explanation of the GD-MS that "The technique is an extension to the earlier forms of mass spectrometry.

Processes inherent to the glow discharge, namely cathodic sputtering coupled with Penning ionization, yield an ion population from which semi-quantitative results can be directly obtained. Quantification in GD-MS is achieved both through standard elemental mass spectrometric procedures and more innovative approaches. The analytical performance of GD-MS compares favorably with competing elemental mass spectrometric methods and newer experiments use this ionization method for both molecular and elemental analysis. As with any analytical technique, the future of GD-MS lies in improvements with respect to the instrumental implementation and extension to new areas of application. Continued efforts to develop improved procedures are needed to provide greater accuracy. The sample to be analyzed forms the cathode in a low pressure (~ 100 Pa) gas discharge or plasma. Argon is typically used as the discharge gas. Argon positive ions are accelerated towards the cathode (sample) surface with energies from hundreds to thousands of eV resulting in erosion and atomization of the upper atom layers of the sample. Only the sputtered neutral species are capable of escaping the cathode surface and diffusing into the plasma where they are subsequently ionized. The atomization and ionization processes are thus separated in space and time, which appears to be a keystone for simplified calibration, quantification and the near matrix independence of this technique".

For this work, the samples from each of the tin and aluminium fixed-point cells were analysed and the types of elemental impurities were determined at the Chemical Metrology, National Research Council (NRC) in Canada. It is in order to investigate the quantity and distribution (or uniformity) of the impurity elements within the "pure" tin and aluminium, before deliberate doping. Subsequently the impurity levels in the tin and aluminium samples, after doping, will be re-measured by using the GD-MS again.

4.4 Thermodynamic and phase equilibrium analysis by MTDATA

The application of a thermodynamic model, the MTDATA software designed at NPL, is used to predict the phase equilibrium in the materials and also to investigate the initial decrease of the freezing temperature and the temperature drop during the freezing process as used in Head's work [Head *et al.*, 2008]. In Head's work, MTDATA was also used to calculate the theoretical curves compared with previously published experimental data of Ancsin [Ancsin, 2003] on aluminium fixed-point doped with a variety of impurities. The results of the comparison showed good agreement in the magnitude of the initial depression (at freeze start) but examples of the wrong curvature on the subsequent freezing curve for impurities that increase the phase transition temperature (while getting agreement in the curvature for elements that depress the Al phase transition temperature). Therefore, MTDATA also is used for simulating to estimate the whole phase transition curves of any metal fixed points in order to compare with the experimental curves.

NPL's MTDATA [Davies *et al.*, 2002] was developed over many years by the Thermodynamics and Process Modelling Group, in the Materials Centre at the National Physical Laboratory (NPL). The MTDATA software package is described in its "advertising literature" as being used to predict the complex chemistry in multicomponent multiphase systems, using critically assessed thermodynamic data. It is used by companies and universities worldwide for understanding such diverse applications as continuous casting of steel, lamp chemistry, pollution control, and pyrometallurgical extraction. It claims a very high reliability. It can be designed to calculate the phase or chemical equilibria with maximum ease and reliability.

Considering the application of MTDATA for thermal metrology, MTDATA is normally performed to predict the phases forming at equilibrium in systems containing many components and many phases. It is based upon critically assessed thermodynamic data. It can be done for simple equilibrium calculations given the composition and the temperature. (Though it is also possible to set paraequilibrium (or quasi equilibrium) conditions in certain circumstances).

For given the description of thermodynamic model, Head and coworkers [2008] also mentioned that "The equilibrium state of a chemical system at a fixed-point temperature, pressure, and overall composition can be calculated by minimizing its Gibbs energy with respect to the amounts of individual species that could possibly

form. The most stable phase or combination of phases at chemical equilibrium can then be predicted for a chosen T and P as that with the lowest Gibbs energy. When impurities are present then additional terms representing the interactions between them and bulk materials must be included in the model of the Gibbs energy."

This work was performed using the MTDATA model to estimate the initial drop in the freezing temperature on tin and aluminium fixed points before doping. Also, the concentrations of the GD-MS results detected from the "undoped" tin and aluminium cells were used to calculate the equilibrium phase curves in the MTDATA program before doping. Then, the equilibrium calculations would be compared with the experimental results before doping any impurities into the tin and aluminium fixed-point cells.

Chapter 5
Experimental Procedures

This chapter describes the experimental procedures for the study of the effect of trace impurities on the temperature realised by a high purity (99.9999%) tin (231.928 ^{o}C) and aluminium (660.323 ^{o}C) fixed-point cell. This chapter will detail the instruments, the chemicals, and the assembly of the fixed-point components in the tin and aluminium cells. In addition, the chapter describes the temperature realisation and measurement of the tin and aluminium fixed-point cells both before and after doping with platinum resistance thermometers (PRTs). The method to dope impurities into each fixed-point cell will be presented. All equipment in this research is provided by National Physical Laboratory (UK).

5.1 Instruments

5.1.1 Tin Fixed Point

The following equipment was used for the tine fixed point experiments:

- Reference Isotech Tin Fixed Point Sealed Cell (Serial Number: Sn184, 99.9999% nominal purity of tin)
- Isotech Tin Fixed Point Opened Cell (Serial Number: Spanish Tin, 99.9999% nominal purity of tin)
- Isotech Tin Fixed Point Mini Opened Cell (Serial Number: Mini Isotech Tin, 99.9999% nominal purity of tin)
- AC Precision Resistance Bridges: Automatic Systems Laboratories (ASL) F18 (Serial Number 1085/002/071 and 1737/003/151)
- Standard Resistor: H. Tinsley & Co. Ltd (Serial Number 268167, 240741 and 222024)
- Three-Zone Furnace: Model Carbolite 902 (Serial Number: 20-602639)
- Three-Zone Furnace: Model Elite (Serial Number: 2048/10/06)
- Long-Stem Platinum Resistance Thermometers (PRTs): Tinsley Model 5187SA (Serial Number: 274728), Isothermal Technology Ltd (Serial Number: 909174, 909069, 909347) and Aerospace delicate PRT (Serial Number: 4849)

- A Tempmaster with 2 (100 ohm) PRT probes: Lab Facility Indicators (Serial Numbers A and B)
- NPL Water Triple Point Cells: (Model 5901-1441, 5901-1442)
- Huber Polystat CC2 Oil Bath Controller: (Serial Number: 55903)
- Oil Bath: Model Kaltebad K15 (Serial Number: 53750/03)
- Pressure Gauge: Model Wallace & Tiernan (Serial Number: I5338)
- Scroll pump: Model Edwards XDS10 (Serial Number: 027216630)
- Helium Leak Detector: Leybold Vacuum PhoeniXL 300
- Variac (Variable Transformer)
- Sartorius Balance Model: CC3000 (up to 1 Kg) (*)
- Mettler AT20 (Balance Scale, Serial Number: K86486) (*), from 1 μg to 20 g.

5.1.2 Aluminium Fixed Point

The following equipment was used for the aluminium fixed point experiments:

- Aluminium Fixed Point Open Cell (Serial number: 298, originally 99.9999% nominal purity and 174, originally 99.9999% nominal purity of aluminium, (but it is expected that they are presently less than the original purity percent quoted)
- National Standard Aluminium Fixed Point Sealed Cell (Serial number: 1205, 99.9999% high purity aluminium)
- AC Precision Resistance Bridges: Automatic Systems Laboratories (ASL) F18 (Serial Number 1085/002/071 and 1737/003/151)
- Standard Resistor: Wilkins design from H. Tinsley & Co. Ltd (Serial Number 268167, 240741 and 222024)
- Huber Polystat CC2 Oil Bath Controller: (Serial Number: 55903)
- Oil Bath: Model Kaeltebad K15 (Serial Number: 53750/03)
- Single-zone furnace: Model Carbolite (Serial number: 2/96/542)
- Three-Zone Furnace: Model Hart Scientific 9114 (Serial Number: A63118)
- Standard Long-Stem Platinum Resistance (25 ohm) Thermometers (SPRTs): (Serial Number: 250329, 261198)
- A Tempmaster with 2 (100 ohm) PRT probes: Lab Facility Indicators (Serial Numbers A and B)
- Water Triple Point Cells (Serial Number: 938, 1058)

- Pressure Gauge: Model Wallace & Tiernan (Serial Number: I5338)
- Scroll pump: Model Edwards XDS10 (Serial Number: 027216630)
- Helium Leak Detector: Leybold Vacuum PhoeniXL 300
- Variac (Variable Transformer)
- Sartorius Balance Model: CC3000 (up to 1 Kg) (*)
- Mettler AT20 (Balance Scale, Serial Number: K86486) (*), from 1 μg to 20 g.

(*) Mass Section, National Physical Laboratory (NPL), UK

5.2 Chemical Substances

The first six high purity metals (metalloid), listed below, are the impurities used for doping the tin and aluminium fixed-point cells. In addition, other chemical substances on the list were used for cleaning the components of the fixed-point cells and the PRTs and the last substance is the fluid used for maintaining the standard resistor temperature in the bath.

Chemicals	Nominal Purity	Supplier
1. Antimony (Sb)	99.5%	Goodfellow Cambridge Limited
2. Cobalt (Co)	99.99+%	Goodfellow Cambridge Limited
3. Copper (Cu)	99.99+ %	Goodfellow Cambridge Limited
4. Lead (Pb)	99.99+%	Goodfellow Cambridge Limited
5. Silicon (Si)	99.998 %	Goodfellow Cambridge Limited
6. Titanium (Ti)	99.8 %	Goodfellow Cambridge Limited
7. Acetone		
8. Absolute ethanol (C_2H_5OH)		
9. Ensolv		
10. Nitric Acid (HNO_3)		
11. High Purity Paraffin Oil		

5.3 Stability of PRTs: Checking by the Triple Point of Water

A platinum resistance thermometer is checked at the triple point of water, which is used as a baseline for the stability and the accuracy of the thermometer. The triple point of water, defined as 273.16 kelvin or 0.01 ^{o}C in the International Temperature Scale of 1990 (ITS-90), is one of the most accurately realisable temperature fixed-points. Therefore, water triple point cells are almost always used in the calibration of thermometers. The triple point cell contains high-purity gas-free water maintained in the thermal equilibrium between the three phases of water: liquid, solid and vapour. For PRTs' measurement and calibration, the water triple point cell is the most important fixed-point. This is because the interpolation equations used for the ITS-90 for a PRT are expressed in terms of the resistance ratio $W(T_{90}) = R(T_{90})/R(0.01\ ^{o}C)$, where $R(T_{90})$ is the resistance value at T_{90} and $R(0.01\ ^{o}C)$ is the resistance value at the triple point of water. The resistance of the PRT at the triple point of water needs to be checked frequently to identify any instability of the PRT. In general, if the resistance value of the PRT at the triple point of water does not change, the thermometer does not need recalibration.

For this procedure, two small water triple point cells, designated as the NPL cells (serial numbers 934 and 1058) were used. Figure 5.1 shows one such water triple point cell. Both water triple point cells were kept in a Dewar containing crushed ice at 0 ^{o}C for 24 hours before the ice mantles were allowed to form. The ice mantles were produced using solid CO_2 (see the detail of preparation of a mantle in Section 2.3.1). Measurements with the PRTs were then made about 24 hours after the ice mantles were formed. The stability of PRTs was determined at the water triple point in between the realisations (both before and after realising tin and aluminium fixed-points). The water triple point values in this research were checked within a few hours after the measurements at tin and aluminium fixed-point temperatures. The results of stability of each PRT were shown in terms of the resistance values, which were obtained by combining the bridge ratio measurements and the standard resistor values. An Automatic Systems Laboratories (ASL) Model F18 ac resistance bridge was used to measure the resistance ratio values of 25 Ω platinum resistance thermometers in the two water triple point cells, against 100 Ω standard resistors.

For improved accuracy in the triple point of water realisation, the cell is required to be kept in storage for 24 hours before it was used. This is to relieve strains

in the ice of the water cell and the prepared ice mantles [Furukawa *et al.*, 1997] as the strain affects the obtained temperature value in the cell. With effective strain relaxation, the uncertainty will be typically less than 150 μK [Nicholas and White, 2001j].

Figure 5.1 NPL small water triple point cell.

5.4 Making and Realisation the Tin Fixed Point Cells

Two standard purity (nominally 99.9999%) tin fixed-point cells were used to study the influence of trace impurities on the equilibrium tin freezing temperature. Both standard tin cells were named after their donors as “Spanish tin” and “Mini Isotech tin”; these tin ingots were donated by Centro Espanñol De Metrología (CEM), Spain, and the Isothermal Technology Company, respectively.

5.4.1 Making and Realisation Spanish Tin Fixed-Point Cell

The methods for the assembly and temperature realisation of high purity Spanish tin fixed-point cell will be presented separately in two sections: Section 5.4.1.1 describes the method for the original “undoped” opened-“sealed cell” whilst Section

5.4.1.2 shows the method for the high purity "undoped" ingot after re-assembly into a new container.

5.4.1.1 Original "Undoped" Spanish Tin Opened-"Sealed Cell"

The Spanish tin cell was a closed cell re-assembled into an open cell by means of a thin quartz tube as seen in Figure 5.2. The cell was purchased in 1993, but it was out of use since 1998; its purity (based on Isotech information) is 99.9999%. The tube and the "cell body" were respectively 30 cm and 25 cm long. The quartz envelope had an outer diameter of 48 mm. Since the quartz envelope of the cell was broken due to a shock to the cell at ambient temperature, it was sent to Isotech for repair but the damage was such that the cell could not be closed effectively. As can be seen in Figure 5.2, the quartz tube and the graphite appeared slightly "burnt" and that prompted the CEM's laboratory to suspect that contamination might have happened during the re-assembly. Despite this, the graphite crucible was in perfect condition and therefore the Spanish tin ingot inside could be used for doping. To dope the ingot, it has to be removed from the quartz envelope and so the cell had to be modified to become an "opened" cell to allow access to the ingot. The afore-mentioned information was obtained from M. Dolores del Campo Maldonado who is the Head of the Temperature Division in CEM, Spain.

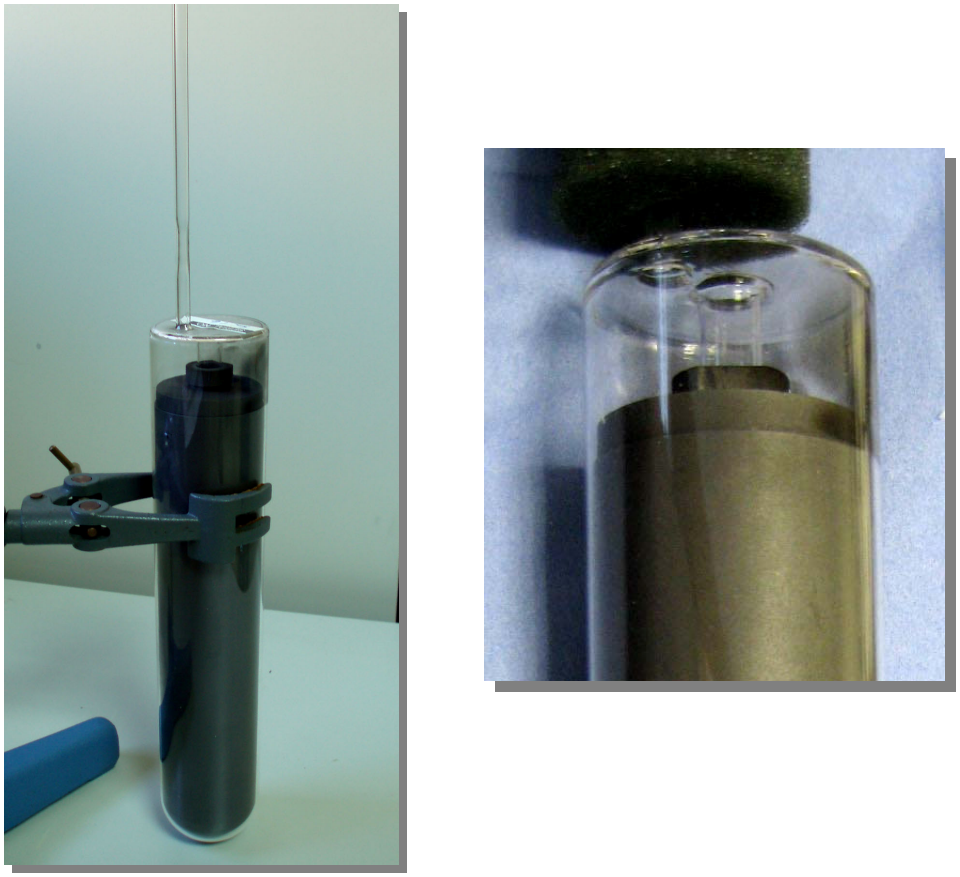

Figure 5.2 An original Spanish tin opened-"sealed cell" obtained from CEM, Spain. The "burnt" area of the quartz and the graphite can see on the right of the figure.

Before the original Spanish tin opened-"sealed cell" was put into the furnace, the cell needed to be assembled with other components in the way that a sealed cell is. The components consist of the Spanish tin cell, the bricks, the metal discs (2 mm thickness) and an inconel block (459 mm long and 50 mm inner diameter) are seen in Figure 5.3. The insulator on top of the cell was made with alternate layers of the bricks and the metal discs, which were designed specially for this cell by the company Isothermal Technology (UK). The bricks and the metal discs had been baked at 1100 ^{o}C for a day before assembling into the cell to eliminate by oxidation any contaminations. Then, all components would be put into the inconel block. The assembly was operated as both of the "sealed" and "open" cells, i.e. the bricks and the metal discs were put outside of the quartz tube (not directly touching the graphite crucible) as the sealed cell while this cell allowed the evacuation of the air and the

filling with high purity argon gas at a pressure of 101.3 kPa at the fixed-point temperature as would the normal open cell, Figure 5.4.

This original silica envelope of the sealed cell had had a silica tube retro fitted to it, connecting the gas space to the outside world – rather like a NIST design of the open cell used for their aluminium points [Strouse, 1995].

Figure 5.3 Components of the original Spanish tin opened-"sealed cell" assembly.

The original Spanish tin opened-"sealed cell" was installed in a three-zone Hart furnace set for maintaining an even temperature distribution around the tin cell. The Hart furnace is specially designed for maintaining and establishing the long freezing plateaus. The temperature range is from 100 ^{o}C up to 680 ^{o}C. It also has an inlet for injecting clean dry air, or an inert gas, to initiate the supercooling in a tin cell. For other methods (normal method) of initiation, the fixed-point cell might be initially removed by hand from the furnace to cause cooling or the temperature of the whole furnace needs to be reduced to remove the heat from the cell surface. Also, this furnace has the external cooling coils for circulation of tap water to reduce heat load to the laboratory.

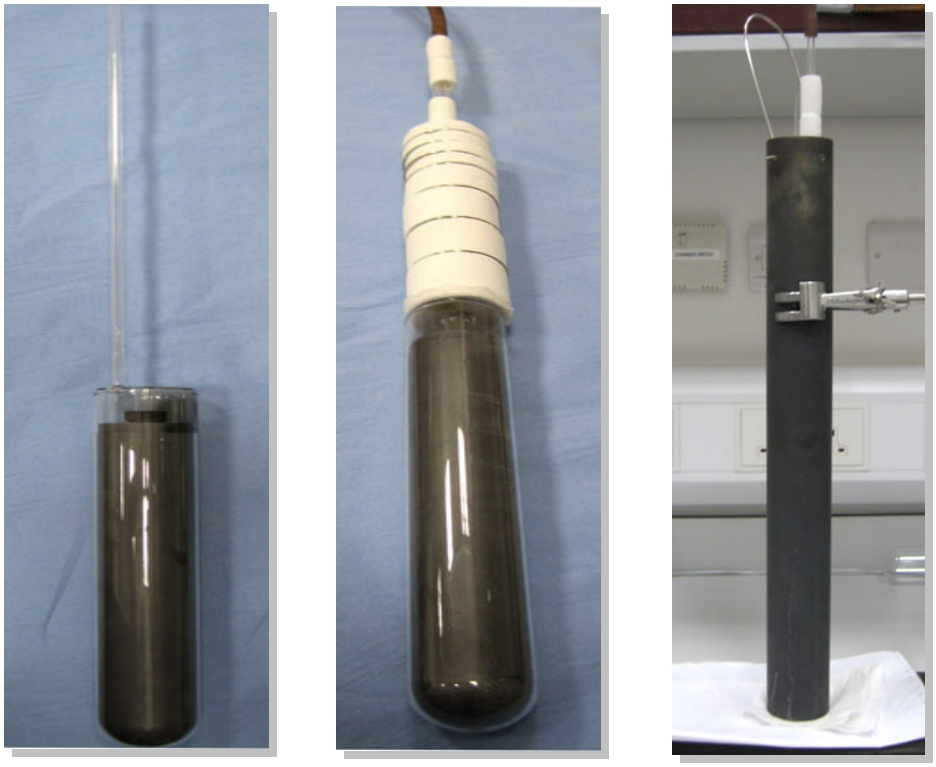

Figure 5.4 Assembly of the original Spanish tin opened-"sealed cell".

The freezing and melting transition temperatures were realised using a 25 ohm platinum resistance thermometer (PRT), serial number 909347. The ASL Model F18 ac Resistance Bridge was used to measure the resistance ratio values of the PRT against a 100 ohm Tinsley standard resistor, which was kept in the oil bath maintained at 20 °C.

In the first stage of the procedure of the freezing point of tin realisation, the tin ingot in the cell must be kept in the liquid state (fully molten) by holding the temperature at 5 ^{o}C above the equilibrium temperature (231.4 ^{o}C for this furnace) of tin. (The "equilibrium temperature" was that calculated to cause no further melting or freezing of the sample when it was already part molten/frozen).

Normally, the temperature for fast melting should be more than 5-10 ^{o}C above the equilibrium temperature to ensure the ingot was completely melted. The furnace temperature is set at half a degree below or above the equilibrium tin fixed point with settings for the cell to be frozen and melted, respectively. This means that the conditions are only quasi-adiabatic, but this was the desired way to carry out the tests, and these are considered the "normal" conditions for the realisation of fixed-points.

In fact, tin exhibits a large amount of supercooling (the process of crystal nucleation of a freezing pure metal at a temperature lower than its freezing point). Some kind of thermal shock is used to initiate the freeze. Two methods that were used are described in this section, namely a) turning the temperature of the whole furnace down by 6 ^{o}C and b) forcing an air flow up the furnace axis and around the tin cell.

In the first method, after the tin metal ingot was fully molten and held for 5 days, the furnace temperature was decreased by 6 ^{o}C below the equilibrium temperature until the temperature indicated by the PRT showed the under cooling. Then, the PRT was taken out of the cell and a cold metal rod inserted into the quartz tube in the tin cell and left there for 4 minutes to induce the freeze and to form a thin mantle of solid tin around the thermometer well. After that, the PRT was inserted back into the cell and the furnace was set to the temperature of the freezing point to realise the freezing plateau. The furnace setting was increased to the freezing temperature that was a half-degree below the equilibrium temperature.

In the second method, the temperature was decreased to the freezing point after the ingot was fully molten. Then, cold air was blown into the bottom of the furnace for 10 minutes to produce an upward airflow around the fixed-point cell until the supercooling started. This is the way to form the roughly uniform thickness of a solid shell at the outer crucible wall of tin. When tin recalescence started, the air flow was shut off and the furnace setting was kept at a stable freezing temperature. As is the case with the first method, the metal rod was inserted to initiate the inner freeze.

For the melting procedure, the furnace temperature was increased to about 5 °C higher than the equilibrium point. Due to the deep supercooling, the furnace was set at 5 °C below the equilibrium and left overnight or the cold air was let in for 10 minutes to obtain the fully frozen state of the ingot (rapidly frozen) before melting started. Then, in the following morning, the furnace temperature was set at half a degree above the equilibrium point. Then, the melting plateaus were realised.

The resistance values for all measurements of the freezing and melting curves were calculated from the resistance ratio of PRT and standard resistor values. The freezing and melting transitions of each initially “pure” tin cell were measured at least three times.

Then, the original “undoped” Spanish tin opened-“sealed cell” was calibrated by comparison against the Reference Isotech Sn184 with four PRTs (i.e. 909347,

909174, 909069, and 4849) noting the direct measurements on the freezing curves. These results were recorded when the Spanish tin cell was originally an opened-"sealed cell". The zero-power resistance values (0 mA) were used to present the resistance values of the thermometers in the work. The zero-power resistance values were calculated from two currents, i.e. 1 mA and $\sqrt{2}$ mA and also converted from the zero-power resistance ratio using the resistance value of the standard resistor. The reason why the zero-power resistance values were used is to eliminate the effect of variations in PRT self-heating in the fixed point cell.

All resistance values have been corrected by application of the hydrostatic pressure correction of each tin fixed-point cell. Nicholas and White [2001k]; Supplementary information for the ITS-90 [1997] reported that the measured temperature is affected by the depth of the fixed-point cell caused by the hydrostatic head of the metal above the PRT sensor. From the definition of fixed points in the ITS-90 scale, it describes "the hydrostatic head" - "the temperature dependence on the depth of the cell caused by the hydrostatic pressure of the metal, and the corrections should be applied" [Preston-Thomas, 1990]. Preston-Thomas [1990] shows the rate of the temperature change with the height of the freezing point of tin is 2.2×10^{-3} Km^{-1}. In theory, that rate of change explains that 1 meter below the surface of the freezing point of tin cell the temperature is 2.2 mK hotter. Then, this value is applied to calculate as in supplementary information to the ITS-90 and become the hydrostatic head value. For high purity Spanish tin and Reference Sn184 fixed-point cells, the hydrostatic head correction values after calculating are -0.265 mK and -0.428 mK, respectively. These two values will be used to correct for all experiments of Spanish tin fixed-point cell. The data of the resistance values include the hydrostatic head pressure corrections for the different those two cells.

All above experiments on high purity Spanish opened-"sealed cell" were tested in the old building of NPL. Then, all the equipment was moved to the new laboratory in the new building. Therefore, the experiment would be tested again. Also, the PRT 909347 was broken by accident, therefore these thermometer measurements would be replaced with PRT 4849 for measuring the temperature measurement in the further experiment steps. Therefore, the freezing and melting curves will be realised again with PRT 4849 by use the same equipment system.

5.4.1.2 High Purity "Undoped" Spanish Tin Fixed-Point Cell after Re-Assembly

a) Assembly of "Undoped" Spanish Tin Open Cell

After completing the initial freezing and melting measurements and obtaining the comparison results with the reference tin cell of high purity Spanish opened-"sealed cell", the quartz envelope of this opened-"sealed cell" was broken intentionally and only the graphite ingot was taken out. For the Spanish tin cell, the ingot (180 mm long and 34.5 mm outer diameter) was contained in a graphite crucible of length 200 mm and diameter 45 mm, which was held in a new container made from Pyrex (borosilicate) of length 470 mm and diameter 49 mm. Cells like this, containing up to about 1 kg of pure metal, are used in most National Metrology Institutes (NMIs) around the world. The total weight of the Spanish tin metal ingot was weighed with a balance, kept in the NPL Mass division. The weight of ingot was also calculated from the drawing dimension, which was measured from the real tin cell. The mass of Spanish tin was estimated by two methods:

a) Based on the dimensions of the Spanish tin ingot and the graphite re-entrance well, the volume of the tin and the graphite was calculated. (Using standard densities this was converted to mass).
b) As well as directly calculating the mass of tin, the calculated mass of graphite was subtracted from actually measured mass of graphite and tin together. (It is not possible to remove the graphite re-entrance-well as the tin clamps onto it during the freezing process.)

This procedure was checked before the high purity Spanish tin ingot was constructed in the new system and also was measured at the end of the experimental measurements. The whole Spanish tin ingot is shown in Figure 5.5.

Figure 5.5 High purity Spanish tin ingot and the graphite lid of the crucible.

In Figure 5.5, it also shows a hole on top of the graphite lid of the crucible, which was a hole in Isotech design. Isotech put it in so as to make it easier to let the air or argon out of the cells when they pump it before refilling with argon gas.

This ingot was put in the "typical arrangements". This Spanish tin cell was re-assembled in a new Pyrex tube with new thermalising components. All components for re-assembly are as labelled in Figure 5.6. The glassware was cleaned with a special cleaning glassware process as described in Section 5.6. Also, the bricks and the graphite discs were baked in the tube at 1100 ^{o}C. The "undoped" Spanish tin opened cell after re-assembly was inserted into the aluminium block (380 mm length), which was already standing in a three-zone Elite furnace. The aluminium block was used to keep the temperature along the length of the cell uniform. The cell was equipped with a re-entrant well of 10 mm outer diameter, for the insertion of a PRT. The bottom of the aluminium block was connected to the stainless tube through which external air could flow up the furnace axis and around the tin cell. Before the experiments, the whole system was tested using a Leybold Vacuum PhoeniXL 300 helium leak detector to verify that the system was completely leak tight (lowest detectable leak rate for helium < 5 x 10^{-12} mbar l /s).

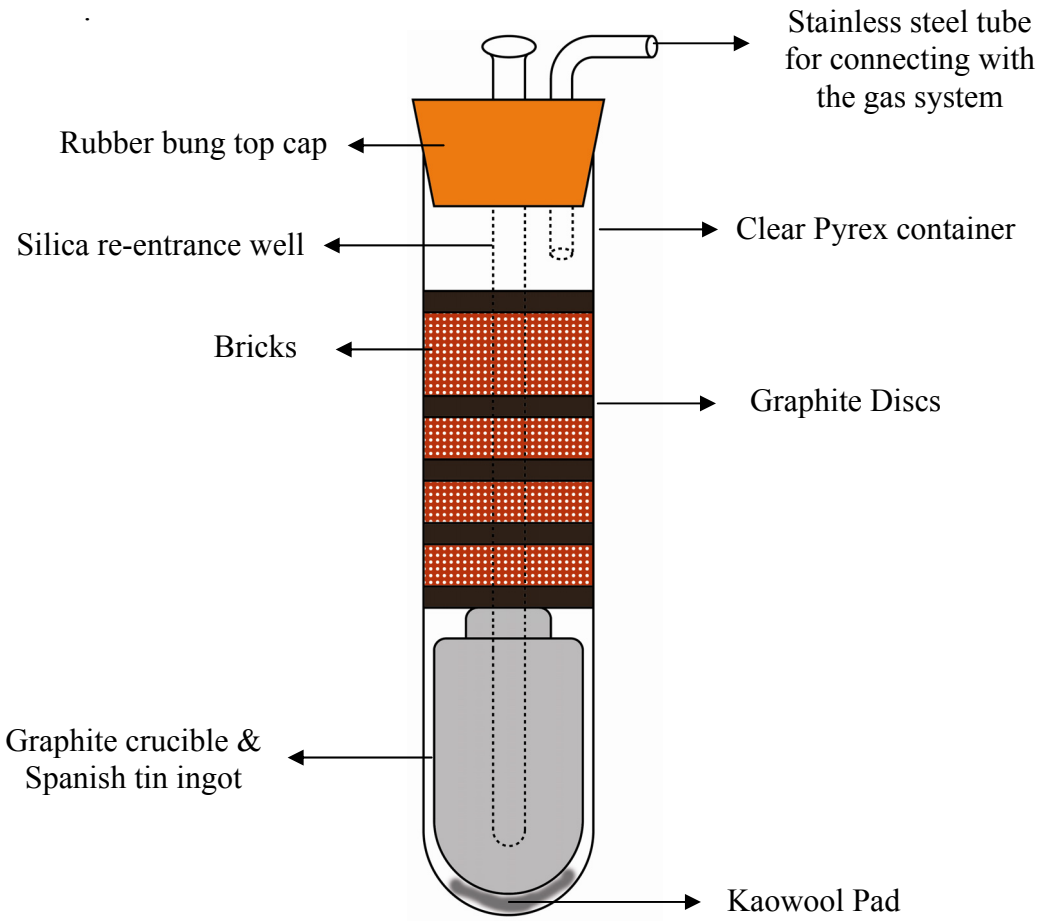

Figure 5.6 Drawing of high purity "undoped" Spanish tin fixed-point opened cell after re-assembly.

b) Temperature Realisation of "Undoped" Spanish Tin Open Cell

After inserting the cell into the furnace, this Spanish tin open cell was filled and evacuated with the argon gas several times and then was filled with pure argon gas with a pressure set at about 101.3 kPa (measured by a Wallace and Tiernan precision pressure Gauge) at its operational temperature to assist thermal exchange inside the cell, to protect the graphite from oxidation and to prevent metal vaporization. A three zone Elite furnace was used for maintaining the temperatures at the tin fixed-point, but the set point temperature was offset by different amounts for the cell to be frozen or melted. This means that the conditions are only quasi-adiabatic -but this is how the tests were intended to be carried out. A Eurotherm controller was used to control the furnace temperature, which applied only 110V (through a transformer) to the heater to reduce the electrical noise. The PRT 4849 was used to

realise the temperature fixed point by reading the resistance ratio from the ASL ac Resistance Bridge against a 100 ohm Tinsley standard resistor.

First of all, the equilibrium temperature of this cell after re-assembly needed to be measured in the new furnace. Then, the temperature was set at 5 ^{o}C above the balance point and maintained for 5 days for the ingot to fully melt and stabilise. After this, the temperature of the furnace was reduced to 5 ^{o}C below the anticipated freeze temperature. When the supercooling started, the PRT was replaced by a cold brass metal in the silica rod. After 4 minutes, the PRT was installed back to the cell and the temperature was increased to the freeze temperature. When the PRT had shown no change for some minutes, the plateau was achieved. The melting realisation procedures were explained in the previous section. All melting curves were obtained after rapid freeze. Three curves of each freezing and melting temperatures were recorded. The resistance values are obtained by combining the bridge ratio measurements and the standard resistor values.

Following the freezing and melting realisations, this tin cell needed to be calibrated by comparison with the Reference Isotech Sn184 fixed-point cell again to check how much the temperature of the cell changed from the initial "pure" tin value, after re-assembling the cell. All resistance values have been corrected by application of the hydrostatic pressure correction of each tin fixed-point cell. The average resistance values for all PRTs in the calibration measurements by comparison method show the calculated values at zero-power dissipation. This is to reduce errors from changes in the self-heating effect. The self-heating effect is the temperature phenomenon as explained in Batageli's report [Batagelj *et al*., 2003]. The average resistance values in the calibration by comparison method were checked with three PRTs, namely PRT 909174, 909069, and 4849. The furnace setting was set to a nominal value of 229.1 ^{o}C for all freezing realisation measurements. Stability performances of three PRTs measured at the triple point of water before and after the calibration by comparison method were also carried out.

c) Elemental Analysis by Glow Discharge Mass Spectrometry (GD-MS)

After completing the initial freezing and melting measurements using the high purity Spanish tin, four small pieces were removed from three areas of the tin ingot, the top, the middle and the bottom, with a small clean hacksaw. An example of cutting

a sample off for a GD-MS analysis of the Al ingot is shown in Figure 5.15. Three of the samples were sent off to the National Research Council of Canada (NRC) for the GD-MS analysis in order to determine the quantity and distribution (or uniformity) of the impurity elements within the "pure" tin before doping. The fourth sample, cut from the middle of the ingot, was kept at NPL; this sample would be sent to NRC subsequently with the doped samples for GD-MS analysis.

d) Mixing Technique

After cutting the samples off from the tin ingot, the originally pure Spanish tin ingots were doped with two types of impurities, namely cobalt and lead, to the total concentrations (in ppmw) of 5.5 and 7.4 for Co, and 7.9 and 31.4 for Pb. After the resistance ratios of the PRTs in "pure" tin were obtained, the masses of pure cobalt (over 99.99%), and lead (over 99.99%) wires, employed as impurities for doping, were weighed with a microbalance (Mettler AT20). The uncertainty components of the weighing scales (Mettler AT20) are as follows:

Negligible for the scale error

1 μg for repeatability (normal distribution)

2 μg for balance resolution (rectangular distribution)

From the above information, obtained from NPL Mass Section, the uncertainty of the "weighing" itself is very small when compared with the total mass of the impurity and the uncertainty due to the mass of the enclosed graphite reentrant well. In other words, the "weighing" uncertainty is negligible.

The presence of impurities in a pure metal normally causes an offset which increases or decreases the temperatures depending on the nature of the impurity. In previous work the Sn-X binary alloy system was studied at larger fractions of impurity X [Hansen, 1958], and the tin temperature was interpolated to be depressed by 0.60 mK/ppmw and 0.133 mK/ppmw for cobalt and lead impurity, respectively. It is discovered that the temperature change depends on the chemical composition of Sn-Co and Sn-Pb alloys as shown in the phase diagram. From the phase diagram calculation, it is found that 1 ppmw of Co can reduce the temperature of pure Sn by 0.6 mK. Therefore, Co was weighed at about 5.2 mg, which equal to 5.5 ppmw, which was expected to decrease the temperature of the "undoped" Spanish cell by 3 mK. After the Spanish Sn had been doped with Co 5.5 ppmw it was further doped with

1.9 ppmw (1.83 mg) more Co, expected to reduce the temperature by 1 mK more (Co 7.8 ppmw and decreased 4 mK in total). Then, the amount of Pb impurity concentrations at 7.9 ppmw (reduced 1 mK) was added into the ingot. After that, an additional amount of lead impurity concentration 23.5 ppmw was put in the ingot, resulting in the total concentration of lead impurity of 31.4 ppmw (4 mK decreasing). The first Co impurity metal was added to the space in the ingot vacated by the samples removed from the top, the middle, and the bottom; then the other impurities would be added to the same locations. An example of the metal wire is given in Figure 5.7.

Figure 5.7 An example of the metal wire used as an impurity for doping in Spanish tin cell.

After each doping, the ingot was re-inserted back into the graphite crucible and the Pyrex container. Then the assembled cell was put into the furnaces and set at 8 ^{o}C above the tin melting temperature for several days to ensure a good mixing of the impurities within the tin. At least three freezing and melting plateaus after each doping were obtained in order to ensure the repeatability of the fixed-point realisation. However, since the tin ingot was found to be stuck to the graphite crucible before adding the second lot of Co impurity; subsequent addition of the Co impurity could only be made through the hole at the top of the graphite lid ingot. To freeze, the furnace controller was set 5 ^{o}C below the freezing temperature. One hour later, the supercooling still had not started; thus the cell was lifted out from the furnace until the curve indicated the under cooling. Then, the cell was installed back to the furnace and two cold metals in silica rod replaced the monitoring PRT. After 4 minutes, the PRT was put back to the cell then the furnace was set to the actual freezing temperature.

After adding the Pb impurity, the freeze process was observed to start by itself without lifting the cell out of the furnace.

During this time the doped cell was compared against the Reference tin cell by cross-transfer of the PRTs. This allowed the measurement of the temperature drop from the initial "pure" tin to the doped tin state. Cross comparison to the reference cell allows the removal of any shift due to any instability in the PRT itself, which is possible at this level of resolution. Stability resistance values of the PRTs also were measured at the triple point of water, before and after the calibration by comparison method. All measurements were recorded at 0 mA.

After completing the freezing and melting measurements after doping with the impurities in the Spanish tin, the samples were removed from the tin ingot with a small-cleaned hacksaw. The previous GD-MS results of the Spanish tin fixed-point cell before impurity doping indicate that the tin and the impurities are well mixed after the tin is properly molten. The impurity levels in the three areas of the tin ingot show homogeneity of the impurity concentration. Therefore, only one piece of the Spanish Sn after doping with Co and Pb impurities was cut from the ingot for the GD-MS analysis. This sample together with the old sample from the ingot before doping and kept at NPL was analysed with the GD-MS. The result from the old sample would be compared with those from the previous three samples from the ingot before doping in order to verify the repeatability of the GD-MS calibration.

5.4.2 Making and Realisation of Mini Isotech Tin Fixed-Point Cell

The explanation on the assembly and the temperature realisation methods of the high purity Mini Isotech tin fixed-point cell will be presented in four sections: Section 5.4.2.1 contains the assembly of "undoped" Mini Isotech tin opened cell, Section 5.4.2.2 shows the method for the temperature realisation of "undoped" Mini Isotech tin opened cell, Section 5.4.2.3 presents the process for preparing the tin samples for elemental Analysis by GD-MS, and Section 5.4.2.4 describes the impurity mixing technique.

5.4.2.1 Assembly of "Undoped" Mini Isotech Tin Opened Cell

A standard purity (nominally 99.9999%) tin fixed-point cell, obtained from the Isotech Technology Company, was used to study the influence of trace antimony impurity on the equilibrium tin temperature. Antimony is the only impurity that is known to elevate the liquidus temperature of tin. This tin cell was also named after its donors as "Mini Isotech tin". The Mini Isotech tin ingot was smaller than normal i.e. it was 110 mm in length, 26 mm in outer diameter, and had an inner diameter of 16 mm. The hydrostatic head values were calculated from this depth of the ingot. The total mass of tin sample put in this cell was approximately 240 g. The total weight of the Mini Isotech tin metal ingot was weighed with a balance, kept in the NPL Mass division. The weight of ingot also was calculated from the drawing dimensions, which was measured from the real tin cell. The mass of Mini Isotech tin was estimated by two methods:

a) Based on the dimensions of the Mini Isotech tin ingot and the graphite re-entrance well, the volume of the tin and the graphite was calculated. Using standard densities the volume was converted to mass.

b) As well as directly calculating the mass of tin, the calculated mass of graphite was subtracted from the actually measured mass of graphite and tin together. (It is not possible to remove the graphite re-entrance-well as the tin clamps onto it during the freezing process.) This procedure was checked before the high purity Mini tin ingot was constructed in the new system and also was measured at the end of the experimental measurements.

The Mini Isotech tin ingot was housed inside a high purity graphite crucible (about 130 mm long and 32 mm outer diameter) contained within a Pyrex tube. They had never been used for assembly; therefore the bricks and the graphite discs were put in a translucent long silica tube and then were baked at 1100 ^{o}C in a three-zone Elite furnace, as shown in Figure 5.8, for a day. All components of Mini Isotech tin cell are presented in Figure 5.9. Also, the Pyrex container and the silica re-entrance well had to be cleaned before using as explained in Section 5.6. The assembly and the drawing of high purity "undoped" Mini Isotech tin fixed-point opened cell are shown in Figures 5.10 and 5.11 respectively.

Figure 5.8 System for baking the bricks and graphite discs at 1100 ^{o}C.

The baking at 1100 ^{o}C was used in this work in order to eliminate any contamination, which can be volatile at high temperature. The completed fixed-point assembled cell was put in the nickel block before putting into a three-zone Carbolite furnace set for maintaining an even temperature distribution around the tin cell. The nickel block was used to maintain the vertical profile temperature for the Mini Isotech tin cell. Also, this block had been specially designed by drilling the bottom to attach the stainless steel tube underneath the block, where the external air could flow through the block hole and up the furnace axis and around the tin cell.

Figure 5.9 Components of the original Mini Isotech tin "opened cell" assembly (left) and Mini Isotech tin ingot (right).

Figure 5.10 Assembly of high purity "undoped" Mini Isotech tin fixed-point opened cell.

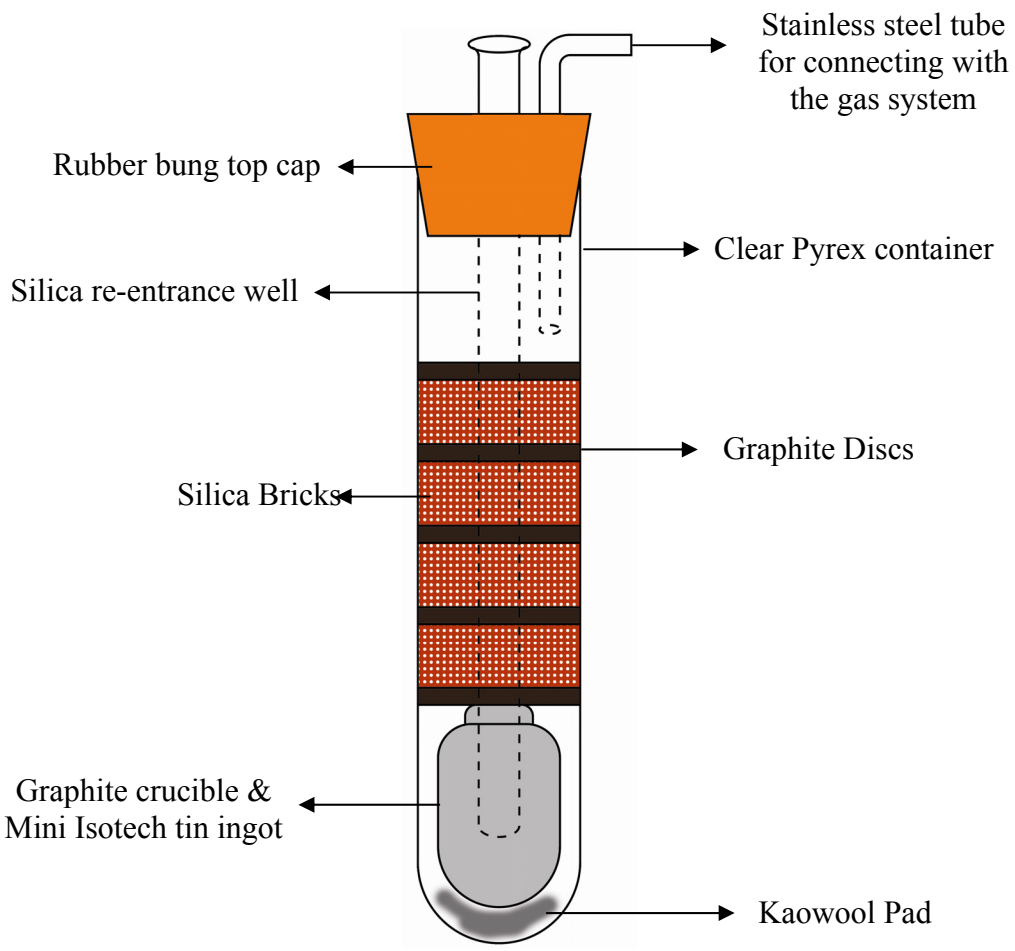

Figure 5.11 Drawing of high purity "undoped" Mini Isotech tin fixed-point opened cell.

Before starting the freezing and melting realisations in the Mini Isotech tin cell, it was argon filled and evacuated several times with the vacuum system to flush out any dust from the cell. The gas system was connected then to the cell. Before the inert gas was added into the fixed-point cell, the whole system was tested using a Leybold Vacuum PhoeniXL 300 helium leak detector. Then, the high purity argon gas was filled into the cell at a pressure of 101.3 kPa at the fixed-point temperature.

5.4.2.2 Temperature Realisation of "Undoped" Mini Isotech tin opened cell

After installing the tin cell in the three-zone furnace, the equilibrium temperature of the tin metal was found by setting about 5 ^{o}C above the expected tin melting temperature. Then, the furnace was left at 5 ^{o}C – 10 ^{o}C above the tin melting temperature to ensure a good mixing within the molten tin and the temperature was

left in this condition for several days. The tin metal was entirely in the liquid phase at this stage. After that, the temperature of the Carbolite furnace was set below or above the equilibrium tin fixed-point with settings for the cell to be frozen or melted respectively. All temperature realisations of the undoped Mini Isotech tin were measured with an F18 ac Resistance Bridge connected to a PRT 909174.

As previous mentioned in Spanish tin cell about the supercooling, the high purity tin metal has the characteristic of deep supercooling. The supercooling of tin can be as much as 10 °C below the freezing temperature. If the furnace was set in the normal method, i.e. let the temperature cool down to the nucleation point by itself, then it would probably not get back in time to realise the freezing plateau. The realisation of the Mini Isotech tin freezing plateau was performed in a manner similar to the Spanish tin. After the metal was fully molten, the furnace controller was set 6 °C below the actual freeze temperature; this was anticipated to be below the bottom of the supercool. The under cooling of tin metal was indicated by the PRT measurement as the temperature curve would turn upwards at that point. However, the results showed that it took about 1 hour to get to the nucleation point. The freezing and melting procedures for this cell was similar to those applied to the Spanish tin cell except that no external air flow was allowed around the cell due to the furnace difference. The freezing and melting transitions of the initially “pure” Mini Isotech tin cell were measured at least three times. The resistance values included the hydrostatic head correction. For high purity Mini Isotech tin and Reference Sn184 fixed-point cells, the hydrostatic head correction values after calculating are -0.149 mK and -0.428 mK, respectively.

Then, the initially “pure” Mini Isotech tin cell was calibrated by comparison on the freezing curves against the Reference Isotech Sn184 with three PRTs (i.e. 909174, 909069, and 4849) at zero-power resistance values (0 mA) to avoid the self-heating effect of the PRTs. The stability of the three PRTs was analysed again by realising the temperature in the triple point of water.

5.4.2.3 Elemental Analysis by GD-MS of “Undoped” Mini Isotech tin cell

After realising the freezing and melting curves of the “undoped” Mini Isotech tin cell, a total of two small pieces were cut from two areas of the tin ingot; namely the middle of the top part and of the bottom half on the opposite side with a small

clean hacksaw. One piece was then analysed to determine the quantity of the impurity elements within the cell using GD-MS technique. The other piece was kept at NPL. After completing the freezing and melting realisations in the doped tin cell, a sample was cut from the Mini Isotech tin. Both this doped sample and the previously undoped sample kept at NPL were now analysed with the GD-MS technique at NRC.

5.4.2.4 Mixing Technique of "doped" Mini Isotech tin cell

The originally pure Mini Isotech tin ingot was doped with antimony (Sb) impurity; total concentrations as follows (in ppmw): Sb 7.8 and 23.2. The Sb impurity metal was put on the top, the middle, and the bottom of this ingot. Sb was chosen as the impurity in this ingot as it is the only substance that is expected to increase the melting temperature of Sn. However previous work [Zhang *et al.*, 2008] has shown unusual results that have not yet been fully explained and which produce melting curves that can not be modelled by MTDATA [see the analogous effect in Figure 9 of Ti in Al in Head's publication [Head *et al.*, 2008]. (MTDATA shows better agreement with impurities that decrease the temperature – see same paper by Head [Head *et al*, 2008]).

The antimony (Sb) impurity was selected to study the trace impurity effect on high purity Mini Isotech tin cell temperature fixed point. In previous work the Sn-X binary alloy system was studied at larger fractions of impurity X [Hansen, 1958], the tin transition plateau was raised by 0.128 mK/ppmw of antimony impurity. Our measurements using lower concentrations of dopants planned to test the interpolation of this previous data obtained using relatively high levels of impurities.

The mass of pure antimony powder (99.5%) was weighed with a microbalance (Mettler AT20). Two lots of antimony powder were used as impurity to produce the concentrations of 7.8 and 23.2 ppmw in the ingot. Each lot was divided into three parts for adding to the top, the middle, and the bottom of the Mini Isotech tin ingot. After re-inserting the ingot into the cell, the assembled cell was put into the furnace set at 10 ^{o}C above the tin melting temperature for 5 days. The freezing and melting procedures were the same as the undoped Mini Isotech tin. Three freezing and melting plateaus after each doping were realised. After obtaining all curves at 7.8 ppmw antimony doping, the PRT 909174 was broken unexpectedly; therefore the PRT 909069 and 280140 were used to re-measure all freezing and melting curves. From the

results, the PRT 280140 showed more stability than 909069. Thus, the PRT 280140 was selected for repeated checking of all freezing and melting curves and also was used for the further experiment on the 23.2 ppmw doped antimony. During this time the freeze peak of the doped Mini Isotech tin cell was compared against the new sealed tin reference cell by cross-transfer of the PRTs. This allowed the measurement of how much the temperature of the doped cell dropped (increased) from the initial "pure" tin value. Cross comparison to the reference cell allows the removal of any shift due to any instability in the PRT itself, which is possible at this level of resolution. Again the water triple point values of the PRT were checked before and after the calibration.

5.5 Making and Realisation the Aluminium Fixed-Point Cells

Two nominally 99.9999% pure aluminium fixed-point cells, according to the NPL design, were used in this study to realise the reference standard temperature. The two cells were fabricated in 1974 (Al 174) and 1998 (Al 298), respectively. Before starting, a note of the size and weight of each cell was made. Their experiments are segregated into two separate experiments as investigate in each aluminium cell namely Al 174 and Al 298 fixed-point cells, respectively.

5.5.1 Making and Realisation Aluminium (Al 174) Fixed-Point Cell

The details of the cell assembly and the process of the experiment studied in Al 174 cell will be described as follows; Section 5.5.1.1 presents the assembly of the Al 174 Opened fixed-point cell, Section 5.5.1.2 discusses the temperature realisation of initially "undoped" Al 174 after re-assembling with the new components, Section 5.5.1.3 mentions the process for preparing the Al samples for GD-MS analysis, and Section 5.5.1.4 explained the mixing technique between impurity doping and Al metal ingot.

5.5.1.1 Assembly of "Undoped" Al 174 Opened Fixed-Point Cell

The old NPL Al 174 opened fixed-point cell was made in 1974. The original Al 174 cell before taking apart and re-assembling in the new components and the new translucent silica container shows in Figure 5.12. Since this cell was quite old, some parts of assembly had been damaged and worn out. The Al 174 ingot and the brass top cap from the original cell had still been used to be the components for a new opened fixed-point cell. First of all, the measurements of the sizes of the Al ingot, the graphite crucible, including the weight of aluminium metal were checked.

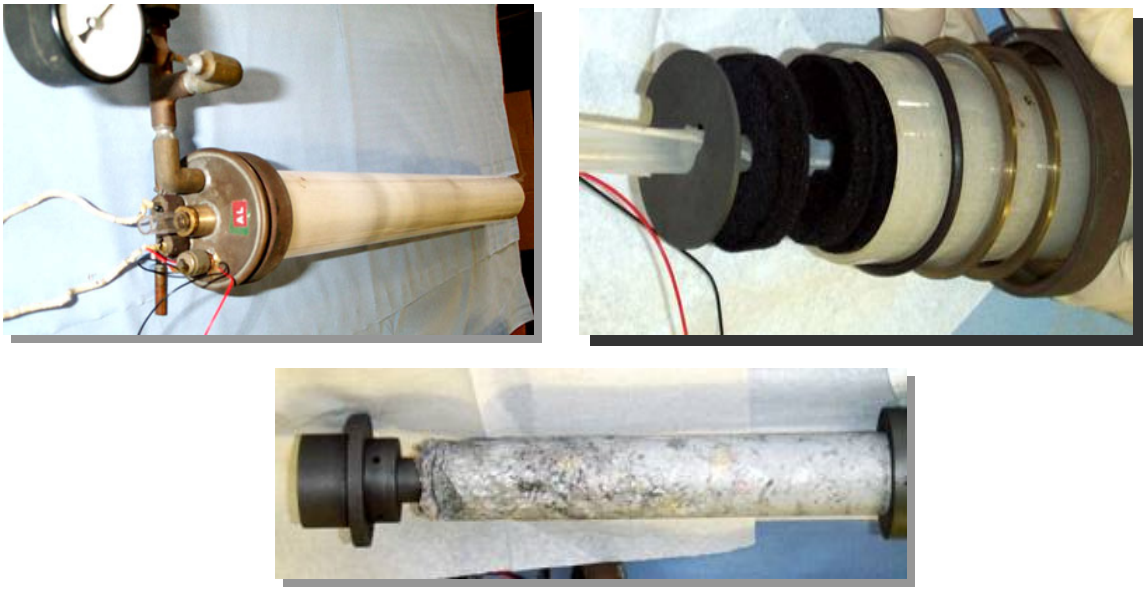

Figure 5.12 original Al174 fixed-point cells before re-assembling.

The weight of ingot also was calculated from the drawing dimension, which was measured from the real aluminium cell. The mass of Al 174 was estimated by two methods. Based on the dimensions of the Al 174 ingot and the graphite re-entrance well, the volume of the Al 174 and the graphite was calculated. (Using standard densities this was converted to mass). As well as directly calculating the mass of aluminium, the calculated mass of graphite was subtracted from actually measured mass of graphite and aluminium together. (It is not possible to remove the graphite re-entrance-well as the tin clamps onto it during the freezing process.) This procedure was carried out before the high purity Al 174 ingot was constructed in the new system and also was measured at the end of the experiments.

The Al 174 opened cell consists of a translucent silica cylinder used as a container of the cell with the brass top cap, a sand-blasted silica thermometer well for inserting the standard platinum resistance thermometer (SPRT), graphite felt discs and graphite discs as a thermal insulator. The components and the assembled cell are shown in Figure 5.13. Before the new translucent container and the silica thermometer well were used, they were cleaned with dilute nitric acid and acetone as explained the glassware cleaning process in Section 5.6. Moreover, the graphite felt discs and the graphite discs were baked in the vacuum system at 1100 ^{o}C for 2 days before using.

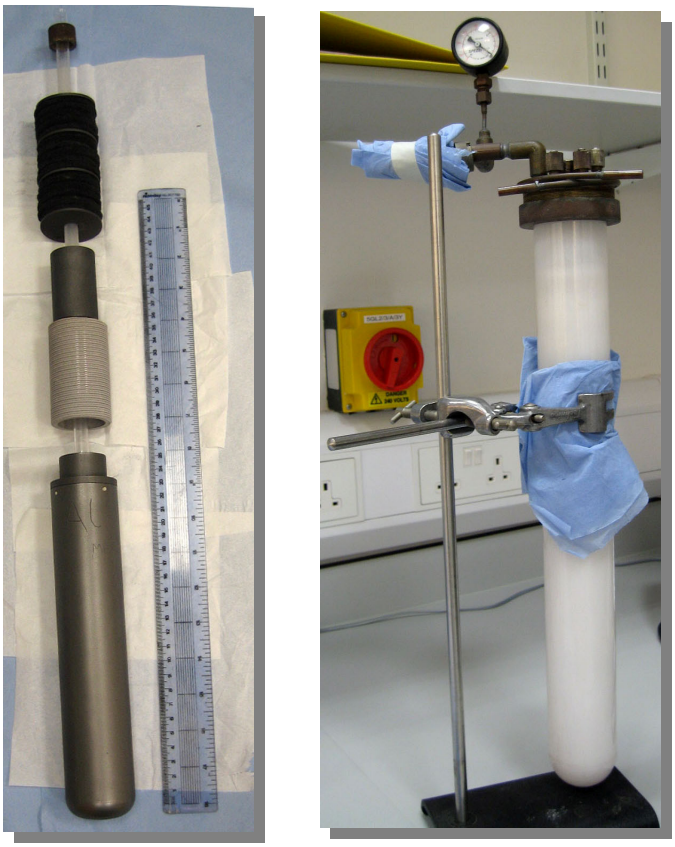

Figure 5.13 Assembly of high purity "undoped" Al 174 fixed-point opened cell.

The aluminium base material of Al 174 ingot was put inside the graphite crucible originally made according to an old NPL design. The ingot is 185 mm long and 29 mm outer diameter. The diagram of the Al 174 fixed-point cell is shown in Figure 5.14. The graphite crucible is 29.5 mm in inner diameter, is 47 mm in outer diameter and is 250 mm in length. This crucible is contained within the translucent silica (460 mm long, 54 mm outer and 49 mm inner diameters) with a brass top cap. The diagram of "undoped" Al 174 fixed-point opened cell assembly is presented in

Figure 5.14. On the brass top cap, there is a cooling water tube, which was connected to a cooling water system at 18 ^{o}C. It was typically used for removing the heat and cooling the temperature down, which it was to ensure that the O-ring was not destroyed by the furnace heat at the Al temperature.

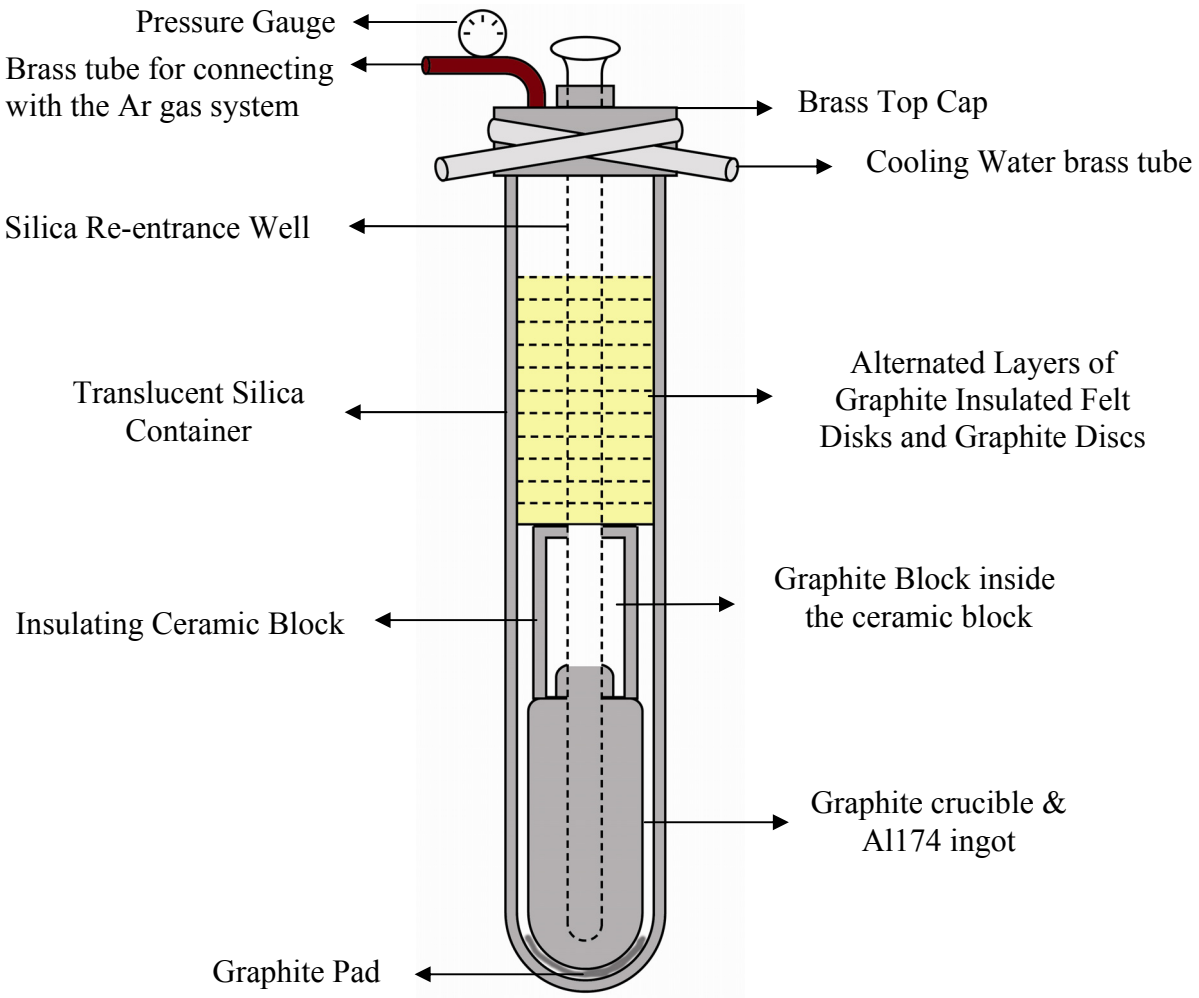

Figure 5.14 Diagram of high purity "undoped" Al 174 fixed-point opened cell assembly.

5.5.1.2 Temperature Realisation of "Undoped" Al 174 Opened Fixed-Point

The assembled cell was inserted in a single zone Carbolite furnace. The Al cell was connected to a gas control system including a vacuum pump (Edwards XDS10 scroll pump) and a Wallace & Tiernan precision pressure gauge. Before the experiments, the whole system was tested using a Leybold Vacuum PhoeniXL 300 helium leak detector to confirm a seal adequate for prohibiting any contamination from the surrounding. Afterwards, the cell, made as "Open" cell, was filled with argon gas and the pressure in the cell was set at about 101.3 kPa at the fixed-point transition to assist thermal exchange inside the cell, to protect the graphite from oxidation and to prevent metal vaporization and other contamination gases into the cell assembly.

The single zone Carbolite furnace was used in conjunction with a potassium heat pipe for maintaining a uniform temperature above or below the phase transition temperature of the Al 174 cell. The function of the potassium heat pipe is to provide the base metal in the ingot with an isothermal environment. A Thyristor controller was used to control the furnace temperature, which applied only 120 volts (through a transformer) to reduce the electrical noise. As the phase transition is powered by an offset in the furnace temperature, it means that the conditions are only quasi-adiabatic, but this was the desired way to carry out the tests, as these are the "normal" conditions for the realisation of fixed-points.

Before the temperature realisation started, the setting point of the balance temperature was investigated. The furnace controller was set to 6 °C higher than the actual equilibrium temperature to ensure the Al metal within the ingot was fully molten for 5 days. A PRT 250329, which was connected with an ac F18 Bridge, was used to record the resistance ratio from the freezing and melting temperatures. The PRT was annealed using the strength annealing, i.e. PRT was left at 670 °C for 3 hours then let it cooled down to 450 °C and remove it to room temperature, before realising the Al temperature. Normally, the Al metal is characterised by a relatively short supercool. The supercooling can be expected to be less than 0.5 °C. To freeze, the suggested setting is 5 °C below the freeze temperature; this is, assuredly, below the bottom of the supercooling quickly. It took about 25 minutes to get the under cooling point. The nucleation occurred at this point and the freeze was started from the bottom of the cell inwards. Then, the PRT was removed and replaced by two ceramics in silica rods (1 minute each). After 2 minutes remove the rod and replace the PRT. This

procedure made a radial freeze from the outside to the inside walls of the Al cell toward the centre. Then, the cell was maintained at an operating temperature, i.e. - 0.5 ^{o}C with respect to the equilibrium temperature, which was the setting for the cell to be frozen. Finally, the freezing plateaus of the "undoped" Al 174 cell were achieved at least three times.

Following the freezing process, the furnace controller was increased to 5 ^{o}C above the equilibrium temperature. The metal in the cell was entirely in the liquid phase. After that, the melting curves were realised after a rapid freeze was obtained. The temperature was set at + 0.5 ^{o}C of the equilibrium temperature, which was the setting for the cell to be melted. The resistance ratios of the PRT measurements were recorded using an Automatic Systems Laboratories Model F18 ac resistance bridge, to monitor the changing or equilibrium temperature of the fixed-point cell. The stability of the PRTs was then determined by comparison with the NPL standard Al 1205 cell. The PRT number 250329 was used to demonstrate the fixed-point realisation.

Before adding the impurities in Al 174 cell, the peak of freezing curve of this initial Al 174 cell had been compared against with the "NPL national standard" (Al 1205) with two PRTs (serial number 250329 and 261198). The reason why the freeze peak had been selected to use was all freezing curves of the initial Al 174 had dropped and were not flat enough to do the comparison between the cells throughout the full length of the freeze. This comparison indicated how good the Al 174 was and how much temperature dropped from the high purity National standard Al cell. All results are corrected for the hydrostatic head pressure of both Al cells. For high purity Al 174 and NPL standard Al, the hydrostatic head correction values after calculating are about -0.198 mK and -0.185 mK, respectively.

5.5.1.3 Elemental Analysis by GD-MS of Al 174 Opened Fixed-Point Cell

Thereafter four small samples of the Al 174 ingot were cut from the top, middle, and bottom by the cleaned small hacksaw. Three pieces were sent for chemical analysis to determine the distribution of the impurity elements within the "pure" aluminium, before deliberate doping, by using GD-MS at the NRC. An example of cutting a sample off is shown in Figure 5.15. One piece was kept in NPL for a year later, which was detected at the same time as the doped sample. Subsequently the

impurity levels in the aluminium sample after doping will be measured again by GD-MS.

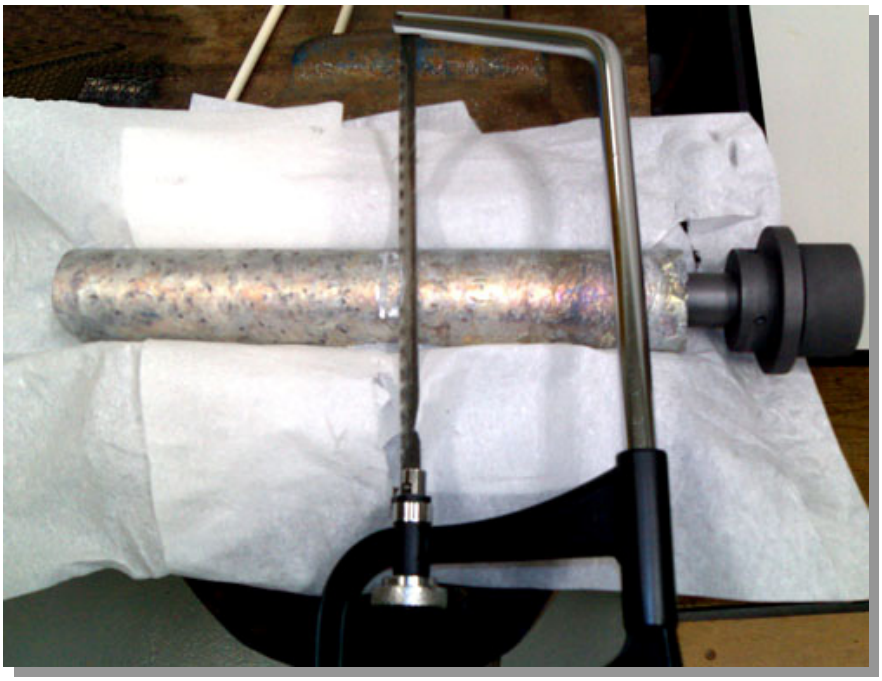

Figure 5.15 Cutting a sample off for a GD-MS analysis of "undoped" Al 174 ingot.

5.5.1.4 Mixing Technique of Al 174 Opened Fixed-Point Cell

After the equilibrium curves of "initial" Al 174 cell were completely measured, two types of impurities; namely copper and silicon were selected for doping. For the Al 174 fixed-point, high purity copper (99.99+%) and silicon (99.998%) were used to perform the study. After the equilibrium curves of "initial" Al 174 cell were completely measured, two types of impurities; namely copper wire and silicon powder were selected for doping. Each impurity was dropped on the top, the middle, and the bottom of the originally pure Al 174 sample in increasing concentrations as follows (in ppmw); Cu 8.3 and 16.2, Si 4.7 and 9.8. In prior experiments on these binary alloy systems, using higher levels of impurities [Hansen, 1958], the fixed-point temperature of aluminium was interpolated to be depressed by 0.37 mK/ppmw of copper and 0.71 mK/ppmw of silicon impurity. The temperature values of pure Al 174 were decreased by the increased amount of the Cu, which were expected to decrease by 3 and 6 mK, respectively. Then, the increased amounts of silicon impurity cause the

aluminium temperature to decease with respect to the Al-Cu by 3 and 6 mK, respectively.

The masses of pure copper (99.99+%), and silicon (99.998%), employed as impurities for doping, were weighed by a microbalance (Mettler AT20).

The uncertainty components of this weighing scale (Mettler AT20) are as follows;

Negligible for the scale error

1 μg for repeatability (normal distribution)

2 μg for balance resolution (rectangular distribution)

From the above information, obtained from NPL Mass section, the uncertainty of the "weighing" itself is very small when compared with total mass of the impurity and the uncertainty due to the mass of the enclosed graphite reentrant well. Therefore, the "weighing" uncertainty is negligible in this research.

The whole sample after each doping was held at 5 ^{o}C - 8 ^{o}C above the aluminium melting temperature for several days to ensure a good mixture of aluminium and their trace impurities. The temperature changes during freezing and melting of the aluminium after each doping were measured and compared with the original curves to find out how much each of the trace impurities affected the equilibrium temperatures of the aluminium fixed point.

After any impurities were doped in the aluminium ingot, the balance point was checked to find what the proper melting and freezing temperature setting would be. (The "balance point" is the furnace setting that should neither freeze nor melt a sample i.e. the setting that would, ideally, hold the ingot at the fixed-point temperature). The freezing/melting processes and the temperature realisations after doping were similar to the previous details in undoped Al 174 temperature realisation.

The shifts and shapes of freezing and melting curves during freezing and melting of the aluminium after doping were measured and compared with the original curves by use of the freeze peak to find out how much the trace impurities affected the temperatures of the Al 174 fixed points. As thermometers drift, a comparison between the doped and NPL standard aluminium cells was carried out to investigate how much the trace impurities affected the temperatures of the initially "undoped" Al 174 fixed-point cell. This is to ensure the reliable measurement of the small temperature shift due to the trace impurities, and not from the PRTs' instability. The offsets of the melting curves need to be corrected following "re-calibration" of the PRTs by

comparison of the peak of the freezing curves against the NPL reference Al 1205 cell. The water triple point was realised to check the stability of the PRTs after doing the comparisons.

5.5.2 Making and Realisation Aluminium (Al 298) Fixed-Point Cell

The aluminium 298 fixed-point ingot was named as the serial number, which appeared on the graphite crucible as shown in Figure 5.16. This cell was made in 1998, according to the NPL design.

Figure 5.16 Aluminium 298 fixed-point ingot.

All processes of this experiment studied in the Al 298 cell will be mentioned in details as follows; Section 5.5.2.1 explains the Al 298 opened fixed-point cell assembly, Section 5.5.2.2 shows the process of the temperature realisation of initially "undoped" Al 298, Section 5.5.2.3 presents the process for preparing the Al samples for GD-MS analysis, and Section 5.5.2.4 discuss the mixing technique for adding the impurities into the Al metal ingot.

5.5.2.1 Assembly of "Undoped" Al 298 Opened Fixed-Point Cell

All components of the assembled Al 298 fixed-point cell never been used excepting the ingot and graphite crucible. The components are presented in Figure 5.17. Because all glassware never had been used; therefore they needed to be cleaned as explained in Section 5.6 (cleaning glassware process). For the graphite felt and graphite discs, they were baked at 1100 ^{o}C for two days. The graphite crucible and all components were assembled to be an opened fixed-point cell as shown in Figure 5.18. Also, the diagram of Al 298 opened cell is presents in Figure 5.19. The measurements of the sizes of the Al ingot, the graphite crucible, including the weight of Al298 metal were checked**.** The total mass of the aluminium (Al 298) fixed-point metal ingot was weighed by a balance, which is in the NPL Mass division.

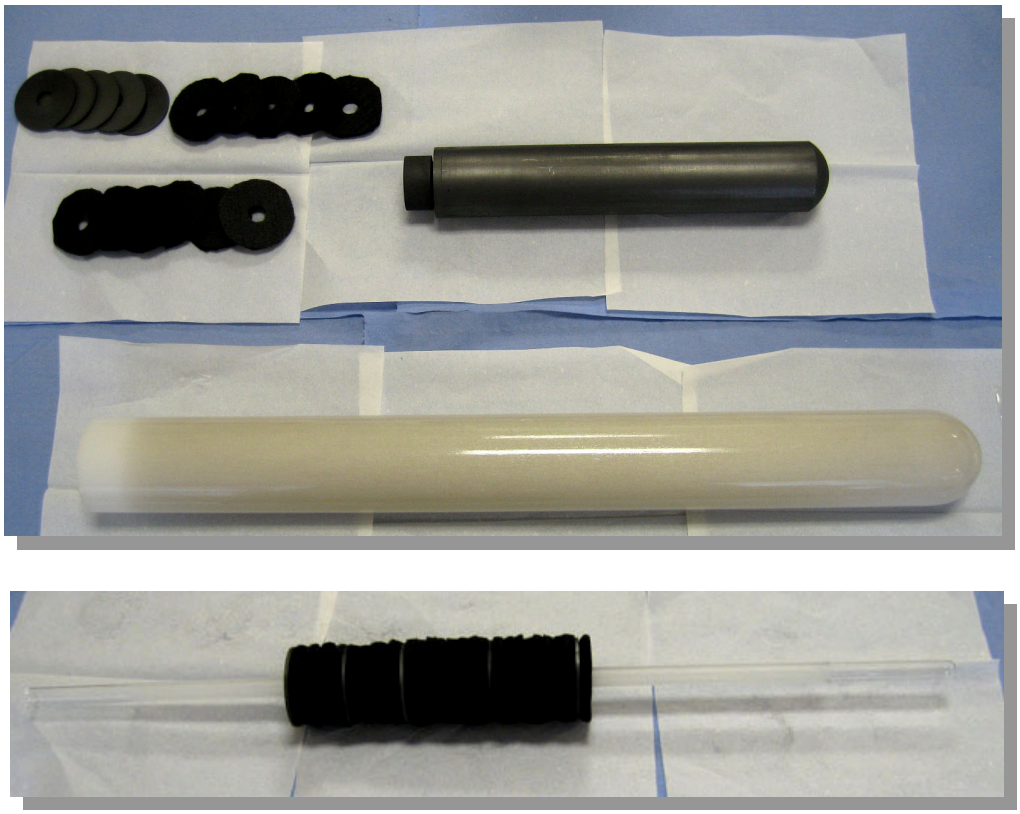

Figure 5.17 Components of aluminium (298) fixed-point cell: namely the graphite crucible, the aluminium 298 ingot (not shown), the graphite felt discs (99.99% purity), the graphite discs, the translucent silica tube. The silica re-entrance well (the bottom) was assembled with the layers of the graphite felt and the graphite discs.

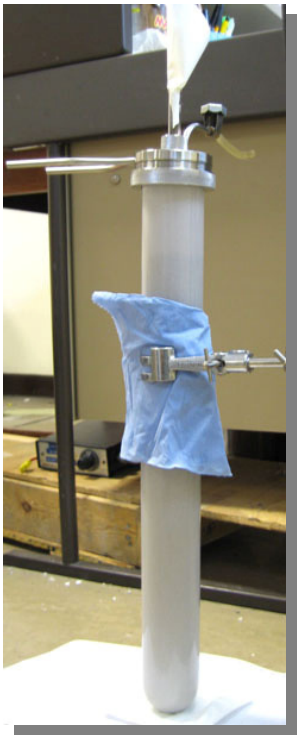

Figure 5.18 "undoped" Al 298 fixed-point opened cell.

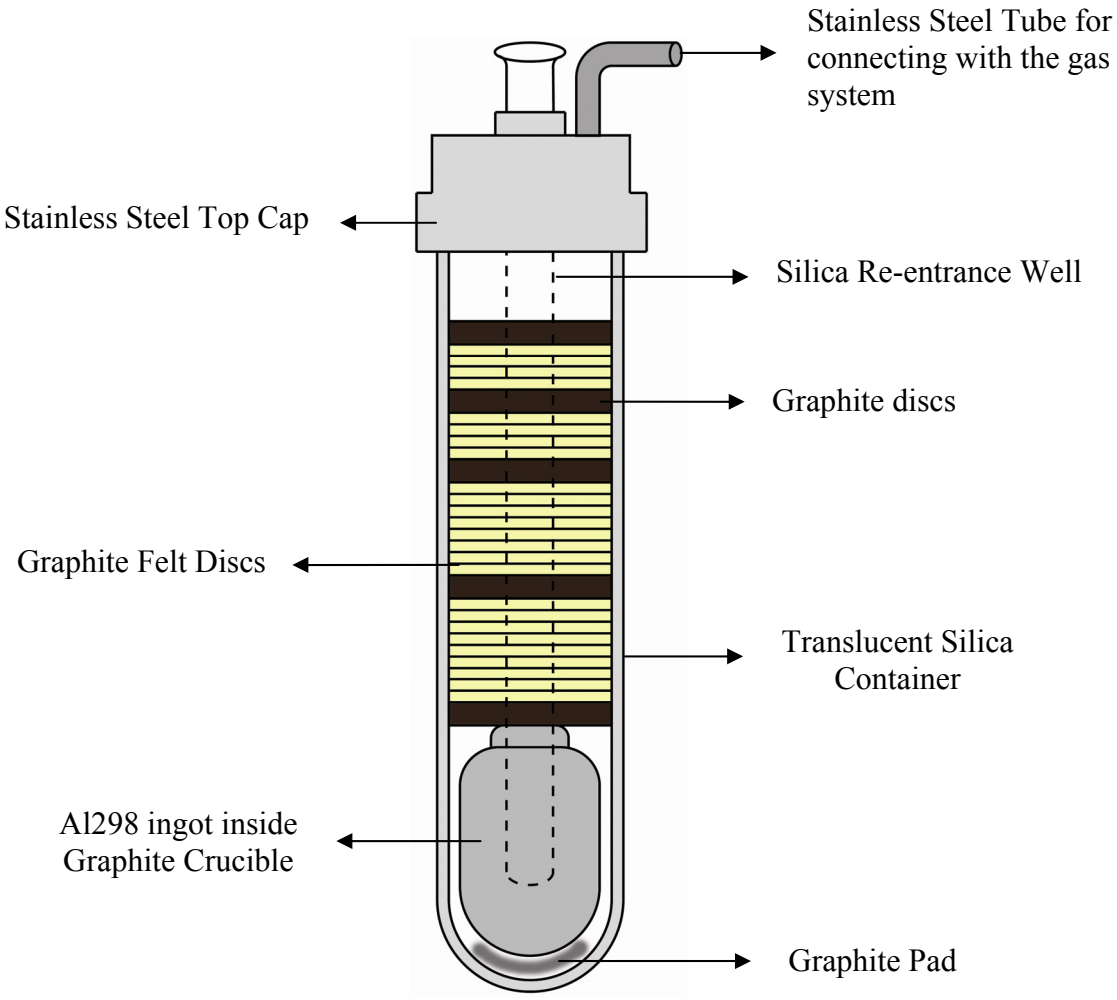

Figure 5.19 Diagram of the aluminium 298 opened fixed-point cell assembly.

5.5.2.2 Temperature Realisation of "Undoped" Al 298 Opened Fixed-Point Cell

A three-zone Hart furnace was used for maintaining a uniform temperature above or below the expected equilibrium of the aluminium fixed-point. This furnace is specially designed for thermal uniformity. The furnace core has a thermal block, which is a heated aluminium-bronze block. This block is attached with the electrical heaters, which the main heater is wound over the whole length of the block. However, additional end zones are wound on the top and bottom, which are there only to control the heat required to equalise the end temperatures to that of the centre zone. Thus, this block is suspended in the cabinet and insulated to minimise heat loss. After completing the assembly of Al 298 cell, the assembled cell was inserted to the Hart furnace. Then, the cell was connected via a copper tube to the system, which was connected by reinforced plastic tube to the vacuum pump and a Wallace & Tiernan precision pressure gauge. Before the experiments, the whole system is tested using a Leybold Vacuum PhoeniXL 300 helium leak detector. Then, the cell was evacuated with the external argon for several times to flush some dust or contaminations out from the cell. Argon is an inert gas, which was used to back fill and to provide approximately 101.32 kPa in the cell at the aluminium temperature.

The resistance ratios of the PRT 261198 measurements are recorded from an ASL F18 resistance bridge, in order to record the melting/freezing plateaus of the fixed-point cell. The fixed-point cell was maintained at the operating temperature, either – 0.5 ^{o}C or + 0.5 ^{o}C of the equilibrium temperature, which were the settings for the cell to be frozen and molten respectively. The freeze and the melt processes were the same as prior mentioned in Al174 fixed-point cell.

The initial freezing temperature of the "high purity" aluminium cell was calibrated several times against a NPL national standard Al 1205 cell by comparison of the thermometers readings (PRT 250329 and 261198) in the two cells. All results are corrected for the hydrostatic head pressure from Al 298 and NPL standard cells. For high purity Al 298 fixed-point cell, the hydrostatic head correction value after calculating is about -0.195 mK.

5.5.2.3 Elemental Analysis by GD-MS of Al 298 Opened Fixed-Point Cell

After obtaining all temperature realisations from the initial "undoped" Al 298 cell, four small pieces of the Al 298 ingot were cut from the top, middle, and bottom. As the same as Al 174 method, three pieces were analysed by GD-MS technique to check the distribution of the impurity elements within the ingot, before doping. The Al 298 ingot was shown in Figure 5.20. The other one was checked the same time as the doped sample. Moreover, the impurity levels in the aluminium samples after doping were measured again by GD-MS to see the level change of titanium impurity concentration after adding some titanium impurity into the ingot.

Figure 5.20 Aluminium 298 fixed-point ingot.

5.5.2.4 Mixing Technique of Al 298 Opened Fixed-Point Cell

After completing the initial measurements of the "undoped" Al 298 cell, the titanium impurity was used for doping. The high purity titanium wire (99.8%) was weighed and cut to be three pieces. They were placed on the top, the middle and the bottom of the originally pure aluminium Al 298 sample increasing the concentrations as follows (in ppmw); Ti: 0.9 and 1.8 in Al 298 cell. Titanium metal was chosen as the impurity in this aluminium ingot because it can affect that is expected to increase the melting and freezing temperatures of aluminium. From the phase diagram calculation, the fixed-point temperature of aluminium was interpolated to be elevated by 3.31 mK/ppmw of titanium impurity. The titanium metal wire (99.8%) was weighed

by a microbalance (Mettler AT20), which the uncertainty was discussed in the Section 5.5.1.4.

After doping in each lot of titanium, the Al 298 ingot was re-inserted back to the graphite crucible and the translucent container. Then the assembled cell was put into the Hart furnace, which was set at $6\,^{o}C - 8\,^{o}C$ above the actual equilibrium temperature for 5 days to ensure a good mixing of the impurities within the cell. Before the melting and the freezing curves of Al 298 after doping titanium display, the instability of the PRT 261198 would be checked by calibration in the NPL standard Al 1205 cell. The freeze peak of this cell was regularly cross-compared to the NPL standard Al 1205 cell by measuring thermometers resistances. This is to ensure the reliable measurement of the small temperature shift due to the trace impurities, and not from the PRTs' instability. The shifts and shapes of freezing and melting curves were investigated.

Following the fully molten process, the freezing and the melting curves of Al 298 were realised by use the same procedure as before doping in Al 298. When all results were completely obtained, the samples were cut off from the Al ingot to check the impurity levels after doping by use the GD-MS technique.

5.6 Cleaning Glassware Process

All glassware used as components of tin and aluminium fixed point open cells was cleaned before assembling. The glassware was made from Laboratory glassware provided by LGC Limited. "LGC is the UK's designated National Measurement Institute for chemical and biochemical analysis and is also the host organisation for the UK's Government Chemist function" [LGC limited, 2009].

The glassware used in this work consists of a set of clear Pyrex tube containers, a set of translucent silica tubes and a set of silica re-entance well tubes, which were used in the assembly of the tin and aluminium opened cells. Before the cleaning process started, the clean areas needed to be prepared and kept clean. The cleaning process of the glassware is as follows;

1. For the initial clean process, the glassware was cleaned with tap water both inside and outside at least three times.
2. Then, the acetone solvent, which is miscible with water, was used to rinse and remove any water from the surface of the glassware. Acetone is a common

solvent for rinsing laboratory glassware. The rinsing with acetone was usually performed 3 times.

3. The glassware was left until its surface was dry. Then, the glassware was cleaned by the Ensolv solvent. It was used to remove oil, grease, or wax contaminations on the glassware's surface. This solvent is very effective for higher cleaning performance and also is non-hazardous to the environment and health. This process was repeated three times

4. Then, the cleaning was followed by the acetone. It was to dissolve Ensolv out from the surface.

5. The glassware was rinsed with distilled water and was dried by acetone.

6. Following the completed cleaning with the Ensolv solvent, the dilute nitric acid was prepared for 10% dilute by adding nitric acid to water. Pour dilute nitric acid into a glass container. Then, the glassware was divided into 2 groups, namely the first group was a set of all containers and the other group was a set of re-entrance well tubes, respectively. For the first group, all containers were directly added the dilute nitric acid and then the rubber bungs were used to be a lid. The containers were shaken to clean the surface inside the containers. For the second group, each tube was put into the larger glass tube as a cleaning holder for small item to soak and shake with dilute nitric acid for 10 minutes. For extra clean surfaces, they were soaked for 24 hours. This process was done in a sink with either running water or a large tank of water available, which it was repeated at least three times. After that, it the used dilute nitric acid was clean and it can be used again, then it was stored in an appropriately labeled container.

7. Remove the dilute nitric acid and rinse thoroughly with distilled water until the glass was cleaned.

8. Finally, the glassware was rinsed with acetone to remove all traces of water.

9. Then, the glassware was turned upside down and was left until they were dried.

Following the completed cleaning process, all glass containers and re-entrance well tubes were ready to use for assembling the tin and aluminium fixed-point cells.

Chapter 6

Results and Discussions of Tin Fixed Point

This chapter describes the experimental results of the study of the quantitative affect of low level impurities on the phase transition temperature of high purity tin (231.928 °C) metal fixed-point cells, specified for use in the International Temperature Scale of 1990 (ITS-90). The accurate realisation of the tin fixed-point temperature, which plays an important role in the provision and dissemination of standard temperature values, strongly depends on the purity level of the tin material used. The trace impurities (of order ~1-30 parts per million by weight (ppmw)) of cobalt, lead, and antimony metals were selected for addition to the originally "pure" tin ingots; total concentrations as follows (in parts per million by weight (ppmw)): Co 5.5 and 7.4, Pb 7.9 and 31.4, Sb 7.8 and 23.2. The effect of these three impurities on Sn temperature had been studied at larger fractions by Hansen [1958], as had been described in Section 5.4.1.2. Our measurements using lower concentrations of dopants planned to test the interpolation of this previous data obtained using relatively high levels of impurities, which would help reduce the uncertainty budget of the tin fixed-point realisation, where impurities are the biggest contribution to the uncertainty budget.

The changes to the offsets of the initial freezing temperature, after deliberate doping with the impurity elements will be discussed in this chapter. Also, the shapes of melting plateaus of the "pure" tin will be compared with MTDATA program to check what shapes of the pure plateaus are. Also, the results of the concentration and distribution (or uniformity) of the impurity elements within the "pure" tin and aluminium ingots, which were detected by the Glow Discharge Mass Spectrometry (GD-MS) analysis, will be given. The experimental results of tin fixed point are divided into two parts, i.e. Spanish tin and Mini Isotech tin as used to study the influence of trace impurities on the equilibrium tin temperature.

6.1 High Purity Spanish Tin Fixed-Point

The experimental results of high purity Spanish tin fixed-point cell will be summarised and formed in terms of the "Family tree" as presented in Figure 6.1. But note that the measurements were done consecutively (not in parallel).

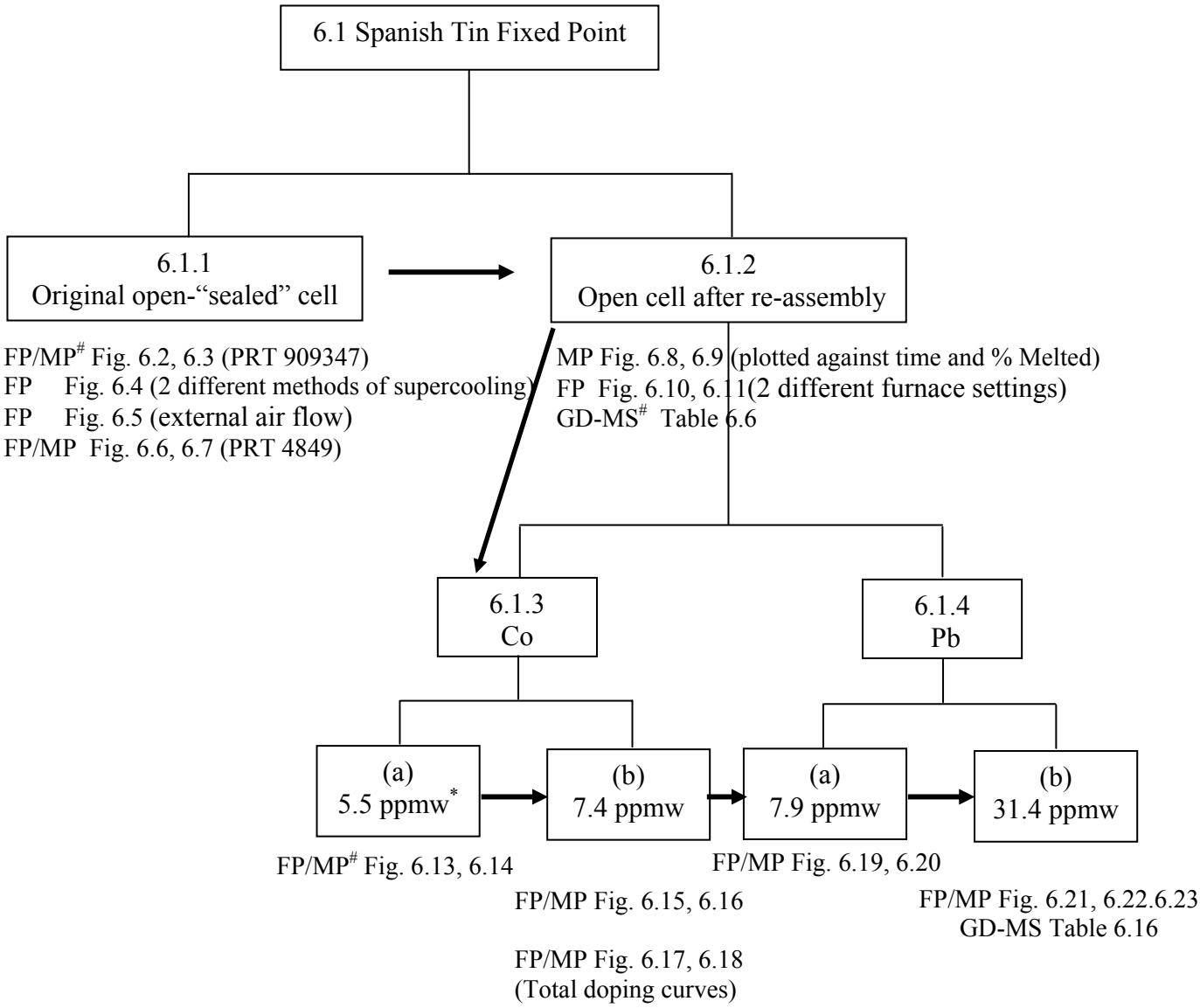

FP/MP = Freezing and Melting curves conducted in this stage.

GD-MS = Glow discharge mass spectrometry analysis performed in this stage.

* ppmw = Parts per million by weight

Figure 6.1 "Family Tree" showing the figure number of the freezing/ melting curves and the analysis technique of Spanish tin fixed point obtained for a particular combination of conditions.

6.1.1 Temperature Realisation of Original Open-"Sealed" Spanish Tin

The freezing and melting transitions of initially 99.9999% nominal "pure" Spanish tin cell were shown in Figures 6.2 and 6.3. The PRT resistance values on the Y axis for all figures in this chapter including the figure in Mini Isotech tin of the freezing and melting curves were calculated from the resistance ratio of PRT and standard resistor values and these values were not included the correction of the hydrostatic head, while the resistance values of PRT calibration by comparison measured at the peak of the freeze include the correction of the hydrostatic head of the cell.

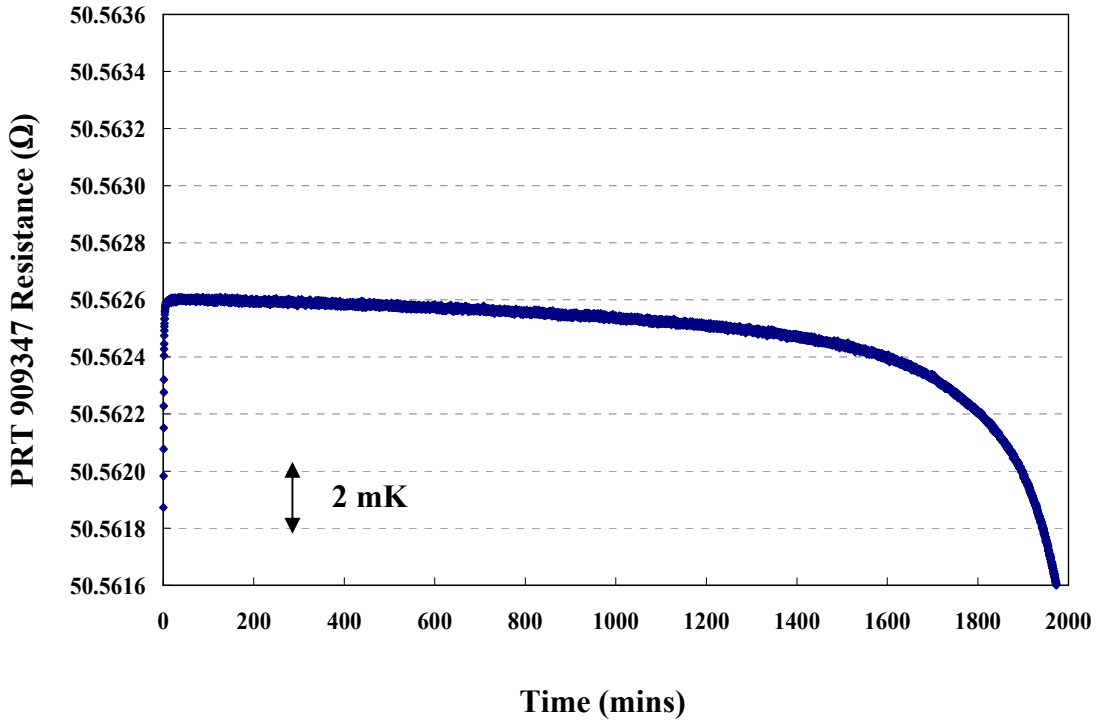

Figure 6.2 A freezing curve of a high purity original Spanish tin open "sealed-cell" in terms of the resistance value of the PRT 909347 (at 230.83 ^{o}C nominal temperature) plotted as a function of time.

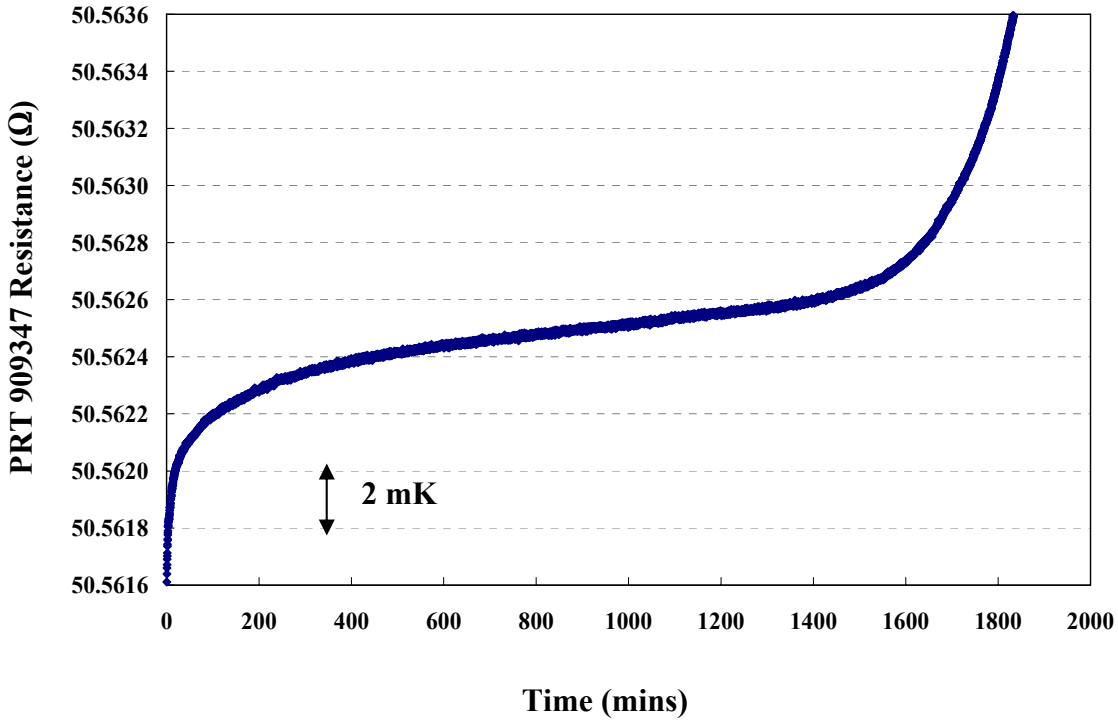

Figure 6.3 A melting curve of a high purity Original undoped "Spanish" tin fixed-point after being rapidly frozen, in terms of the resistance value of the PRT 909347 (at 231.83 ^{o}C nominal temperature) plotted as a function of time.

Figures 6.2 and 6.3 show examples of freezing and melting curves of original "undoped" Spanish tin cell plotted as the relationship between the PRT resistance values and a function of time. The melting curve was obtained after rapid freezing. The impurity segregation of the prior freezing process occur in either slowly or rapidly frozen metals affects the shape of the subsequent melting curve as had been discussed in Section 3.1. Ideally, the melting curve should be flat but it is difficult or impossible to obtain 100% pure metal, therefore, the curve would slightly incline. The rapid frozen (quenching) would stop any dispersion of impurities from their original positions in the metal fixed point. The temperature of the melting curve slowly increases until the liquidus point (100% liquid) occurred. It is the phase transition change from the solid to liquid. The results illustrate that the curve has a small slope (a few mK) due to the impurity distributed within the cell.

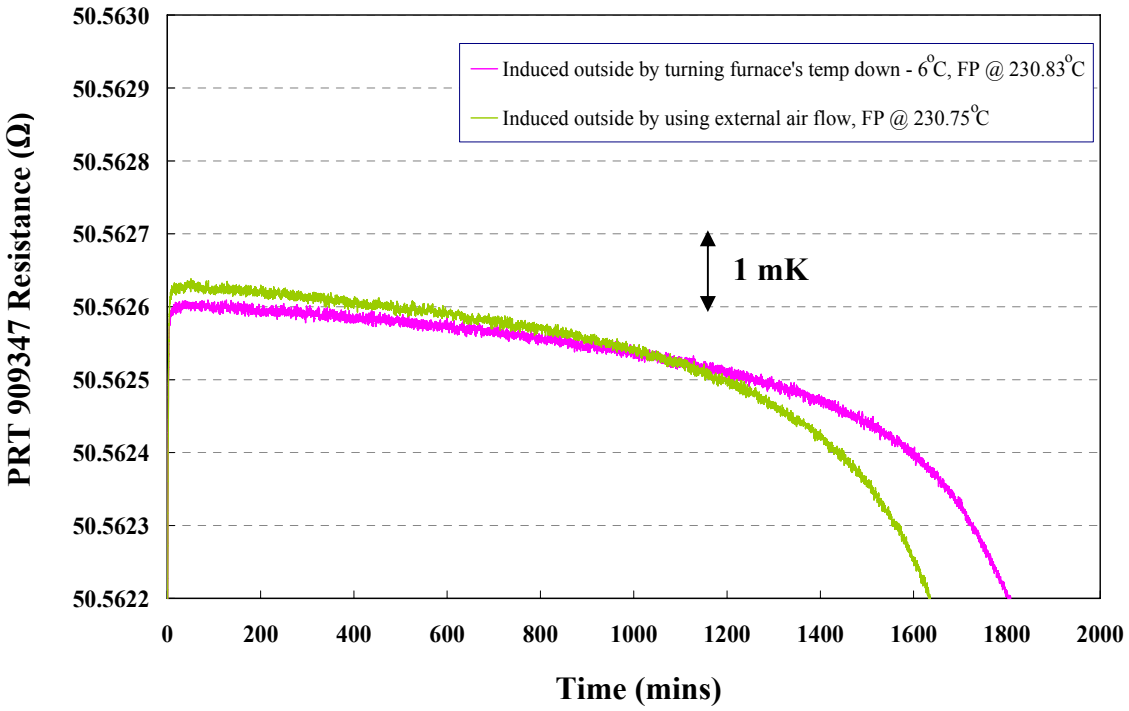

Figure 6.4 Freezing curves of original "undoped" Spanish Sn plotted as a function of time. The supercooling needed to induce tin recallescence was provided by two different methods, i.e. turning the temperature of the whole furnace down 6 °C or by using an external forced air flow up the furnace axis and around the tin cell.

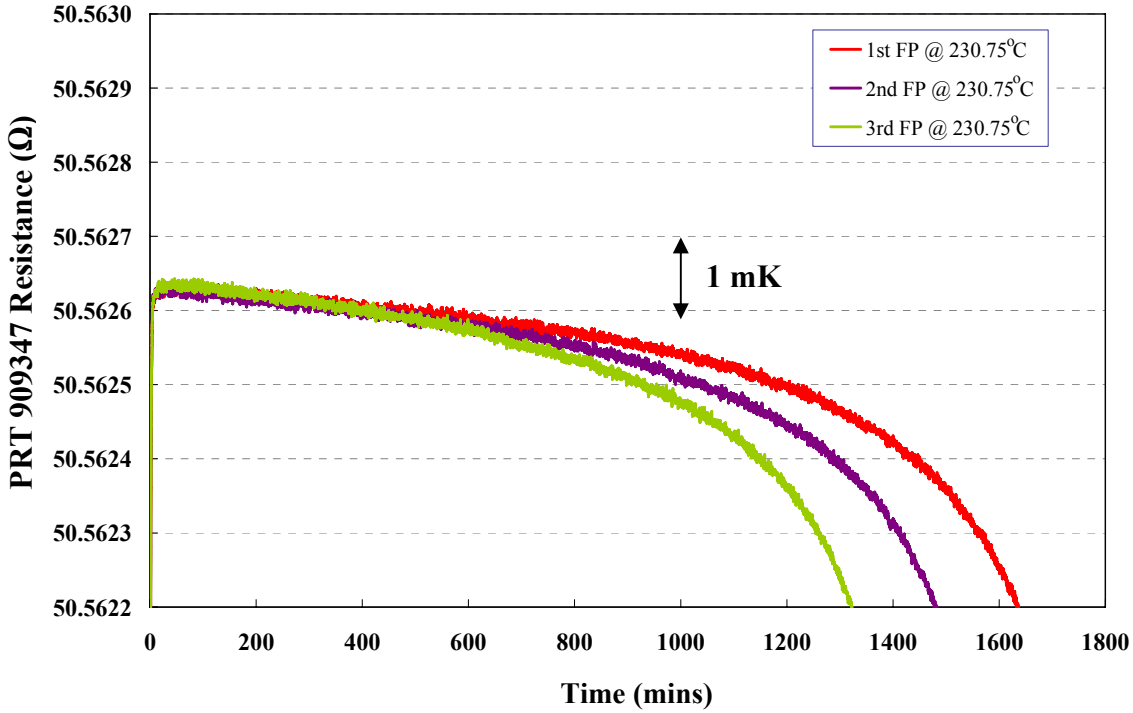

Figure 6.5 Three freezing curves of high purity original "Spanish tin" plotted as a function of time. The furnace set point for all three measurements is set at the same temperature. All freezing curves use the external air flow inside the furnace around the tin cell to initiate the recalescence.

Figure 6.4 indicates that the peak of the resistance values of the freezing curve obtained from the external air flow of the Hart furnace initiation method is a bit higher (~0.2 mK) from the normal initiation method as explained in Section 5.4.1.1. The period of the freezing time is different due to variations in the amount frozen at recallescence and difference of the furnace setting (the temperatures quoted are only nominal values as indicated on the furnace controller.

The results, as plotted in Figure 6.5, show the reproducibility of three freezing curves of original "undoped" Spanish tin. These freezing curves indicate the different period of time even though the three-zone Hart furnace is set in the same temperature. However, the peaks of all curves are exactly the same resistance values. Considering the solidus of these curves in Figure 6.5, it found that the temperature drop from the peak along the curve is about 1 mK. These three freezing curves also provide the reproducibility of better than 1 mK.

Table 6.1 Resistance values measured at the freezing point of high purity "undoped" Spanish Sn fixed-point cell. These values were calculated from the resistance ratio of PRT and standard resistor values. Also, the resistance values include the correction of the hydrostatic head of this cell. The temperature setting of the furnace was maintained at 230.75 ^{o}C (nominal). The resistance values are measured at the peak of the freeze.

Resistance values at freezing point of tin	**Date**	**Platinum Resistance Thermometers (PRTs) (Serial Number)**		
R_T (*i*) / Ω	-	**909069**	**274728**	**909347**
R_T (*1*)	04/06/07	48.249953	48.895843	50.562408
R_T (*2*)	05/06/07	48.249968	48.896149	50.562412
R_T (*3*)	06/07/07	48.249858	48.896375	50.562386
Standard deviation (2s)	-	**0.12 mΩ**	**0.53 mΩ**	**0.03 mΩ**
Mean of the R_T (Ω)	-	**48.249926** ± 0.00012	**48.896122** ± 0.00053	**50.562402** ± 0.00003

In Table 6.1, *i* represent the order of the resistance measurements of the PRTs at the freezing point of Spanish tin.

In Table 6.1, it shows the resistance values at the freezing temperature are similar in each measured PRT. The standard deviation (2s) for all measurements was 0.55 mΩ which is equivalent to 5.9 mK approximately The standard deviation value is not good, which is higher than ideal. It is because only the old PRTs can be used in this research, as only these PRTs were available. Hence, the use of several thermometers would help to obtain the most stable and/or to take the average of the resistance values. The biggest change is from the PRT 274728, which has a wide range of results. A PRT serial number 909347 proved to be more stable than other two thermometers during the thermal cycling. Its standard deviation is equivalent to $\pm$ 0.03 mΩ. This is the primary result to show the most stable of these PRTs is the PRT 909347.

Nevertheless, the stability of three PRTs needs to be tested again by realising the temperature in the triple point of water. According to Physikalisch-Technische Bundesanstalt (PTB) - the German national metrology measurement institute -the peak of the freeze is the most reproducible part of the freezing curve, from which good results can be obtained. The reason is that the maximum temperature does not strongly depend on the homogeneity and stability of the furnace temperature [Rudtsch *et al.*, 2008]. Furthermore, the graphite crucible and an inert gas environment, which are the part of the components for the metal fixed-point cell assembly, must be the high purity grade. This is to prevent the contamination from the surrounding impurities affecting the temperature values.

Table 6.2 Measurement of the stability of four PRTs measured from the resistance values at the triple point of water. These values were checked before using the PRTs in the comparison measurements at the freezing curves of tin fixed point between high purity "Undoped" Spanish and Reference Isotech Sn 184 fixed-point cells.

Resistance values at triple point of water (Ω)	**Date**	**Platinum Resistance Thermometers (PRTs) (Serial Number)**			
Cycle number and differences	-	**909069**	**909174**	**909347**	**4849**
$R_{TPW}(1)$	18/05/07	25.493319	25.501499	-	-
$R_{TPW}(2)$	19/05/07	25.493318	25.501508	26.715184	25.443919
$\Delta T_1 = \Delta R_1 * 10.8$ #	-	-0.011 mK	+0.097 mK	-	-
$R_{TPW}(3)$	06/06/07	25.493482	-	26.715175	-
$\Delta T_2 = \Delta R_2 * 10.8$ #	-	+1.77 mK	-	-0.097 mK	-
$R_{TPW}(4)$	21/06/07	25.493447	25.501236	26.715225	25.443956
$\Delta T_3 = \Delta R_3 * 10.8$ #	-	-0.38 mK	-2.94 mK	+0.54 mK	+0.40 mK
Mean of the ΔT	-	**+0.46 mK**	**-2.84 mK**	**+0.22 mK**	**+0.40 mK**
Standard deviation (2s)	-	**0.172 mΩ**	**0.310 mΩ**	**0.053 mΩ**	**0.052 mΩ**

In Table 6.2, *i* represent the order of the resistance measurements of the PRTs at the triple point of water; # 10.8 (mK/mΩ) is the appropriate conversion factor of sensitivity of $R(T_{90})$ from 10^{-6} μΩ to mK [Rusby, 2008].

The resistance values measured at the triple of water cell as listed in Table 6.2 can give an indication of the thermometer stability. The water triple point values in this research were checked within a few hours after the measurements at tin fixed-point temperature. The standard deviation (2s) for all measurements of all thermometers was 0.31 mΩ which is equivalent to 3.3 mK approximately. In practice, the shift differences of the thermometers during the thermal cycling result from the influences of increased strain in the wire during the temperature change or a slightly different wire composition.

Table 6.2 lists the resistance value and standard deviation of the resistance changes obtained at the triple point of water for the four PRTs. The first two PRTs as

presented in Table 6.2, i.e. 909069 and 909174, show the lower stability behaviour with the standard deviation 2s within 0.35 mΩ. Other two PRTs, i.e. 909347 and 4849, display good stability with a standard deviation of less than 0.06 mΩ during the thermal cycles. This proves that PRT 909347 and PRT 4849 are the better thermometers to use for realising the tin temperature fixed point.

(a) Tin Fixed-Point Calibration by Comparison between High Purity Spanish and Reference Isotech Sn 184 cells

In the first stage, the original "undoped" Spanish tin fixed-point cell was calibrated by comparison against the Reference Isotech Sn 184, by noting direct measurements on the freezing curves, listed in Table 6.3.

Table 6.3 Summary of the average resistance values in the comparison measurements of the freezing curves of tin fixed point between original high purity "Spanish" and "Reference Isotech Sn 184" cells with four PRTs. These results were recorded when the Spanish tin cell was originally an opened-"sealed cell".

PRTs serial number	**Date**	**R_T Original Spanish Sn (0 mA)**	**R_T Reference Sn 184 (0 mA)**	**Equivalent Temperature difference between Original Spanish Sn and Sn184 cells** $[\Delta T = 10.8 * \Delta R_T]^{\#}$ [Rusby, 2008]
909069 I	20/06/07	48.249885	48.250048	-1.76 mK
909069 II	21/06/07	48.249879	48.250058	-1.93 mK
909174 I	20/06/07	48.265319	48.265458	-1.50 mK
909174 II	21/06/07	48.265300	48.265448	-1.60 mK
909347 I	20/06/07	50.562431	50.562568	-1.48 mK
909347 II	21/06/07	50.562407	50.562563	-1.69 mK
4849 I	20/06/07	48.152663	48.152808	-1.57 mK
4849 II	21/06/07	48.152626	48.152808	-1.97 mK
Overall Mean		-	-	**- 1.69 mK**
∴ Standard deviation (2s) = ± 0.24 mK				
∴ Mean of Temperature difference Original Spanish - Reference Sn184 tin fixed-point cells = - 1.69 ± 0.24 mK				

[#]10.8 (mK/mΩ) is the appropriate conversion factor of sensitivity of $R(T_{90})$ from 10^{-6} μΩ to mK [Rusby, 2008].

Table 6.3 indicates that the average temperature difference between the original "undoped" Spanish tin and Reference Sn184 fixed-point cells is - 1.69 ± 0.24 mK. That means the temperature of the original "undoped" Spanish tin is lower than the Reference Sn184 by around 1.69 mK. That also means the Spanish tin ingot contained some pre-existing contamination affecting its freezing and melting temperatures (this was expected, and part of the reason why it could be used for doping, which effectively destroys the value of the cell). The standard deviation (2s) for all measurements is 0.24 mK. Table 6.3 also shows the important thing is that the Reference Sn 184 cell has good repeatability for good thermometers, which is better than water triple points.

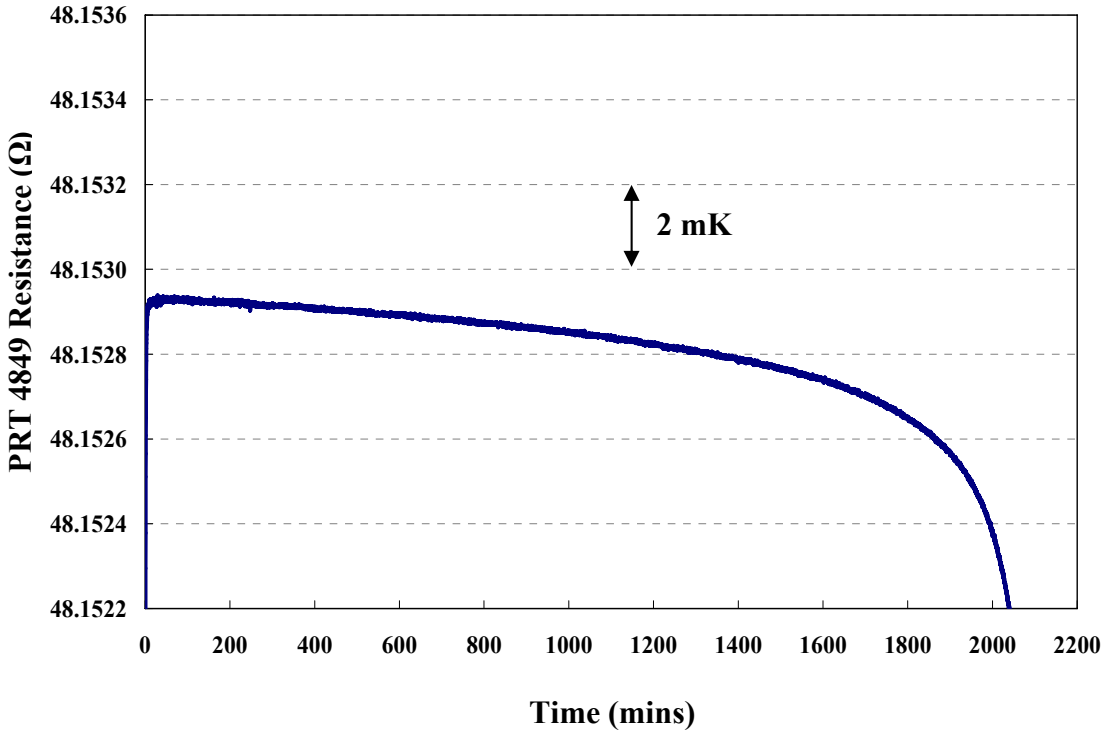

Figure 6.6 Freezing curves of a high purity original Spanish tin open "sealed-cell" in terms of the resistance value of the PRT 4849 used instead of the PRT 909347 at 230.75 ^{o}C (nominal temperature) plotted as a function of time.

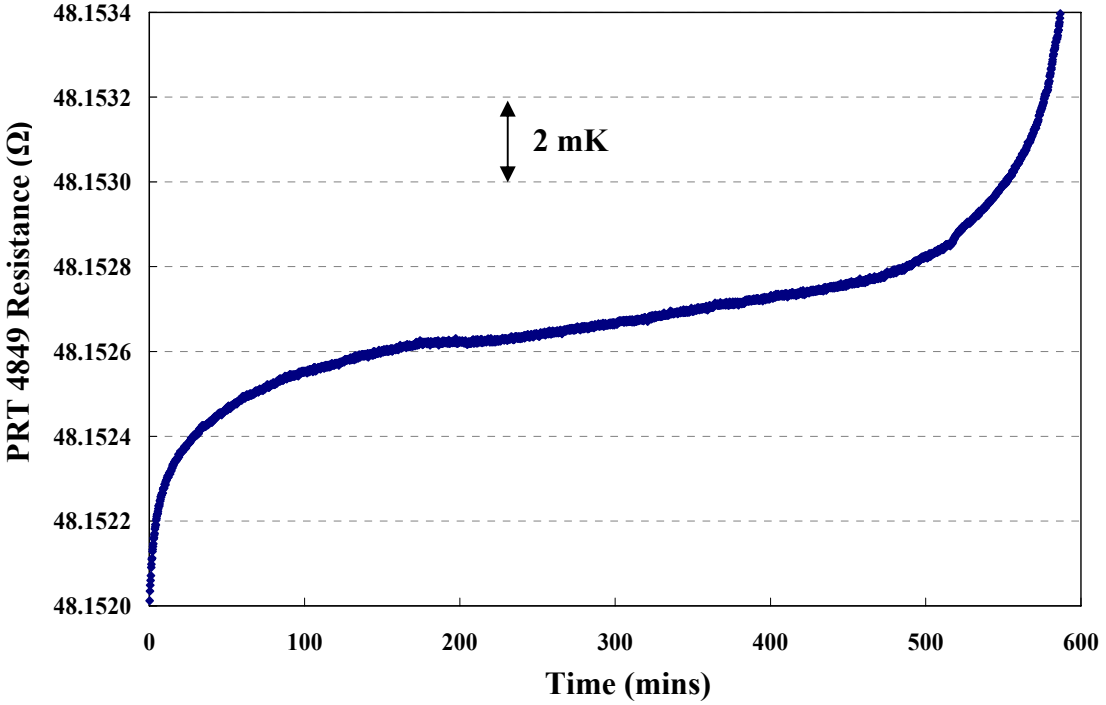

Figure 6.7 Melting curves of a high purity original Spanish tin open "sealed-cell" in terms of the resistance value of the PRT 4849 used instead of the PRT 909347 at 233.25 ^{o}C (nominal temperature; +2 ^{o}C from the equilibrium temperature) plotted as a function of time.

Figure 6.6 and 6.7 show the freezing and melting curves, which were recorded by PRT 4849 used to replace the broken PRT 909347 using the same equipment system. Once the results of the calibration and realisation were completely recorded, the high purity Spanish tin open "sealed-cell" was broken apart and then was re-assembled into the new component system and container. It would be made to be an "Open" cell. The results will be revealed in the next section.

6.1.2 Temperature Realisation of "Undoped" Opened Spanish Tin after Re-Assembly

The melting curves, as shown in Figure 6.8, are taken from the high purity undoped "Spanish" tin fixed-point curves after re-assembly and plotted as a function of time. In Figure 6.9, these melting curves are plotted as a function of percentage melted in preparation for future comparison of these shapes with the output of the MTDATA program. The reproducibility of these melting curves is of order of 1 mK. Also, the high purity Spanish tin freezing curves, before doping, are shown in Figure 6.10.

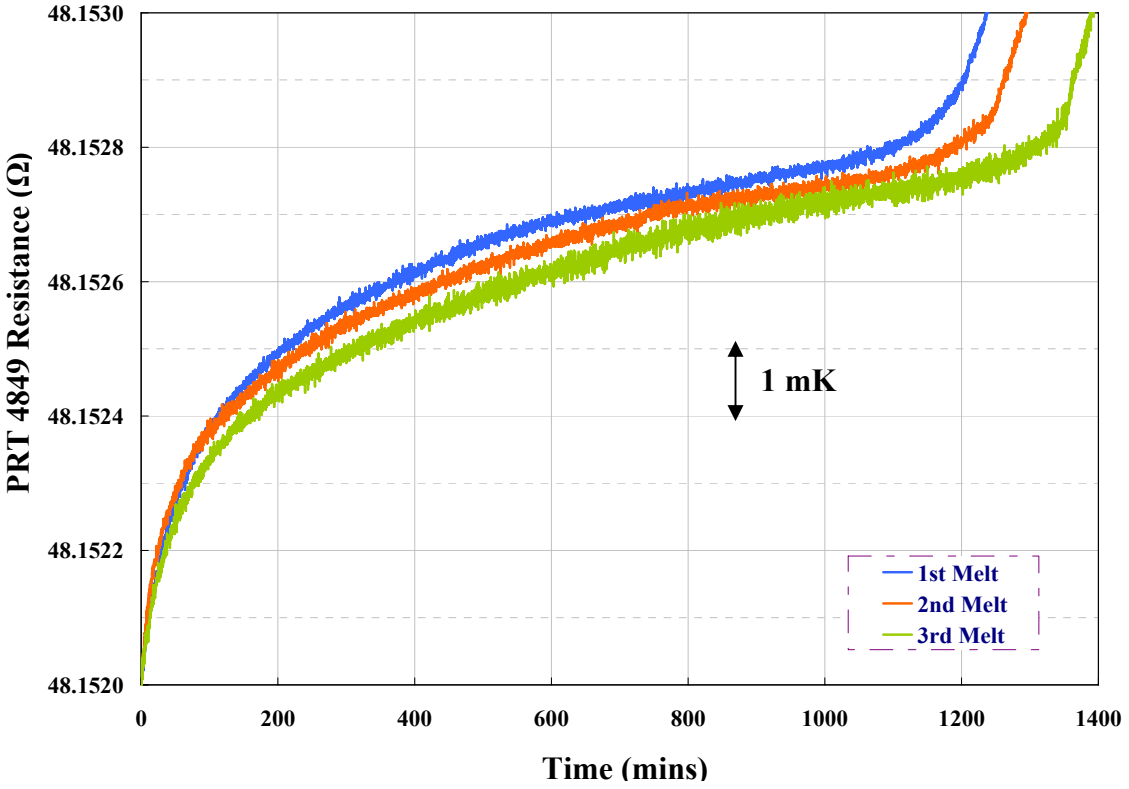

Figure 6.8 Three melting curves of a high purity undoped "Spanish" tin fixed-point after re-assembly plotted as a function of time. The furnace setting point for all three measurements is set at the same temperature (nominally half a degree above the melting point).

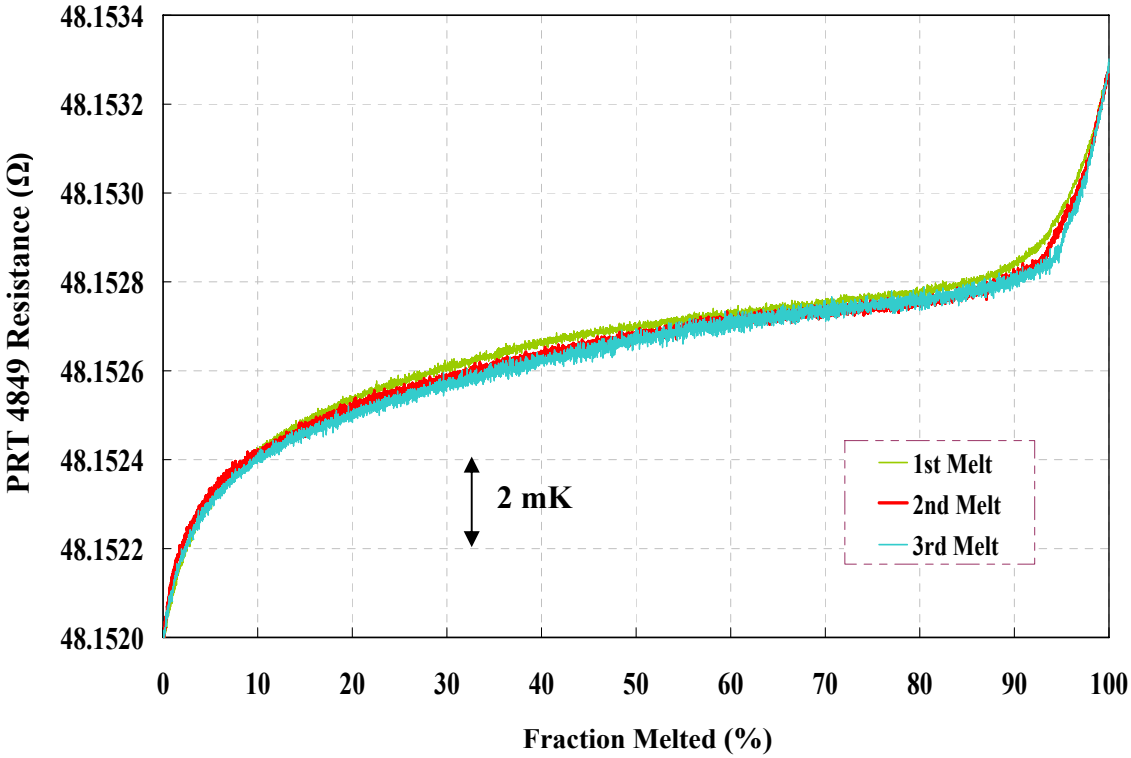

Figure 6.9 Three melting curves of high purity "undoped" Spanish tin. The curves have been normalised to an approximate percentage melted.

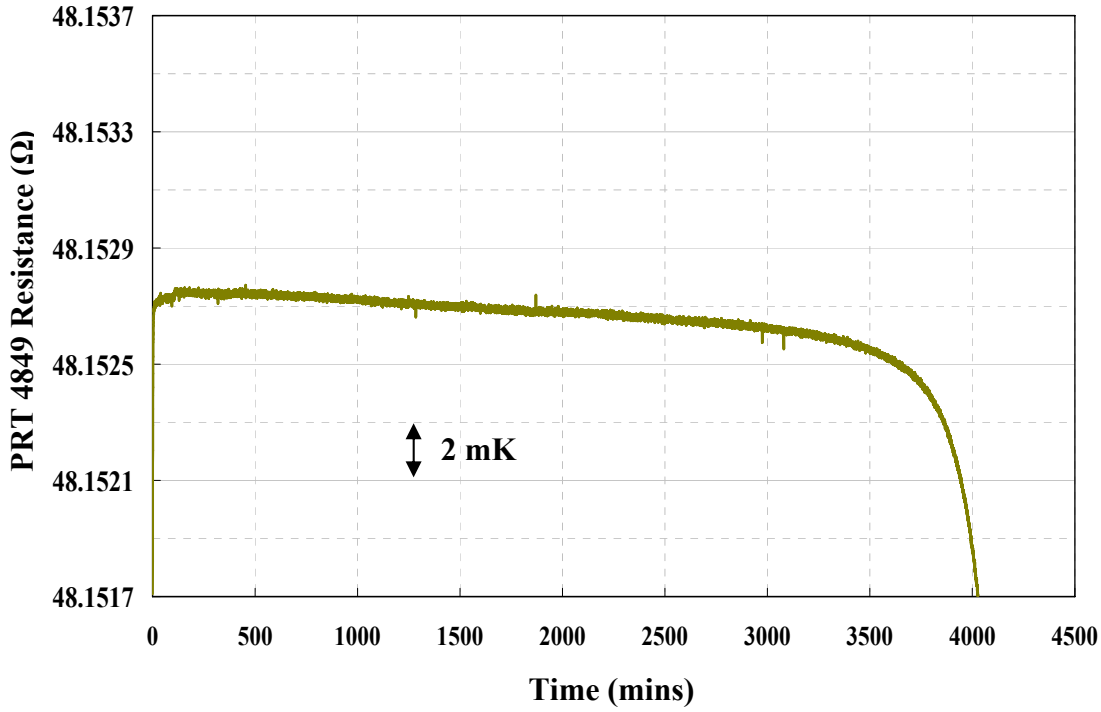

Figure 6.10 A freezing curve of the high purity "undoped" Spanish tin plotted as a function of time. The furnace setting is set at 229.3 °C (nominally half a degree below the equilibrium point).

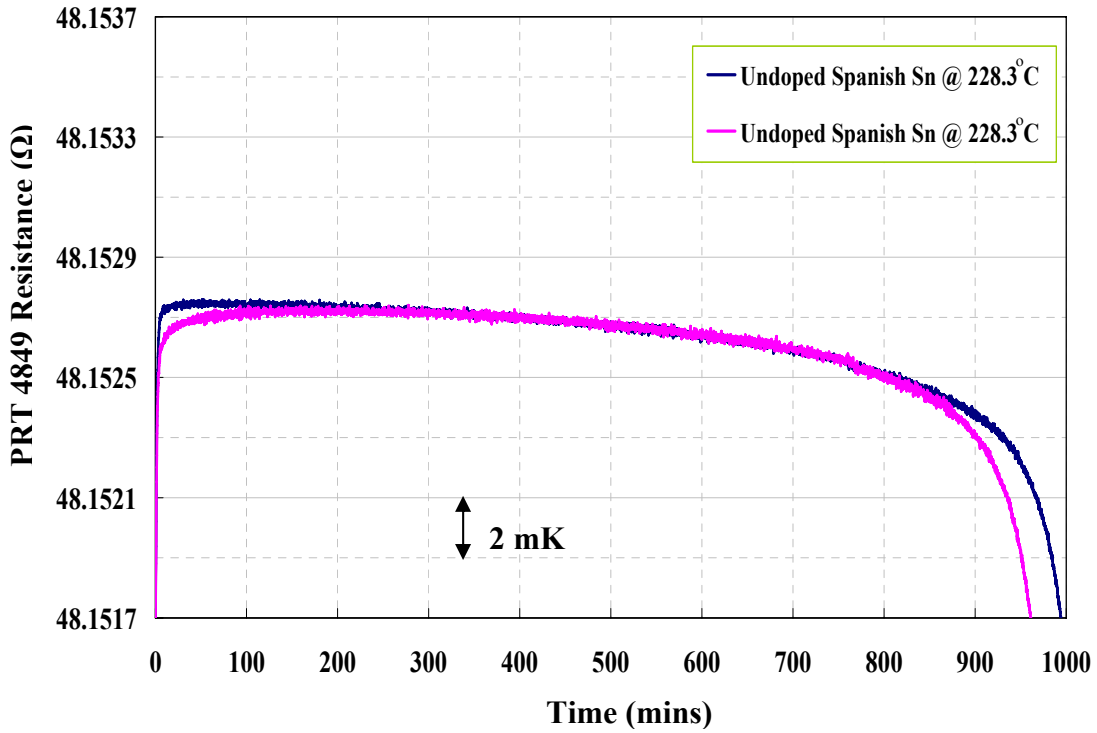

Figure 6.11 High purity "undoped" Spanish tin freezing curves plotted as a function of time. The furnace control point for these curves is set at the same temperature at 228.3 °C (nominal value).

All the melting and freezing curves of the undoped Spanish tin confirm the reproducibility of the measurements of this tin fixed-point cell. In Figure 6.10, the period of the freezing curve from the liquidus until solidus points is approximately 4000 minutes or 70 hours when the furnace setting is set at -0.5 ^{o}C below the equilibrium point. It is too long a curve for normal realisations. The setting point of the furnace can be set at 1 ^{o}C below the equilibrium point, i.e. 228.3 ^{o}C (nominal), which is enough temperature difference to get the long curve in this experiment, as seen in Figure 6.11. The temperature change of the curve between the approximate liquidus and solidus points is about 2 mK as showed in Figure 6.11. For the standard tin fixed-point cell, the temperature change of the flat curve should be within 0.5 mK. This confirms that this Spanish tin has been contaminated with some impurities. The temperature curves are smooth and no sharp structural changes take place in these melting curves during melting and the following freeze.

Table 6.4 Stability performances of three PRTs (PRT serial number 909069, 909174, and 4849) measured at the triple point of water before and after the calibration by comparison between "undoped" Spanish tin and Reference Isotech Sn 184 fixed-point cells.

Resistance values at triple point of water/Ω	**Date**	**Platinum Resistance Thermometers (PRTs) (Serial Number)**		
Cycle number and differences	**-**	**909069**	**909174**	**4849**
$R_{TPW}(1)_A$	21/06/07	25.493447	25.501236	25.443956
$R_{TPW}(2)_B$	22/10/07	25.493368	25.501197	25.443907
$\Delta T_1 = \Delta R_1 * 10.8^{\#}$	-	-0.85 mK	-0.42 mK	-0.53 mK
R_{TPW} *(3)*	23/10/07	25.493280	25.501383	25.443961
$\Delta T_2 = \Delta R_2 * 10.8^{\#}$	-	-0.95 mK	+2.01 mK	+0.58 mK
R_{TPW} *(4)*	24/10/07	25.493416	25.501218	25.443949
$\Delta T_3 = \Delta R_3 * 10.8^{\#}$	-	+1.47 mK	-1.78 mK	-0.13 mK
Mean of the ΔT	-	**-0.11 mK**	**-0.06 mK**	**-0.03 mK**
Standard deviation (2s)	-	**0.145 mΩ**	**0.169 mΩ**	**0.005 mΩ**

In Table 6.4, *i* represent the order of the resistance measurements of the PRTs at the triple point of water. # 10.8 (mK/mΩ) is the appropriate conversion factor of sensitivity of $R(T_{90})$ from 10^{-6} μΩ to mK [Rusby, 2008].

The stability of three PRTs was monitored by means of the triple point of water cells, as illustrated in Table 6.4. The standard deviation (2s) for all measurements was 0.17 mΩ, which is equivalent to 1.8 mK approximately. However, PRT 4849 shows the best stability of the resistance values at the triple point of water (the standard deviation is 0.005 mΩ which is about 0.05 mK). This confirms that PRT 4849 is good for measuring at this tin cell.

Table 6.5 Summary of the average resistance values in the calibration by comparison method between a new undoped "Open cell" Spanish Sn and the Reference Isotech Sn184 fixed-point cells with three PRTs on 23rd and 24th October 2007, respectively. The furnace setting was set to a nominal value of 229.1 °C for all freezing realization measurements.

PRTs serial number	**Date**	**R_T "undoped" Spanish Sn (0 mA)**	**R_T Reference Sn 184 (0 mA)**	**Equivalent Temperature difference between "undoped" Spanish Sn and Sn184 cells** $[\Delta T = 10.8 * \Delta R_T]^{\#}$ [Rusby, 2008]
909069 I	23/10/07	48.249687	48.250004	- 3.42 mK
909069 II	24/10/07	48.249701	48.250022	- 3.47 mK
909174 I	23/10/07	48.265258	48.265554	- 3.20 mK
909174 II	24/10/07	48.265258	48.265558	- 3.24 mK
909174 III	23/10/07	48.265265	48.265561	- 3.20 mK
909174 IV	24/10/07	48.265265	48.265562	- 3.21 mK
4849 I	23/10/07	48.152602	48.152897	- 3.19 mK
4849 II	24/10/07	48.152602	48.152901	- 3.23 mK
Overall Mean	-	-	-	**- 3.27 mK**
∴ Standard deviation (2s) = ± 0.22 mK				
∴ Mean of Temperature difference "undoped" Spanish Sn – Reference Sn 184 fixed-point cells = - 3.27 mK				

10.8 (mK/mΩ) is the appropriate conversion factor of sensitivity of $R(T_{90})$ from 10^{-6} μΩ to mK [Rusby, 2008].

Table 6.5 summarises the calibration by comparison and takes the average values from the resistance ratio in the "undoped" Spanish tin cell; it indicates that the

temperature difference between the “undoped” Spanish tin cell and Reference Isotech Sn 184 cell is 3.27 ± 0.22 mK. That means the temperature of the “undoped” Spanish tin cell is lower than the Reference Sn184 cell by around 3.27 mK. The standard deviation can be calculated as 0.22 mK, which is equivalent 2.4 mK.

After comparison with the reference tin cell, the initial freezing temperature of the Spanish cell was found to be 3.27 mK lower than the Reference Isotech Sn 184 cell. That means the Spanish tin ingot contained some pre-existing contamination affecting its freezing and melting temperatures (this was expected, and part of the reason why it could be used for doping, which effectively destroys the value of the cell). Moreover, transferring and assembling the Spanish tin cell from the old to the new components and container were also the one factor to increase its contamination by more than it would be expected. We understand that the influence of each of the impurities in the host material remains independent of each other at low concentrations. The magnitude of each effect on the temperature depends on both the species type and the amount of that particular species and the total temperature change is the sum of the individual effects, taking account of any sign. The impurities in the original Sn sample can be detected by using the Glow Discharge Mass Spectrometry (GD-MS), which will be discussed in the next part.

6.1.2.1 Impurity Analysis of Spanish Tin Fixed-Point before Doping

Glow Discharge Mass Spectrometry (GDMS) Characteristics

Table 6.6 lists the impurity elements detected in three areas of the tin metal ingot. The uncertainty of this GD-MS analysis is considered to be accurate within a factor of two of the values obtained, at a confidence level of 95% though there is anecdotal evidence that the results are more accurate than quoted. GD-MS is the best technique (most sensitive) available at present to determine the amount of the impurities.

Table 6.6 GD-MS analysis results of the initial impurity concentration of the "undoped" Spanish tin fixed point before doping [NRC report number: 30337R1 (checked on 14/12/07)]. These elements were detected in term of mass fraction (in parts per billion by weight, ppbw). The uncertainty is quoted as a "factor of 2" i.e. 50% to 200% of the reported value, though this is probably a conservative overestimate.

Element	Top	Middle	Bottom	Element	Top	Middle	Bottom
	ppbw				ppbw		
Li	<0.3	<0.4	<0.3	**Br**	<25	<20	<25
Be	<0.1	<0.2	<0.1	**Rb**	<0.3	<0.9	<0.3
B	<0.3	<0.4	<0.2	**Sr**	<0.2	<0.3	<0.2
C	1500	2100	1300	**Y**	<0.2	<0.2	<0.2
N	85	500	170	**Zr**	<0.2	<0.2	<0.2
O	290	880	430	**Nb**	<0.2	<0.3	<0.2
F	<1	<1	<0.6	**Mo**	<1	<1	<1
Na	<0.3	<0.4	<0.2	**Pd**	-	-	-
Mg	<0.3	<0.3	<0.3	**Ag**	<2	<2	<2
Al	<0.2	<0.2	<0.2	**Cd**	<20	<30	<20
Si	0.8	0.3	0.3	**In**	3600	4200	4000
P	2	<0.3	0.8	**Sn**	Matrix	Matrix	Matrix
S	400	120	550	**Sb**	<45	<50	<35
Cl	0.8	3	<0.4	**Te**	<2	<3	<3
K	<45	<45	<45	**I**	<6	<6	<4
Ca	<5	<6	<5	**Cs**	<0.5	<0.5	<0.6
Sc	<0.2	<0.3	<0.2	**Ba**	<0.2	<0.3	<0.4
Ti	<0.1	<0.2	<0.2	**La**	<0.3	<0.2	<0.4
V	<0.1	<0.1	<0.1	**Ce**	<0.2	<0.2	<0.3
Cr	<0.4	<0.6	<0.4	**Hf**	<0.6	<0.8	<0.6
Mn	<0.2	<0.3	<0.3	**Ta**	-	-	-
Fe	<4	<4	<3	**W**	<0.6	<0.7	<0.5
Co	<100	<100	<100	**Pt**	<2	<2	<2
Ni	<16	<20	<17	**Au**	<10	<10	<10
Cu	<1	<1	<1	**Hg**	<8	<10	<7
Zn	<2	<2	<2	**Tl**	<1	<1	<1
Ga	<0.8	<1	<0.8	**Pb**	14	10	20
Ge	<2	<2	<2	**Bi**	<0.5	<0.7	<0.5
As	<10	<12	<13	**Th**	<0.2	<0.2	<0.2
Se	<80	<80	<40	**U**	<0.3	<0.3	<0.7

The pre-existing impurities would contribute to the initial 3.27 mK offset with respect to the reference cell. From the GD-MS results we see that the impurity levels are the same throughout the cell, which shows the homogeneity of the impurity

concentration (within the uncertainty quoted). This indicates that the tin is sufficiently well mixed after properly melting the sample. In future only one sample will need to be cut out for analysis after doping. (Cutting out of samples is a risky procedure).

C, N, and O show as large amounts of impurity, when compared with other background impurities, even though GDMS is not expected to be so accurate with these elements.

6.1.2.2 MTDATA Analysis

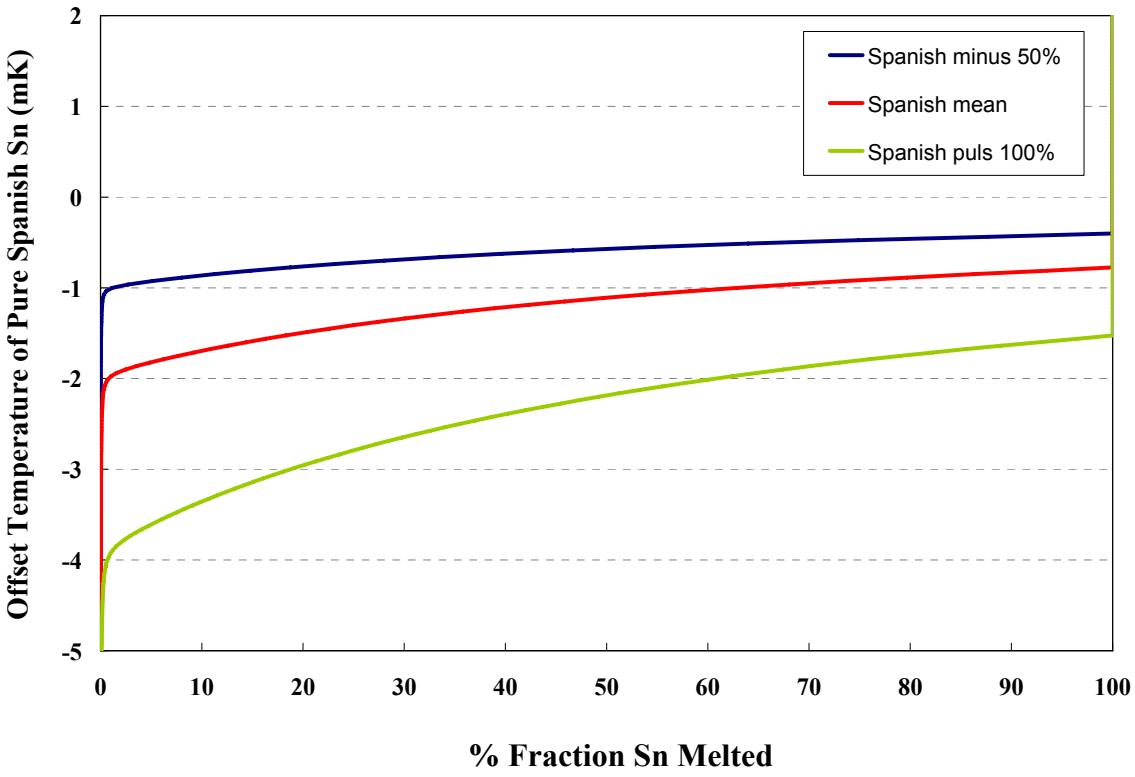

Figure 6.12 Melting curves of pure Spanish fixed point obtained from MTDATA calculation analysis. The red line shows the curve calculated using the GD-MS result (impurity effect on the curve), the blue and the green lines show the calculated bounds (based on the quoted uncertainty of the GD-MS analysis i.e. factor of 2 which translates to –50% and +100% of reported value)

Considering the red line (Spanish mean) obtained from MTDATA as shown in Figure 6.12, the depression of the Spanish Sn melting temperature at 100% is about 0.8 mK (i.e. 0% of freezing). This is not in agreement with the experimental results, i.e. the initial temperature (0% “frozen”) obtained from experiment results, compared

to the Isotech reference Sn cell, is depressed by 3.27 mK. This difference is beyond the uncertainties. However at 100% to 50% melted [as defined on MTDATA curve], the temperature depression is approximately 0.4 mK. This does match with the experimental results, which is a 0.5 mK drop, as based on 100% to 50% melted and 0% to 50% frozen on melting and freezing curves, respectively. In light of the aluminium data (see chapter 7) there is some evidence that there may be more impurity effect present than is calculated by MTDATA based on the GD-MS analysis – this MIGHT be due to some undetected impurity.

Also, the comparison of the pre-doped Sn cells (and Al cells) with MTDATA seems to show much more rounding in the experimental melt data (though the experimental data is repeatable, but then the same "fast freeze" technique was always used i.e. reduce the furnace by 5 degrees, giving a freeze duration of about one hour). It might be that in large cells, as used in this work as compared to Ancsin's small cells [Ancsin, 2008], that the thermal inertia of the cell/furnace means that "fast freeze" rates are not as fast as one might expect, and that to get a freeze that will truly quench the impurities in place it would have to be "Very" fast – such as by pulling the ingot into air (see comment below**,** regarding the recent work of Qiu [Qiu *et al*., 2008] in the section on the 23.2 ppmw Sb doped Mini Isotech tin). We note that Head [Head *et al*., 2008] showed good agreement between the doping experiments of Ancsin and MTDATA. However Ancsin was using very small samples that could be easily and very quickly pulled into air to cause "Ultra fast" freezing. (Ancsin also had higher levels of impurity and a special adiabatic container).

It may be that to properly compare our "fast frozen" melt data will need a more sophisticated model than just MTDATA that will allow for temporal affects and impurity redistributions. Work on such models has been started by Hunt [2008] and Malik [2009] but their application to the data here is beyond the present work. (However it could be considered as useful "Further work").

6.1.3 Influence of Cobalt on High Purity Spanish Tin Fixed Point

6.1.3.1 High Purity Spanish Tin doped 5.5 ppmw of Cobalt

The offsets and shapes of the melting and freezing curves doped with 5.5 ppmw of Co in tin sample are shown in Figure 6.13 and 6.14.

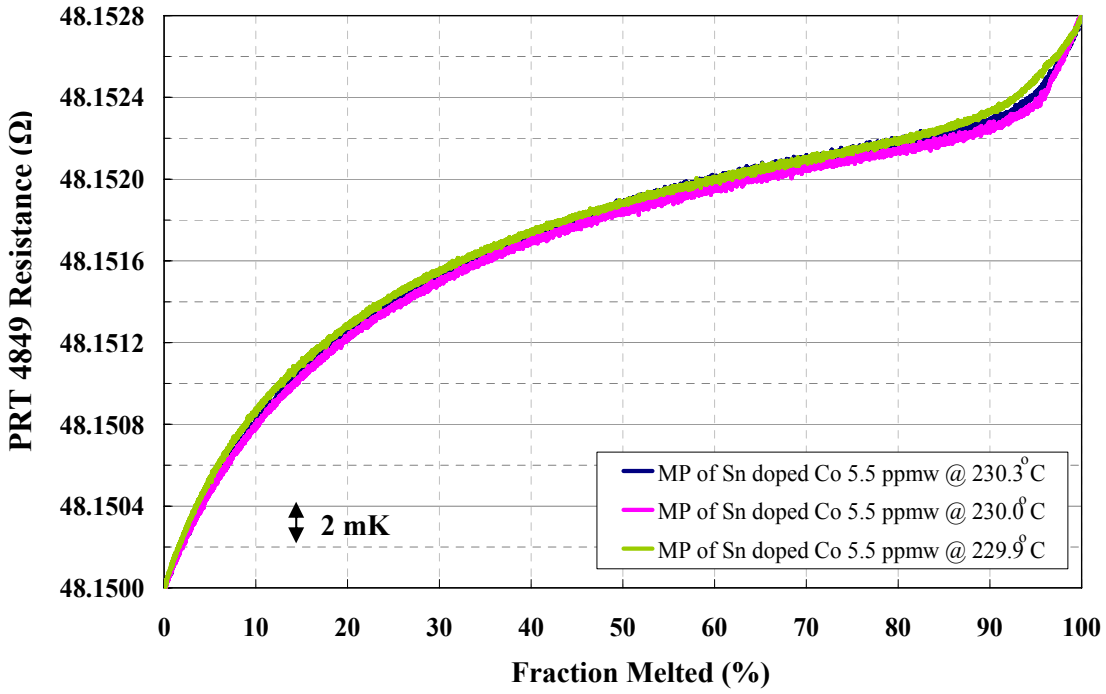

Figure 6.13 Three melting curves of Spanish Sn fixed point after doping with 5.5 ppmw cobalt impurity. The curves have been normalised to an approximate percentage melted of Sn fixed-point sample. These melting curves are realised at different nominal temperature furnace settings.

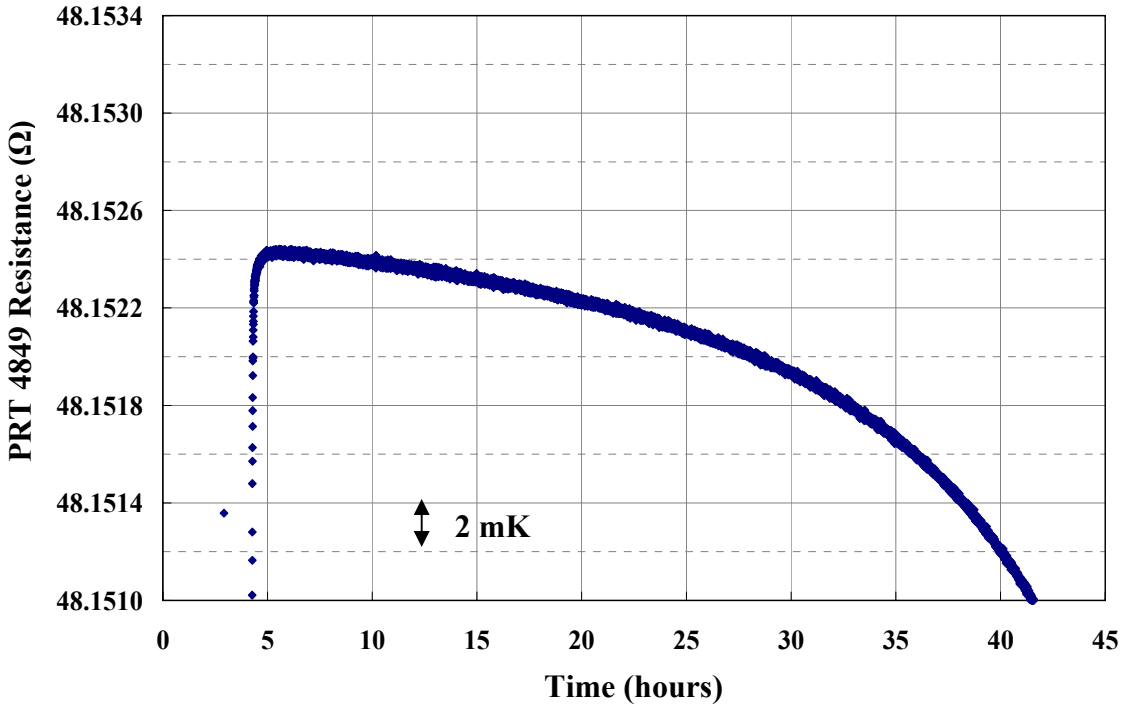

Figure 6.14 An example of freezing curve of Spanish Sn fixed point doped with 5.5 ppmw cobalt impurity. This curve is recorded at nominal furnace setting of 229.1 °C.

Melting curves are dependent on the thermal history of the sample. This is a result of changes in impurity segregation during the former freezing process. If ingot/impurities are left molten for a long time we assume they will become uniformly distributed. However, if the freezing process takes a long period, there will be time for segregation to occur: this does not happen, as noticeably, if the sample is frozen quickly. Therefore, all melting curves in this work were measured following a rapid freeze (approximately 1 hr). More melting curves, plotted as a function of time, will be presented in Appendix B. Three melting curves of Spanish Sn fixed point after doping with 5.5 ppmw cobalt impurity confirm, as shown in Figure 6.13, the reproducibility of the temperature measurements in these fixed-point cells. However, the slope of the freezing curves after cobalt doping, as seen in Figure 6.14, decline dramatically when they are compared with undoped ones.

After comparison with Reference Isotech Sn184, the initial freezing temperature of the Spanish cell after doping 5.5 ppmw was found to be 7.07 ± 0.81 mK reduced from the Reference Isotech Sn184 cell, as displayed in Table 6.7. Therefore, the temperature difference between “doped Co 5.5 ppmw” and “undoped” Spanish Sn was decreased by 3.80 ± 0.84 mK. That means the Co impurity results in a reduction in the freezing and melting temperatures of the Spanish tin ingot. The equilibrium curves of the Spanish tin after doping with Co 5.5 ppmw fixed-point and the temperature difference after calibration by comparison decreased roughly in line with expectations derived from interpolation of previous experiments as increasing amounts of impurities was introduced; the measured rates is as follows: Co - 0.69 mK/ppmw.

Table 6.7 Summary of the average resistance values in the calibration measurements by comparison method between the Spanish Sn doped with Co 5.5 ppmw and the Reference Isotech Sn 184 fixed-point cells with three PRTs. The nominal furnace setting was maintained at 229.1 ^{o}C. These resistance values are compared by using the peak of the freeze values as explained in section 6.1.1.

PRTs serial number	**Date**	**R_T Spanish Sn doped "Co 5.5 ppmw" (0 mA)**	**R_T Reference Sn 184 (0 mA)**	**Equivalent Temperature difference between Spanish Sn doped Co 5.5 ppmw and Sn184 cells** $[\Delta T = 10.8 * \Delta R_T]^{\#}$ [Rusby, 2008]
909174 I	22/01/08	48.264841	48.265538	- 7.53 mK
909174 II	23/01/08	48.264919	48.265554	- 6.86 mK
4849 I	22/01/08	48.152193	48.152911	- 7.75 mK
4849 II	23/01/08	48.152279	48.152927	- 7.00 mK
4849 III	23/01/08	48.152292	48.152937	- 6.97 mK
4849 IV	24/01/08	48.152276	48.152898	- 6.72 mK
909069 I	23/01/08	48.249332	48.249995	- 7.16 mK
909069 II	24/01/08	48.249403	48.250008	- 6.53 mK
Overall Mean	-	-	-	**- 7.07 mK**
∴ Standard deviation (2s)-Temperature difference between Co 5.5 ppmw doped Spanish Sn and Reference Sn ± 0.81 mK				
∴ Temperature difference between Co 5.5 ppmw "doped" and "undoped" Spanish Sn (-7.07) - (-3.27) = - 3.80 mK				
∴ Standard deviation (2s) Difference -Temperature difference between "Co 5.5 ppmw doped" and "undoped" Spanish Sn (by quadrature addition) ± 0.84 mK				

10.8 (mK/mΩ) is the appropriate conversion factor for the sensitivity of $R(T_{90})$ [Rusby, 2008].

Table 6.8 Stability Resistance results from three PRTs (PRT serial number 909069, 909174, and 4849) measured at the triple point of water before and after the calibration by comparison between Spanish tin doped Co 5.5 ppmw and Reference Isotech Sn184 fixed-point cells.

Resistance values at triple point of water/Ω	**Date**	**Platinum Resistance Thermometers (PRTs) (Serial Number)**		
Cycle number and differences	**-**	**4849**	**909174**	**909069**
$R_{TPW}\ (1)_A$	22/01/08	25.443974	25.501230	25.493358
$R_{TPW}\ (2)_B$	22/01/08	25.443978	25.501241	-
$\Delta T_1 = \Delta R_1 * 10.8^{\#}$	-	+0.043 mK	+0.12 mK	-
$R_{TPW}\ (3)$	23/01/08	25.443985	25.501256	25.493440
$\Delta T_2 = \Delta R_2 * 10.8^{\#}$	-	+0.076 mK	+0.16 mK	+0.89 mK
$R_{TPW}\ (4)$	24/01/08	25.443971	-	25.493433
$\Delta T_3 = \Delta R_3 * 10.8^{\#}$	-	-0.15 mK	-	-0.076 mK
Mean of the ΔT	-	**-0.01 mK**	**+0.14 mK**	**+0.41 mK**
Standard deviation (2s)	-	**0.012 mΩ**	**0.026 mΩ**	**0.091 mΩ**

In Table 6.8, *i* represents the order of the resistance measurements of the PRTs at the triple point of water; B means the measurements were taken before comparison calibration between Spanish Sn and Reference Sn184; A refers to the measurements were taken after comparison calibration between Spanish Sn and Reference Sn184. # 10.8 (mK/mΩ) is the appropriate conversion factor for the sensitivity of $R(T_{90})$ [Rusby, 2008].

The standard deviation (2s) for all measurements from three PRTs was 0.10 mΩ, which is equivalent to 1.08 mK approximately. However, PRT 4849 still shows the best stability of the resistance values at the triple point of water. However, the water stability is not all good as mentioned above. The resistance values at the Reference Sn184 are much better than the water stability and this is a better argument that these data from the Reference Sn 184 cell can be used in this research. The better repeatability of Reference Sn184 values are presented from the results of both the tin and water resistance values the as shown in Table 6.15 and accompanying text.

6.1.3.2 High Purity Spanish Tin doped 7.4 ppmw of Cobalt

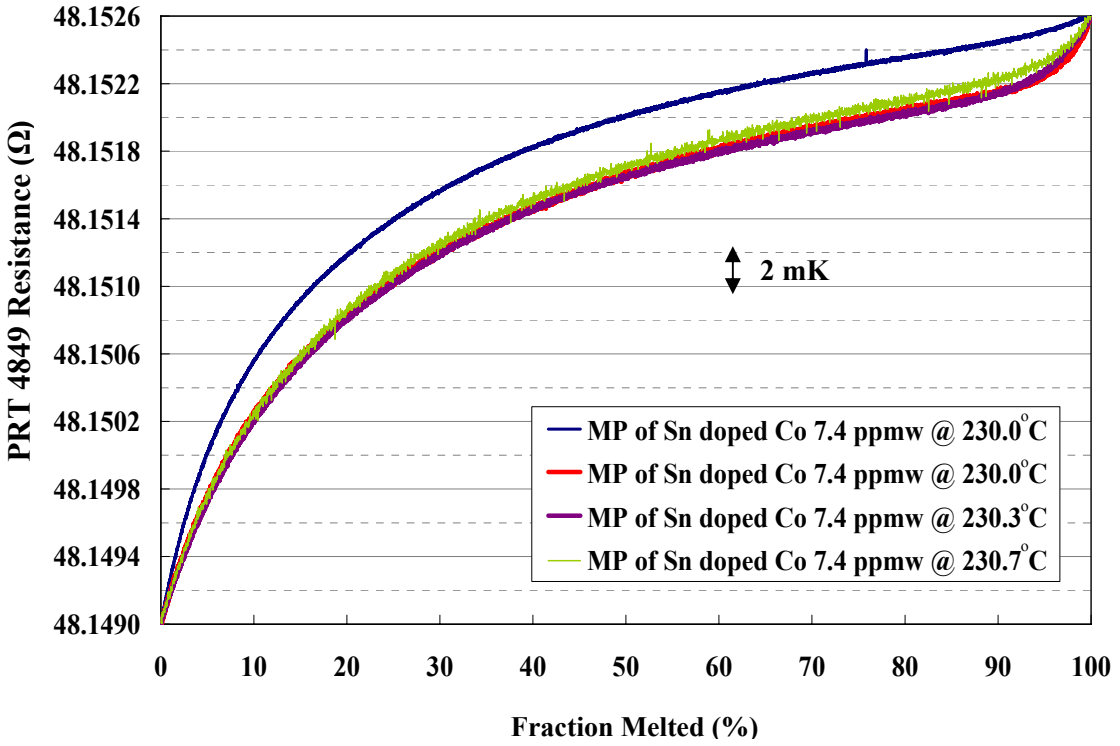

Figure 6.15 The equilibrium melting curves of the Spanish Sn sample containing an amount of Co 7.4 ppmw concentration plotted as the percentage of fraction melted. These curves were realised at different temperature furnace settings.

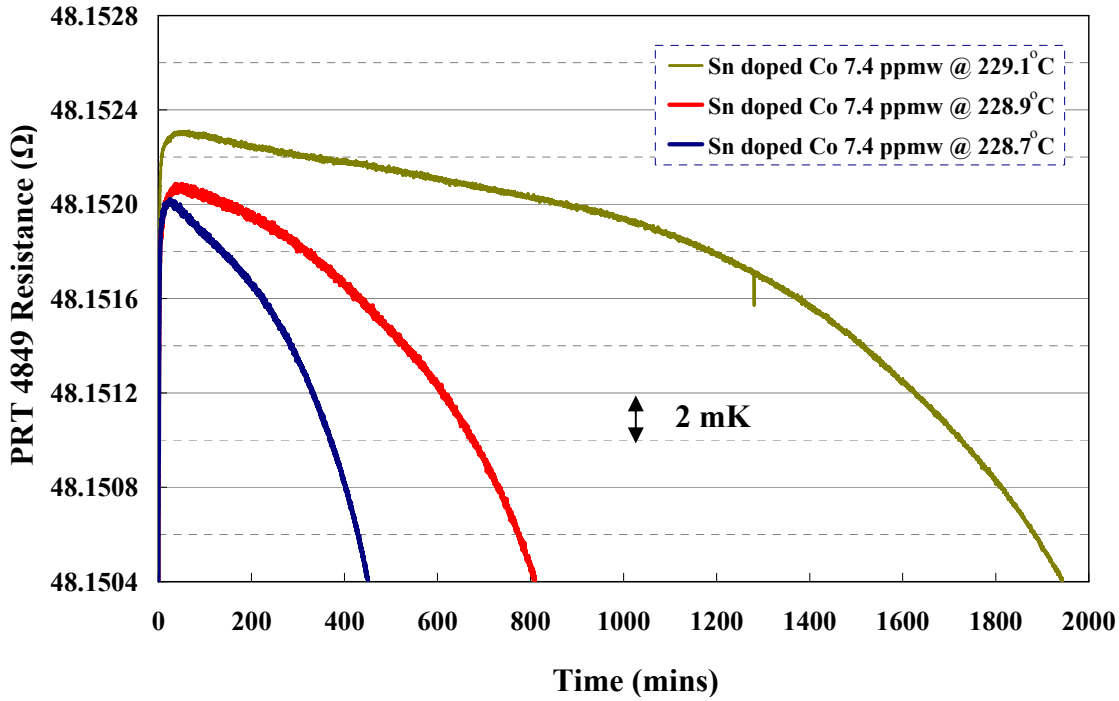

Figure 6.16 The equilibrium freezing curves of the Spanish Sn sample containing an amount of Co 7.4 ppmw concentrations plotted as a fraction of time. These curves were realised at different settings of the furnace temperature.

Figure 6.15 shows typical examples of melting curves obtained after a rapid rate of freezing. The first melting curve, which is clearly separate from the other three, indicates that the Spanish Sn and cobalt impurity was not well mixed. However, the remaining three melting curves confirm the reproducibility of the temperature measurements in this doped fixed-point cell. The results from Figure 6.16 display the different period of time of the freezing curves doped with the same amount of Co 7.4 ppmw due to the different furnace temperature settings. The first freezing curve confirms that the mixture of Spanish Sn and cobalt impurity is not well mixed as seen in the previous Figure on the melting curve. Furthermore, the remaining two freezing curves shows similar temperature values, which were recorded on the freezing point in these fixed-point cells.

Table 6.9 Summary of the average resistance values in the calibration by comparison method between the Spanish Sn doped with Co 7.4 ppmw and the Reference (Sn184) tin fixed-point cells with two PRTs. The furnace setting of was maintained at a nominal 228.6 ^{o}C for all freezing realisation measurements.

PRTs serial number	**Date**	**R_T Spanish Sn doped "Co 7.4 ppmw" (0 mA)**	**R_T Reference Sn 184 (0 mA)**	**Equivalent Temperature difference between Spanish Sn doped Co 7.4 ppmw and Sn184 cells** $[\Delta T = 10.8 * \Delta R_T]^{\#}$ [Rusby, 2008]
4849 I	26/03/08	48.152087	48.152915	- 8.94 mK
4849 II	01/04/08	48.152090	48.152928	- 9.05 mK
274728 I	26/03/08	49.037796	49.038618	- 8.88 mK
274728 II	01/04/08	49.037780	49.038606	- 8.92 mK
Overall Mean	-	-	-	**- 8.95 mK**
∴ Standard deviation (2s)-Temperature difference between Co 7.4 ppmw doped Spanish Sn and Reference Sn ± 0.15 mK				
∴ Temperature difference between "Co 7.4 ppmw doped" and "undoped" Spanish Sn (-8.95) – (-3.27) = - 5.68 mK				
∴ Standard deviation (2s) Difference -Temperature difference between "Co 7.4 ppmw doped" and "undoped" Spanish Sn (by quadrature addition) ± 0.27 mK				

10.8 (mK/mΩ) is the appropriate conversion factor for the sensitivity of $R(T_{90})$ [Rusby, 2008].

The standard deviation (2s) for all measurements of the equivalent temperature difference between Spanish Sn doped Co 7.4 ppmw and Reference Sn184 cells is 0.15 mK. The freezing temperature of the Spanish cell after Co doping 7.4 ppmw was found to be 8.95 ± 0.15 mK reduced from the Reference Isotech Sn184 cell. That means the adding Co 7.4 ppmw impurity decreases the temperature of the freezing and melting of undoped Spanish tin ingot by 5.68 ± 0.27 mK. The equilibrium curves of the Spanish tin after doping with Co 7.4 ppmw fixed-point and the temperature difference after calibration by comparison decreased as increasing amounts of impurities was introduced; the measured rates is as follows: Co - 0.77 mK/ppmw.

Table 6.10 Stability Resistance results from two PRTs measured at the triple point of water before and after the calibration by comparison between Spanish tin doped Co 7.4 ppmw and Reference Isotech tin (Sn184) fixed-point cells.

Resistance values at triple point of water/Ω	**Date**	**Platinum Resistance Thermometers (PRTs) (Serial Number)**	
Cycle number and differences	**-**	**4849**	**274728**
R_{TPW} (*1*)	19/03/08	25.443976	25.909939
R_{TPW} (*2*)	26/03/08	25.443977	25.909898
$\Delta T_1 = \Delta R_1 * 10.8$	-	+0.011 mK	-0.44 mK
R_{TPW} (*3*)	01/04/08	25.443980	25.909880
$\Delta T_2 = \Delta R_2 * 10.8^{\#}$	-	+0.032 mK	-0.19 mK
Mean of the ΔT	-	**+0.022 mK**	**-0.32 mK**
Standard deviation (2s)	-	**0.004 mΩ**	**0.06 mΩ**

In Table 6.10, *i* represent the order of the resistance measurements of the PRTs at the triple point of water. # 10.8 (mK/mΩ) is the appropriate conversion factor for the sensitivity of $R(T_{90})$ [Rusby, 2008].

Table 6.10 presents the stability of the PRTs calibrated at the triple point of water during the comparison between Spanish tin doped Co 7.4 ppmw and Reference Isotech Sn184 fixed-point. This shows that there are no large shifts in the PRTs during the measurement cycle. The standard deviation (2s) for all measurements was 0.06 mΩ which is equivalent to -0.65 mK approximately.

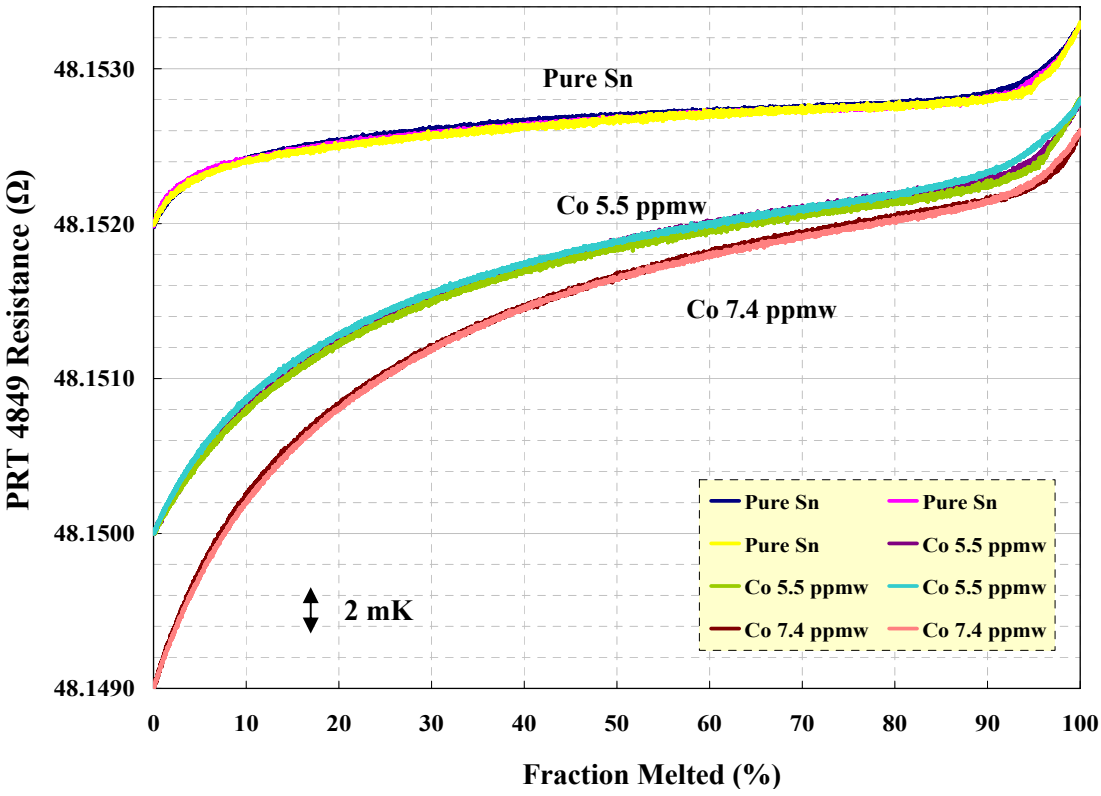

Figure 6.17 Three melting curves of high purity "Spanish" tin and the shift of these curves after doping the tin with increasing concentration of cobalt impurities. The curves have been normalised to an approximate percentage melted

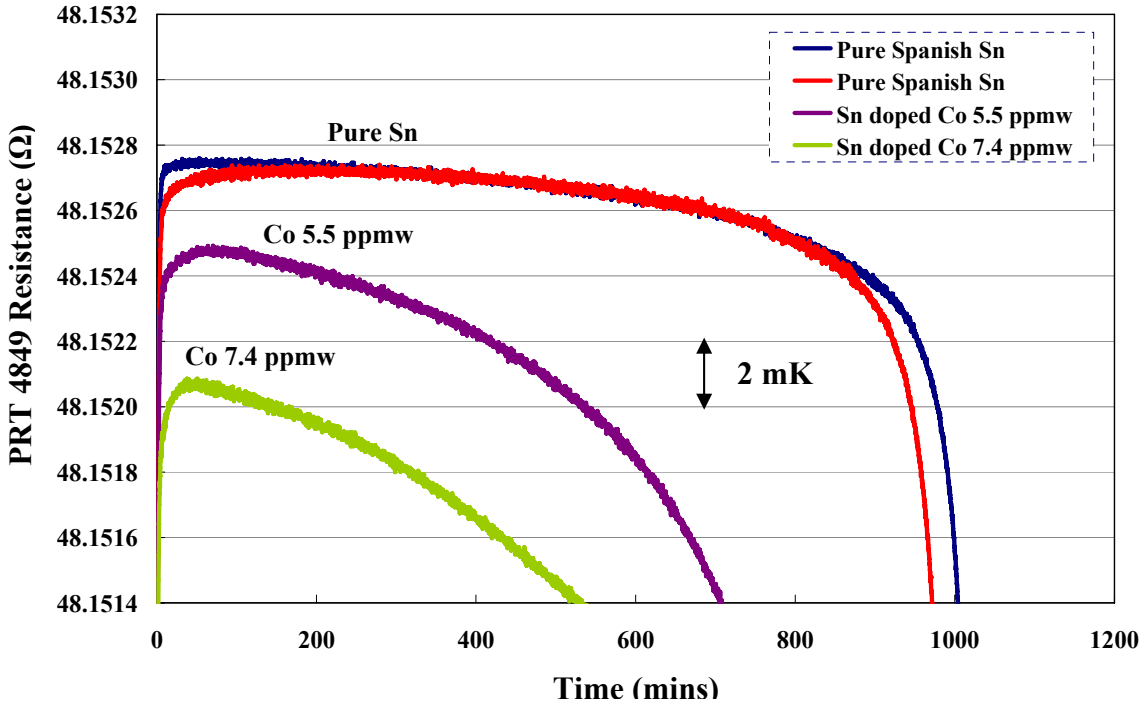

Figure 6.18 Example of high purity tin freezing curves and the shift of these curves after doping the Spanish tin with increasing concentrations of cobalt impurities, plotted as a function of time. The period of time for all curves is different due to differences in the furnace setting.

The offsets and shapes of the melting and freezing curves for the undoped and Co doped samples of tin are shown in Figure 6.17 and 6.18. The results confirm that cobalt depresses the phase transition temperature as expected. The peak of the freezing curves after doping had dropped by 3.7 mK and 5.4 mK (compared to initial undoped Spanish tin cell analysis) for concentrations of 5.5 ppmw and 7.4 ppmw of cobalt, respectively. Moreover, the set of three melting curves of undoped and Co doped Spanish tin confirm the reproducibility of the temperature measurements of this fixed-point cell. Total Co impurities in the Sn sample can be checked by the amount of concentrations by using the GD-MS, after finishing the last experiment of Pb doping.

6.1.4 Influence of Lead Impurity on High Purity Spanish Tin Fixed Point

6.1.4.1 Spanish Tin doped 7.9 ppmw of Lead

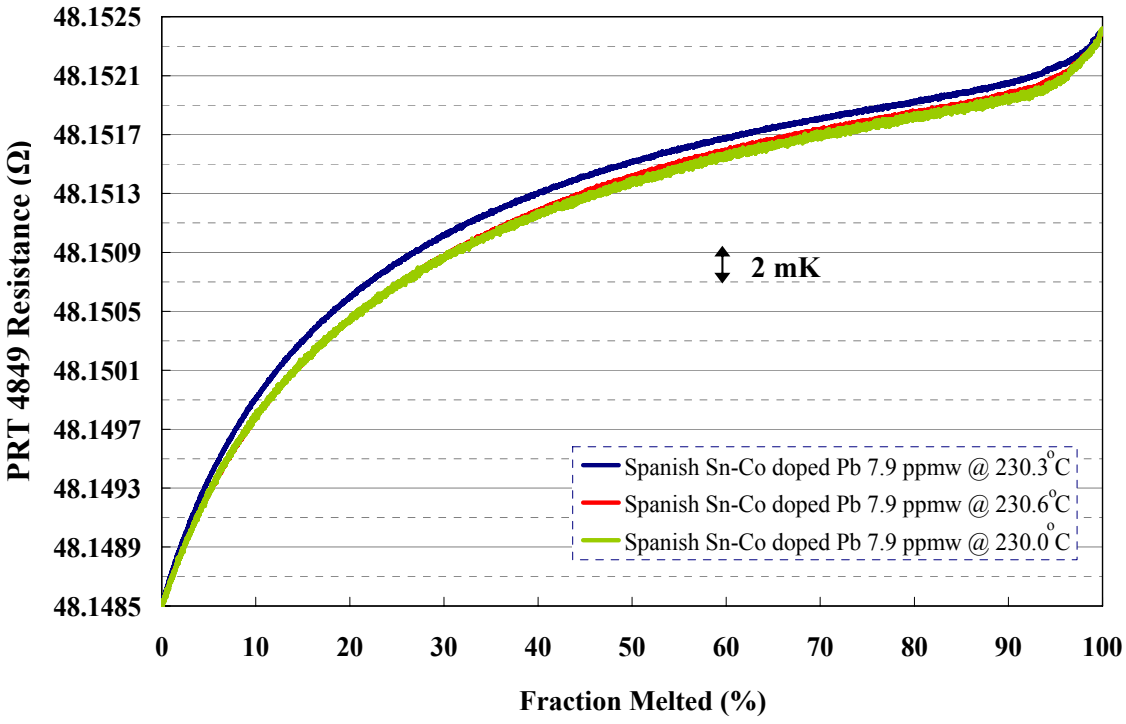

Figure 6.19 Three melting curves of high purity "Spanish" tin after doping the tin with 7.9 ppmw of lead impurity. The curves have been normalised to an approximate percentage melted.

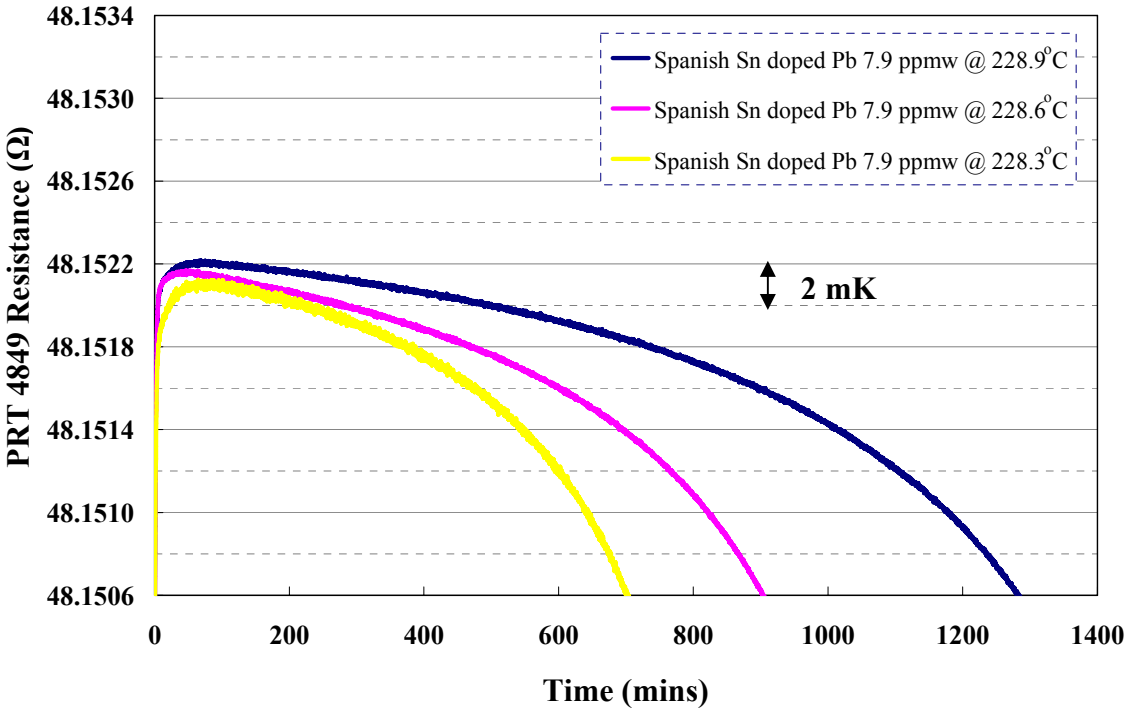

Figure 6.20 The equilibrium freezing curves of the Spanish Sn sample containing an amount of lead at 7.4 ppmw concentration plotted as a function of time. These curves were realised at different settings of the furnace temperature.

Figure 6.19 and 6.20 shows the significant impurity dependence of the tin melting point affected by a low concentration of lead (as compared to the "Sn-Co" in Figure 6.17 and 6.18). This first set of Spanish doping with 7.9 ppmw of lead is slightly separated from the other two melting curves. This may be explained that the tin after adding lead impurity is not well mixed, while the rest of two melting curves show the highly reproducibility of the temperature measurements of this fixed-point cell.

Table 6.11 Summary of the average resistance values in the calibration measurements by comparison method between the Spanish Sn-Co alloy systems doped with Pb 7.9 ppmw and the Reference (Sn184) tin fixed-point cells with three PRTs. The furnace setting of was maintained 229.1 ^{o}C for all freezing realisation measurements. The hydrostatic head corrections values are included in all resistance values.

PRTs Serial number	**Date**	**R_T Spanish Sn-Co Doped "Pb 7.9 ppmw" (0 mA)**	**R_T Reference Sn 184 (0 mA)**	**Equivalent Temperature difference between Spanish Sn-Co and Sn184 cells** $[\Delta T = 10.8 * \Delta R_T]^{\#}$ [Rusby, 2008]
4849 I	03/05/08	48.151952	48.152918	- 10.43 mK
4849 II	03/05/08	48.151913	48.152916	- 10.83 mK
4849 III	04/05/08	48.151985	48.152930	- 10.21 mK
274728 I	03/05/08	49.037664	49.038668	- 10.84 mK
274728 II	03/05/08	49.037619	49.038667	- 11.32 mK
909069 I	04/05/08	48.249069	48.250016	- 10.23 mK
Overall Mean	-	-	-	**- 10.64 mK**
∴ Standard deviation (2s)-Temperature difference between Pb 7.9 ppmw doped Spanish Sn and Reference Sn ± 0.86 mK				
∴ Temperature difference between "Pb 7.9 ppmw doped" and "Sn-Co" Spanish Sn (-10.64) – (-8.95) = - 1.69 mK				
∴ Standard deviation (2s) Difference -Temperature difference between "Pb 7.9 ppmw doped" and "Sn-Co" Spanish Sn (by quadrature addition) = ± 0.87 mK				

10.8 (mK/mΩ) is the appropriate conversion factor of sensitivity of $R(T_{90})$ [Rusby, 2008].

After comparison with the Reference Isotech Sn184 cell, the freezing temperature of the Spanish Sn-Co cell doped Pb 7.9 ppmw as listed in Table 6.11 was found to be 10.64 ± 0.86 mK lower than the Reference Isotech Sn184 cell. Therefore, the temperature difference between "Pb 7.9 ppmw doped" and Spanish Sn-Co was

decreased by 1.69 ± 0.87 mK. That means the Pb impurity results in a reduction in the freezing and melting temperatures of the Spanish tin ingot.

The equilibrium curves of the Spanish tin after doping with Pb 7.9 ppmw fixed-point and the temperature difference after calibration by comparison decreased roughly in line with expectations derived from interpolation of previous experiments as increasing amounts of impurities was introduced; the measured rates is as follows: Pb - 0.21 mK/ppmw. Figure 6.19 shows the significant impurity dependence of the tin melting point affected by a low concentration of Pb 7.9 ppmw. Total Pb impurities in the based Sn-Co sample can be checked the amount of concentrations by using the GD-MS, after finishing the last experiment of Pb doping.

Table 6.12 Stability Resistance results from three PRTs measured at triple point of water before and after the calibration by comparison between Spanish Sn-Co doped Pb 7.9 ppmw and Reference Isotech tin (Sn184) fixed-point cells. All measurements were recorded at 0 mA.

In Table 6.12, *i* represents the order of the resistance measurements of the PRTs at the triple point of water. # 10.8 (mK/mΩ) is the appropriate conversion factor of sensitivity of $R(T_{90})$ [Rusby, 2008].

Resistance values at triple point of water/Ω	**Date**	**Platinum Resistance Thermometers (PRTs) (Serial Number)**		
Cycle number and differences	**-**	**4849**	**274728**	**909069**
R_{TPW} (*1*)	02/05/08	25.444003	25.909952	25.493323
R_{TPW} (*2*)	03/05/08	25.444014	25.909959	-
$\Delta T_1 = \Delta R_1 * 10.8^{\#}$	-	+0.12 mK	+0.076 mK	-
R_{TPW} (*3*)	04/05/08	25.444004	-	25.493394
$\Delta T_2 = \Delta R_2 * 10.8^{\#}$	-	-0.11 mK	-	+0.77 mK
Mean of the ΔT	-	**+0.005 mK**	**+0.076 mK**	**+0.77 mK**
Standard deviation (2s)	-	**0.012 mΩ**	**0.01 mΩ**	**0.1 mΩ**

Table 6.12 presents the perform stability of the PRTs calibration at the triple point of water cells comparison between Spanish tin doped Pb 7.9 ppmw and Reference Isotech Sn184 fixed-point. This explains that the PRT number 4849 and 274728 have the small change with the measured cycling in the Spanish tin fixed-point temperature, while the values of PRT 909069 has a big change. The standard deviation (2s) for all measurements was within 0.1 mΩ which is equivalent to 1 mK approximately.

6.1.4.2 Spanish Tin doped 31.4 ppmw of Lead

A set of melting curves of Spanish Sn after doping with lead at 31.4 ppmw is presented in Figure 6.21.

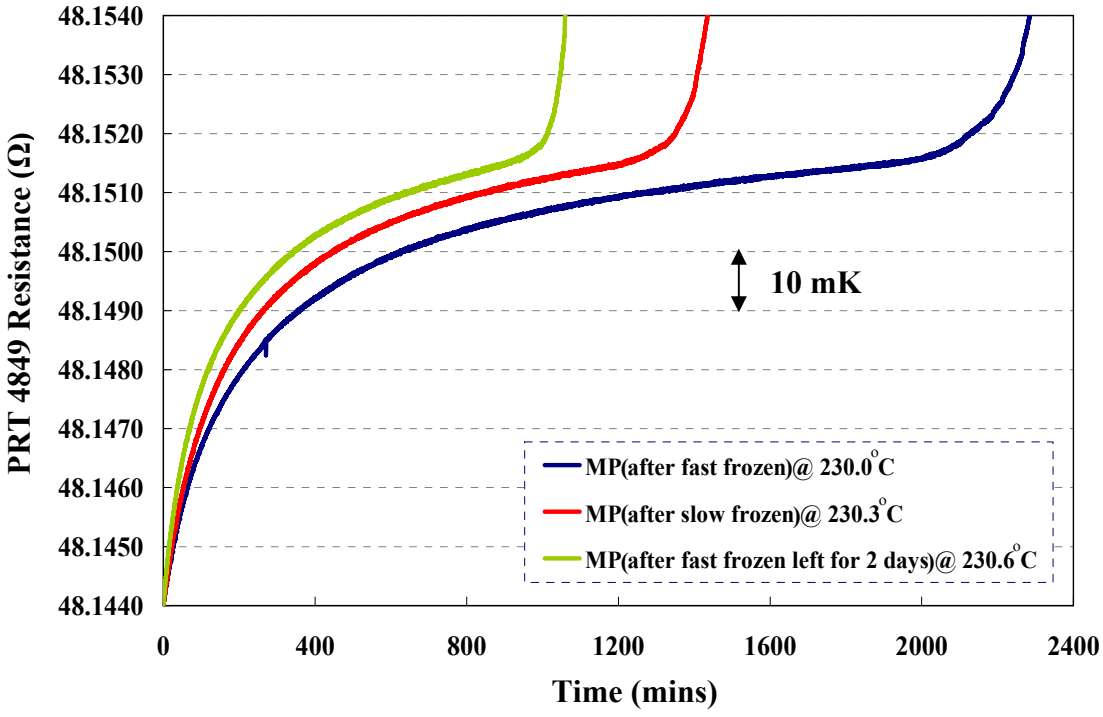

Figure 6.21 Melting curves of Spanish Sn sample containing an amount of lead concentrations at 31.4 ppmw plotted as a function of time. These curves were measured after different rates of prior freezing. The furnace was set at a different nominal furnace setting temperature for each melting curve.

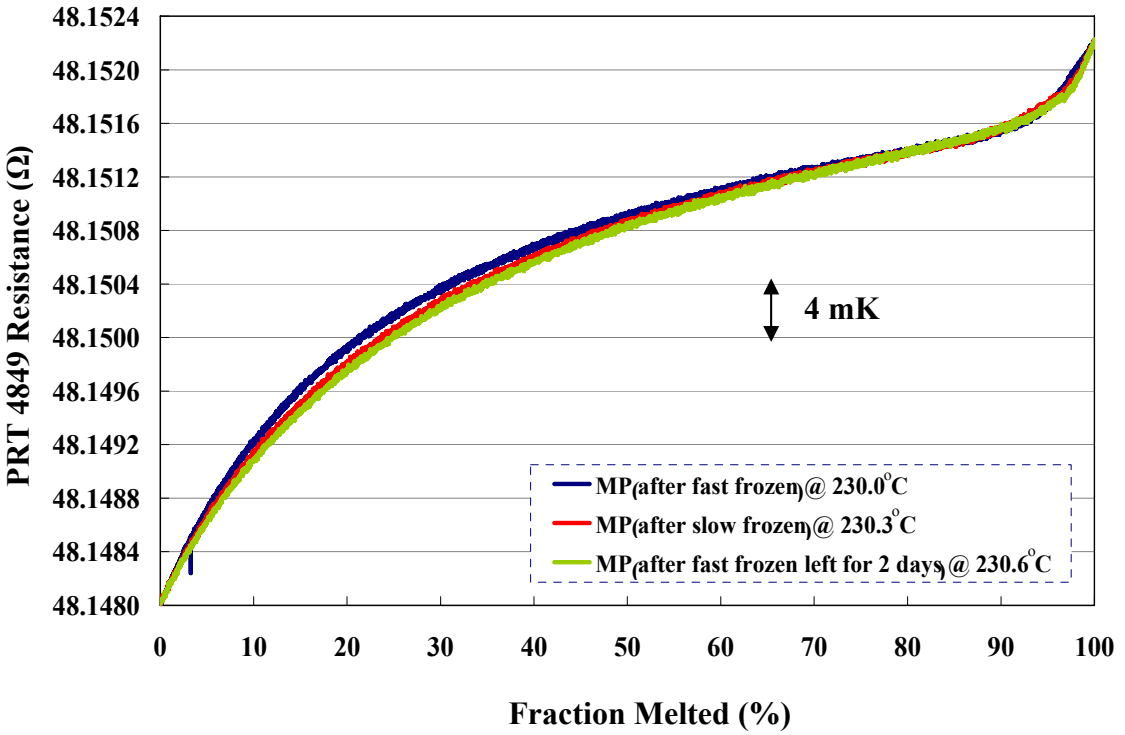

Figure 6.22 Melting curves of Spanish Sn sample doped with an amount of lead at concentration of 31.4 ppmw plotted as a fraction of sample melted. These curves were measured after different rate of prior freezing. The furnace setting of each melting curve was set at a different nominal temperature.

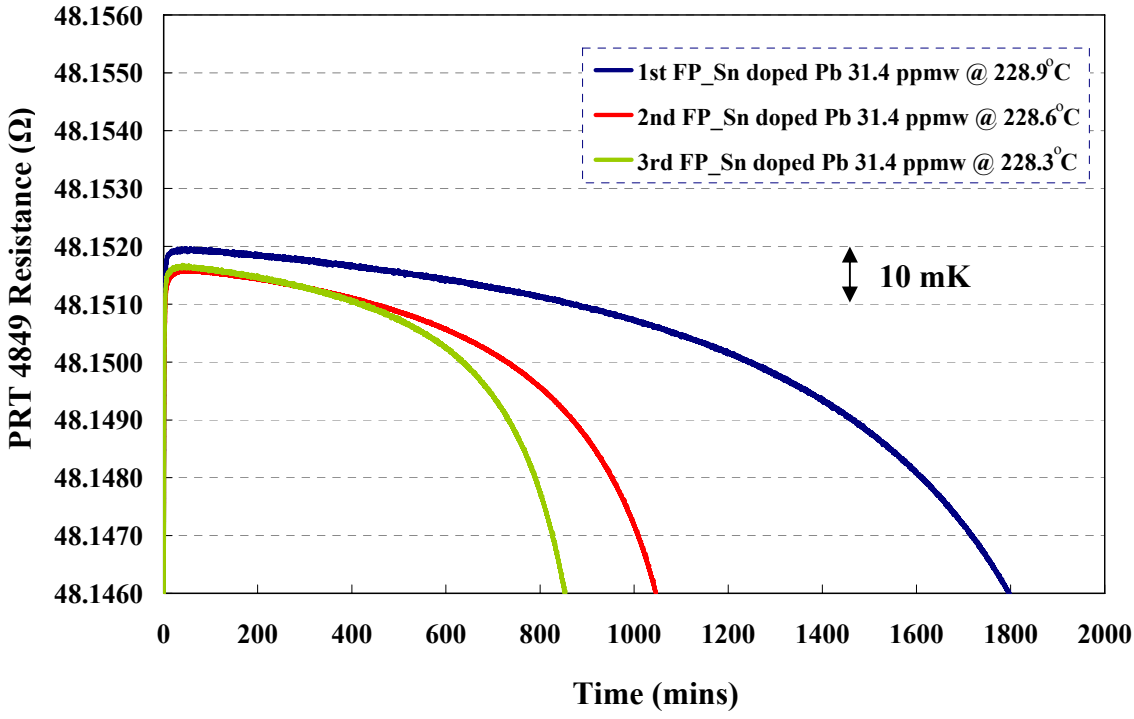

Figure 6.23 The equilibrium freezing curves of the Spanish Sn sample containing an amount of lead concentrations at 31.4 ppmw plotted as a function of time. These curves were realised at different settings of the temperature furnace.

Figure 6.22 shows the similar shape of Spanish Sn after doping lead for all measured melting curves. The prior frozen rate of the melting curves shows an insignificant influence to the shape of their curves as shown on the 2nd (red) and 3rd (green) curves.

In Figure 6.23, the first freezing curve presents a higher resistance value than the other two curves. This is mentioned that the base sample and impurity are not well mixed in the fixed-point ingot as agreed with the melting curves, in which the shape of the first melting curve is slightly separated from the other two. The other two freezing curves indicate the reproducibility of the resistance values. Because the temperature offset is different, therefore, the period of time is also different.

The peak of the freezing curves has been used to calibrate the PRTs by comparison method between the Spanish Sn-Co alloy system doped with 31.4 ppmw Pb and the Reference (Sn184) tin fixed-point cells with three PRTs. From Table 6.13, it indicates that the freezing temperature of the Spanish Sn-Co cell doped Pb 31.4 ppmw was found to be 15.47 ± 0.66 mK lower than the Reference Isotech Sn184 cell. Therefore, the temperature difference between “Pb 31.4 ppmw doped” and Spanish Sn-Co was decreased by 6.51 ± 0.68 mK.

Table 6.13 Summary of the average resistance values in the calibration measurements by comparison method between the Spanish Sn-Co alloy system doped with 31.4 ppmw Pb and the Reference (Sn184) tin fixed-point cells with three PRTs. The furnace setting was maintained at 229.1 °C for all freezing realisation measurements.

PRTs serial number	**Date**	**R_T Spanish Sn-Co doped "Pb 31.4 ppmw" (0 mA)**	**R_T Reference Sn 184 (0 mA)**	**Equivalent Temperature difference between Spanish Sn-Co and Sn184 cells** $[\Delta T = 10.8 * \Delta R_T]^{\#}$ [Rusby, 2008]
4849 I	06/06/08	48.151483	48.152940	- 15.73 mK
4849 II	10/06/08	48.151522	48.152936	- 15.27 mK
4849 III	11/06/08	48.151530	48.152933	- 15.15 mK
274728 I	06/06/08	49.037173	49.038652	- 15.97 mK
274728 II	11/06/08	49.037202	49.038634	- 15.47 mK
280140 I	10/06/08	47.511229	47.512635	- 15.18 mK
Overall Mean	-	-	-	**- 15.46 mK**
∴ Standard deviation (2s)-Temperature difference between Pb 31.4 ppmw doped Spanish Sn and Reference Sn ± 0.66 mK				
∴ Temperature difference between "doped Pb 31.4 ppmw" and "Sn-Co" Spanish Sn (-15.46) – (-8.95) = - 6.51 mK				
∴ Standard deviation (2s) Difference -Temperature difference between "Pb 31.4 ppmw doped" and "Sn-Co" Spanish Sn (by quadrature addition) ± 0.68 mK				

10.8 (mK/mΩ) is the appropriate conversion factor for the sensitivity of $R(T_{90})$ [Rusby, 2008].

The equilibrium curves of the Spanish tin after doping with Pb 31.4 ppmw fixed-point and the temperature difference after calibration by comparison decreased as increasing amounts of impurities was introduced; the measured rates is as follows: Pb - 0.21 mK/ppmw.

Table 6.14 Stability Resistance results from three PRTs measured at triple point of water before and after the calibration by comparison between Spanish Sn-Co doped Pb 31.4 ppmw and Reference Isotech tin (Sn184) fixed-point cells. All measurements were recorded at 0 mA.

Resistance values at triple point of water/Ω	**Date**	**Platinum Resistance Thermometers (PRTs) (Serial Number)**		
Cycle number and differences	**-**	**4849**	**274728**	**280140**
R_{TPW} (*1*)	06/06/08	25.444028	25.909966	25.103496
R_{TPW} (*2*)	10/06/08	25.444019	-	25.103486
$\Delta T_1 = \Delta R_1 * 10.8^{\#}$	-	-0.097 mK	-	-0.11 mK
R_{TPW} (*3*)	11/06/08	25.444019	25.909953	-
$\Delta T_2 = \Delta R_2 * 10.8^{\#}$	-	0 mK	-0.14 mK	-
Mean of the ΔT	-	**-0.097 mK**	**-0.14 mK**	**-0.11 mK**
Standard deviation (2s)	-	**0.01 mΩ**	**0.018 mΩ**	**0.014 mΩ**

In Table 6.14, *i* represent the order of the resistance measurements of the PRTs at the triple point of water. # 10.8 (mK/mΩ) is the appropriate conversion factor for the sensitivity of $R(T_{90})$ [Rusby, 2008].

The standard deviation (2s) for all measurements agreed to within 0.02 mΩ which is equivalent to 0.22 mK approximately. These measurements were checked within a few hours after the measurements at the tin temperature. However, the water stability for all PRTs does not show the repeatability for good thermometers when compared with the resistance values of the measurements at the Reference Sn184 cell. It shows a better repeatability than water triple point values as presented in Table 6.15 and accompanying text.

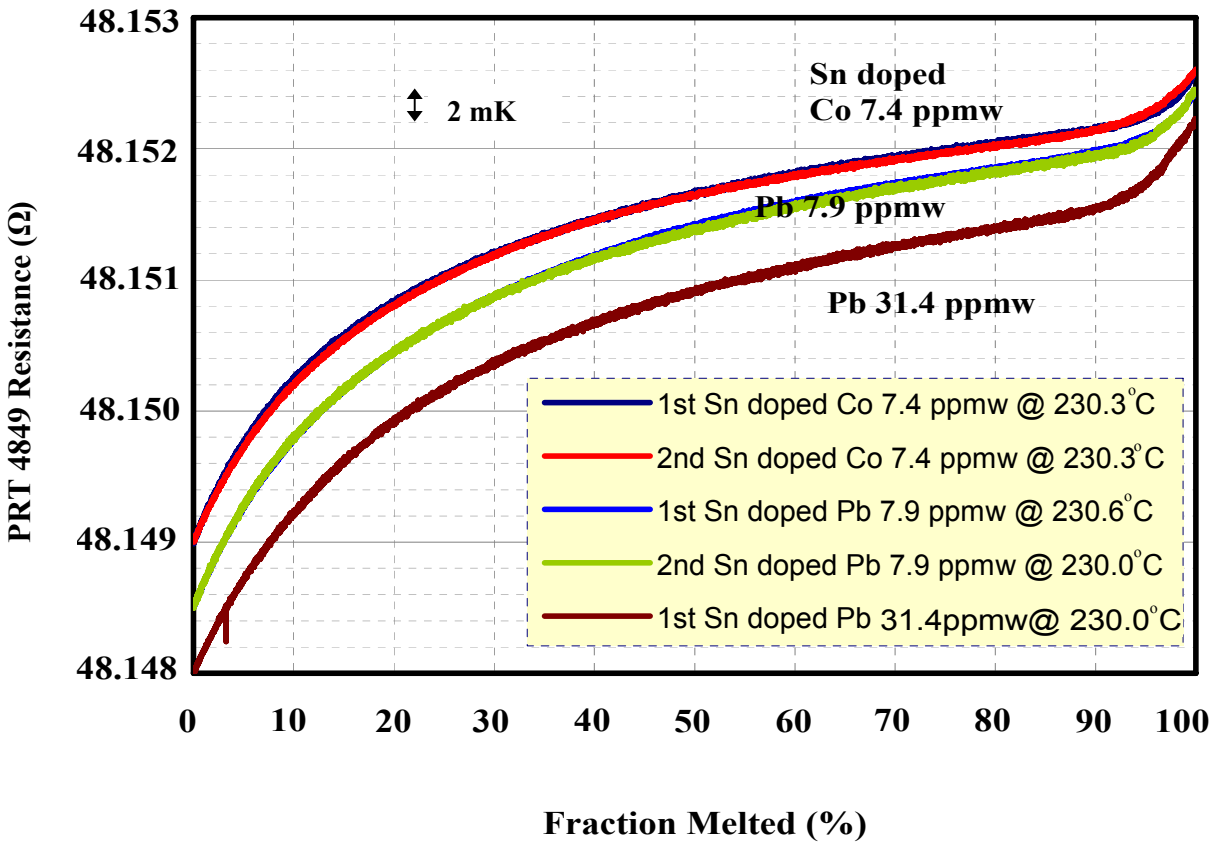

Figure 6.24 Example of melting curves of "Spanish Tin" after doping with low-level concentrations of lead. The curves are compared with the previous curves of Spanish tin doped with cobalt. The temperatures are nominal settings of the furnace.

The results obtained after doping with cobalt and lead support the previous data that the temperatures of the fixed point were affected at these low impurity levels. Moreover, their curves, before and after doping, confirm the reproducibility of the temperature measurements in these fixed-point cells. Figure 6.24 and 6.25 show the shift of the melting and freezing curves after doping the tin with increasing concentrations of cobalt and lead impurities From this work, the temperature change of the freezing and melting curves of the tin fixed point were affected by amounts as follows: Co -0.69 mK/ppmw (obtained at Co 5.5 ppmw), Co -0.77 mK/ppmw (obtained at Co 7.4 ppmw) and Pb -0.21 mK/ppmw (obtained at Pb 7.9 ppmw), Pb - 0.21 mK/ppmw (obtained at Pb 31.4 ppmw). Therefore, The equilibrium curves of the tin fixed-point decreased roughly in line with expectations derived from interpolation of previous experiments as increasing amounts of impurities were introduced; the average measured rates are as follows: Co -0.73 and Pb -0.21 in units of mK/ppmw. This expectation is compared with Hansen's book [Hansen, 1958],

which was interpolated to be depressed by 0.60 mK/ppmw and 0.133 mK/ppmw for cobalt and lead impurity, respectively.

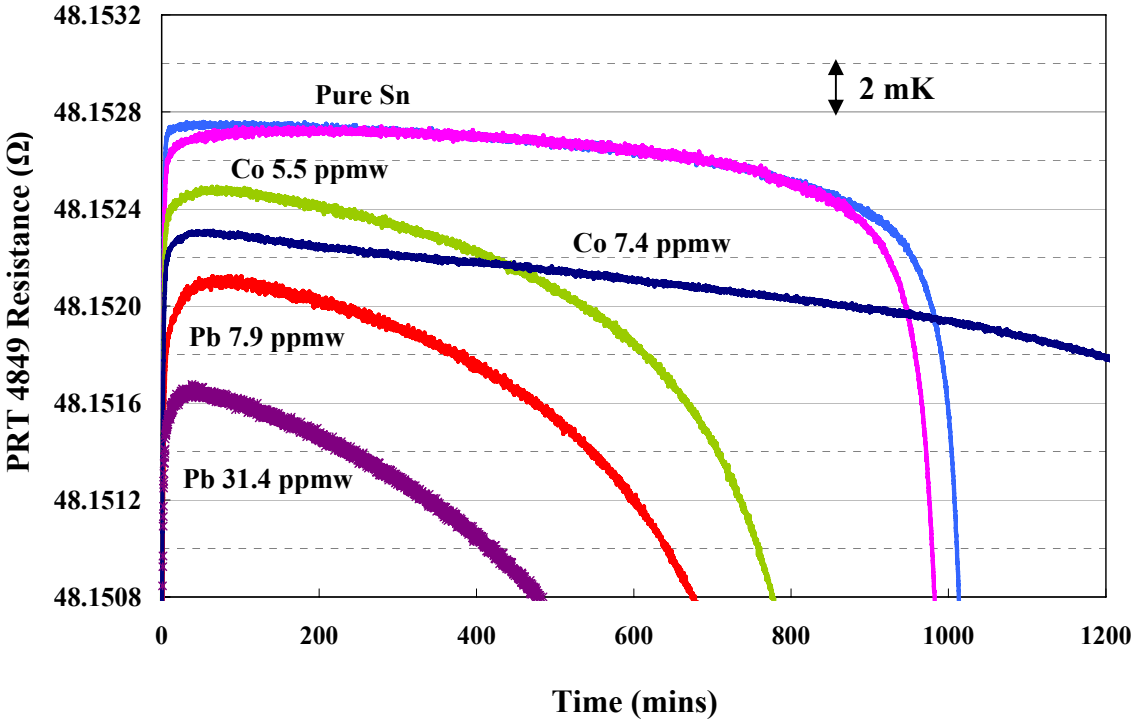

Figure 6.25 Example of high purity tin freezing curves and the shift of these curves after doping the tin with increasing concentrations of cobalt and lead impurities, plotted as a function of time. The end of the curve tin doped with 7.4 ppmw cobalt continues off the graph due to the small furnace temperature offset.

Table 6.15 The stability of the PRT 4849, which was checked at the freezing point of the Reference Sn184 cell at 0 mA and in a water point.

Date	Resistance Values (R_T, Ω)	Resistance values at triple point of water/Ω
20/06/07	48.152808	25.443956
21/06/07	48.152808	25.443956
23/10/07	48.152897	25.443961
24/10/07	48.152901	25.443949
22/01/08	48.152911	25.443974
23/01/08	48.152932	25.443985
24/01/08	48.152898	25.443971
26/03/08	48.152915	25.443977
01/04/08	48.152928	25.443980
03/05/08	48.152917	25.444014
06/06/08	48.152940	25.444028
10/06/08	48.152936	25.444019
11/06/08	48.152933	25.444019
Standard deviation (2s)	0.09 mΩ	0.06 mΩ

Table 6.15 shows all measurements of PRT 4849 at the freezing point of the Reference Sn 184 cell and at the triple point of water after checking in the Reference Sn cell. If one takes into account that the affect of any change in the water point is amplified by a factor of W at the tin point temperature then the resistance values in Reference Sn 184 cell shows much better repeatability of than the PRT values in the water triple point. (The water values also have a greater range than the Sn values).

6.1.5 Impurity Analysis of Spanish Tin Fixed-Point after Doping with Co and Pb Contents

Glow Discharge Mass Spectrometry (GD-MS) Characteristics after Doping Impurities

The previous GD-MS results of the Spanish tin fixed-point cell before impurity doping indicate that the tin metal and the impurities are well mixed after the tin is properly molten. The impurity levels in three areas of the tin ingot show the homogeneity of the impurity concentration. Therefore, only one piece of the Spanish Sn after doping with Co and Pb impurities was cut from the ingot to detect the impurity concentrations by the GD-MS technique. Also, one piece of ingot before doping, which was cut almost a year ago and kept in NPL, was checked the GD-MS at the same time as the after doping piece. The GD-MS result of these two pieces, compared with the previous results, which were measured before doping, is shown in Table 6.16.

Table 6.16 GD-MS analysis results of the impurity concentrations of the "Spanish" tin before and after doping [NRC report number: 30337R1 (checked on 14/12/07) & 30817 (checked on 22/08/08)]. These elements were detected in term of mass fraction (in parts per billion by weight, ppbw). The uncertainty is quoted as a "factor of 2", though this is probably a conservative overestimate

Element	Spanish Sn Before Doping (Average from three areas)	Spanish Sn Before doping (Cut a year ago)	Spanish Sn After Doping	Element	Spanish Sn Before Doping (Average from three areas)	Spanish Sn Before doping (Cut a year ago)	Spanish Sn After Doping
	ppbw				ppbw		
Li	<0.3	<0.2	<0.2	**Br**	**<23**	**<480**	**<480**
Be	<0.1	<0.07	<0.08	**Rb**	<0.5	<0.1	<0.2
B	<0.3	<0.1	<0.1	**Sr**	<0.2	<0.1	<0.09
C	1600	940	1100	**Y**	<0.2	<0.09	<0.08
N	250	25	35	**Zr**	<0.2	<0.2	<0.2
O	530	110	210	**Nb**	<0.2	<0.09	<0.1
F	<0.9	<2	<1	**Mo**	<1	<0.5	<0.5
Na	<0.2	<0.1	<0.1	**Pd**	-	-	-
Mg	<0.3	<0.2	<0.1	**Ag**	<2	<1	<0.9
Al	<0.2	0.6	2	**Cd**	<23	<40	<40
Si	<0.5	<0.4	0.8	**In**	**3900**	**<3800**	**<3200**
P	1	<0.2	<0.1	**Sn**	Matrix	Matrix	Matrix
S	350	480	440	**Sb**	**<43**	**<370**	**<290**
Cl	1.4	<0.5	<0.6	**Te**	<3	<2	<2
K	<45	<10	<45	**I**	<5	<11	<9
Ca	<5	<3	<2	**Cs**	<0.5	<2	<2
Sc	<0.2	<0.1	<0.1	**Ba**	<0.3	<1	<5
Ti	<0.2	<0.1	<0.07	**La**	<0.3	<1	<6
V	<0.1	<0.07	<0.07	**Ce**	<0.2	<1	<6
Cr	<0.5	<0.3	<0.2	**Hf**	<0.7	<0.3	<0.3
Mn	<0.3	<0.2	<0.1	**Ta**	-	-	-
Fe	<4	<2	8	**W**	<0.6	<0.2	<0.2
Co	**<100**	**<100**	**<100**	**Pt**	<2	<0.9	<0.9
Ni	<18	<9	<10	**Au**	**<10**	**<60**	**<80**
Cu	<1	<0.7	17	**Hg**	<8	<3	<3
Zn	<2	<1	<2	**Tl**	<1	<0.6	<0.9
Ga	<0.9	<1	<2	**Pb**	**<15**	**12**	**23000**
Ge	<2	<1	<1	**Bi**	<0.6	<0.3	<0.6
As	<12	<7	<8	**Th**	<0.2	<1	<0.9
Se	<67	<250	<550	**U**	<0.4	<3	<2

Table 6.16 presents the GD-MS analysis results of the impurity concentrations of the "Spanish" tin before and after doping. The uncertainty of this GD-MS analysis is considered to be accurate within a factor of two of the values obtained, at a confidence level of 95% though there is anecdotal evidence that the results are more accurate than quoted. Considering the Co impurity concentrations, it was found that the amount of Co had not changed even though the cobalt was deliberately introduced into the Spanish tin sample. Subsequently we discovered that for GD-MS analysis, the Co signal is an "interfering signal" on the predominant Sn peak and therefore not resolvable. Therefore, it results in a GD-MS (VG-9000) detector that cannot measure the amount of Co.

Considering Pb, it shows that the increased amount of Pb after adding total 31.4 ppmw (31400 ppbw). The total amount of Pb from GD-MS presents 23000 ppbw, which is less than the real amount added.

Considering Indium (In) impurity in Table 6.15, it shows a large and variable amount. Anecdotally, we have been told that In is a common impurity in tin "pure" sample.

Considering Table 6.16 as a whole: the GD-MS measurements show a variable amount of Se, Br, Sb and Au. However, we note that these background values show better agreement in the measurements made at the same time; even though the samples were cut from the ingot at different times of its life (pre and post doping). Conversely samples cut from the ingot at the same time (pre-doped), but GD-MS measured a year apart, show a bigger difference in their results.

Consequently, the time of measurement of the sample is one important factor for the GD-MS results. That is the different samples, i.e. Spanish Sn before and after doping, measured at the same time give more similar amounts of background impurities than the "same sample" at different times (Except for the doping impurities).

6.1.6 Photographs of Spanish Tin Cell

The photographs of Spanish tin fixed-point ingot before and after doping with any impurities will be shown in Section 6.2.4. As the colour of the ingot's surface of the Mini tin ingot shows interesting changes, then the photographs of Spanish tin will be considered in the same section as Mini Isotech tin.

6.1.7 Mass of Spanish Tin Fixed-Point Ingot

The measured mass method for Spanish ingot had been described in Section 5.4.1.2.(a). The uncertainty on this balance scale (a large scale) can be corrected by adding 1.09 mg to the value of the weight. The uncertainty components are as follows;

0.05 mg for the scale error (rectangular distribution)

0.06 mg for repeatability (normal distribution)

0.1 mg for balance resolution (rectangular distribution)

From the above information, obtained from NPL Mass section, the uncertainty of the weighing itself is very small when compared with the total mass of Spanish tin ingot (~1 Kg). Thus, the uncertainty is negligible compared to that of the included graphite re-entrant well, where the two methods for accounting for the graphite in Table 6.17 differ by 0.6g. The measured mass of Spanish tin metal after cutting some samples off for the undoped GD-MS testing was used in calculation of the doping concentrations (in ppmw).

Table 6.17 Mass of Spanish tin fixed-point ingot as calculated based on a mass measurement (of the tin and central graphite) before doping the impurities.

Component(s) of Spanish Tin Cell	Mass (g)
Calculated Mass of Spanish tin metal (Originally)	961.99 g
Measured Mass {Spanish tin metal and graphite re-entrance well} (Originally) less the calculated mass of graphite	961.32 g
Measured Mass of Spanish tin metal (Samples cut off) less the calculated mass of graphite	954.58 g

6.2 High Purity "Mini Isotech" Tin Fixed Point

6.2.1 Temperature Realisation of "Undoped" Mini Isotech Tin

The experimental results of high purity Spanish tin fixed-point cell will be summarised and formed in terms of the "Family Tree" as presented in Figure 6.26.

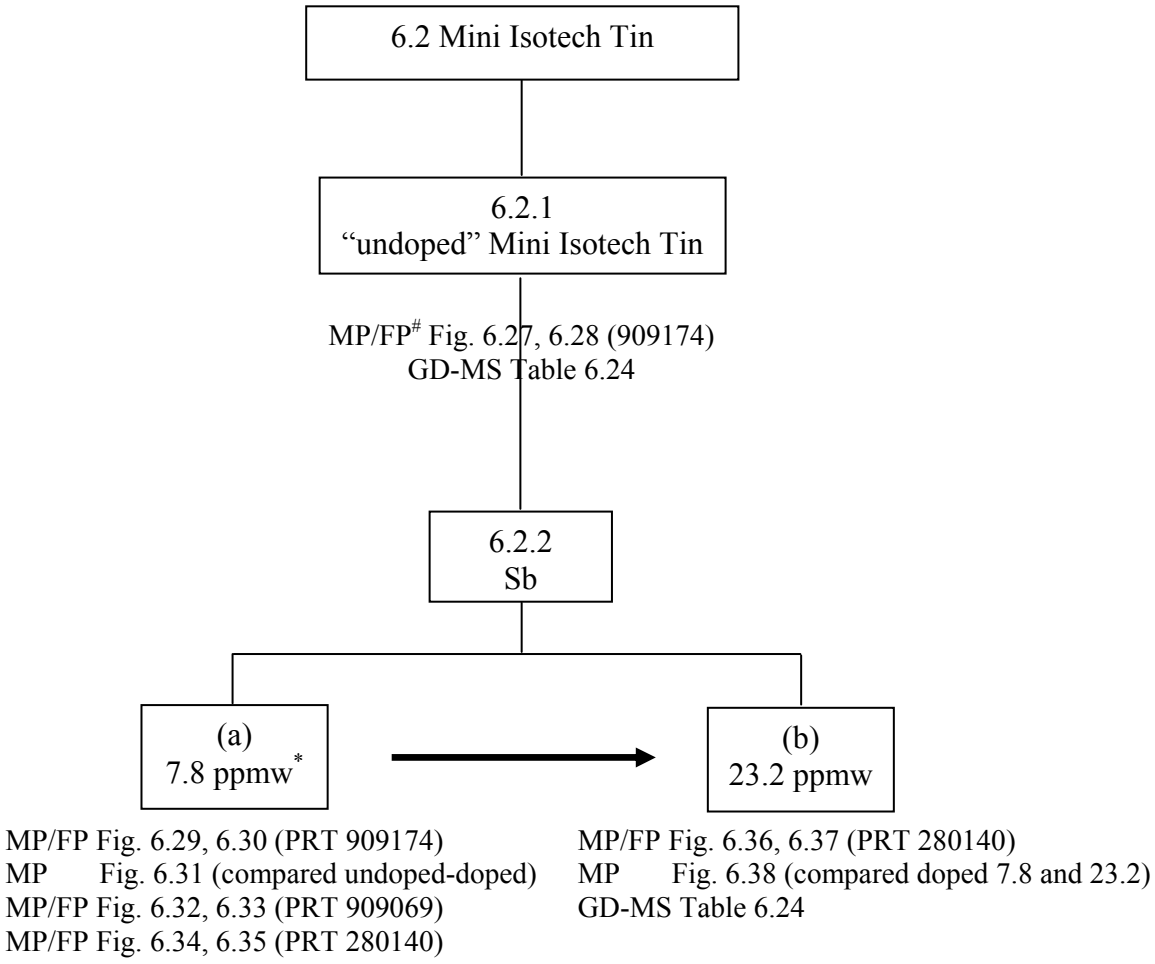

MP/FP = Melting and Freezing curves conducted in this stage.

GD-MS = Glow discharge mass spectrometry analysis performed in this stage.

* ppmw = Parts per million by weight

Figure 6.26 "Family Tree" showing the figure number of the freezing/ melting curves and the analysis technique of Mini Isotech tin obtained for a particular combination of conditions.

The melting transitions after rapid freezing of initially 99.9999% nominal high purity “Mini Isotech” tin cell presented in Figure 6.27. The PRT resistance values on the Y axis for all figures of the freezing and melting curves of Mini Isotech tin cell were calculated from the resistance ratio of PRT and standard resistor values but these values did not include the correction of the hydrostatic head, while the resistance values of PRT calibration by comparison measured at the peak of the freeze do include the correction of the hydrostatic head of the cell.

Figure 6.27 and 6.28 show the reproducibility of the resistance values measured at the melting and freezing temperatures of this tin cell. Also, the figures confirm that the time period of the transition is related to the furnace setting. In Figure 6.28, red and green lines show transitions where the furnace was set at 231.6 ^{o}C and indicate a similar time to the solidus point (100% solid) on the curves. All melting temperature realisations were obtained after rapid freezing, which is the best method to get a good shape of the melting curves. The rate of the freeze preceding the melting curve influences the impurity distribution in the solid metal ingot, which that would also affect the shape of the melting curve. This is confirmed by Ancsin’s [Ancsin, 2007] and Zhang’s publications [Zhang *et al*., 2008].

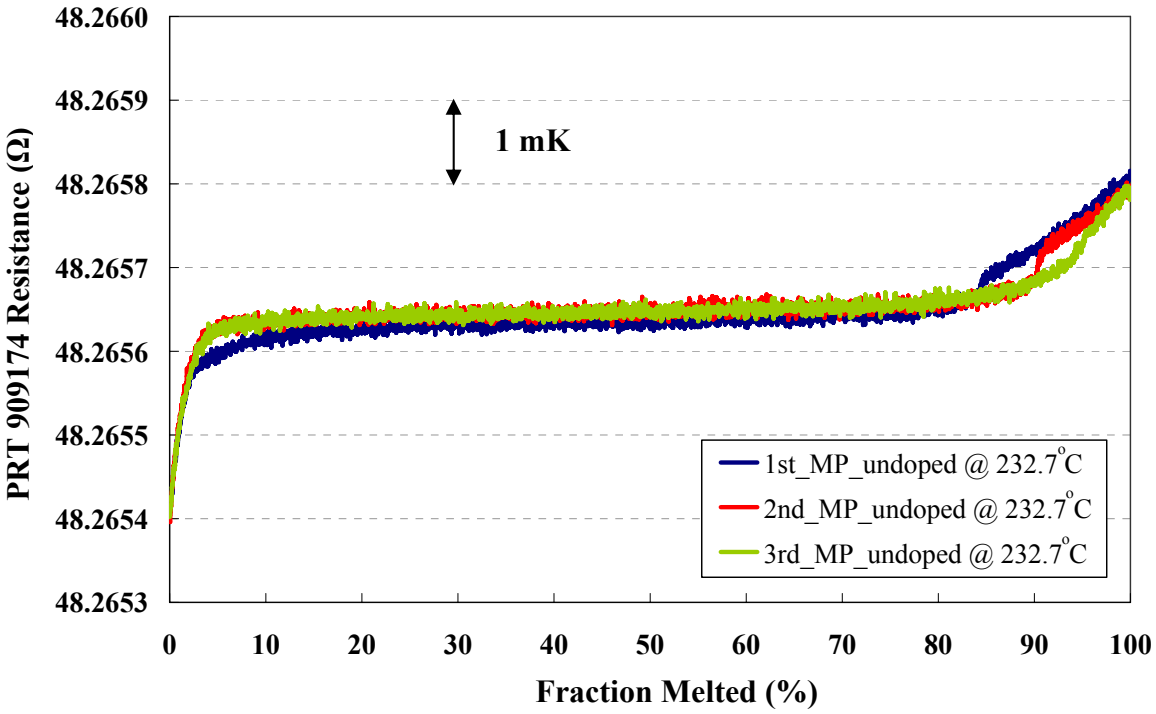

Figure 6.27 A set of melting curves obtained on high purity "Mini Isotech". The furnace setting for all realisations is set at the same temperature.

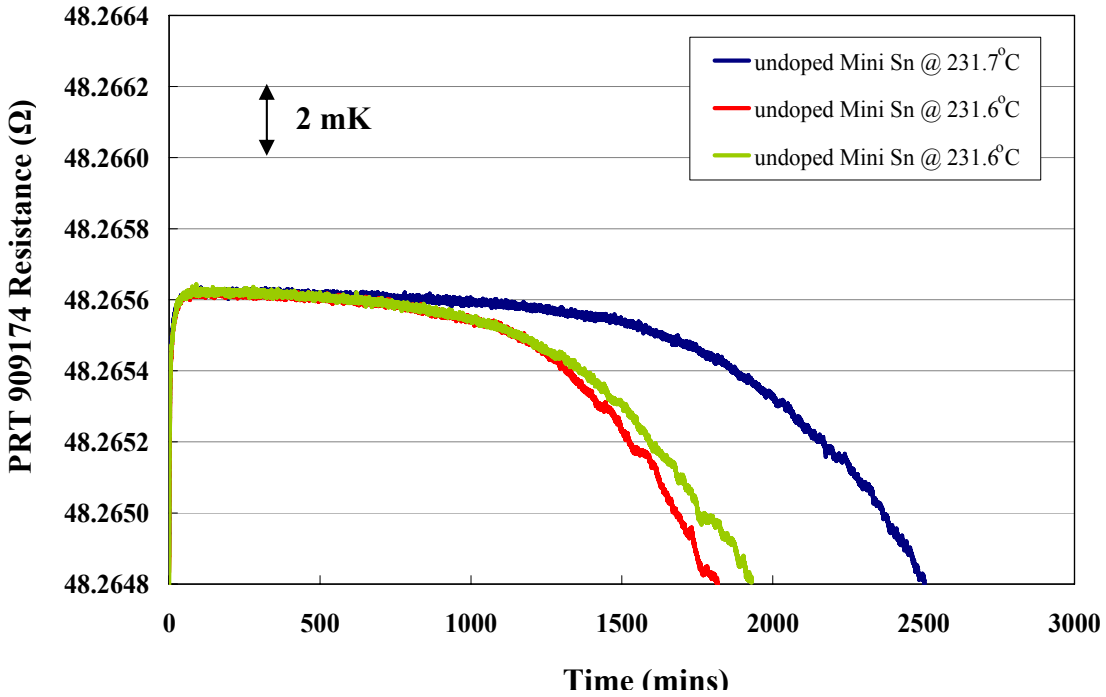

Figure 6.28 Three freezing curves of "undoped" Mini Isotech Sn fixed-point cell plotted as a function of time.

Table 6.18 Summary of the average resistance values in the calibration measurements by comparison method between the High purity "Mini Isotech" and the Reference (Sn184) tin fixed-point cells with three PRTs. The furnace setting was 231.7 ^{o}C for all freezing realisation measurements.

PRTs serial number	**Date**	**R_T High purity "Mini Isotech" (0 mA)**	**R_T Reference Sn 184 (0 mA)**	**Equivalent Temperature difference between High purity "Mini Isotech" and Sn184 cells** $[\Delta T = 10.8 * \Delta R_T]^{\#}$ [Rusby, 2008]
909174 I	05/11/07	48.265479	48.265533	- 0.58 mK
909174 II	06/11/07	48.265483	48.265545	- 0.67 mK
909174 III	06/11/07	48.265475	48.265555	- 0.86 mK
909174 IV	07/11/07	48.265480	48.265530	- 0.54 mK
909069 I	05/11/07	48.249878	48.250034	- 1.68 mK
909069 II	06/11/07	48.249885	48.250051	- 1.79 mK
4849 I	06/11/07	48.152814	48.152902	- 0.95 mK
4849 II	07/11/07	48.152826	48.152873	- 0.51 mK
Overall Mean	-	-	-	**- 0.95 mK**
∴ Standard deviation (2s)-Temperature difference between High purity Mini Isotech Sn and Reference Sn ± 1.02 mK				
∴ Temperature difference between "Mini Isotech" Sn and Reference Sn184 = - 0.95 mK				

10.8 (mK/mΩ) is the appropriate conversion factor for the sensitivity of $R(T_{90})$ [Rusby, 2008].

The standard deviation (2s) for all measurements as listed in Table 6.18 is about 1.02 mK. After comparison with the reference tin cell, the initial freezing temperature of the Mini Isotech tin cell was found to be 0.95 ± 1.02 mK lower than the reference tin cell. That means the Mini Isotech tin ingot contained some pre-existing contamination affecting its freezing and melting temperatures.

We presume that the influence of each impurity in the host material remains independent of each other at low concentrations. The magnitude of each effect on the temperature depends on both the species type and the amount of that particular species and the total temperature change is the sum of the individual effects, taking account of any sign. The kinds of impurities, which contaminated this cell before deliberate doping would be analysed with the GD-MS technique. The GD-MS result before doping presents in Table 6.24, which is the same Table as GD-MS after doping.

Table 6.19 Resistance values from three PRTs measured at the triple point of water before and after the calibration by comparison between "undoped" Mini Isotech tin and Reference Isotech tin (Sn184) fixed-point cells.

Resistance values at triple point of water/Ω	**Date**	**Platinum Resistance Thermometers (PRTs) (Serial Number)**		
Cycle number and differences	**-**	**4849**	**909174**	**909069**
R_{TPW} (*1*)	03/11/07	25.443992	25.501256	25.493409
R_{TPW} (*2*)	05/11/07	-	25.501258	25.493461
$\Delta T_1 = \Delta R_1 * 10.8^{\#}$	-	-	**+0.022 mK**	**+0.56 mK**
R_{TPW} *(3)*	06/11/07	25.443983	25.501276	25.493451
$\Delta T_2 = \Delta R_2 * 10.8^{\#}$	-	**-0.097 mK**	**+0.19 mK**	**-0.11 mK**
R_{TPW} *(4)*	07/11/07	25.443981	25.501258	-
$\Delta T_3 = \Delta R_3 * 10.8^{\#}$	-	**-0.022 mK**	**-0.19 mK**	-
Mean of the ΔT	-	**-0.06 mK**	**+0.022 mK**	**+0.23 mK**
Standard deviation (2s)	-	**0.012 mΩ**	**0.019 mΩ**	**0.056 mΩ**

In Table 6.19, *i* represent the order of the resistance measurements of the PRTs at the triple point of water. # 10.8 (mK/mΩ) is the appropriate conversion factor for the sensitivity of $R(T_{90})$ [Rusby, 2008].

The standard deviation (2s) for all measurements was 0.056 mΩ which is equivalent to 0.60 mK approximately. This shows that these PRTs have no gross instabilities during the measurement cycle in this tin fixed-point temperature. From Table 6.19, the PRT 4849 shows the smallest amount of the standard deviation, i.e.

0.012 mΩ (0.13 mK), to check the resistance values at the triple point of water. However, this PRT was not available to use because it was used to calibrate in Spanish tin cell. Therefore, the next PRT, which shows the small change of the standard deviation (0.019 mΩ) and the ΔT is the PRT 909174. This is the reason why the PRT 909174 was used to calibrate in Mini Isotech tin cell.

6.2.2 Influence of Antimony on High Purity Mini Isotech Tin Fixed-Point

The originally pure Mini Isotech tin ingot was doped with antimony (Sb) impurity; total concentrations as follows (in ppmw): Sb 7.8 and 23.2, respectively.

6.2.2.1 Mini Isotech Tin doped with 7.8 ppmw of Antimony

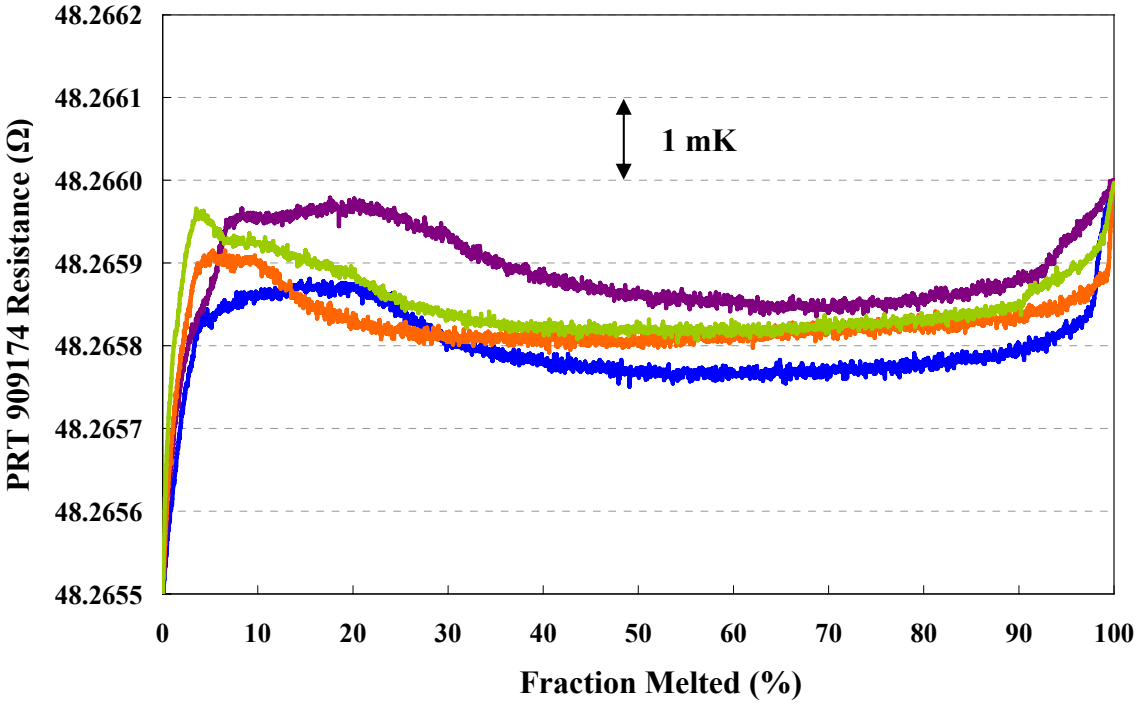

Figure 6.29 PRT resistance value at the melting temperature for "Mini Tin" after doping with 7.8 ppmw of antimony as a function of the approximate tin percentage melted. All curves were melted at different temperature settings. The light blue and purple lines refer to the recorded curves at 232.7 °C; the orange colour represents the measured curve at 232.6 °C; and the green line is the melting curve produced at 232.9 °C. The PRT number 909174 was used to measure the fixed-point temperature. (All quoted temperatures are nominal settings of the controller).

In Figure 6.29, the offset of the "Mini Isotech tin" fixed point, after doping with low levels of antimony, is presented. The melting temperature of the 7.8 ppmw antimony doped tin is higher than for the "pure" Mini tin. It indicates that at low levels, antimony elevates the melting and freezing temperatures although the temperature change is less than expected as compared with Figure 6.27 and 6.28.

However for the antimony doping very unusual melting traces have been produced – with a pronounced bump/ increase in the temperature for several hours at the start of the melt, before settling back (antimony is expected to increase the temperature of the whole plateau). PTB has also reported "bumps", but of a much shorter duration [Zhang *et al.*, 2008]. It may be the result of non-uniform distribution of the antimony, but how that would produce this curve shape, and why it is roughly reproducible remains unexplained. It may be that the antimony is being concentrated in the solid phase during the preceding freeze, so that it tends to be near the well and the outside wall of the ingot. This is particularly possible, as a preceding fast melt/freeze cycle had not been performed before all these meltings. (Other results presented later (see Fig 6.32) seem to support this suggestion as larger peaks were seen after slower freezes). The freeze shapes themselves are not especially affected by the length of the freeze. A set of freezing curves take different lengths of time depending on the furnace offset temperature are shown in Figure 6.30.

In Figure 6.31, the offset of the "Mini Isotech tin" fixed point, after doping with low levels of antimony, is presented. All melting curves were obtained after the rapid freeze. The melting temperature of the 7.8 ppmw antimony doped tin is higher than for the "pure" Mini tin. It indicates that at low levels, antimony elevates the melting and freezing temperatures although the temperature change is less than expected as compared from the Figure of Mini Isotech tin before and after Sb doping.

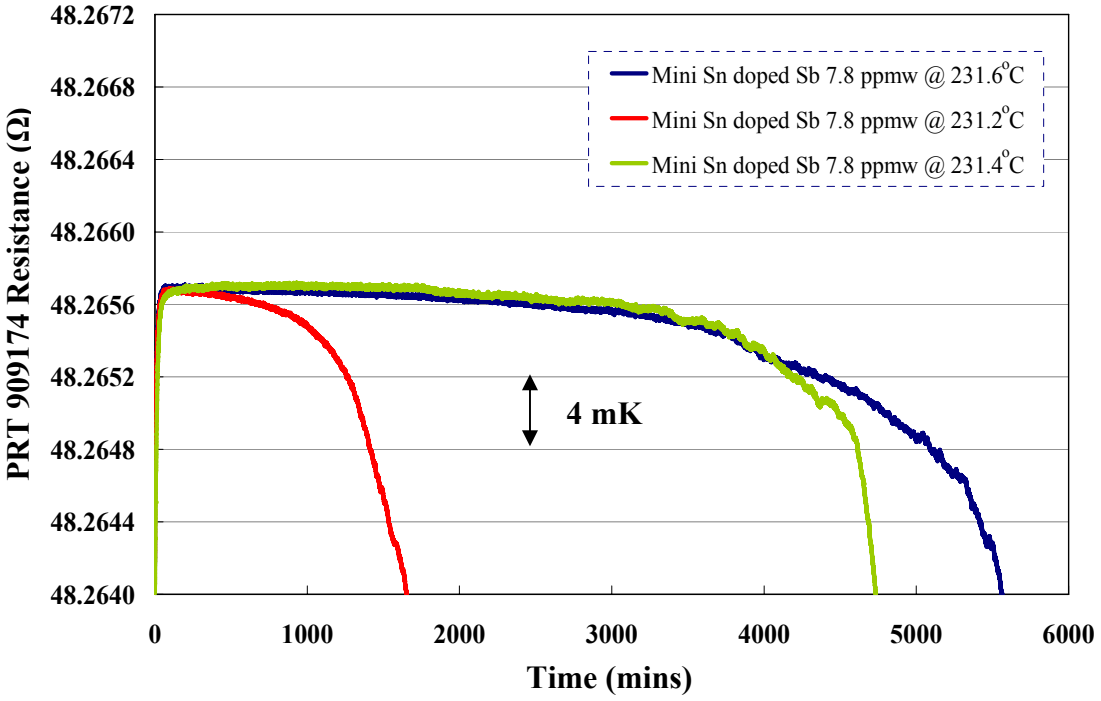

Figure 6.30 Three freezing curves of Mini Isotech Sn fixed-point cell after adding 7.8 ppmw of antimony plotted as a function of time. The furnace setting was set at different temperatures. The PRT number 909174 was used to calibrate the fixed-point temperature.

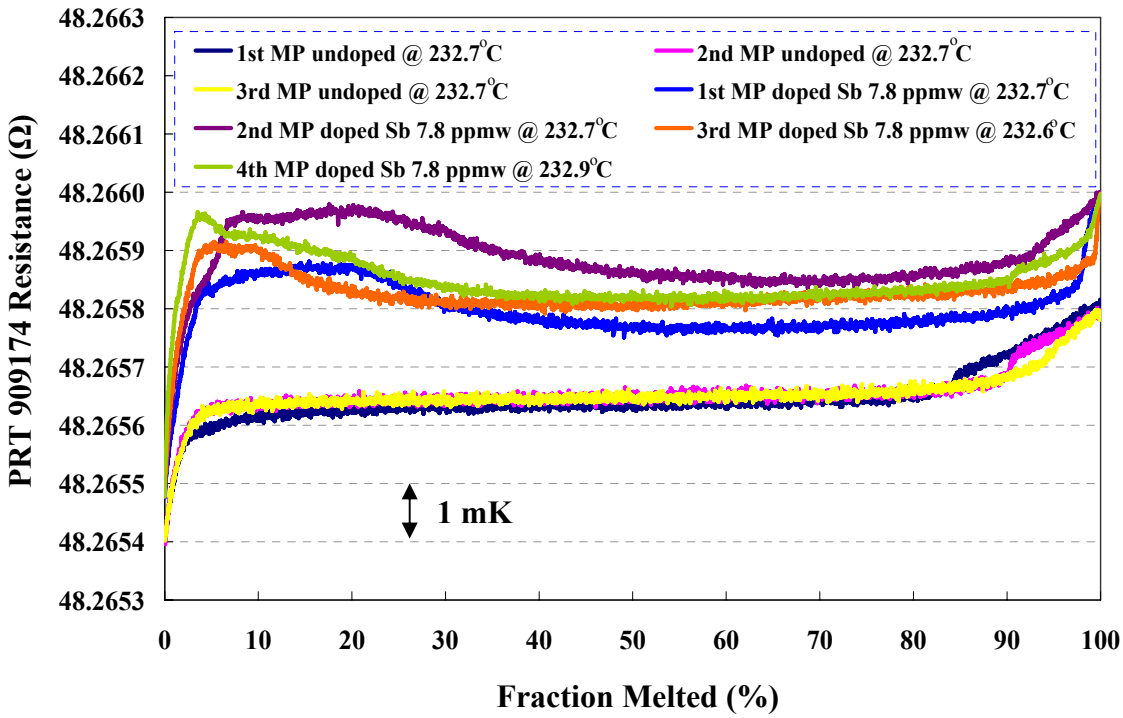

Figure 6.31 Changes in the PRT resistance value changing for "Mini Tin" after doping with antimony at 7.8 ppmw as a function of the approximate tin percentage melted. The PRT number 909174 was used to calibrate the fixed-point temperature.

Table 6.20 Summary of the average resistance values from the comparison measurements between Mini Isotech after doping with antimony at 7.8 ppmw and the reference (Sn184) tin fixed-point cells with three. As measurement is made on the same ASL F18 Bridge and standard resistor for each PRT then, the resistance values can be compared for each PRT. The furnace is set at 231.6 ^{o}C.

PRTs serial number	**Date**	**R_T "Mini Isotech" Doped Sb 7.8 ppmw (0 mA)**	**R_T Reference Sn 184 (0 mA)**	**Equivalent Temperature difference between "Mini Isotech" Doped Sb 7.8 ppmw and Sn184 cells** $[\Delta T = 10.8 * \Delta R_T]^{\#}$ [Rusby, 2008]
909174 I	27/02/08	48.265553	48.265584	- 0.33 mK
909174 II	04/03/08	48.265578	48.265600	- 0.24 mK
909174 III	04/03/08	48.265584	48.265605	- 0.23 mK
909174 IV	12/03/08	48.265611	48.265629	- 0.19 mK
4849 I	04/03/08	48.152922	48.152917	+ 0.054 mK
4849 II	12/03/08	48.152901	48.152927	- 0.28 mK
280140	09/05/08	47.512594	47.512653	- 0.64 mK
274728	09/05/08	49.038633	49.038672	- 0.42 mK
Overall Mean	-	-	-	**- 0.28 mK**
∴ Standard deviation (2s)-Temperature difference between Sb 7.8 ppmw doped Mini Isotech Sn and Reference Sn ± 0.40 mK				
∴ Temperature difference between "Sb 7.8 ppmw doped" and "undoped" Mini Isotech tin cell (-0.28) - (-0.94) = + 0.66 mK				
∴ Standard deviation (2s) Difference -Temperature difference between "Sb 7.8 ppmw doped" and "undoped" Mini Isotech Sn (by quadrature addition) ± 1.10 mK				

10.8 (mK/mΩ) is the appropriate conversion factor for the sensitivity of $R(T_{90})$ [Rusby, 2008].

After comparison with the reference tin cell, the peak of the freezing curves after doping with Sb at 7.8 ppmw had increased 0.66 ± 1.10 mK as presented in Table 6.20. It indicates that at low levels, antimony elevates the melting and freezing

temperatures although the temperature change is less than expected. The equilibrium curves of the tin fixed-point increased as increasing amounts of impurities were introduced; the measured rate is: Sb +0.08 in units of mK/ppmw.

After obtaining all results from the realisations of the Mini Isotech tin after adding with the first lot of antimony at 7.8 ppmw, the PRT 909174 was broken by accident. Therefore, the measurement would be done again with the new PRTs, i.e. the PRT 909069 and 280140. The PRT 909069 was the first PRT used to measure the melting and freezing curves as shown in Figure 6.32 and 6.33.

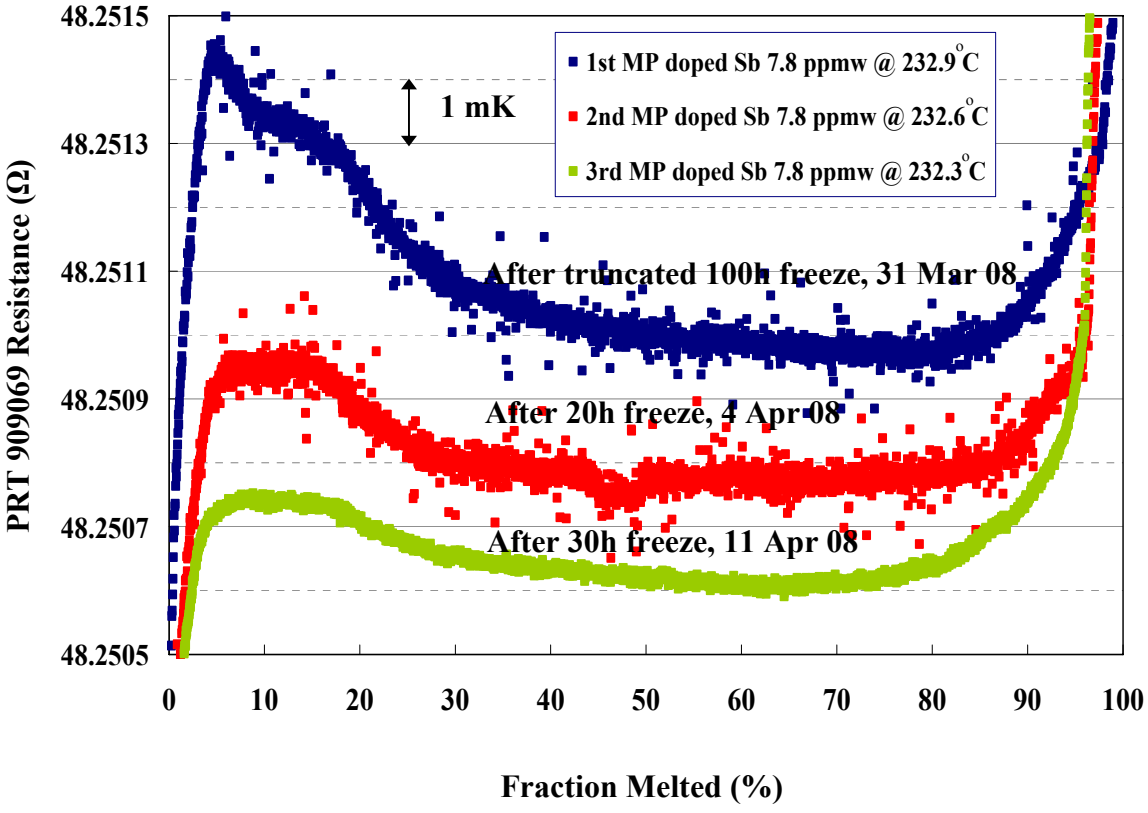

Figure 6.32 PRT 909069 resistance value at the melting temperature for "Mini Isotech Tin" after doping with 7.8 ppmw of antimony as a function of the approximate tin percentage melted. (All temperatures are nominal settings of the controller; as thermometer 909069 seemed to be "noisy" it wasn't used in subsequent dopings).

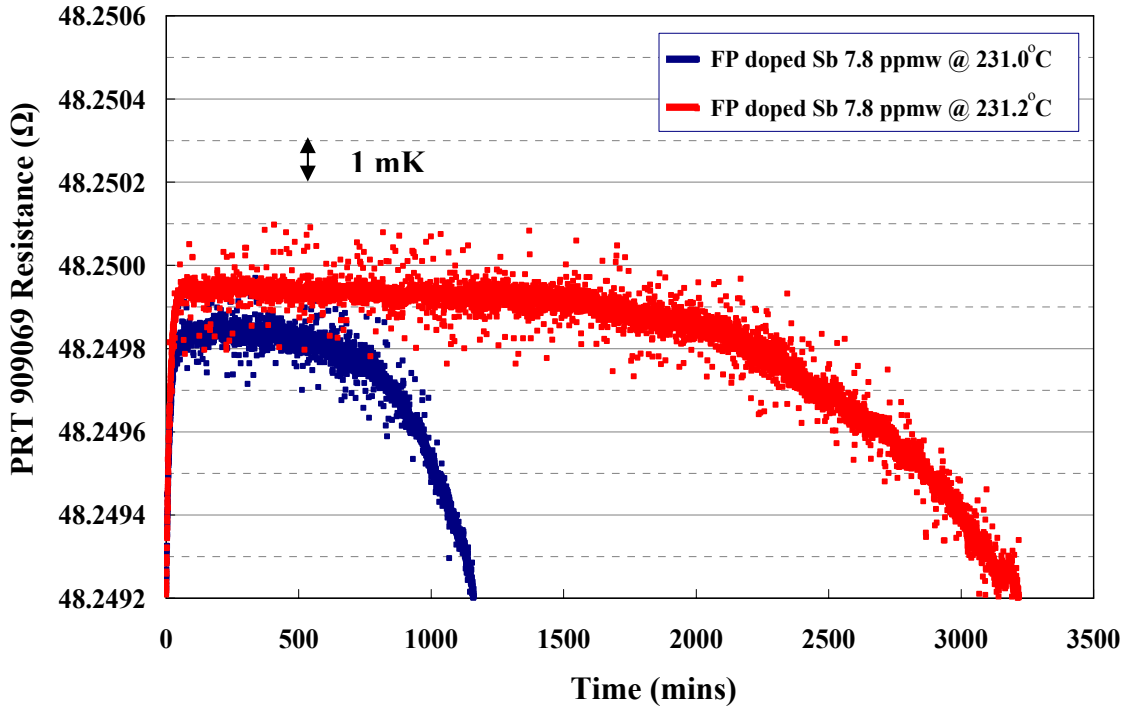

Figure 6.33 PRT 909069 resistance values at the freezing temperature for "Mini Isotech Tin" after adding 7.8 ppmw of antimony as a function of time.

Three melting curves after doping with antimony 7.8 ppmw, which were measured by PRT 909069, show a peak at the start of the first curve (blue line) as presented in Figure 6.32. This curve was measured on 31st of March 2008. The big effect appears after a slow freeze, which was truncated at 100 hours duration. The peak of this melting curve is around 5 mK high, which is the highest one for all obtained melting curves. Considering the second melting curve, this curve was recorded after 20 hours freezing curve and the height of the peak is 2 mK approximately. The starting peak of the bottom curve, which was measured after a 30 hour freezing curve, is about 1 mK. Normally melting curves are only measured after an intervening "fast" freeze; however these unusual results followed after only a slow freeze. Figure 6.32 also shows the shift of three melting curves, the shift might be due to the thermometer but this is unlikely to account for all the change as thermometer stability is supported from the results of the reproducibility of the resistance values of PRT 909069, when checked at the water triple point. However, this PRT was only used for calibrating in Mini Isotech cell after doping with 7.8 ppmw of antimony. A set of the freezing curves as presented in Figure 6.33 (obtained either side of the 2nd melt) showing the change in the freeze value of this tin

cell, but the change is less that that of the melts, suggesting their change is more than due to thermometer instability. Then, PRT 280140 was selected to use in the further experiment because this PRT is less noisy than 909069. Because the Mini Isotech tin would have additional antimony added (+15.4 ppmw) in the next step (to see the antimony impurity effect on the tin metal fixed-point temperature) the previous step needs to be repeated to find out how much the temperatures change from the prior step to the next step with the PRT 280140.

Table 6.21 Resistance values from three PRTs measured at triple point of water after the calibration by comparison between Mini Isotech tin doped with 7.8 ppmw Sb and Reference Isotech tin (Sn184) fixed-point cells. Also, the stability of PRT 280140, which was used instead of PRT 909174, has been shown.

Resistance values at triple point of water/Ω	**Date**	**Platinum Resistance Thermometers (PRTs) (Serial Number)**		
Cycle number and differences	**-**	**4849**	**909174**	**280140**
$R_{TPW}\ (1)_A$	27/02/08	-	25.501279	-
$R_{TPW}\ (2)$	04/03/08	25.443980	25.501293	-
$\Delta T_1 = \Delta R_1 * 10.8^{\#}$	-	-	+0.15 mK	-
$R_{TPW}\ (3)$	12/03/08	25.444021	25.501330	-
$\Delta T_2 = \Delta R_2 * 10.8^{\#}$	-	+0.44 mK	+0.40 mK	-
$R_{TPW}\ (4)$	09/05/08	-	-	25.103437
$R_{TPW}\ (5)$	02/06/08	-	-	25.103451
$\Delta T_3 = \Delta R_3 * 10.8^{\#}$	-	-	-	+0.15 mK
$R_{TPW}\ (6)$	20/06/08	-	-	25.103457
$\Delta T_4 = \Delta R_4 * 10.8^{\#}$	-	-	-	+0.065 mK
Mean of the ΔT	-	+0.44 mK	+0.28 mK	+0.11 mK
Standard deviation (2s)	-	**0.058 mΩ**	**0.052 mΩ**	**0.02 mΩ**

In Table 6.21, *i* represent the order of the resistance measurements of the PRTs at the triple point of water. # 10.8 (mK/mΩ) is the appropriate conversion factor for the sensitivity of $R(T_{90})$ [Rusby, 2008].

Table 6.21 shows that these PRTs have no gross instabilities during the measurement cycle in this tin fixed-point temperature. The standard deviation (2s) for all measurements was 0.06 mΩ which is equivalent to 0.65 mK approximately. For the PRT 280140, it shows the stability of the PRT calibration with the standard deviation 0.02 mΩ which is equivalent to 0.22 mK. The melting and freezing curves of the Mini Isotech tin after adding with the antimony at 7.8 ppmw were repeatedly checked by the PRT 280140 instead of PRT 909174. Those curves are presented in Figure 6.34 and 6.35.

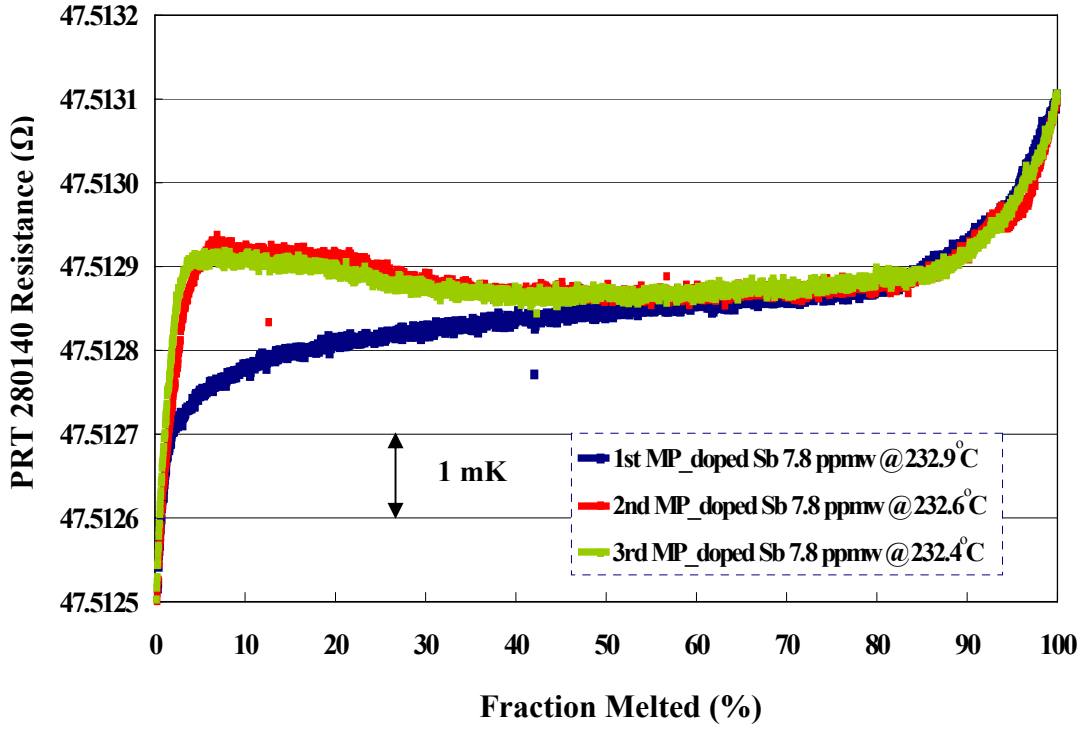

Figure 6.34 A set of three melting curves from the high purity Mini Isotech tin doped with antimony at 7.8 ppmw fixed-point cell. These curves are measured from PRT 280140.

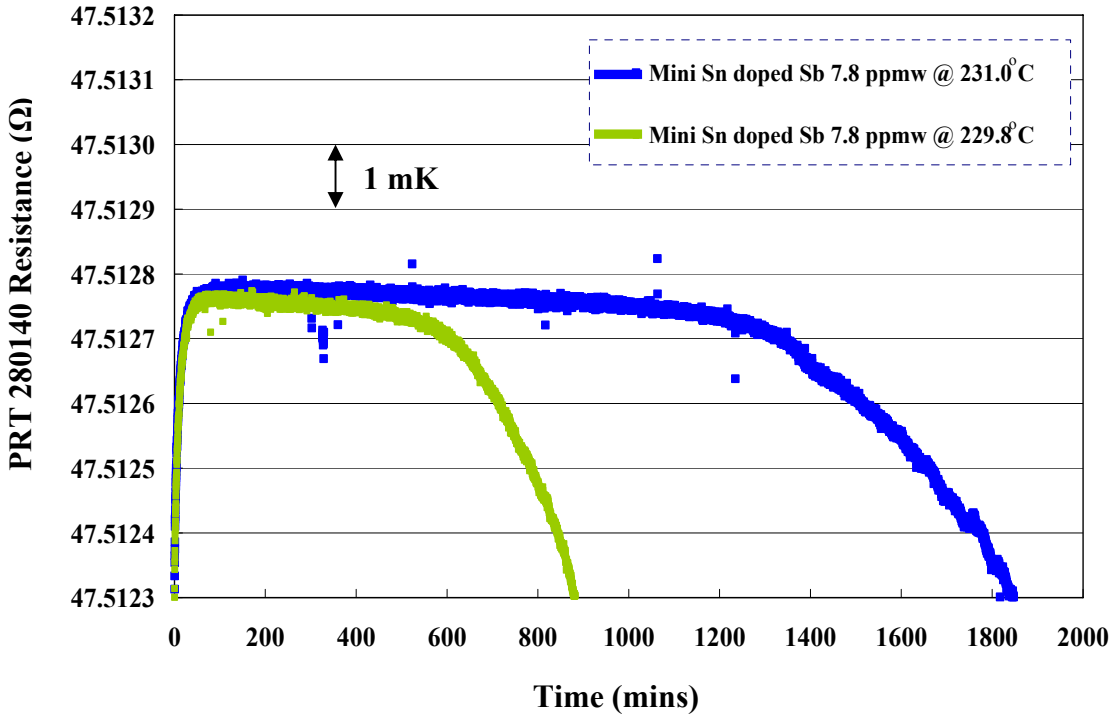

Figure 6.35 A set of two freezing curves from the high purity Mini Isotech tin doped antimony 7.8 ppmw fixed-point cell. These curves are measured from PRT 280140.

In Figure 6.34, the first curve has no bump at the start of the melting curve, while the next two melting curves show a bump. The 1st and 3rd melts were after fast freezes and the 2nd melt was after slow freeze. (Based on later results may be the 3rd melt "remembered" the slow freeze before the 2nd melt). Figure 6.35 shows the reproducibility of the resistance values measured at the freezing temperatures after doping with 7.8 ppmw Sb in this Mini Isotech tin cell. Melts seem to show that they are very dependent on the thermal history.

6.2.2.2 Mini Isotech Tin doped with 23.2 ppmw of Antimony

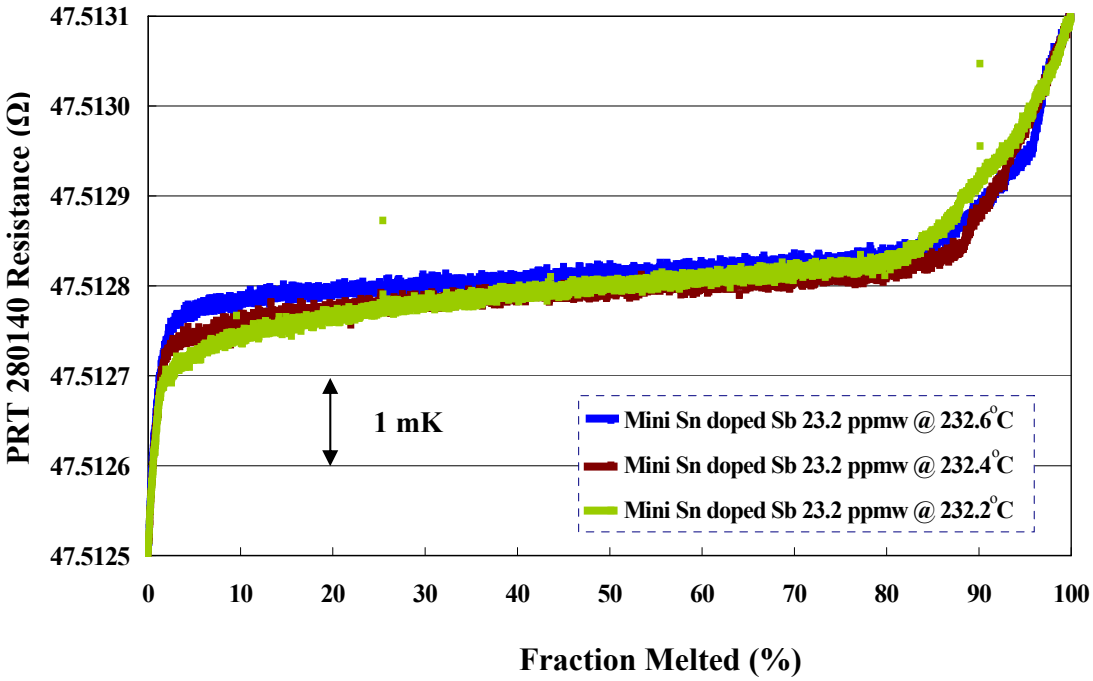

Figure 6.36 A set of three melting curves from the high purity Mini Isotech tin doped with 23.2 ppmw antimony fixed-point cell. These curves are measured with PRT 280140.

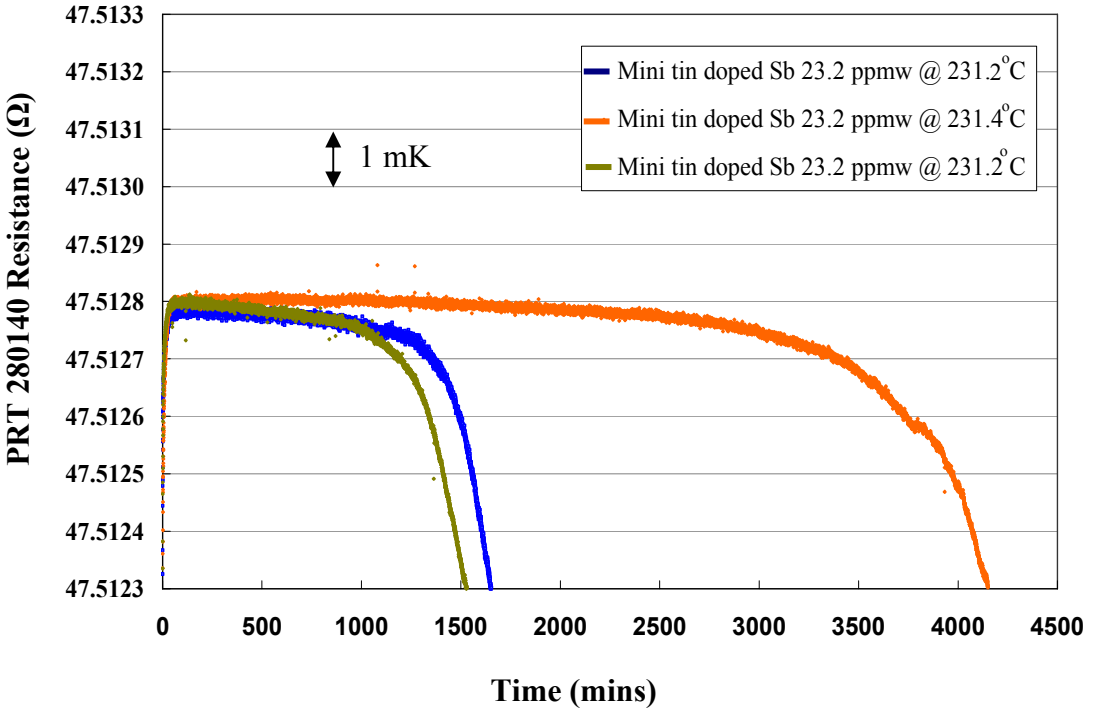

Figure 6.37 A set of three freezing curves from the high purity Mini Isotech tin doped antimony 23.2 ppmw fixed-point cell. The furnace setting was set in different temperature. The PRT number 280140 was used to measure the fixed-point freeze.

In Figure 6.36, the liquidus melting temperatures are at the same level (or lower) as the first melting curves of Mini Isotech tin after doping with only 7.8 ppmw Sb. Figure 6.37 shows the reproducibility of the resistance values measured at the freezing temperatures after doping 23.2 ppmw Sb into this tin cell. The peaks of three freezing curves are a little bit increased compared to the freezing curve after doping with Sb at 7.8 ppmw. In passing we again note that the period of time on the curves shows the effect of difference furnace settings.

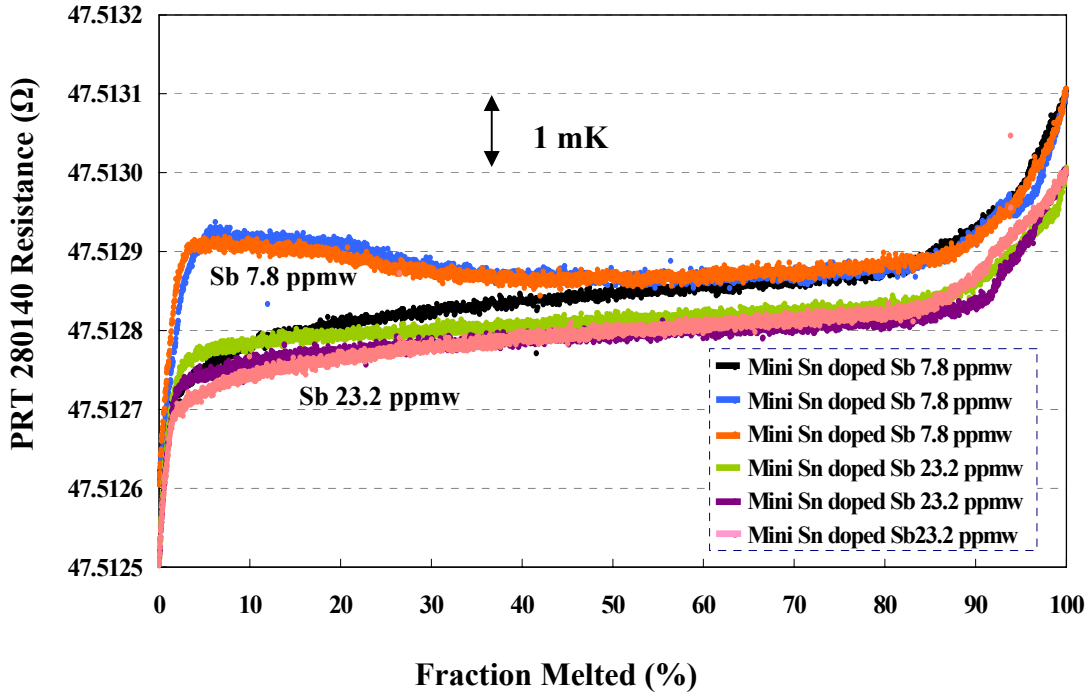

Figure 6.38 PRT resistance value changes for "Mini Tin" after doping with antimony at 23.2 ppmw compared to the 7.8 ppmw doping as a function of the approximate tin percentage melted. The PRT number 280140 was used to measure the fixed-point resistance.

Figure 6.38 illustrates the impurity dependence of the tin melting point affected by a low concentration of antimony. Considering the Mini Isotech tin after doping with Sb 23.2 ppmw, the melting curves (Green, Purple, and Pink lines) show the reproducibility of the resistance values. The results we have obtained are not as expected and we are unable to give a convincing explanation. The fact of the repeatability of the curves shows that this is not simply a measurement error. We wonder if the melt-freeze cycle has somehow caused a redistribution of the impurity

(as evidenced by the bump in the 7.8 ppmw Sb). Redistribution has been shown (more convincingly) in the work of Zhang at PTB [Zhang *et al.*, 2008]. Perhaps at 23.2 ppmw Sb the distribution is more even (avoiding the peak) but then one might expect the 23.2 ppmw liquidus to come higher). As the curves from Sb 23.2 ppmw are lower than Sb 7.8 ppmw it might suggest that some antimony has been "lost".

It appears that the 23.2 ppmw antimony is not manifesting itself. A possible explanation of this happening is that the antimony might have been moved to the top area in the ingot when it was frozen and it could not be moved down to get the well mixed when it was fully molten. This is just feasible if other impurities might MECHANICALLY obstruct or "pin" the antimony at the molten temperature, and the over melt temperature prior to the freeze was not high enough. (Subsequent to the experimental work we found that we could still see where the samples had been cut out of the aluminium ingot even though it had been left molten at 5 degrees above the mp for several days.

The peaks of the freezing curves were used for the comparison measurements between the Mini Isotech Sn (after doping with antimony at 23.2 ppmw) and the reference (Sn184) tin fixed-point cells with three PRTs, as presented in Table 6.22. The resistance values after doping with Sb at 23.2 ppmw had increased 0.78 ± 1.08 mK. The standard deviation for all measurements is 0.35 mK. The equilibrium curves of the tin fixed-point increased as increasing amounts of impurities were introduced; the measured rates are as follows: Sb +0.03 mK/ppmw (This rate was obtained from the calculation based on the 23.2 ppmw measurements). The standard book value for the affect of Sb on the tin transition plateau is that it is raised by 0.128 mK/ppmw of antimony impurity [Hansen, 1958].

Table 6.22 Summary of the average resistance values from the comparison measurements between Mini Isotech after doping with antimony at 23.2 ppmw and the reference (Sn184) tin fixed-point cells with three PRTs on 30th June, 2nd July, 4th July and 14th July 2008, respectively. As measurements are made on the same ASL F18 Bridge and standard resistor for each PRT then, the resistance values can be compared for each PRT.

PRTs serial number	**Date**	**R_T "Mini Isotech" Sn doped 23.2 ppmw Sb (0 mA)**	**R_T Reference Sn 184 (0 mA)**	**Equivalent Temperature difference between doped Mini Isotech Sn and Sn184 cells** $[\Delta T = 10.8 * \Delta R_T]^{\#}$ [Rusby, 2008]
280140 I	30/06/08	47.512615	47.512659	- 0.48 mK
280140 II	02/07/08	47.512614	47.512652	- 0.41 mK
280140 III	02/07/08	47.512629	47.512646	- 0.18 mK
280140 IV	04/07/08	47.512603	47.512636	- 0.36 mK
280140 V	14/07/08	47.512614	47.512643	- 0.31 mK
274728 I	02/07/08	49.038611	49.038609	+ 0.02 mK
274728 II	04/07/08	49.038643	49.038647	- 0.04 mK
4849 I	30/06/08	48.152942	48.152941	+ 0.01 mK
4849 II	02/07/08	48.152961	48.152934	+ 0.29 mK
Overall Mean	-	-	-	**- 0.16 mK**
∴ Standard deviation (2s)-Temperature difference between Sb 23.2 ppmw doped Mini Isotech Sn and Reference Sn ± 0.35 mK				
∴ Mean of Temperature difference "Sb 23.2 ppmw Doped" and "Undoped" Mini Isotech tin (-0.16) – (-0.94) = + 0.78 mK				
∴ Standard deviation (2s) Difference -Temperature difference between "Sb 23.2 ppmw doped" and "undoped" Mini Isotech Sn (by quadrature addition) ± 1.08 mK				

10.8 (mK/mΩ) is the appropriate conversion factor for the sensitivity of $R(T_{90})$ [Rusby, 2008].

Table 6.23 Resistance values from three PRTs measured at triple point of water before and after the calibration by comparison between Mini Isotech tin doped antimony at 23.2 ppmw and Reference Isotech tin (Sn184) fixed-point cells.

Resistance values at triple point of water/Ω	**Date**	**Platinum Resistance Thermometers (PRTs) (Serial Number)**		
Cycle number and differences	**-**	**4849**	**280140**	**274728**
R_{TPW} (*1*)	30/06/08	25.443943	25.103420	-
R_{TPW} (*2*)	02/07/08	25.443962	25.103434	25.909855
$\Delta T_1 = \Delta R_1 * 10.8^{\#}$	-	+0.21 mK	+0.15 mK	-
R_{TPW} *(3)*	04/07/08	-	25.103433	25.909898
$\Delta T_2 = \Delta R_2 * 10.8^{\#}$	-	-	-0.011 mK	+0.46 mK
R_{TPW} *(4)*	14/07/08	-	25.103393	-
$\Delta T_3 = \Delta R_3 * 10.8^{\#}$	-	-	-0.43 mK	-
Mean of the ΔT	-	+0.21 mK	-0.29 mK	+0.46 mK
Standard deviation (2s)	-	**0.02 mΩ**	**0.035 mΩ**	**0.06 mΩ**

In Table 6.23, *i* represent the order of the resistance measurements of the PRTs at the triple point of water. # 10.8 (mK/mΩ) is the appropriate conversion factor for the sensitivity of $R(T_{90})$ [Rusby, 2008].

The results obtained after doping with antimony at low impurity levels can be summarised that the melting and freezing curves, before and after doping, confirm the reproducibility of the temperature measurements in this tin fixed-point cell. The freezing temperatures of the Mini Isotech tin after adding antimony 7.8 and 23.2 ppmw are higher than for the "pure" ones. It indicates that at low levels, antimony elevates the melting and freezing temperatures although the temperature change is less than expected. At 7.8 ppmw antimony in tin the freezing maximum temperature increased by 0.60 mK, while at 23.2 ppmw the curves had increased by 0.77 mK compared with the reference high purity tin cell.

The measured rate of increased temperature after adding amounts of Sb was calculated from the previous results. It found that the measured rate at Sb 7.8 ppmw is Sb +0.08 in units of mK/ppmw and the measured rate at 23.2 ppmw is Sb +0.03 in units of mK/ppmw. Therefore, the equilibrium curves of the freezing tin fixed-point

temperature as increasing amounts of impurities of Sb were introduced; the average of the measured rate is: Sb +0.06 in units of mK/ppmw. Total Sb impurities in the based Mini Isotech tin sample can be checked the amount of concentrations by using the GD-MS.

Looking at both the 7.8 and 23.3 ppmw curves and at the beginning of the curve (bump for 7.8 ppmw) and near the curves liquidus then one can calculate several different values for the impurity sensitivity, varying between 0.03 mk/ppmw and 0.33 mK/ppmw. (The Hansen book value is 0.128 mK/ppmw). We might expect that the 7.8 ppmw peak value would overestimate the sensitivity (0.33 mK/ppmw), as the peak suggests that the level of antimony has been increased by some form of impurity consolidation. (We might then expect that the liquidus of the 7.8 ppmw would give a much lower sensitivity, but in fact it does not go below the book value.)

However when thinking of the 23.2 ppmw results we note that the GD-MS results detect a much lower level of Sb (3.8 ppmw) than the 23.2 ppmw that had been added. If we assume that a large portion of the antimony had been "taken out of play" after the second stage of doping, and that the GD-MS was actually measuring the remaining active antimony then we can work "backwards". Looking at the increased temperature at the start and end of the "23.2 ppmw" curve but using a concentration of 3.8 ppmw then we calculate sensitivities of 0.18 and 0.29 mK/ppmw. It is interesting to observe that this range is closer to the book value of 0.128 mK/ppmw. This is an intriguing suggestion that might lend us to have more trust in GD-MS results, but unfortunately at this time we can only leave it as an interesting speculation, for some future work.

The freezes show that Sb increases the temperature of the Sn phase transition, but not by the expected amount. The melts further suggest that the Sb distribution is strongly dependent of the prior freeze and it may be that our "fast freeze" is not fast enough. During Qiu's recent work [Qiu *et al*., 2008] when studying the affect of impurities in zinc, it has been shown that to reduce the rounding at the start of the melt (which we subsequently assume to be due to uneven distribution of impurities) then a VERY "fast freeze" has to be carried out before the melt. They pulled the ingot into the air to get their (very) fast freeze.

6.2.3 Impurity Analysis of High Purity Mini Isotech Tin before and after Doping with Antimony (Sb) Impurity

GDMS Characteristics of High Purity Mini Isotech Tin before and after Doping with Sb

Table 6.24 lists the impurity elements detected in the Mini Isotech tin metal ingot. It indicates the increased amount of Sb after adding total 23.2 ppmw (23200 ppbw). However, the total amount of Sb from GD-MS is just 3800 ppbw, which is less than the real added amount as expected at 23200 ppbw. This may be the reason why the elevation of the melting and freezing temperatures change after doping with antimony less than expected. It might be because of the limitations of Sb solubility in this tin metal.

Moreover, two samples were cut from the Mini Isotech tin before deliberate doping; one was tested soon after while the other was tested a ~year later at the same time as the doped sample, i.e. two similar samples were tested by GD-MS at different times, i.e. the first undoped sample was checked a year ago, while the other undoped sample was detected as the same time as the doping sample. From the GD-MS results we see the amount of "background" Sb in this tin cell (i.e. prior to doping) shows different amounts, namely the amount at the first measurement is 360 ppbw, while the second one is <260 ppbw. Similar larger variations in nominally the same background impurities can be seen between the measurements e.g. B, Se, S, Br, Au to name some; but note some such as C, N, O so not show a large variation even though GD-MS is not expected to be so accurate with these elements. These results can show some evidence of the uncertainty of the GD-MS technique.

Considering Indium (In) impurity in Table 6.22, it shows the large amount and variable as also appeared in Spanish tin ingot in Table 6.15 (Indium is know by materials experts to be a common impurity in Sn – private communication [Quested, 2008]. Also, we can see the different amount of In when the two samples before doping were checked the GD-MS at the different time. The second measurement, which was checked at the same time as after doping, has the amount nearly the sample after doping.

For Sulphur (S) impurity, we can see the big different amount of this impurity in this cell.

Table 6.24 GD-MS analysis results of the impurity concentrations of the "Mini" Isotech tin before and after doping [NRC report number: 30337R1 (checked on 14/12/07) & 30817 (checked on 22/08/08)]. These elements were detected in term of mass fraction (in parts per billion by weight, ppbw). The uncertainty is quoted as a "factor of 2", though this is probably a conservative overestimate.

Element	Mini Sn Before Doping	Mini Sn Before doping (Kept a year until time of doped analysis)	Mini Sn After Doping	Element	Mini Sn Before Doping	Mini Sn Before doping (Kept a year until time of doped analysis)	Mini Sn After Doping
	ppbw				ppbw		
Li	<0.3	<0.3	<0.2	**Br**	<23	<1000	<750
Be	<0.1	<0.1	<0.08	**Rb**	0.8	<0.3	<0.1
B	80	<0.2	3	**Sr**	<0.2	<0.2	<0.1
C	2800	1100	2000	**Y**	<0.2	<0.2	<0.08
N	390	320	240	**Zr**	<0.2	<0.3	<0.2
O	3700	1700	6300	**Nb**	<0.2	<0.2	<0.08
F	<0.4	<2	<2	**Mo**	<0.9	<0.9	<0.5
Na	2	<0.2	4	**Pd**	-	-	-
Mg	<0.3	<0.3	<0.2	**Ag**	<2	<2	<0.9
Al	4	4	2	**Cd**	<21	<70	<40
Si	130	0.8	90	**In**	**<330**	**<770**	**<670**
P	3	<0.2	0.8	**Sn**	Matrix	Matrix	Matrix
S	**3700**	**7**	**1300**	**Sb**	**360**	**<280**	**3800**
Cl	13	<0.8	35	**Te**	<20	<11	<35
K	<90	<50	<20	**I**	<9	<20	<12
Ca	<6	<5	<6	**Cs**	<1	<3	<45
Sc	<0.2	<0.2	<0.2	**Ba**	<0.6	<1	<30
Ti	<0.2	<0.1	<0.1	**La**	<0.5	<0.8	<2
V	<0.1	<0.1	<0.07	**Ce**	<0.4	<0.9	<25
Cr	7	<0.4	13	**Hf**	<0.6	<0.6	<0.3
Mn	0.5	<0.3	<0.1	**Ta**	-	-	-
Fe	8	<10	<5	**W**	<0.4	<0.4	<0.2
Co	<100	<100	<100	**Pt**	<2	<2	<0.9
Ni	<19	<15	<8	**Au**	<10	<200	<80
Cu	<1	<1	2	**Hg**	<7	<6	<3
Zn	<3	<3	<2	**Tl**	<1	<1	<0.6
Ga	<0.8	<2	<0.7	**Pb**	6	6	11
Ge	<2	<2	<0.9	**Bi**	7	4	10
As	<10	<3	<7	**Th**	<0.2	<0.4	<0.8
Se	<41	<500	<300	**U**	<0.4	<1	<2

6.2.4 Photograph of Mini Isotech Tin Cell

(a)

(b)

Figure 6.39 Photographs of Mini Isotech tin fixed-point ingot (a) shows the original pure tin ingot before doping; and (b) shows the colour change of the surface on the ingot after doping with antimony impurity and having undergone several (very) long melts and freezes. "Fresh" tin can just be seen where the GDMS sample has been cut out on top of (b).

The colour on the surface of Mini Isotech tin ingot before doping, as shown in Figure 6.39(a), is totally different from the surface of the ingot after doping with antimony and undergoing several (very) long melts and freezes (Figure 6.39(b)). The surface before doping has a dark grey colour, which is a not unusual colour for an old tin metal ingot, while the yellow-brown is the colour on the surface after doping experiments. Looking at the GDMS results of the Mini Sn ingot (and comparing with the Spanish Sn) it is noted that there is a relatively large amount of sulphur in the impurity list and therefore it is wondered if sulphur has been redistributed to the surface. Other possible (but less plausible possibilities) could be related to Si or Cs elements (larger amount of these elements were detected from the GD-MS analysis after doping) that might be formed with the oxygen and become SiO-glassy solid (blown black) or Cs_2O (yellow-orange). It can be assumed that some impurities might be reacted with oxygen gas, which (with large variations in amounts) is detected in the

GD-MS results. Initially the sulphur hypothesis seems more plausible. This hypothesis needs to be confirmed and proved by scraping the surface off to check the chemical analysis, which is left as an interesting speculation, for the future work.

(a)

(b)

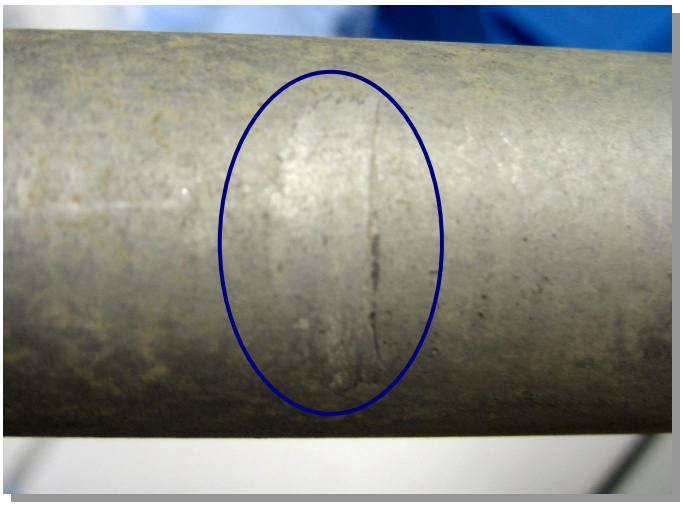

(c)

Figure 6.40 Photographs of Spanish tin fixed-point ingot (a) shows the original whole ingot before doping; (b) shows the top part of the ingot after doping with cobalt and lead impurities (we can see the space on the right hand side, which appeared after cutting the sample off for GD-MS analysis); and (c) shows a fully re-fill the sample hole (in the blue circle line) after re-melting and re-freezing the ingot in several times.

Considering the surface colour of Spanish tin ingot, this has the dark grey outside of the ingot before doping (someone has wondered if there was some organic contamination based on the colour and its mottled distribution), while after doping etc it has a less greyer surface than the undoped Spanish tin. It might be some tin oxide, which has a whitening effect. However, the surface structure suggests a good mixing in the ingot because it has no holes or crevices on the surface. Also, the sample hole after cutting the samples out was fully refilled, as shown in Figure 6.40(c); this trace still appears even after re-melting and re-freezing several times. Scraping off the surface layer makes it harder, but not impossible, to see this trace, suggesting that whatever is on the surface is not mobile (otherwise it would cover over the trace) and that the "surface contaminant" hasn't been introduced after the post cut re-melting.

6.2.5 Mass of Mini Isotech Tin Fixed-Point ingot

Table 6.25 Mass of Mini Isotech tin fixed-point ingot as calculated based on a mass measurement (of Mini Isotech tin and central graphite well) before and after doping the impurities.

Component(s) of Mini Tin Cell	Mass (g)
Calculated Mass of Mini tin metal (Originally)	262.28 g
Measured Mass {Mini tin metal and graphite re-entrance well} (Originally) less the calculated mass of graphite	243.05 g
Measured Mass of Mini tin metal (Samples cut off) less the calculated mass of graphite	240.76 g

The difference in the amount of tin, estimated from the two methods is just under 10%. Therefore the uncertainty in the mass of added impurities is negligible (see mass balance uncertainties in Spanish tin section). However the uncertainties in the measurement of the affect of Sb doping in Sn appear to be dominated by the question of whether the antimony is being "removed from play", either due to the freeze process or some other process that is pinning the impurity away from the thermometric (and GD-MS) measurement area. The measured mass of Mini Isotech tin metal after cutting some samples off for the undoped GD-MS testing was used in calculation of the doping concentrations (in ppmw).

Chapter 7

Results and Discussions of Aluminium Fixed-Point

Two originally nominally 99.9999% pure aluminium point cells constructed according to the NPL design were used in this study to realise as the test cells to measure before and after doping and compare against a reference cell. These two cells were designated after the year they were fabricated in 1974 (Al 174) and 1998 (Al 298). The offsets and shapes of melting and freezing plateaus of high purity aluminium are investigated as a function of the impurities (concentrations of order ~1-16 ppmw) of copper, silicon, and titanium pure metals. In prior experiments on these binary alloy systems, using higher levels of impurities [Hansen, 1958], the fixed-point temperature of Aluminium was interpolated to be depressed by 0.37 mK/ppmw of copper and 0.71 mK/ppmw of silicon impurity. Conversely the aluminium transition temperature is interpolated to be increased by 3.31 mK/ppmw of titanium impurity.

The following impurities were added to the “pure” aluminium samples in increasing concentrations as follows (in ppmw); Cu 8.3 and 16.2, Si 4.7 and 9.8, to Al174 and Ti 0.9 and 1.8 to Al298, respectively.

7.1 High Purity Aluminium (Al 174) Fixed Point

The order and location of the experimental results of high purity Al 174 fixed-point cell are summarised below in terms of a “Family tree” as presented in Figure 7.1. But note that the measurements were done consecutively (not in parallel).

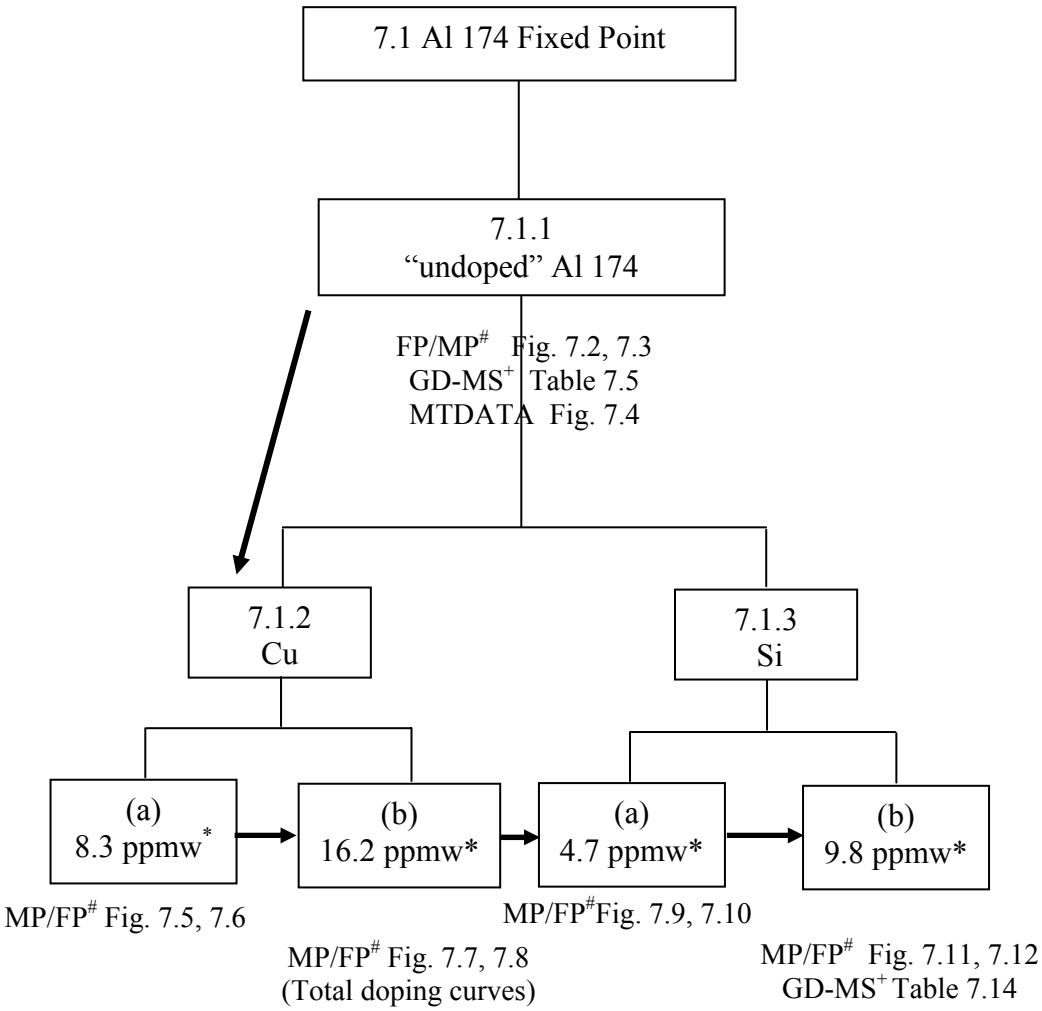

FP/MP = Freezing and Melting curves conducted in this stage.

+ GD-MS = Glow discharge mass spectrometry analysis performed in this stage.

* ppmw = Parts per million by weight (nominal doping amounts)

Figure 7.1 "Family Tree" summarising the experiments giving the section numbers, figure numbers of the freezing/ melting curves, the nominal doping amounts, and the table number of results from the chemical analysis technique for Al 174 fixed point obtained for a particular combination of conditions.

7.1.1 Temperature Realisation of "Undoped" Aluminium (Al 174)

Considering the high purity "Al 174" aluminium fixed point results: a set of three freezing curves of "Al 174" aluminium fixed-point cell, before the doping process, is shown in Figure 7.2. There is a region in the Figure 7.2 where the temperature is almost stable (within about 2 mK), and that is called the "plateau". All freezing measurements were determined at the same setting of the furnace temperature. (All furnace values quoted in this chapter are nominal settings of the controller(s)). Examples of Al 174 melting curves, before doping, are also shown in Figure 7.3.

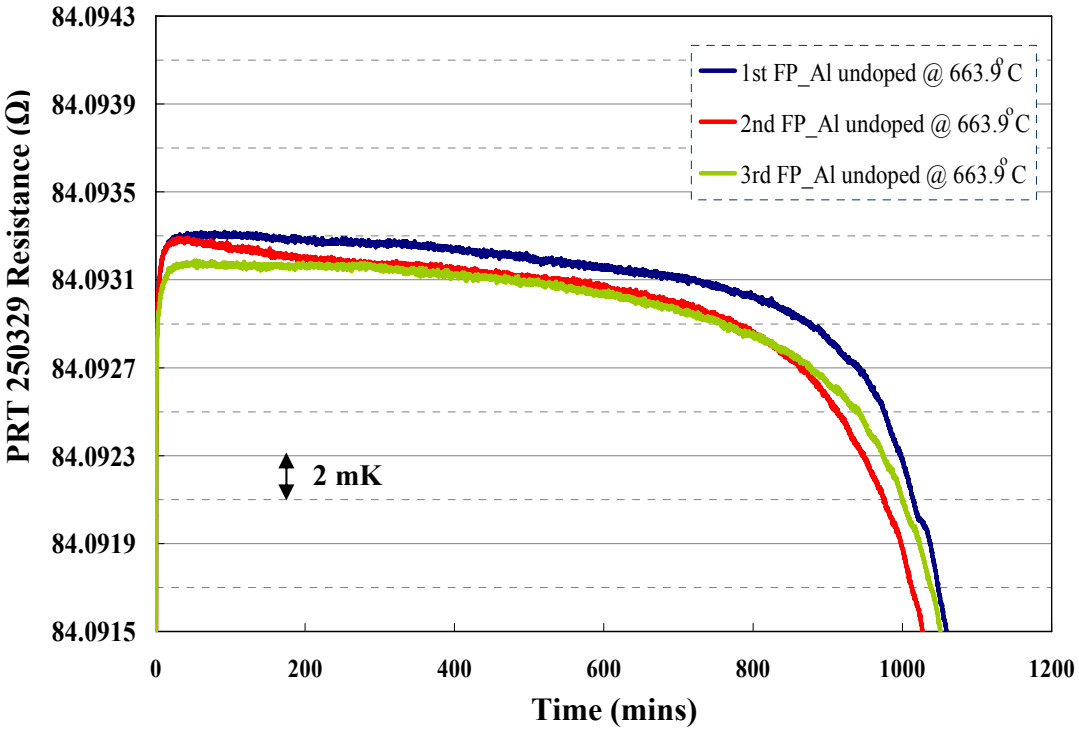

Figure 7.2 Three freezing curves of high purity Undoped "Al 174" aluminium fixed-point plotted as a function of time. The furnace set point for all three measurements is maintained at the same temperature (nominally half a degree below the melting point).

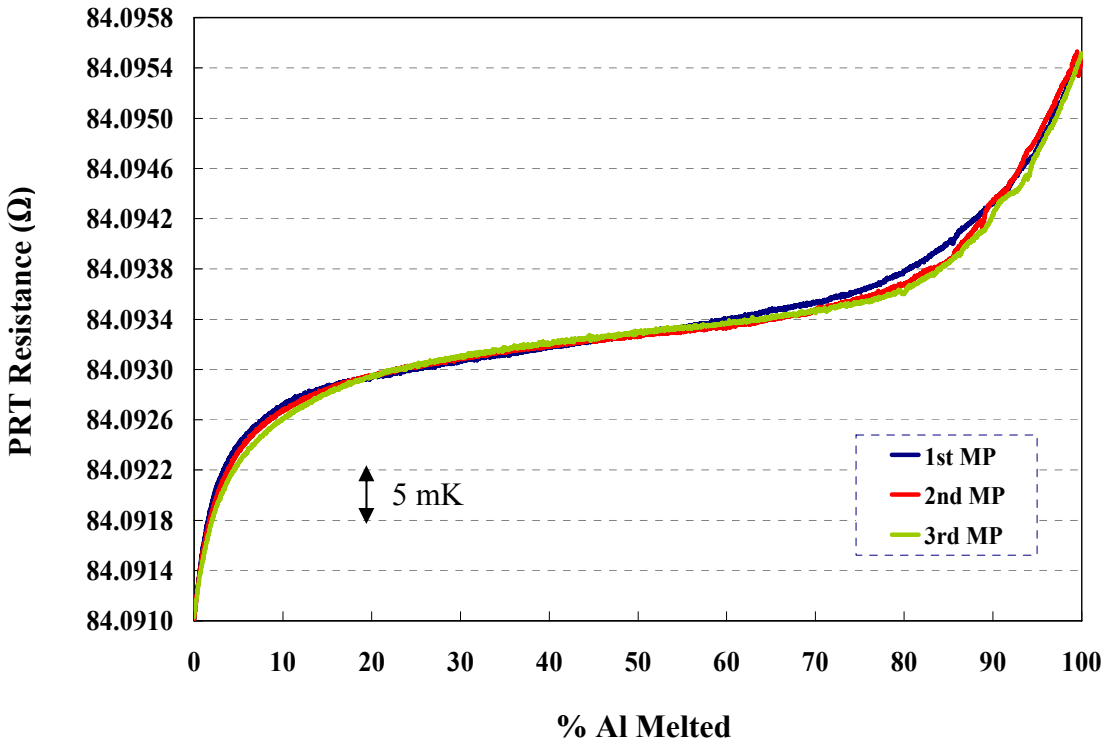

Figure 7.3 Melting curves of high purity Undoped "Al 174" aluminium fixed-point plotted as a function of aluminium percentage melted. The curves have been normalised to an approximate percentage melted (the best means for this normalisation is still a topic for discussion in the community) [Lowe *et al.,* 2007].

Our method of determination of 0% and 100% was slightly arbitrary. For 0%, we chose a resistance that was same distance below the actual plateau "start", i.e. almost vertical and for 100% some way above the plateau, where the temperature was obviously rising above the plateau. This means that 0% and 100% may not be fully correct; but any offset will be common to all the curves being measured by the same thermometer on the same cell and the same furnace system.

All the melting and freezing curves of high purity Al 174 aluminium confirm the general reproducibility of the temperature realisations over a short time scale, and intercomparison with a reference fixed-point cell, ensures longer-term measurement accuracy. However, we can see some shift of the resistance values of the PRT at the freezing and melting curves. The average of these freezing temperatures shifts, as shown in Table 7.1, is about 1.5 mK. Thermometers are not normally as stable at the aluminium temperature as at tin temperatures, hence we expect that there may be more noticeable shifts in thermometer values over shorter time scales in the aluminum experiments.

Since the impurity segregation tends to induce a decrease of the equilibrium fixed-point temperature during the freezing process itself (irrespective of whether the impurities raise or depress the overall (average) freeze value), then the best estimate of the "liquidus point" of the fixed-point is the maximum point of the freezing curve. Therefore, the comparison for measuring the PRTs' differences between the Al 174 or Al 298 and the NPL national standard aluminium cells in this work was realised by use of the peak of the freezing point(s).

It can be difficult to find PRTs that are stable for extended periods of time at the aluminium fixed-point. Further the best PRTs are kept for use with the national standard calibration service. Consequently, the PRTs that were available were not optimal for this job. To overcome possible drift we investigated the use of water triple points and reference back to a standard aluminium cell. (Results soon showed that calculating W values from water triple points did not provide any advantage- similar to what we found with tin.)

Table 7.1 Resistance values measured at the freezing point of the "Undoped" Al 174 aluminium fixed-point cell. These values were calculated from the resistance ratio of PRT and standard resistor values. Also, the resistance values include the correction of the hydrostatic head of this cell. The temperature setting of the furnace was maintained at 663.9 ^{o}C. The resistance values are measured at the peak of the freeze.

Resistance values at freezing point of Al 174	**Date**	**Platinum Resistance Thermometer (PRT) (Serial Number)**
$\boldsymbol{R_T(i)/\Omega}$	-	**250329 (1 mA)**
$R_T(1)$	23/08/07	84.093280
$R_T(2)$	24/08/07	84.093269
$R_T(3)$	29/08/07	84.093158
Standard deviation (2s)	-	**0.135 mΩ**

Because the resistance values of the impure (or doped) aluminium point changed too quickly (especially at the peak), the values are not stable enough for the

measured cycling currents at 1 mA and $\sqrt{2}$ mA. For that reason, the resistance values were measured the freeze peak at 1 mA instead of 0 mA. In Table 7.1, the peak of each freezing temperature was measured to show the resistance values of a PRT 250329 at Al 174 fixed point cell. The standard deviation (2s) of the samples, which was used to show the stability, for all three measurements was 0.135 mΩ, which is equivalent to 1.46 mK approximately. We can see the peak drop in Figure 7.2. The stability of this PRT needs to be evaluated again by measuring in the triple point of water. All resistance values checked in the triple point of water have been corrected by application of the hydrostatic pressure correction of each aluminium fixed-point cell as shown in Table 7.2.

Table 7.2 Measurement of the stability of the PRT 250329 measured from the resistance values at the triple point of water. These values were checked before using the PRT in the comparison measurements at the freezing curves of aluminium fixed point between high purity "undoped" Al 174 and Al 298 cells.

Resistance values at triple point of water/Ω	**Date**	**Platinum Resistance Thermometer (PRT)**
Cycle number and differences	**-**	**250329 (0 mA)**
R_{TPW} *(1)*	27/08/07	24.915017
R_{TPW} *(2)*	05/10/07	24.915078
R_{TPW} *(3)*	13/10/07	24.915096
R_{TPW} *(4)*	14/10/07	24.915074
Standard deviation (2s)	-	**0.068 mΩ**

The stability of this PRT was monitored by means of the triple point of water cells, as illustrated in Table 7.2. The resistance values are obtained by combining the bridge ratio measurements and the standard resistor values. The standard deviation (2s) for all measurements was 0.068 mΩ, which is equivalent to 0.85 mK approximately.

(a) Aluminium Fixed-Point - Calibration by Comparison for the PRTs between High Purity Al 174 and High Purity Al 298 Cells

Before adding the impurities in Al 174 fixed-point cell, the peak of the freezing curve of this aluminium cell had needed to be compared against with the "reference cell" (Al 1205), which is related to NPL national standard. However, this Al cell was in a different room to Al 174 and the Al 174 cell itself had been put in a single zone heat pipe Carbolite furnace, which was very hard to move to the same room as the Al 1205 cell. Therefore, the Al 174 needed to be compared with the Al 298 instead of the "Al 1205" cell because the furnace of the Al 298 cell stands was on a trolley, making it is easier to move Al 298 to the Al 1205 reference cell. In the first stage, the Al 174 aluminium fixed-point cell was calibrated by comparison with the Al 298 fixed-point cell using the recording of the peak on the freezing curves of each cell, listed in Table 7.3. The Al 298 cell had been already compared against the peak freeze of "Al 1205 reference cell" aluminium fixed-point cell as shown in Table 7.17.

Both Al 174 and Al 298 fixed-point cells were used in this study because they have already been contaminated with the impurities, which had affected their freezing curves. Their freezing curves had dropped and were not flat enough to do the calibration by comparison between the cells throughout the full length of the freeze; therefore the freeze peak was selected to compare the initial freezing temperatures. A freeze peak was measured separately in each Al cell.

Because segregation has not progressed at the initial freeze front, it tends to make the first layer of frozen Al more representative/reproducible than the rest and because freezes are normally performed after sufficient time for the melt to become homogenised, then it is believed that it gives a better representation of the fixed point temperature. Thus, the best estimate of the liquidus point in a freeze is the early maximum point of the freezing curve. Also, according to Physikalisch-Technische Bundesanstalt (PTB) - the German national metrology measurement institute - the peak of the freeze is the most reproducible part of the freezing curve (because it is least affected by the furnace thermal conditions), from which good results can be obtained. The reason is that the maximum temperature does not strongly depend on the homogeneity and stability of the furnace temperature [Rudtsch *et al.*, 2008]. Therefore, the temperature comparisons between the Al 174 or Al 298 and the NPL

national standard aluminium cell in this work were realised by using the peak of the freezing point curve.

Table 7.3 Summary of the average resistance values (R_{Al}) in the comparison measurements at the peak of the freezing curves of the aluminium fixed points between Al 174 and Al 298 cells with two PRTs (serial number 250329 and 261198). The stability performance of the two PRTs, as measured at the triple point of water after the calibration, is also shown in this Table.

PRTs serial number	**Date**	**R_{Al} Al 174, (Ω) (1 mA)**	**R_{Al} Al 298, (Ω) (1 mA)**	**Temperature difference between Al 174 and Al 298 cells** $[\Delta T = 12.5 * \Delta R_{Al}]^{+}$	**R_{TWP} (Ω) (1 mA)**
250329 I	01/10/07	84.093166	84.092913	+3.16 mK	24.915337
250329 II	03/10/07	84.093222	84.093121	+1.26 mK	-
250329 III	03/10/07	84.093272	84.093116	+1.95 mK	24.915328
261198 I	02/10/07	84.996034	84.996000	+0.43 mK	-
261198 II	02/10/07	84.996012	84.996033	-0.26 mK	25.183047
Overall Mean	-	-	-	+1.31 mK	-
∴ Standard deviation (2s) = ± 2.66 mK					
∴ Temperature difference between "undoped" Al 174 and "undoped" Al 298 fixed-point Al 174-Al 298 = + 1.31 mK					

+12.5 (mK/mΩ) is the appropriate conversion factor for the sensitivity of $R(T_{90})$ at Al fixed-point temperature [Rusby, 2008].

Before the PRTs were calibrated by comparison, the PRTs had been annealed at 670.0 ^{o}C for 2 hrs. Table 7.3 summarises the comparison between Al 174 and Al 298; it lists the resistance values at the peak of the aluminium freezing curves, the subsequent triple point of water values and the mean difference between Al cells. The temperature difference, which was measured from the resistance values, between the original "undoped" Al 174 and Al 298 fixed-point cells shows that the temperature of Al 174 is higher than Al 298 by 1.31 mK. The values in Table 7.3 were also used to calculate the W values as shown in Table 7.4. The results indicate that the temperature difference between the original "undoped" Al 174 and Al 298 cells is +1.31 mK. This gives the same value as obtained from the resistance values. The standard deviation

(2s) for all measurements is ± 2.66 mK. From Table 7.18, it shows the temperature difference, from the comparison of the resistance values, between the peak of the original "undoped" Al 298 and the reference cell (Al 1205), which is 11.30 mK approximately. Therefore, it can be calculated that the value of the peak freezing point of Al 174 is 9.99 mK lower than the NPL standard Al cell.

Table 7.4 Summary of resistance ratios $W_{(Al)}$ values in the calibration by comparison method between Al 174 and Al 298 cells for two PRTs. [$W_{(Al)} = R_{(Al)}/R_{(TPW)}$]

PRTs Serial number	**Date**	**$W_{Al\ 174}$ (Ω) (1 mA)**	**$W_{Al\ 298}$ (Ω) (1 mA)**	**Temperature difference between Al 174 and Al 298 cells** $\Delta T = 312 * \Delta W$ [Rusby, 2008]
250329 I	01/10/07	3.37515667	3.37514653	+3.16 mK
250329 II	03/10/07	3.37516008	3.37515603	+1.26 mK
250329 III	03/10/07	3.37516211	3.37515583	+1.96 mK
261198 I	02/10/07	3.37512903	3.37512770	+0.41 mK
261198 II	02/10/07	3.37512818	3.37512901	-0.26 mK
Overall Mean	-	-	-	+1.31 mK
∴ Standard deviation (2s) = ± 2.67 mK				
∴ Temperature difference between "undoped" Al 174 and "undoped" Al 298 fixed-point Al 174 - Al 298 = + 1.31 mK				

The results above imply that Al 174 ingot (prior to doping) probably contained some initial impurities affecting its freezing and melting temperatures (this is as expected as it is an old cell retired due to some previous contamination). Also, the shape of the curves is no longer flat when compared with the NPL standard Al cell. For an ideal pure aluminium fixed point, a purer metal usually shows a flatter plateau on the freezing and melting curves.

Because measurements of the PRTs at the water triple point did not shift in proportion, the W values obtained from the experiment also moved. (W is the ratio of the thermometer resistance at the fixed point to the resistance at the water triple point).

It was found that the resistance values were more reproducible than W values. (Hence this is a reason why the resistance values were selected to show on all Figures). The offsets of the melting curves need to be corrected following "re-calibration" of the PRTs by comparison of the peak of the freezing curves against the NPL reference Al cell. Also, the results of the temperature difference as shown in Table 7.3 and 7.4 confirm the same value between Al 174 and Al 298 fixed-point cells. Therefore, all calibrations by comparison on the peak of freezing temperatures would use the resistance values to find out how much the trace impurities affected the temperatures of the aluminium fixed-points.

As the test cell(s) contained some existing impurities it was necessary to carry out an elemental analysis of this aluminium fixed-point cell(s) using the GD-MS technique, before doping the aluminium cell(s) with any impurity elements in the next step of the procedure.

7.1.1.1 Impurity Analysis of Aluminium (Al 174) Fixed-Point before Doping

Glow Discharge Mass Spectrometry (GD-MS) Characteristics

An example result of the impurity determination for the "high purity" aluminium (Al 174) fixed point by GD-MS analysis is reported in Table 7.5. This shows the impurity content measured in three areas of the aluminium ingot. This GD-MS analysis is considered to be accurate within a factor of two of the values obtained, at a confidence level of 95%. From the results we see that the impurity levels are the same throughout the cell (within the uncertainty quoted). This shows that the aluminium is sufficiently well mixed and that only one sample will need to be cut out for analysis after doping. (Cutting out of samples is a risky procedure).

Table 7.5 An example of the GD-MS analysis results of the initial "high purity" (6N) aluminium fixed point Al 174 (NRC report number: 30337R1). The aluminium samples were cut from the three areas of the ingot, which are the top, the middle, and the bottom. These elements were detected in term of mass fraction (in parts per million by weight, ppmw). The uncertainty is quoted as a "factor of 2", though this is probably a conservative overestimate.

Element	Top	Middle	Bottom	Element	Top	Middle	Bottom
Li	<0.004	<0.003	<0.003	**Br**	<0.02	<0.02	<0.02
Be	<0.001	<0.001	<0.001	**Rb**	<0.001	<0.001	<0.002
B	0.01	0.007	0.003	**Sr**	<0.001	<0.001	<0.001
C	6	6	5	**Y**	<0.001	<0.001	<0.001
N	1	1	0.3	**Zr**	0.005	0.006	0.009
O	12	8	3	**Nb**	<0.001	<0.001	<0.001
F	<0.02	<0.01	<0.01	**Mo**	<0.003	<0.003	<0.003
Na	<0.002	<0.001	<0.002	**Pd**	-	-	-
Mg	<0.003	<0.003	<0.002	**Ag**	<0.009	<0.007	<0.008
Al	Matrix	Matrix	Matrix	**Cd**	<0.02	<0.01	<0.02
Si	0.2	0.1	0.2	**In**	<0.005	<0.01	<0.003
P	<0.003	<0.002	<0.002	**Sn**	<0.03	<0.02	<0.03
S	<0.003	<0.003	<0.003	**Sb**	<0.009	<0.006	<0.007
Cl	0.006	0.004	0.003	**Te**	<0.009	<0.007	<0.008
K	<0.02	<0.02	<0.02	**I**	<0.004	<0.003	<0.003
Ca	<0.03	<0.03	<0.03	**Cs**	<0.001	<0.001	<0.001
Sc	0.05	0.05	0.05	**Ba**	<0.007	<0.001	<0.001
Ti	0.09	0.1	0.07	**La**	<0.001	<0.0007	<0.001
V	0.08	0.09	0.07	**Ce**	<0.001	<0.0007	<0.0009
Cr	0.02	0.02	0.03	**Hf**	<0.003	<0.002	<0.003
Mn	0.04	0.05	0.05	**Ta**	-	-	-
Fe	0.2	0.2	0.3	**W**	<0.004	<0.003	<0.003
Co	<0.001	<0.0006	<0.0007	**Pt**	<0.01	<0.01	<0.01
Ni	0.01	0.007	0.03	**Au**	<0.2	<0.2	<0.2
Cu	0.1	0.1	0.1	**Hg**	<0.04	<0.03	<0.03
Zn	0.1	0.09	0.1	**Tl**	<0.01	<0.008	<0.008
Ga	<0.007	<0.005	<0.006	**Pb**	<0.004	<0.003	<0.004
Ge	<0.01	<0.01	,0.01	**Bi**	<0.005	<0.004	<0.004
As	<0.007	<0.003	<0.004	**Th**	<0.001	<0.001	<0.001
Se	<0.1	<0.1	<0.05	**U**	<0.001	<0.001	<0.001

7.1.1.2 MTDATA Analysis

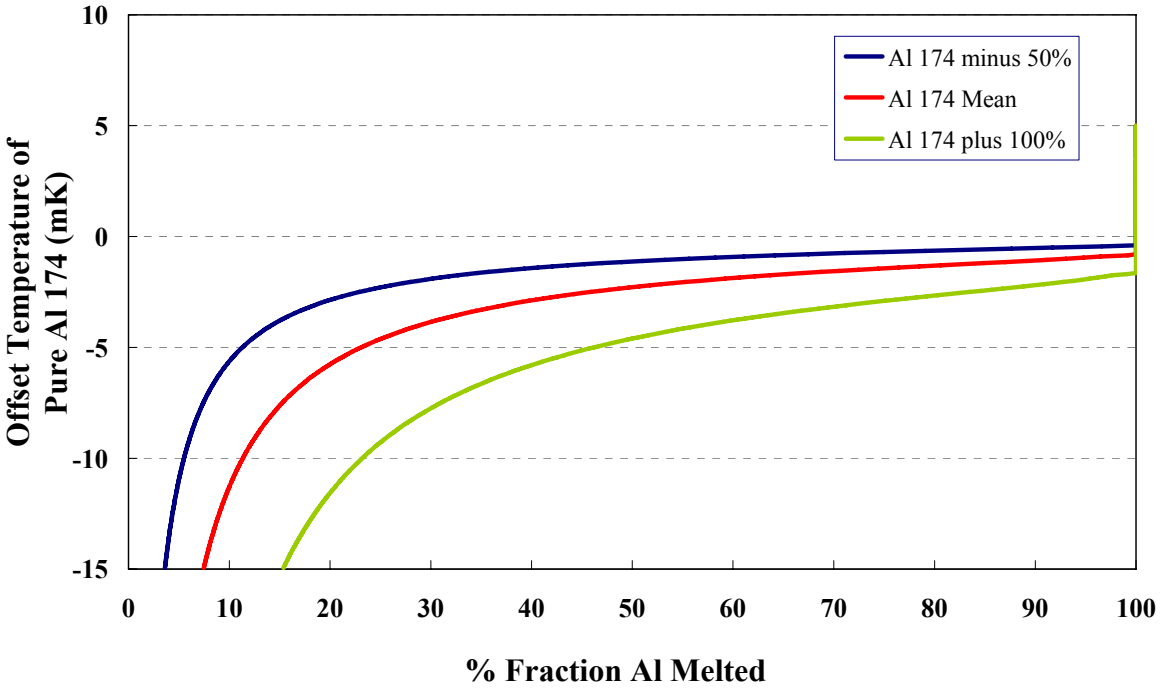

Figure 7.4 Melting curves of pure Al 174 fixed point obtained from MTDATA calculation analysis. The red line shows the curve calculated using the GD-MS result (impurity effect on the curve), the blue and the green lines show the calculated bounds (based on the quoted uncertainty of the GD-MS analysis i.e. factor of 2 which translates to –50% and +100% of reported value)

The melting of the initial undoped Al 174 curve compared to MTDATA experiments show much more rounding, which does not agree very well with MTDATA analysis. MTDATA also appears to grossly underestimate the melting point depression. If the MTDATA calculations are correctly done then it would imply that the GD-MS is unable to pick up a significant impurity component. We were informed – private communication [Head, 2009] - that a "back of the envelope" calculation assuming Raoult's law applied suggested that the total impurities would give a depression of around 20mK, while the depression (excluding the C, N and O) would be between 0.5 to 1 mK. This suggests that the MTDATA calculation have no gross errors. If there were some other impurity component we might speculate on this and one might wonder if some organic compound was having some effect. As an old open cell it would have been vacuum pumped using oil based pumps and there is

noticeable C, Si and O presence, but there is no way to distinguish its source in the above GD-MS analysis. This remains a speculation. Calculation of the MTDATA results was dependent on the availability of the appropriate specialist and constraints on the resources of MTDATA meant that they were not able to pursue this during the period of this work. We are aware of two new fixed point cells, manufactured at NPL, in the past; using "old" graphite that produced cells with low values, of order 1 mK. (NPL now uses post machined purified graphite, manufactured in Germany [Head, 2009]).

7.1.2 Influence of Copper on High Purity Al 174 Fixed Point

7.1.2.1 High Purity Al 174 doped with 8.3 ppmw of Copper

Considering the instability of the PRT 250329, this PRT was calibrated to check its resistance values in the reference Al cell as shown in Table 7.6.

Table 7.6 Stability of the PRT 250329, as checked at the peak of the reference Al cell (Al 1205) at 1 mA.

Checking Time	**Date**	**Resistance Values (R_T, Ω)**	**Average R_T Values (Ω)**
Measurement in Al 1205 before Al 174 was doped	18/09/07	84.093960	84.093915
	20/09/07	84.093870	
Checked when Al 1205 Compared with Al 174 doped Cu 8.3 ppmw	18/01/08	84.093791	84.093791
The shift of PRT 250329 during the calibration = 0.125 m **Ω**			

In Table 7.6, the shift of PRT 250329 during the thermal cycling checked against the reference Al cell decreases by 0.125 mΩ. It is equivalent to 1.56 mK approximately. Therefore, this number would be used to correct on the resistance values of freezing and melting curves of Al 174 fixed point after doping with Cu 8.3 ppmw.

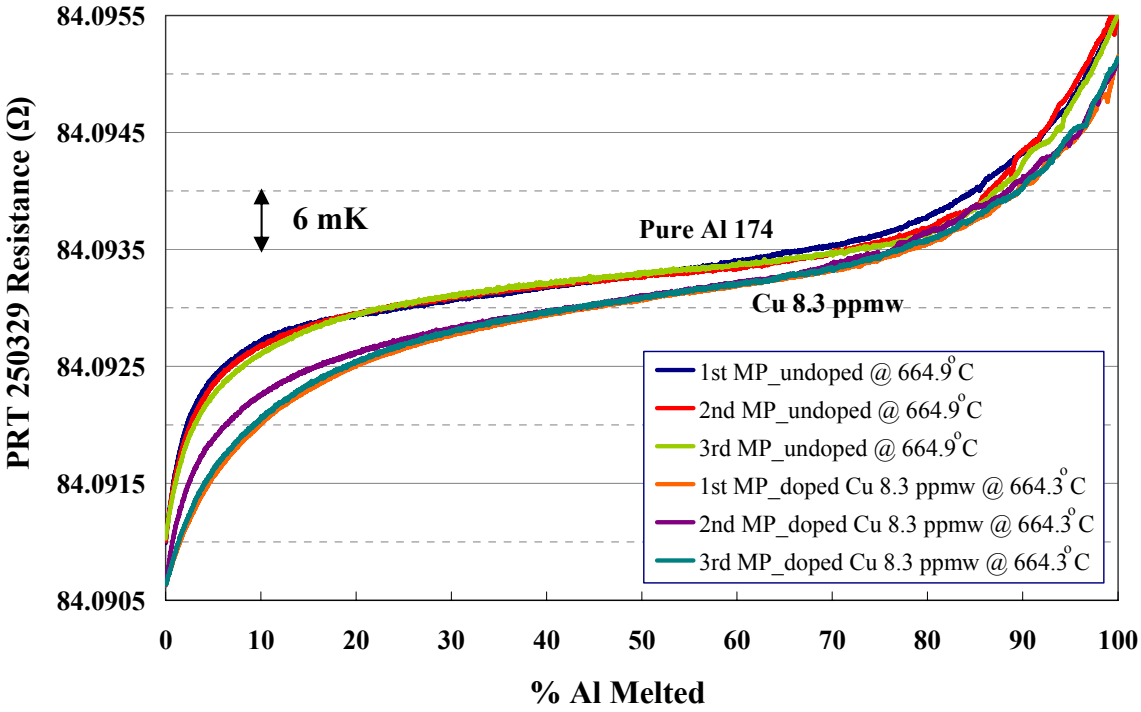

Figure 7.5 Melting curves of "Al 174" high purity aluminium fixed-point and the shift of these curves after doping the aluminium with a concentration of copper at 8.3 ppmw, plotted as a function of aluminium percentage melted. The curves have been normalised to an approximate percentage melted.

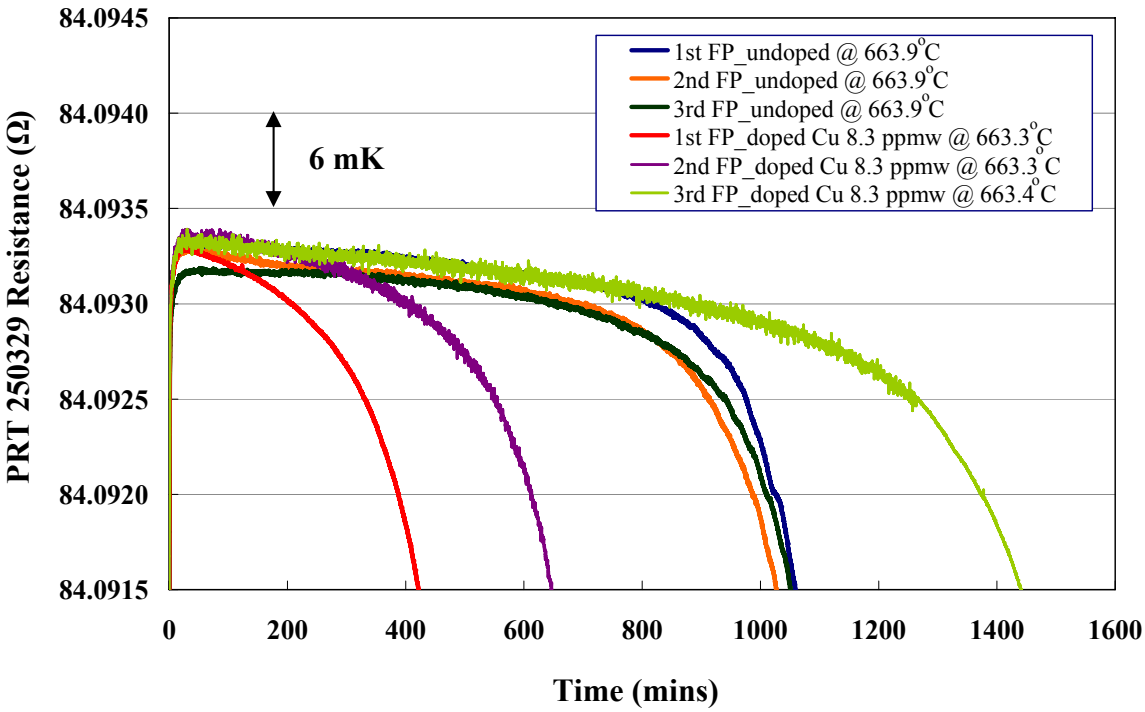

Figure 7.6 Freezing curves of "Al 174" high purity aluminium fixed-point and the shift of these curves after doping the aluminium with a concentration of copper at 8.3 ppmw, plotted as a function of time.

The melting curves, before and after doping, compared with 8.3 ppmw copper concentration curves are shown in Figure 7.5. All freezing curves are presented in Figure 7.6. All doped curves were corrected with the values obtained from Table 7.6.

The curves, before and after doping, indicate the limitations of the reproducibility of the temperature conditions in this fixed-point cell. The length of the freeze does not correlate with the nominal setting of the furnace, which suggests that the furnace control is also moving with time. Figure 7.5 shows the shift of the melting curves after doping the Al with a concentration of 8.3 ppmw copper impurity while the freeze peaks from the set of freezing curves after doping do not change as presented in Figure 7.6. While the y-axis of the graphs in this chapter are plotted in terms of thermometer resistance, a temperature scale arrow (of 6 mK or 2.5 mK) dimension are placed within each graph. The scale arrow sign was calculated using the number (12.5 mK/mΩ for Al), which is the appropriate sensitivity factor of $R(T_{90})$ for converting uncertainties to the temperature equivalents in mK. These come from those used sensitivity factors, in determining mK equivalents of uncertainties in an uncertainty budget [Rusby, 2008].

The peak freeze is from Al 174 (after doping) and reference Al cells were used to compare the temperature changes as shown in Table 7.7. However, the peak can be compared separately; it does not need to be compared directly between two cells at the same time. Therefore, the measurements as shown in Table 7.7 were investigated on different days. (Although it is more ideal to cross compare the peaks at the same time – to minimize any changes in the thermometer, it was not always practical to get both freeze peaks occurring at a similar time on the same day).

Table 7.7 Summary of the average resistance values (R_{Al}) in the comparison measurements at the peak freezing curves of aluminium fixed point between Al 174 and reference (Al 1205) cells with two PRTs (serial number 250329 and 261198).

PRTs serial number	**Date**	**R_T Al 174 doped Cu 8.3 ppmw (1 mA)**	**R_T reference Al 1205 (1 mA)**	**Equivalent Temperature difference between Al 174 doped Cu 8.3 ppmw and Al 1205 cells** $[\Delta T = 12.5 * \Delta R_T]^+$ [Rusby, 2008]
250329	18/01/08	-	84.093791	-
250329	21/01/08	84.093215	-	- 7.20 mK
250329	24/01/08	84.093195	-	- 7.45 mK
261198	18/01/08	-	84.996800	-
261198	28/01/08	84.995883	-	- 11.46 mK
Overall Mean	-	-	-	**- 8.7 mK**
∴ Standard deviation (2s) = ± 4.78 mK				
∴ Mean of Temperature difference Cu 8.3 ppmw doped Al 174 – NPL standard fixed-point = - 8.7 mK				
∴ Mean of Temperature difference Cu 8.3 ppmw doped Al 174 – "undoped" Al 174 = - 8.7 - (-9.99) = +1.3 mK				
∴ Standard deviation (2s) of Difference: Temperature difference between " Cu 8.3 ppmw doped" and "undoped" Al 174 (by quadrature addition) ± 5.52 mK				

+12.5 (mK/mΩ) is the appropriate conversion factor for the sensitivity of $R(T_{90})$ at Al fixed-point temperature [Rusby, 2008].

Table 7.7 shows the temperature difference between Al 174 doped Cu 8.3 ppmw and NPL standard obtained from the calibration of the freeze peaks. It indicates that the Al 174 cell after doping at 8.3 ppmw is lower than the NPL standard cell by 8.7 mK. From the previous section the "undoped" Al 174, the temperature difference is 9.99 mK lower than the reference cell. Hence, if anything, the freeze value appears to have slightly increased on doping. The mean of temperature difference Cu 8.3 ppmw doped and undoped of Al 174 is +1.3 ± 5.52 mK. From comparison measurement of the freeze peaks, at 8.3 ppmw of copper, the initial freezing point value did not change from the original aluminium temperature as

expected (which was slightly surprising – perhaps some unexpected segregation of the impurity had occurred). From Hansen's work [1958], the temperature difference of aluminium is interpolated as expected to decrease by about 3 mK when doped at 8.3 ppmw. However, as shown in Figure 7.5, the offsets at the estimated liquidus point of the melting curves were slightly decreased (subsequent melting/freezing may have provided sufficient dispersion of the impurity as that it produced an effect).

7.1.2.2 High Purity Al 174 doped 16.2 ppmw of Copper

Considering the instability of the PRT 250329, this PRT was calibrated to check the values in the reference Al cell again as shown in Table 7.8.

Table 7.8 Stability of the PRT 250329, as checked at the peak of the reference Al cell (Al 1205) at 1 mA.

Checking Time	**Date**	**Resistance Values (R_T, Ω)**	**Average R_T Values (Ω)**
Checked when Al 1205 Compared with Al 174 doped Cu 8.3 ppmw	18/01/08	84.093791	84.093791
Checked when Al 1205 Compared with Al 174 doped Cu 16.2 ppmw	26/02/08	84.093696	84.093715
	06/03/08	84.093700	
	07/03/08	84.093750	
The shift of PRT 250329 during the calibration = 0.075 m **Ω**			

In Table 7.8, the shift of PRT 250329 during the thermal cycling checked at the reference Al cell decreases by 0.075 mΩ. It is equivalent to 0.94 mK approximately. Therefore, this number would be used to correct the resistance values of freezing and melting curves of Al 174 fixed point after doping with Cu 16.2 ppmw. A set of melting curves of Al 174 after doping with copper at 16.2 ppmw is presented in Figure 7.7. All freezing curves are presented in Figure 7.8.

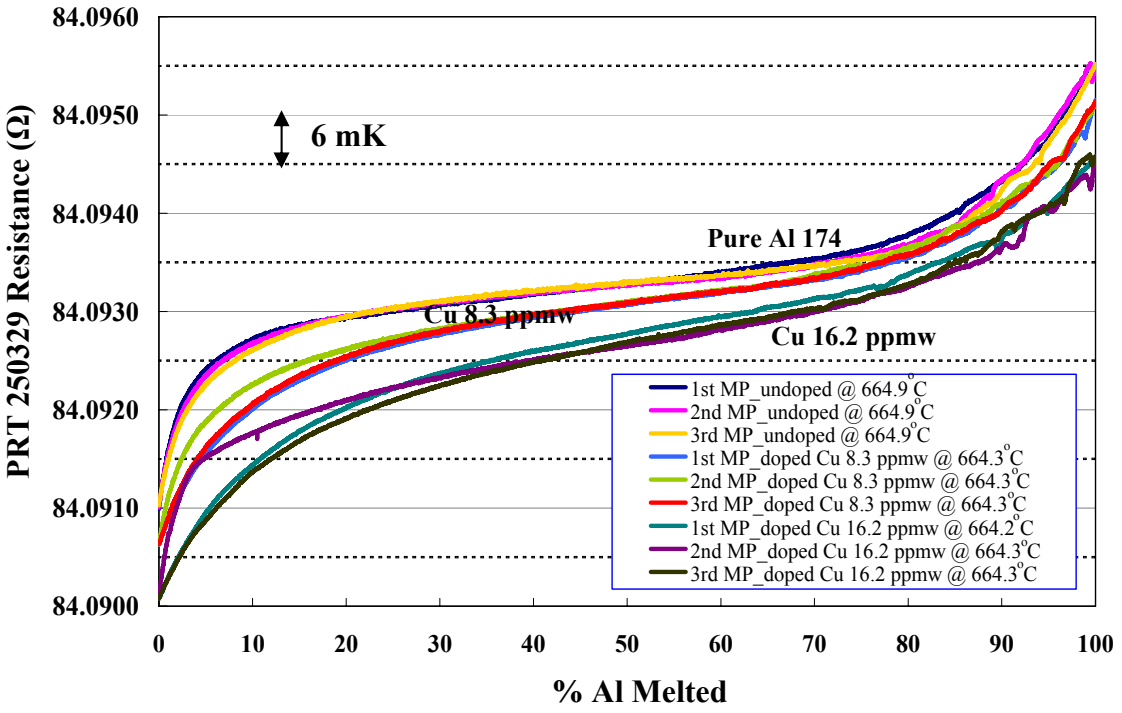

Figure 7.7 Melting curves of "Al 174" high purity aluminium fixed-point and the shift of these curves after doping the aluminium with increasing concentrations of copper, plotted as a function of aluminium percentage melted. The curves have been normalised to an approximate percentage melted.

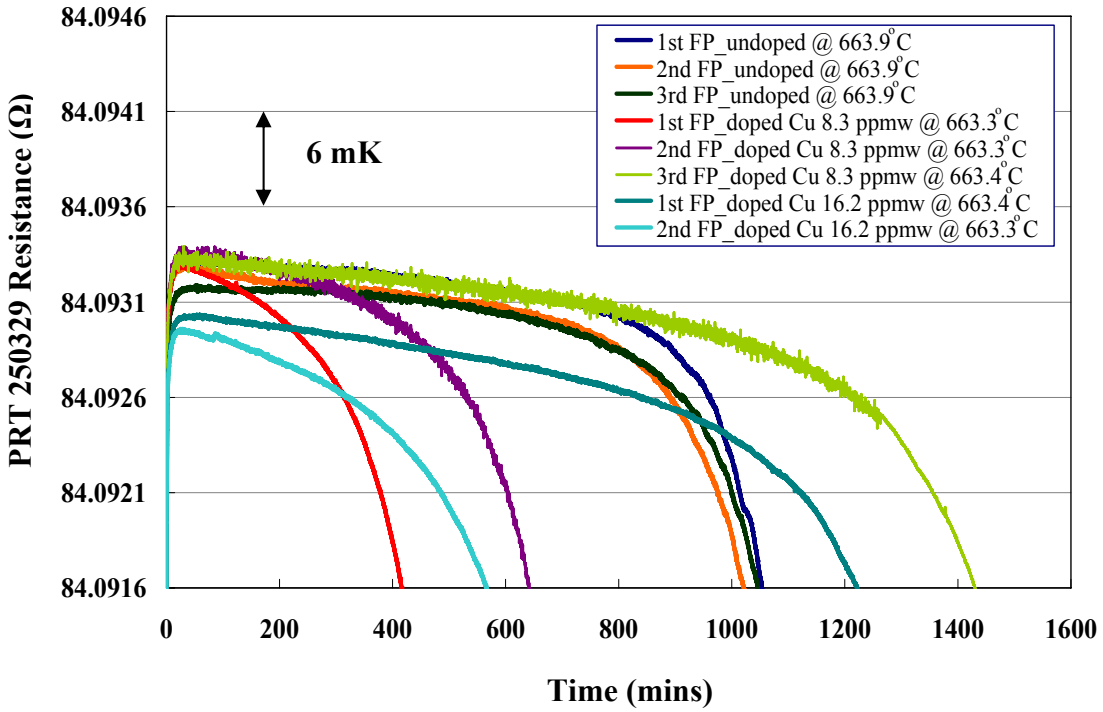

Figure 7.8 Freezing curves of high purity Al 174 fixed-point and the shift of these curves after doping the aluminium with increasing concentrations of copper, plotted as a function of time.

Figure 7.7 illustrates the reproducibility of the melting curves of Al 174 high purity aluminium fixed-point and the shift of these curves after doping the aluminium with increasing concentrations of copper. The curves of Al 174 after doping with copper 16.2 ppmw show the decrease of the liquidus point. All freezing curves as shown in Figure 7.8 present the effect of copper impurity on the freeze peak. The peak of the freezing curves after further doping had dropped, so the value of the decrease could be obtained from the comparison of the peak with the National standard Al cell as shown in Table 7.9.

From the peak comparison between undoped and doped Al 174 with the copper 8.3 ppmw as presented in Table 7.9, the temperature did not change as expected. For the Al 174 with the copper at 16.2 ppmw concentration, depression of the freezing temperature was observed to be 1.7 ± 3.52 mK (expected decrease was ~6 mK from the undoped Al 174). While the mean of temperature difference between Cu 16.2 ppmw and Cu 8.3 ppmw doped Al 174 is 2.99 mK. However if we assume that the initial dopant was inactivated in some way then from our latter experimental results the temperature change of the freezing and melting curves of the aluminium fixed point was affected by the amount of copper at -0.38 mK/ppmw. Then the 2nd doping results are in reasonable agreement with the work of Hansen [1958] and Ancsin [2003] where the fixed-point temperature of aluminium were interpolated to be depressed by 0.37 and 0.29 mK/ppmw of copper, respectively. The results of this work confirm the influence of very low-level copper impurity on the freezing/melting curves of the aluminium fixed point.

Table 7.9 Summary of the average resistance values (R_{Al}) in the comparison measurements at the peak of the freezing curves of the aluminium fixed points between Al 174 after doping with copper at 16.2 ppmw and reference (Al 1205) cells with two PRTs (serial number 250329 and 261198). All results are corrected for the hydrostatic head pressure in both Al cells.

PRTs serial number	**Date**	**R_T Al 174 doped Cu 16.2 ppmw (1 mA)**	**R_T reference Al 1205 (1 mA)**	**Equivalent Temperature difference between Al 174 doped Cu 16.2 ppmw and Al 1205 cells** $[\Delta T = 12.5 * \Delta R_T]^+$ [Rusby, 2008]
250329	21/02/08	84.092725	-	-12.13 mK
250329	22/02/08	84.092851	-	- 10.56 mK
250329	26/02/08	-	84.093696	-
250329	06/03/08	84.092850	84.093700	- 10.63 mK
250329	07/03/08	84.092865	84.093750	- 11.06 mK
261198	06/03/08	84.995277	84.996283	- 12.58 mK
261198	07/03/08	84.995236	84.996290	- 13.18 mK
Overall Mean	-	-	-	**- 11.69 mK**
∴ Standard deviation (2s) = ± 2.19 mK				
∴ Mean of Temperature difference Cu 16.2 ppmw doped Al 174 – NPL standard = - 11.69 mK				
∴ Mean of Temperature difference between Cu 16.2 ppmw doped – Cu 8.3 ppmw doped = (-11.69) - (-8.7) = - 2.99 mK				
∴ Mean of Temperature difference between Cu 16.2 ppmw doped - undoped Al 174 = (-11.69) - (-9.99) = - 1.7 mK				
∴ Standard deviation (2s) Difference: Temperature difference between " Cu 16.2 ppmw doped" and "undoped" Al 174 (by quadrature addition) ± 3.23 mK				

+12.5 (mK/mΩ) is the appropriate conversion factor for the sensitivity of $R(T_{90})$ at Al fixed-point temperature [Rusby, 2008].

7.1.3 Influence of Silicon on High Purity Al 174 Fixed Point

7.1.3.1 High Purity Al 174 Doped with 4.7 ppmw of Silicon

Before the melting and the freezing curves of Al 174 after doping with silicon are measured, the instability of PRT 250329 was checked by calibration in the reference Al cell as shown in Table 7.10.

Table 7.10 Stability of PRT 250329, which was checked at the freeze peak of the reference Al cell (Al 1205) at 1 mA.

Checking Time	**Date**	**Resistance Values (R_T, Ω)**	**Average R_T Values (Ω)**
Checked when Al 1205 Compared with Al 174 doped Cu 16.2 ppmw	26/02/08	84.093696	84.093715
	06/03/08	84.093700	
	07/03/08	84.093750	
Checked when Al 1205 Compared with Al 174 doped Si 4.7 ppmw	25/03/08	84.093746	84.093720
	01/04/08	84.093693	
The shift of PRT 250329 during the calibration = 0.005 m **Ω**			

The shift of PRT 250329 during the thermal cycling checked at the reference Al cell decreases by 0.005 mΩ as seen in Table 7.10. It is equivalent to 0.063 mK approximately. Therefore, this number would be used to correct the resistance values of freezing and melting curves of Al 174 fixed point after doping with silicon 4.7 ppmw. The melting curves of "Al 174" high purity aluminium fixed-point and the shift of these curves after doping the aluminium with 4.7 ppmw concentration of silicon is presented in Figure 7.9. All freezing curves are presented in Figure 7.10.

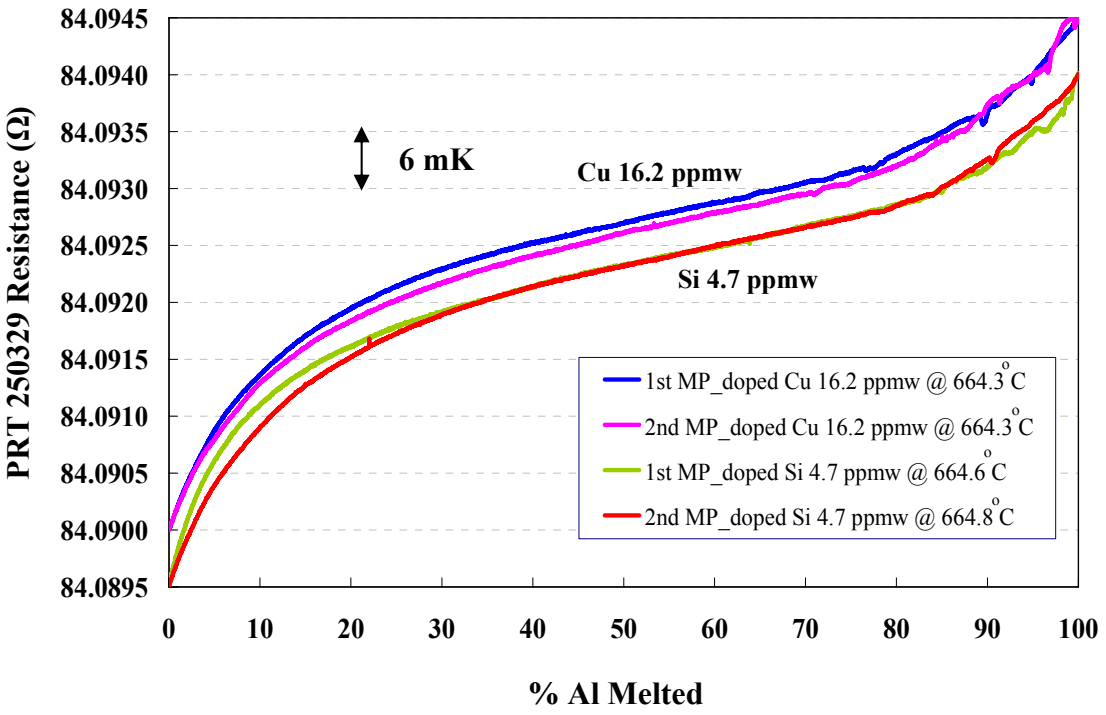

Figure 7.9 Melting curves of Al-Cu binary fixed-point and the shift of these curves after doping with silicon, plotted as a function of aluminium percentage melted. The curves have been normalised to an approximate percentage melted.

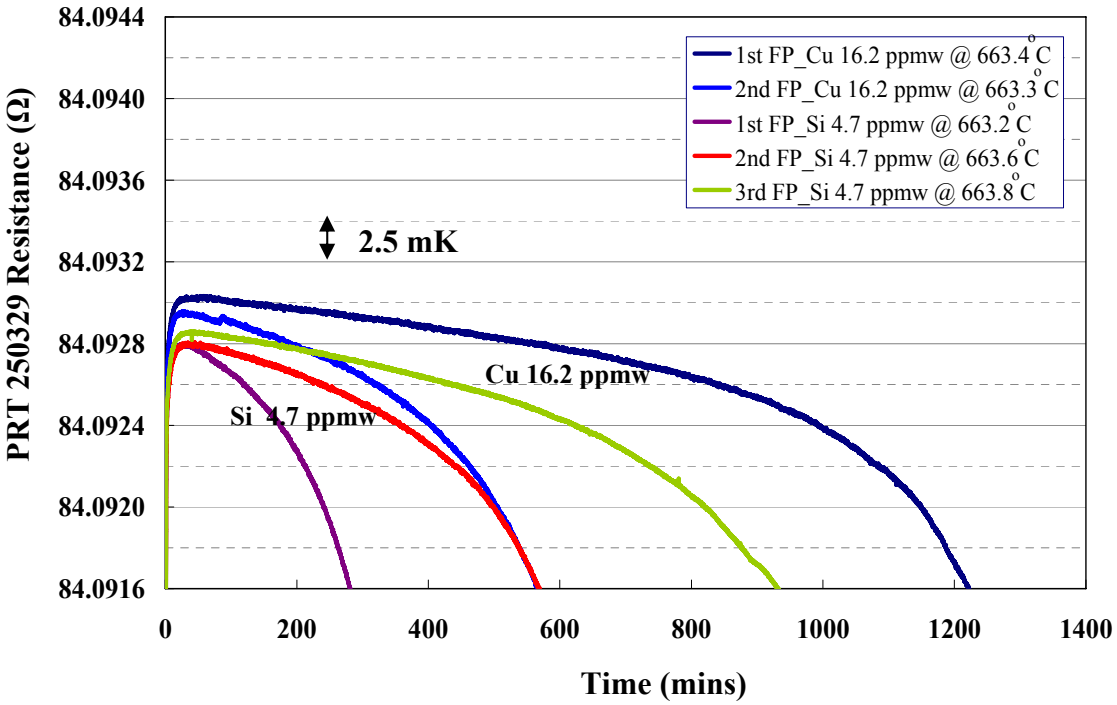

Figure 7.10 Freezing curves of Al-Cu binary fixed-point and the shift of these curves after doping with silicon, plotted as a function of time.

Figure 7.9 shows typical examples of melting curves obtained after a rapid rate of freezing. The set of melting curves confirm the reproducibility of the temperature measurements in this doped fixed-point cell. The results confirm that silicon depresses the phase transition temperature as expected. The results from Figure 7.10 display the different period of time of the freezing curves doped with Cu 16.2 ppmw and Si 4.7 ppmw due to the different furnace temperature settings. The length of the freeze does not appear to be strongly correlated to the furnace setting, suggesting that the furnace control thermometer experiences some drift with time and/or there is a variation in the latent heat lost in the undercool (but the latter would not be expected to cause the amount of variations seen). The undercool of all freezing curves in Figure 7.10 have been checked and they had the same amount, which means the latent heat lost in undercool does not effect the length of the curve. The length of the freeze is affected from variations in the furnace itself. The peak of the freezing curves after doping had dropped.

Table 7.11 Summary of the average resistance values (R_{Al}) in the comparison measurements at the peak of freezing curves of aluminium fixed point between Al 174 after doping with silicon at 4.7 ppmw and reference Al 1205 cells with two PRTs (serial number 250329 and 261198).

PRTs serial number	**Date**	**R_T Al 174 doped Si 4.7 ppmw (1 mA)**	**R_T reference Al 1205 (1 mA)**	**Equivalent Temperature difference between Al 174 doped Si 4.7 ppmw and Al 1205 cells** $[\Delta T = 12.5 * \Delta R_T]^+$ [Rusby, 2008]
250329	14/03/08*	84.091989	-	-
250329	15/03/08	84.092794	-	-
250329	17/03/08#	-	84.093315	-
250329	20/03/08	84.092455	-	-
Average	-	**84.092625**	-	**- 14.00 mK**
250329	25/03/08	-	**84.093745**	-
250329	31/03/08	84.092779	-	-
250329	01/04/08	-	84.093693	-
Average	-	-	**84.093719**	-
250329	07/04/08	84.092856	-	-
Average	-	**84.092818**	-	**-11.30 mK**
261198	04/04/08	84.994878	-	-13.69 mK
261198	05/04/08	-	84.995973	-
Overall Mean	-	-	-	**- 13.00 mK**
∴ Standard deviation (2s) = ± 2.96 mK				
∴ Mean of Temperature difference Al 174 doped Si 4.7 ppmw – NPL standard fixed-point = - 13.00 mK				
∴ Mean of Temperature difference between Al doped Si 4.7 ppmw - Al 174 doped Cu 16.2 ppmw = (-13.00) - (-11.69) = - 1.31 mK				
∴ Standard deviation (2s) Difference: Temperature difference between Al doped Si 4.7 ppmw - Al doped Cu 16.2 ppmw (by quadrature addition) ± 3.68 mK				

* and # represent the exceptional resistance values of PRT 250329 measured in the Al 174 doped Si 4.7 ppmw and NPL standard Al 1205, respectively, e.g. cf. Table 7.9, and so were not used. +12.5 (mK/mΩ) is the appropriate conversion factor for the sensitivity of $R(T_{90})$ at Al fixed-point temperature [Rusby, 2008].

For the Al 174 with the Si at 4.7 ppmw concentration, depression of the freezing temperature was observed to be 13.0 mK relative to the reference Al cell. That means the adding Si 4.7 ppmw impurity decreases the temperature of the freezing and melting of Al ingot by 1.31 ± 3.68 mK (expected decrease was ~3 mK). The measured rate of the Al 174 after doping with silicon 4.7 ppmw in this work is Si -0.23 mK/ppmw, which is lower than the value as expected in Hansen's work [1958], which was 0.71 mK/ppmw. This may be because the instability of the PRT on cycling, which can see from the standard deviation (2s) of the measurements.

7.1.3.2 High Purity Al 174 doped 9.8 ppmw of Silicon

Table 7.12 Stability of the PRT 250329, which was checked at the peak of the reference Al cell (Al 1205) at 1 mA.

Checking Time	**Date**	**Resistance Values (R_T, Ω)**	**Average R_T Values (Ω)**
Checked when Al 1205 Compared with Al 174 doped Si 4.7 ppmw	25/03/08	84.093745	84.093719
	01/04/08	84.093693	
Checked when Al 1205 Compared with Al 174 doped Si 9.8 ppmw	15/05/08	84.093497	84.093333
	27/05/08	84.093474	
	31/05/08	84.093208	
	20/06/08	84.093266	
	09/07/08	84.093219	
The shift of PRT 250329 during the calibration = 0.386 m **Ω**			

The shift of PRT 250329 during the thermal cycling checked against the reference Al cell decreases by 0.386 mΩ as seen in Table 7.12. It is equivalent to 4.83 mK approximately. Therefore, this number would be used to correct the resistance values of freezing and melting curves of Al 174 fixed point after doping with silicon 9.8 ppmw. The melting curves of "Al 174" high purity aluminium fixed-point and the shift of these curves after doping the aluminium with increasing concentrations of silicon at 4.7 and 9.8 ppmw is presented in Figure 7.11. All freezing curves of Al-Cu binary fixed-point and the shift of these curves after doping with increasing concentrations of silicon are presented in Figure 7.12.

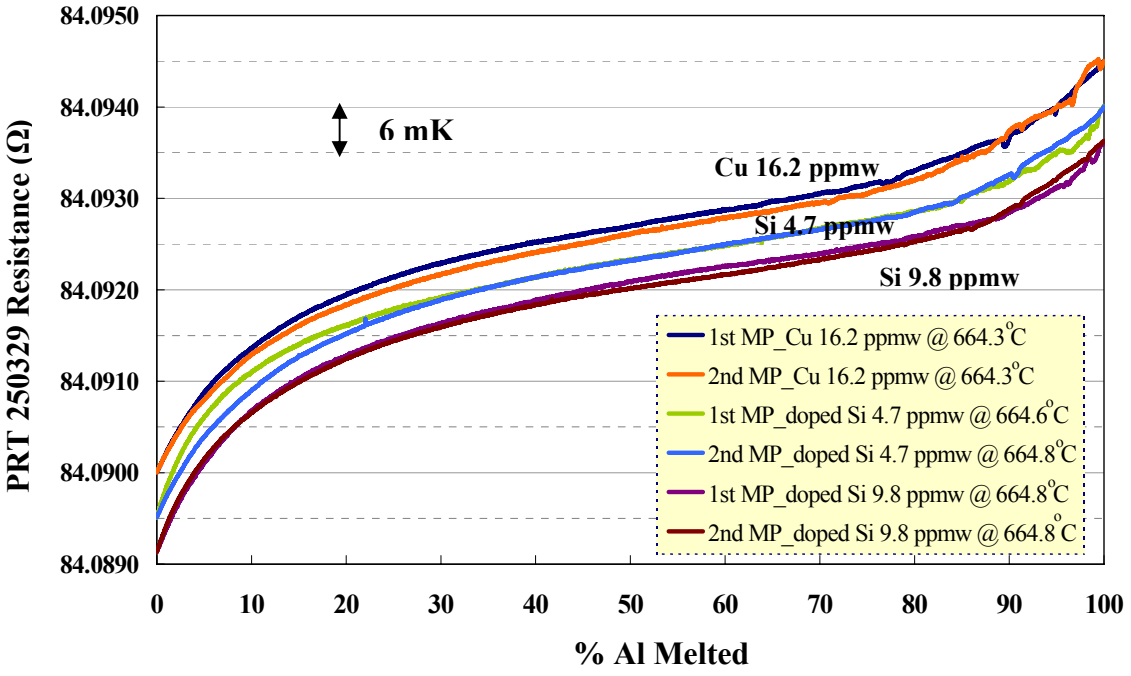

Figure 7.11 Melting curves of "Al-Cu" aluminium fixed point (after further doping with increased amounts of Si) plotted as a function of aluminium percentage melted. The curves have been normalised to an approximate percentage melted.

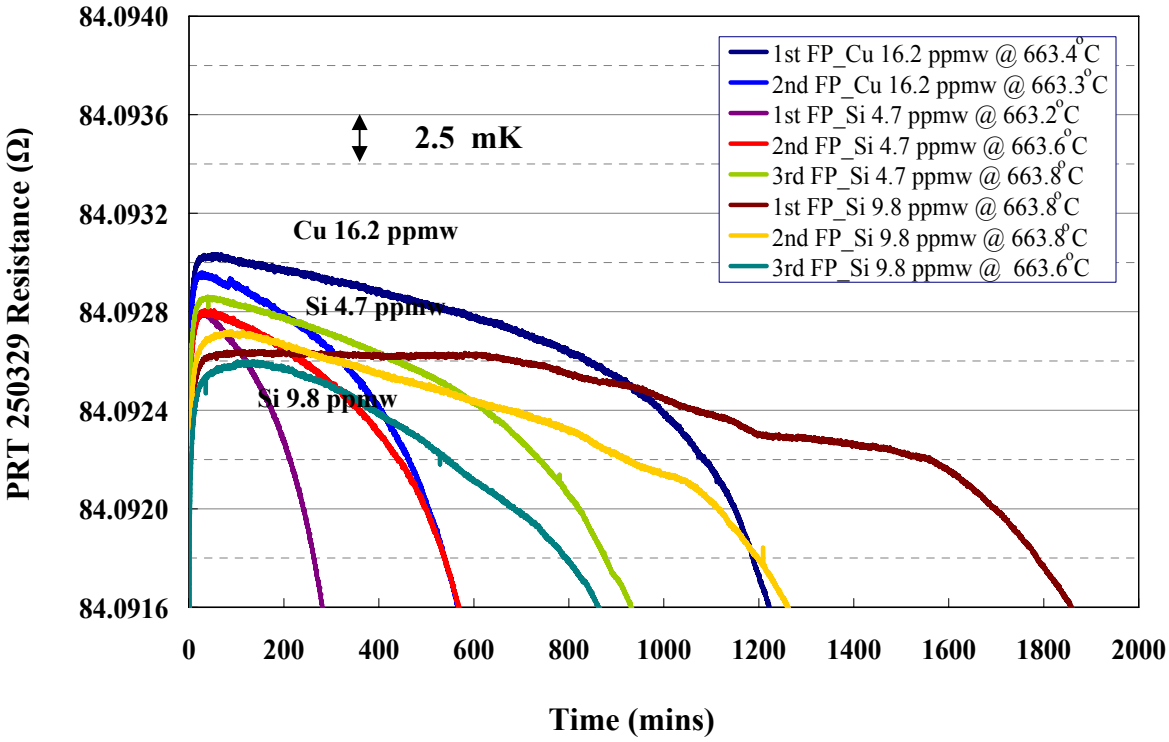

Figure 7.12 Freezing curves of Al-Cu binary fixed-point and the shift of these curves after doping with increasing concentrations of silicon, plotted as a function of time.

Figure 7.11 shows the melting curves obtained after a rapid rate of freezing. The set of melting curves confirm the reproducibility of the temperature measurements in this doped fixed-point cell. Figure 7.11 and 7.12 show the shift of the melting and freezing curves after doping the tin with increasing concentrations of silicon impurities excepting the melting curves after doping 9.8 ppmw of silicon, which there were not changed or shifted from the previous doping. The peak of the freezing curves after doping also had dropped**.** There appear to be repeatable bumps in the three freeze curves of the more heavily Si doped sample (the furnace setting were not altered during the freezes). We do not have an explanation for this, but wonder if some segregation was/had occurring/ed.

For this Al-Si system, the sample with silicon at 4.7 ppmw shows a decrease for the whole of the melting curve. From the freeze peak as shown in Table 7.13, it is about 1.31 ± 3.68 mK lower than the previous aluminium doped with the copper impurity. The results of the first silicon doping (4.7 ppmw) did not agree with interpolation from the previous data [Hansen, 1958] at the freeze peak, and the outcome of Al 174 doped with the silicon at 9.8 ppmw did not give the results as expected again at the freeze peak. The temperature at the freeze peak of the Al 174 after doping with Si 9.8 ppmw shows 14.72 ± 2.31 mK decrease from NPL standard Al, which is just 3.03 ± 3.18 mK different from the Al-Cu system (expected decrease was ~6 mK). The measured rate of the Al 174 after doping with silicon 9.8 ppmw in this work is Si -0.31 mK/ppmw. However, the offsets and shapes of the melting curves showed the depression of the temperature for the whole curve. However, the amount of copper and silicon concentrations in Al 174 ingot can be detected by GD-MS analysis, which is presented in the next section. Therefore, it can be summarised that the temperature change of the freezing and melting curves of the Al fixed point were affected by amounts as follows: Cu (no change) mK/ppmw (obtained at Cu 8.3 ppmw), Cu -0.38 mK/ppmw (obtained at Cu 16.2 ppmw) and Si -0.23 mK/ppmw (obtained at Si 4.7 ppmw), Si – 0.31 mK/ppmw (obtained at Si 9.8 ppmw). The average measured rates in this work are as follows: Cu -0.38 and Si -0.27 in units of mK/ppmw. This expectation is compared with Hansen's book [Hansen, 1958], which was interpolated to be depressed by 0.37 mK/ppmw and 0.71 mK/ppmw for Cu and Si impurity, respectively.

Table 7.13 Summary of the average resistance values (R_{Al}) in the comparison measurements at the aluminium freezing curve peaks between Al 174 after doping with 9.8 ppmw silicon at and reference Al 1205 cells with two PRTs (serial number 250329 and 261198). All results are corrected for the hydrostatic head in both Al cells.

PRTs serial number	**Date**	**R_T Al 174 doped Si 9.8 ppmw (1 mA)**	**R_T reference Al 1205 (1 mA)**	**Equivalent Temperature difference between Al 174 doped Si 9.8 ppmw and Al 1205 cells** $[\Delta T = 12.5 * \Delta R_T]^+$ [Rusby, 2008]
250329	15/05/08	-	84.093497	-
250329	19/05/08	84.092355	-	- 14.28 mK
250329	25/05/08	84.092160	-	- 16.72 mK
250329	27/05/08	-	84.093474	-
250329	28/05/08	84.092231	-	- 15.54 mK
250329	06/06/08	84.092307	-	- 14.59 mK
250329	20/06/08	84.092175	84.093266	- 13.64 mK
250329	09/07/08	-	84.093219	-
250329	10/07/08	84.092151	-	- 13.35 mK
261198	09/07/08	-	84.995621	-
261198	10/07/08	84.994425	-	- 14.95 mK
Overall Mean	-	-	-	**- 14.72 mK**
∴ Standard deviation (2s) = ± 2.31 mK				
∴ Mean of Temperature difference Al 174 doped Si 9.8 ppmw – NPL standard fixed-point = - 14.72 mK				
∴ Mean of Temperature difference between Al doped Si 9.8 ppmw - Al 174 doped Cu 16.2 ppmw = (-14.72) - (-11.69) = - 3.03 mK				
∴ Standard deviation (2s) Difference -Temperature difference between Al doped Si 9.8 ppmw - Al 174 doped Cu 16.2 ppmw (by quadrature addition) ± 3.18 mK				

+12.5 (mK/mΩ) is the appropriate conversion factor for the sensitivity of $R(T_{90})$ at Al fixed-point temperature [Rusby, 2008].

7.1.4 Impurity Analysis of High Purity Aluminium (Al 174) Fixed-Point after Doping with Cu and Si Contents

Glow Discharge Mass Spectrometry (GD-MS) Characteristics after Doping Impurities

The previous GD-MS results of the Al 174 fixed-point cell before impurity doping indicate that the Al 174 metal and the impurities are well mixed after the aluminium is properly molten for a reasonable time. The impurity levels in three areas of the Al 174 ingot show the homogeneity of the impurity concentration. Therefore, after doping only one piece of the Al 174 was cut from the ingot to detect the impurity concentrations by the GD-MS technique. Also, one piece of ingot before doping, which was cut almost a year before and kept in NPL, was measured by GD-MS. Measurement of the two pieces at the same time enabled a check on the absolute values of the GD-MS analysis, i.e. it is for testing the repeatability of the GD-MS technique. However, when the doped sample was analysed the surface pre-cleaning process using an acid, (believed 50% hydrofluoric or hydrofluoric/nitric acid mixture) damaged a large part of the sample, making the subsequent analysis suspect. Also the sample appeared to have a larger than usual number of voids or pits allowing the acid to penetrate inside the sample. NRC reported that the GD-MS measurements did not stabilize as normal, so making the results rather suspect; some elements seemed unexpectedly high e.g. oxygen and tin.

Therefore, a doped sample needed to be cut out and measured again by GD-MS at a different time to the results obtained from the fourth undoped sample. Three sets of the GD-MS results, for the background impurities detected from both undoped and doped samples is shown in Table 7.14.

Table 7.14 GD-MS analysis results of the impurity concentrations of the Al 174 before and after doping [NRC report number: Al30337R1 (checked on 14/12/07, before doping), Al30817 (checked on 22/08/08), before and after doping and Al31121 (checked on 24/03/09), after doping]. These elements were detected in term of mass fraction (in parts per billion by weight, ppmw).

Element	Al 174 Before Doping (Average from three areas 2007)	Al 174 Before doping (Measured Aug 08)	*Al 174 (suspect results measured August 08)*	Al 174 After Doping (Measured Mar 09)	Element	Al 174 Before Doping (Average from three areas 2007)	Al 174 Before doping (Measured Aug 08)	*Al 174 (suspect results August 08)*	Al174 After Doping (Measured Mar 09)
	ppmw					ppmw			
Li	<0.003	<0.002	*0.8*	0.61	**Br**	<0.02	<0.04	*<0.02*	<0.015
Be	<0.001	<0.0006	*<0.001*	<0.001	**Rb**	<0.001	<0.0009	*<0.002*	<0.003
B	<0.007	0.004	*0.04*	0.073	**Sr**	<0.001	<0.0004	*<0.003*	<0.0006
C	6	74	*55*	100	**Y**	<0.001	<0.0005	*<0.001*	<0.0005
N	0.77	2.6	*4.4*	3.8	**Zr**	0.007	0.01	*<0.006*	<0.002
O	7.7	15	*1000*	1000	**Nb**	<0.001	<0.0004	*<0.0009*	<0.0005
F	<0.01	<0.025	*<0.01*	0.025	**Mo**	<0.003	<0.001	*<0.003*	<0.002
Na	<0.002	0.012	*0.2*	0.4	**Pd**	-	-	-	-
Mg	<0.003	0.005	*0.1*	0.049	**Ag**	<0.008	0.018	*<0.009*	0.024*
Al	Matrix	Matrix	*Matrix*	Matrix	**Cd**	<0.02	<0.009	*<0.1*	<0.035
Si	**0.2**	**0.38**	***1-2***	**1.8**	**In**	<0.007	<0.001	*<0.1*	0.017
P	<0.002	0.004	*0.005*	<0.002	**Sn**	<0.03	<0.004	*30*	3.1*
S	<0.003	0.23	*0.04*	0.068	**Sb**	<0.007	<0.003	*<0.007*	0.009
Cl	0.004	<0.004	*0.06*	0.13	**Te**	<0.008	<0.004	*<0.01*	<0.007
K	<0.02	<0.03	*<0.04*	0.046	**I**	<0.003	<0.002	*<0.004*	<0.003
Ca	<0.03	<0.015	*0.5*	0.53	**Cs**	<0.001	<0.0005	*<0.001*	<0.0009
Sc	0.05	0.047	*0.06*	0.062	**Ba**	<0.003	<0.001	*<0.002*	<0.001
Ti	0.087	0.16	*0.09*	0.073	**La**	<0.003	<0.0005	*<0.001*	<0.0008
V	0.08	0.049	*0.05*	0.055	**Ce**	<0.0009	<0.0005	*<0.001*	<0.0007
Cr	0.02	0.022	*0.04*	0.029	**Hf**	<0.003	<0.002	*<0.005*	<0.002
Mn	0.05	0.038	*0.1*	0.067	**Ta**	-	-	-	-
Fe	0.2	0.73	*6.5*	6.1*	**W**	<0.003	<0.001	*<0.003*	<0.002
Co	<0.0008	<0.0004	*<0.002*	<0.002	**Pt**	<0.01	<0.006	*<0.02*	<0.01
Ni	0.016	0.015	*0.08*	0.22	**Au**	<0.2	<0.95	*<1*	<1.4
Cu	**0.1**	**0.16**	***2.9***	**5.5**	**Hg**	<0.03	<0.015	*<0.04*	<0.03
Zn	0.1	0.094	*0.4*	0.65*	**Tl**	<0.009	<0.004	*<0.009*	<0.007
Ga	<0.006	<0.005	*<0.008*	0.005	**Pb**	<0.004	<0.002	*0.04*	0.36*
Ge	<0.01	<0.01	*<0.03*	0.025	**Bi**	<0.004	<0.002	*<0.004*	<0.003
As	<0.0005	<0.003	*<0.007*	0.003	**Th**	<0.001	<0.0005	*<0.001*	<0.001
Se	<0.083	<0.05	*<0.05*	0.06	**U**	<0.001	<0.0006	*<0.001*	<0.001

Table 7.14 lists the impurity elements detected in the Al 174 metal ingot. The uncertainty of this GD-MS analysis is considered to be accurate within a factor of two of the values obtained, at a confidence level of 95% though there is anecdotal evidence that the results are usually more accurate than quoted. However our results may not be bearing that out when doping at low concentrations. Four samples were cut from the Al 174 before deliberate doping; three samples from three areas were tested soon after while the other one was tested a ~year later, i.e. four similar samples were tested by GD-MS at different times, i.e. the first three undoped sample were checked a year ago, while the other undoped sample was detected later. After doping, one sample also removed from the ingot to check the impurity concentrations.

Unfortunately as just mentioned, the pre-cleaning process damaged the sample making the Aug 08 analysis suspect. It appeared that the ingot had not been frozen fast enough and/or the sample was cut too high up the ingot. Consequently there were grain or volume boundaries going into the sample and the acid therefore etched from the inside as well as the outside. Subsequent study of the ingot showed that there was finer "grain" nearer the bottom of the cell – where the pressure due to the metal weight seemed to have kept the metal together but higher up the aluminium seemed more "rough". The ingot was left molten for over a day and then physically lifted into the air to produce ultra fast cooling. New samples were cut out and sent for GD-MS analysis.

Looking at the results that have been obtained and comparing the signals for the "background impurities" of Al 174 before doping i.e. not those deliberately added, the larger variations in nominally the same background impurities can be seen between the measurements at different times e.g. Na, S, Ti, Fe, Cu, Ag and Au even though the samples were cut from the ingot at same time of its life (though most of these differences are within the factor of 2 uncertainty). Again, the impurity concentrations of the background impurities after doping show a bigger difference from the undoped results e.g. Li, B, Na, Mg, Ca, Fe, Ni, Zn, Ag, Cd, In and Sn. S appears to have gone down after doping. Considering Copper (Cu) impurity in Table 7.14, it shows the different amounts before doping were checked the GD-MS at the different time, i.e. 0.1 and 0.16 ppmw (but within the x2 uncertainty range). It also happens with Sulphur (S) impurity, we can see the big different amounts when were checked in different time in this Al 174 cell, i.e. <0.003 and 0.23 ppmw, respectively (beyond a factor 2). The results indicate that the amounts of "background" impurities

in the undoped samples are different as the checked time of GD-MS. These results can show some evidence of the uncertainty of the GD-MS technique. It is possible that some of this variation is due to contamination of the sample by material other than the deliberate dopants. As most of the results from the "suspect" analysis are similar to the final analysis, it may be that it was actually representative. The suspect and final analysis together support some additional contamination, though it is difficult to think where e.g. lithium might have come from. For the iron then there are ageing components on the old top cap that might be a source of iron. We note an increased value for Sn and Pb and therefore wonder if some cross contamination could have occurred at the time of sampling – though the results go in opposite directions with time, and they are not in proportion. Some changes can be attributed to resolution of conflicting peaks on the spectrometer e.g. NRC mention that the Au peak is obscured by the TaO peak (Ta being a component of the machine and not measurable) [NRC GD-MS services, 2009].

Looking at the impurity concentrations in Table 7.14 after doping of the Cu and Si metals in the Al 174 ingot, it shows that the increased amount of Cu and Si after adding a total of 16.2 ppmw (16200 ppbw) and 9.8 ppmw (9800 ppbw), respectively. The actual amount of Cu and Si detected by GD-MS was 5500 ppbw and 1800 ppbw respectively, which are less than the real amount added. From the phase diagram calculation [Hansen, 1958], the fixed-point temperature of aluminium was interpolated to be depressed by 0.37 and 0.71 mK/ppmw of Cu and Si impurity, respectively. Therefore, the decreasing of the freezing and the melting temperatures of Al 174 ingot from the experiment as calculated from the amount of Cu impurity in Table 7.14 would be 1.99 mK, which is reasonable agreed with the experimental results after doping Cu 16.2 ppmw compared the undoped Al 174. Considering the amount of Si impurity in GD-MS results, the temperature would be decreased by 1.07 mK.

7.1.5 Photograph of Al 174 Fixed-Point Cell

After all experiments have been done on the Al 174 ingot it was noticed that changes in the ingot's structure could be seen in the pictures taken at different times of the experiments (i.e. before doping, after doping with Cu 8.3 ppmw and after doping with Si impurities) - as shown in Figure 7.13, Figure 7.14, and Figure 7.15, respectively.

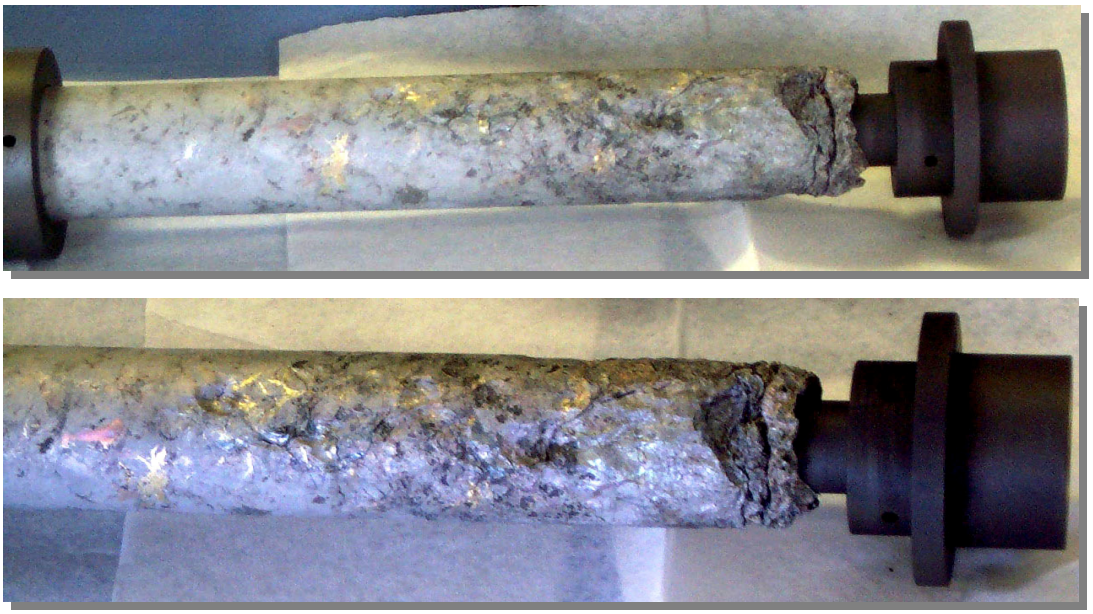

Figure 7.13 Original pure Al 174 ingot before doping with Cu and Si impurities.

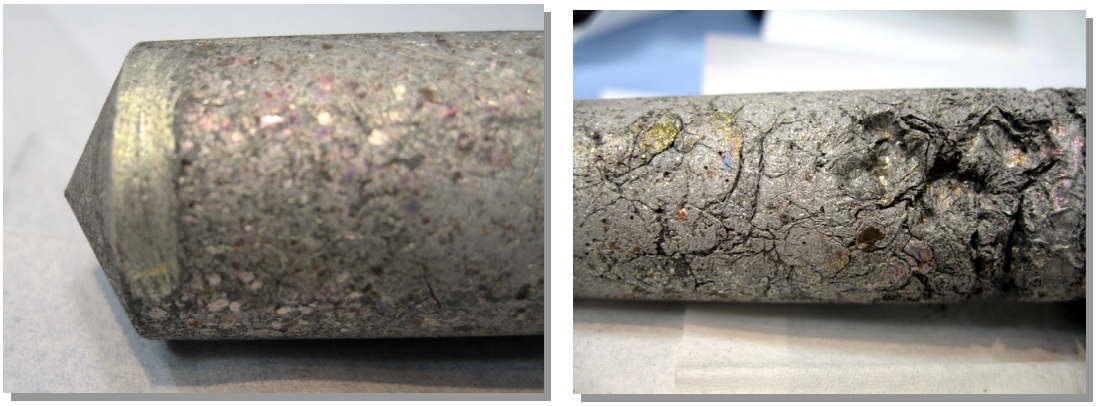

(a) **(b)**

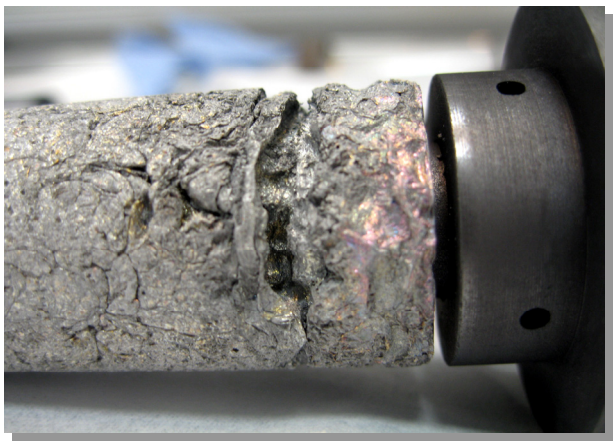

(c)

(d)

Figure 7.14 Al 174 ingot after doping with Cu 8.3 ppmw, where the melt and freeze had been realised at least three times each: (a) shows the shiny surface formed by re-filling of the hole made by cutting the GD-MS sample off the bottom of the ingot (b) shows crevices near the top of the ingot, (c) shows a fissure around the circumference near the top of the ingot and (d) shows the overview of the Al 174 ingot (including the shiny area of two infills where the sample was cut out and the rougher top section.)

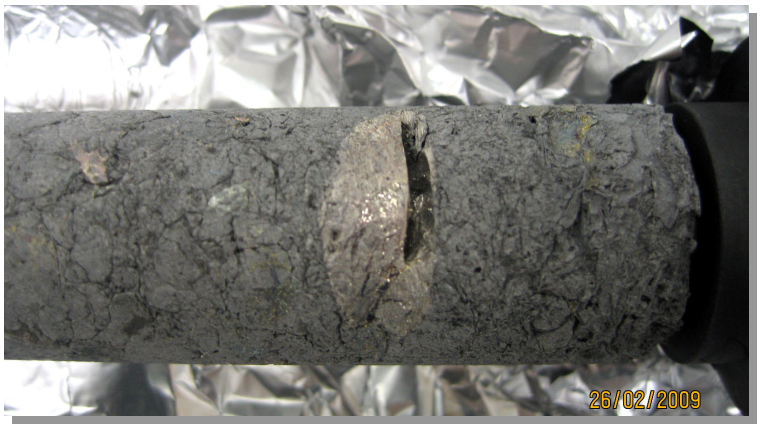

(a)

(b)

Figure 7.15 Al 174 ingot after doping with Cu and Si impurities, which had been re-melted. The ingot was left molten for over a day at high temperature (666 ^{o}C in the Hart Furnace) and then physically lifted into the air to produce ultra fast cooling. (a) shows the Al did not fully re-fill the sample hole on a first remelting and (b) shows the overview of the Al ingot showing the grey surface in contrast with the fresh Al (filling the other sample hole) after 2nd remelting and ultra fast freeze.

The original Al ingot as shown in Figure 7.13 shows the original surface structure, obtained before realising any melting and freezing curves, was not mixed well on the surface and possible near the very top (see the hole around the top of the ingot). We have no information as to what the prior history of the ingot was. Figure 7.14 and 7.15 show the mixing and molten processes may not be effective at the top and/or surface of the Al 174 ingot because it still had the crevices and the Al did not fully re-fill the sample hole after cutting the samples out. However, it should be noted that the original three GD-MS samples suggested that the impurity distribution below the surface was similar from three sites along the ingot length. It may be that the

effects at the top of the ingot are because the furnace temperature was not set to high enough to reduce the viscosity of the molten aluminium within the ingot. Also, the surface colour of the ingot after doping with Cu and Si impurities has a grey outside, which is greyer than the undoped Al ingot. It is wondered if this could be either the Si dopant that might be rejected from the Al or it is a layer of Al_2O_3. If rejected Si then that might explain why the temperature was not decreased as expected. However this hypothesis needs to be confirmed and proved by scraping the surface off to check the chemical analysis as part of any future work. It is also possible that these effects are related to the surface. Perhaps the surface contamination stays still while the aluminium flows behind it. Where the surface contamination is removed due to a sample cut off, the Al fills the gap but without contamination on the surface. If a crust formed during deformed cooling, making the crevice seen, it may be that possible some surface effect doesn't allow the aluminium "out" to subsequently fill the crevice. It appears that the gaps fill faster lower down the cell, presumably due to the pressure head of the aluminium itself. It was possible to scrape off the surface greyness in the bottom half of the cell to reveal a more aluminium like colour below.

7.1.6 Mass of Aluminium (Al 174) Fixed-Point Ingot

Table 7.15 Mass of Al 174 fixed-point ingot as calculated based on a mass measurement (of the aluminium and central graphite) before doping the impurities.

Component(s) of Al 174 Cell	Mass (g)
Calculated Mass of Al 174 metal (Originally)	236.67
Measured Mass {Al 174 metal and graphite re-entrance well} (Originally) less the calculated mass of graphite	216.80
Measured Mass of Al 174 metal (Samples cut off) less the calculated mass of graphite	211.84

The uncertainty on this balance scale (a large scale) can be corrected by adding 1.09 mg to the value of the weight. The uncertainty components are as follows;

0.05 mg for the scale error (rectangular distribution)

0.06 mg for repeatability (normal distribution)

0.1 mg for balance resolution (rectangular distribution)

From the above information, obtained from NPL Mass section, the uncertainty of the weighing itself is very small when compared with the total mass of Al 174 ingot (~200 g). Thus, the uncertainty is negligible compared to that of the included graphite re-entrant well, where the two methods for accounting for the graphite in Table 7.15 differ by 20 g, i.e. ~10%. The measured mass of Al 174 metal after cutting some samples off for the undoped GD-MS testing was used in calculation of the doping concentrations (in ppmw).

7.2 High Purity Aluminium (Al 298) Fixed Point

The experimental process of high purity Al 298 fixed-point cell is summarised in terms of a "Family tree" as presented in Figure 7.16. But note that the measurements were done consecutively (not in parallel).

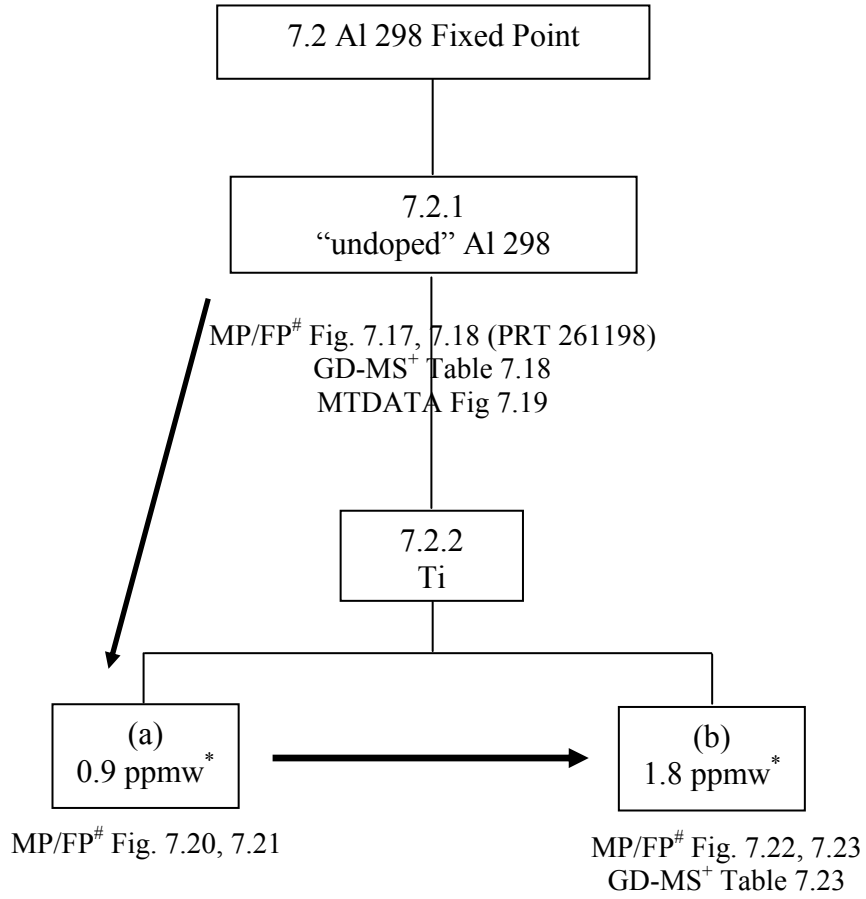

FP/MP = Freezing and Melting curves conducted in this stage.

+ GD-MS = Glow discharge mass spectrometry analysis performed in this stage.

* ppmw = Parts per million by weight (nominal doping amounts)

Figure 7.16 "Family Tree" showing the section number, figure numbers of the freezing/ melting curves and the table number of the results from the chemical analysis technique of Al 298 fixed point obtained for a particular combination of conditions. The arrows show the order of experiments.

7.2.1 Temperature Realisation of "Undoped" Aluminium (Al 298)

A long-stem platinum resistance thermometer (PRT serial number 261198) was selected for measurements in this aluminium (Al 298) fixed-point cell. To check the repeatability of the fixed-point curve, melting, and freezing curves of this aluminium cell have been recorded three times.

Examples of Al 298 melting curves, before doping, are shown in Figure 7.17. A set of three freezing curves of the "Al 298" aluminium fixed-point cell, before the doping process, is shown in Figure 7.18. All freezing measurements were determined at the same furnace setting. The resistance values on the y-axis for all figures do not include the hydrostatic head value of this Al 298 cell.

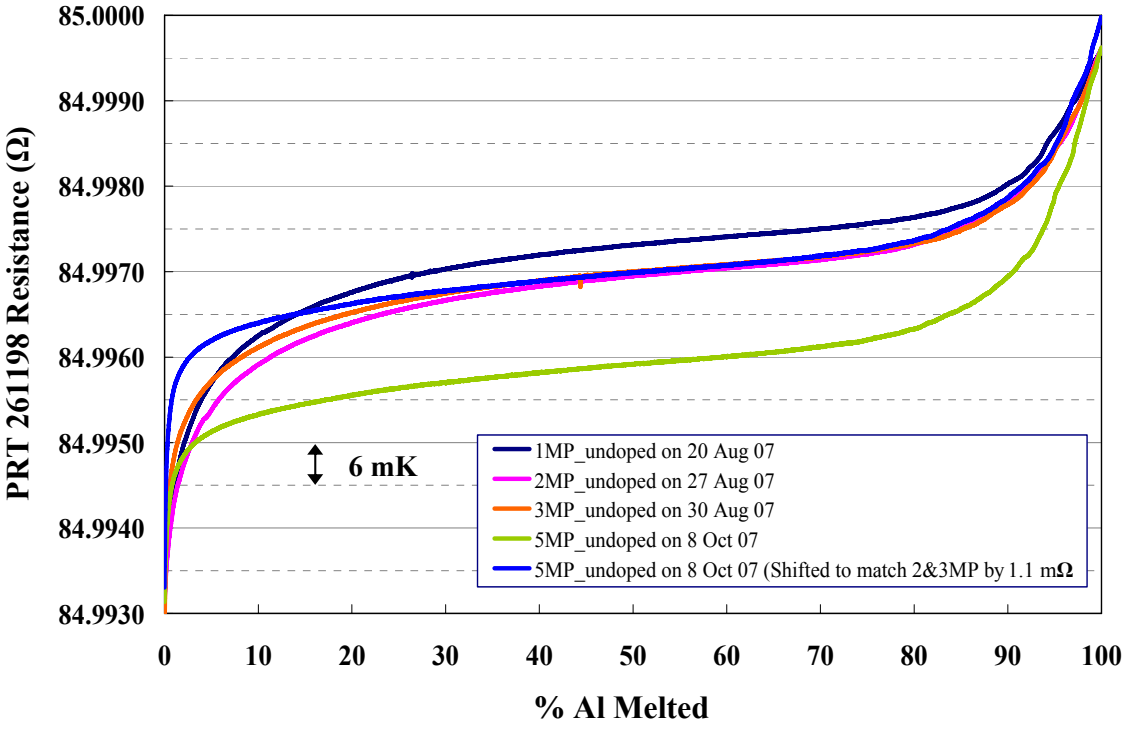

Figure 7.17 Melting curves of high purity undoped "Al 298" aluminium fixed-point plotted as a function of aluminium percentage melted. The curves have been normalised to an approximate percentage melted. The furnace was set at the same temperature of 660.5 ^{o}C for all measurements. PRT 261198 was used to measure in this cell. The blue line is the green line shifted by 1.1 x 12.5 "mK", to match with the pink and orange lines, which corrects a shift in the PRT that occurred during the time gap in the measurements by the PRT (Aug to Oct 07).

Four melting curves indicate the instability of PRT 261198. All melting curves obtained after a rapid freeze are shown in Figure 7.17. The second and the third lines confirm the reproducibility of the temperature measurements in this fixed-point cell. This is because they were measured at times close to each other. The green line of the melting curve was measured just before adding the titanium impurity into the Al 298 ingot for checking the stability of this PRT. It shows that the PRT had moved down from the previous point. From the melting curves, the shift of the curve is around 1.1 mΩ, which is equivalent 13.8 mK.

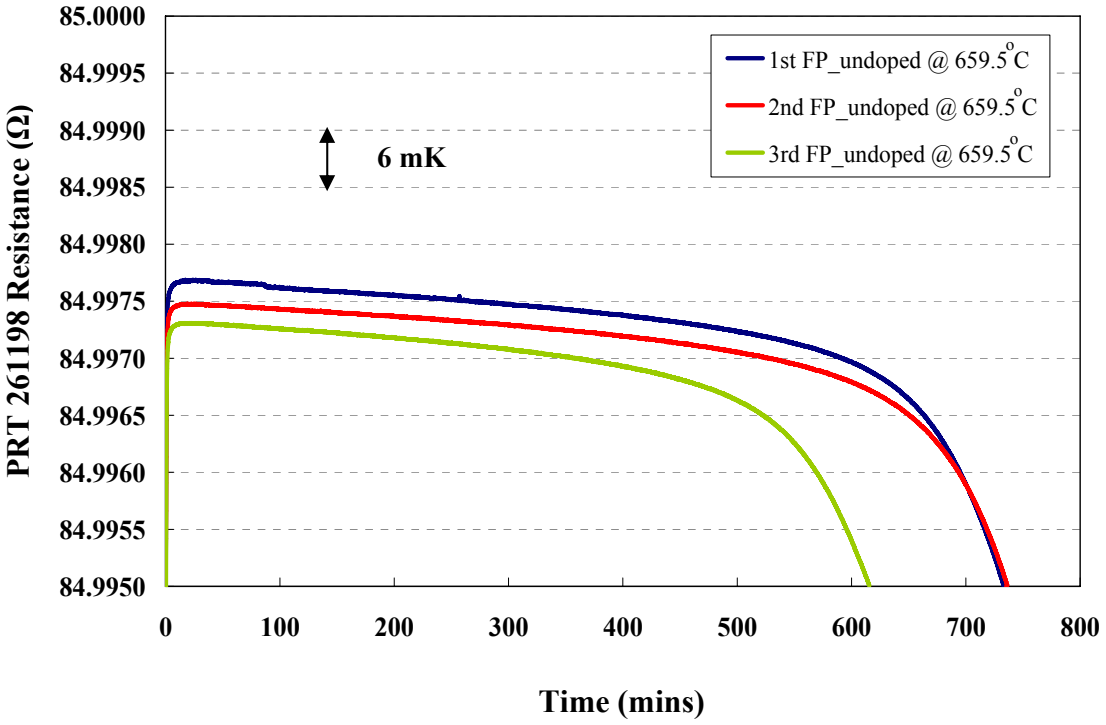

Figure 7.18 Three freezing curves of high purity undoped "Al 298" aluminium fixed-point plotted as a function of time. The furnace set point for all three measurements is set at the same temperature (nominally half a degree below the freezing point).

Figure 7.18 shows the shift of the freezing curves on the undoped Al 298 fixed point due to the instability of the PRT 261198. They were measured on 21st, 22nd and 24th of August 2007, respectively. We can see the shifts of these freeze peaks due to the instability of the PRT.

The Hart furnace was always set at 659.5 ^{o}C, which gave the freezing curves a period of about 12 hours. When the Hart furnace was changed to 659.2 ^{o}C, the length of the freezing curve reduced to 8 hours. This shows more reproducibility than the Carbolite furnace. (The former uses a PRT rather than a thermocouple for its control sensor).

Table 7.16 Resistance values measured at the freezing point of high purity "undoped" Al 298 aluminium fixed-point cell. These values were calculated from the resistance ratio of PRT 261198 and the standard resistor values. Also, the resistance values include the correction of the hydrostatic head of this cell. The temperature setting of the furnace was maintained at 659.5 ^{o}C. The resistance values are measured at the peak of the freeze.

Resistance values at freezing point of Al(298)	**Date**	**Platinum Resistance Thermometer (PRT) (Serial Number)**
R_T (*i*) / Ω	-	**261198 (1 mA)**
R_T (*1*)	21/08/07	84.997663
R_T (*2*)	22/08/07	84.997455
R_T (*3*)	25/08/07	84.997288
R_T (*4*)	29/08/07	84.997215
R_T (*5*)	31/08/07	84.997200
R_T (*6*)	19/09/07	84.995954
R_T (*7*)	02/10/07	84.996017
Standard deviation (2s)	-	**± 1.38 mΩ**

i represent the order of the resistance measurements of the PRTs at the freezing point of Al 298.

The first three resistance values were taken from the peak of each freezing curve from Figure 7.18. These values in Table 7.16 have been corrected with the hydrostatic head of this aluminium cell. The standard deviation (2s) for all measurements was 1.38 mΩ. The results show that the freeze peak of the curves decreased a total around 19 mK. Such a big change is due to the shift of this PRT over the period of time. The resistance values at the freezing point of Al 298, listed as the 6th and 7th result in Table 7.16, were obtained from the freeze peak of the comparisons with Al 174 cell (as presented in Table 7.18 and 7. 3, respectively) and these have

sharply dropped from the previous values. Therefore, each initial freezing curve shown in Figure 7.18 would be corrected with the shift value, before it would be used to compare with Ti doped Al in the next section.

Table 7.17 Measurement of the Stability of the PRT 261198 measured from the resistance values at the triple point of water. These values were checked before using the PRT in the comparison measurements at the freezing curves of aluminium fixed point between high purity "undoped" Al 298 and reference Al 1205 cells.

Resistance values at triple point of water/Ω	**Date**	**Platinum Resistance Thermometer (PRT)**
Cycle number and differences	**-**	**261198 (0 mA)**
R_{TPW} (*1*)	27/08/07	25.183233
R_{TPW} (*2*)	29/08/07	25.183173
R_{TPW} *(3)*	31/08/07	25.183124
Standard deviation (2s)	-	**± 0.1 mΩ**

Table 7.18 Summary of the average resistance values (R_{Al}) in the comparison measurements at the peak freezing curves of aluminium fixed point between Al 298 and reference Al 1205 cells with two PRTs (serial number 250329 and 261198).

PRTs serial number	**Date**	**$R_{Al\ 298}$ (Ω) (1 mA)**	**$R_{Al\ 1205}$ (Ω) (1 mA)**	**Temperature difference between Al 298 and Al 1205 cells** $[\Delta T = 12.5 * \Delta R\ ]^{+}$ [Rusby,2008]	**R_{TPW} (Ω) (1 mA)**
250329 I	18/09/07	84.093220	84.093960	-9.25 mK	24.915368
250329 II	20/09/07	84.092953	84.093870	- 11.46 mK	24.915332
261198 I	19/09/07	84.995954	84.997009	- 13.18 mK	25.183060
Overall Mean	-	-	-	- 11.30 mK	-
∴ Standard deviation (2s) = ± 3.94 mK					
∴ Temperature difference between Al 298 and reference Al 1205 cells - 11.30 mK					

+12.5 (mK/mΩ) is the appropriate conversion factor for the sensitivity of $R(T_{90})$ at Al fixed-point temperature [Rusby, 2008].

Table 7.18 indicates the average resistance values at the aluminium freezing curve peaks for comparison between Al 298 and reference Al 1205 cells. It shows the resistance values of the freezing point of Al and the triple point of water after calibration. The temperature difference illustrates that the temperature at Al 298 is less than reference Al 1205 by 11.30 ± 3.94 mK. All results in Table 7.18 are corrected for the hydrostatic head pressure in both Al cells. For high purity Al 298 and reference Al 1205 fixed-point cells, the hydrostatic head correction values are calculated at about -0.195 mK and -0.184 mK, respectively.

The shape of the Al 298 curve (prior to doping) is not flat and decreases noticeably during the freeze, when compared with the reference Al cell. Moreover, the freeze peak of the Al 298, compared with the resistance values of the reference Al cell plateau, are much lower; therefore this Al ingot contained some initial impurities affecting its freezing and melting temperatures.

For ideal pure aluminium fixed point, a purer metal usually shows a flatter plateau on the freezing and melting curves. The presence of initial impurities can be shown from the GD-MS analysis to find the quantity and distribution (or uniformity) of the impurity elements within the "undoped" Al 298 cell, before deliberate doping.

7.2.1.1 Impurity Analysis of High Purity Aluminium (Al 298) Fixed Point before Doping

Glow Discharge Mass Spectrometry (GD-MS) Characteristics

The results of the impurity determination for the "high purity" aluminium (Al 298) fixed point by GD-MS analysis is reported in Table 7.19. This shows the impurity content measured in three areas of the aluminium ingot. From the results we see that the impurity levels are the same throughout the cell (within the uncertainty quoted). This shows that the aluminium is sufficiently well mixed and that only one sample will need to be cut out for analysis after doping. (Cutting out of samples is a risky procedure).

Table 7.19 An example of the GD-MS analysis results of the initial "high purity" (6N) aluminium fixed point (Al 298) (NRC report number: Al30337R1), detected on 14/12/07. The elements were detected in term of mass fraction (in parts per million by weight, ppmw). The uncertainty is quoted as a "factor of 2", though this is probably a conservative overestimate.

Element	Top	Middle	Bottom	Element	Top	Middle	Bottom
Li	<0.003	<0.003	<0.003	**Br**	<0.02	<0.01	<0.02
Be	<0.001	<0.001	<0.001	**Rb**	<0.001	<0.002	<0.002
B	<0.002	0.01	0.005	**Sr**	<0.001	<0.001	<0.001
C	2	4	6	**Y**	<0.001	<0.001	<0.001
N	0.2	0.2	1	**Zr**	0.02	0.02	0.03
O	5	6	80	**Nb**	<0.001	<0.001	<0.001
F	<0.01	<0.02	<0.01	**Mo**	<0.003	<0.003	<0.003
Na	<0.002	<0.002	0.006	**Pd**	-	-	-
Mg	0.09	0.07	0.1	**Ag**	0.03	0.03	0.04
Al	Matrix	Matrix	Matrix	**Cd**	<0.02	<0.02	<0.02
Si	0.7	0.6	0.8	**In**	<0.003	<0.003	<0.003
P	<0.002	<0.003	<0.002	**Sn**	<0.03	<0.03	<0.03
S	<0.003	0.009	0.02	**Sb**	<0.007	<0.007	<0.007
Cl	0.04	0.004	0.1	**Te**	<0.008	<0.008	<0.008
K	<0.02	<0.02	<0.02	**I**	<0.003	<0.003	<0.003
Ca	<0.03	<0.04	0.1	**Cs**	<0.001	<0.001	<0.001
Sc	0.08	0.06	0.07	**Ba**	<0.001	<0.001	<0.002
Ti	0.1	0.2	0.3	**La**	<0.001	<0.0005	<0.0008
V	0.05	0.07	0.1	**Ce**	<0.0004	<0.001	<0.0008
Cr	0.1	0.1	0.1	**Hf**	<0.003	<0.003	<0.003
Mn	0.1	0.1	0.1	**Ta**	-	-	-
Fe	0.1	0.1	0.1	**W**	0.04	0.04	0.05
Co	<0.0007	<0.0008	<0.0007	**Pt**	<0.01	<0.01	<0.01
Ni	<0.005	<0.005	<0.004	**Au**	<0.2	<0.2	<0.2
Cu	0.09	0.06	0.07	**Hg**	<0.03	<0.03	<0.03
Zn	0.07	0.07	0.1	**Tl**	<0.008	<0.008	<0.008
Ga	<0.006	<0.007	<0.006	**Pb**	<0.003	<0.003	<0.003
Ge	<0.01	<0.01	<0.01	**Bi**	<0.004	<0.004	<0.004
As	<0.004	<0.004	<0.004	**Th**	<0.001	<0.001	<0.001
Se	<0.05	<0.05	<0.05	**U**	<0.001	<0.001	<0.001

7.2.1.2 MTDATA Analysis

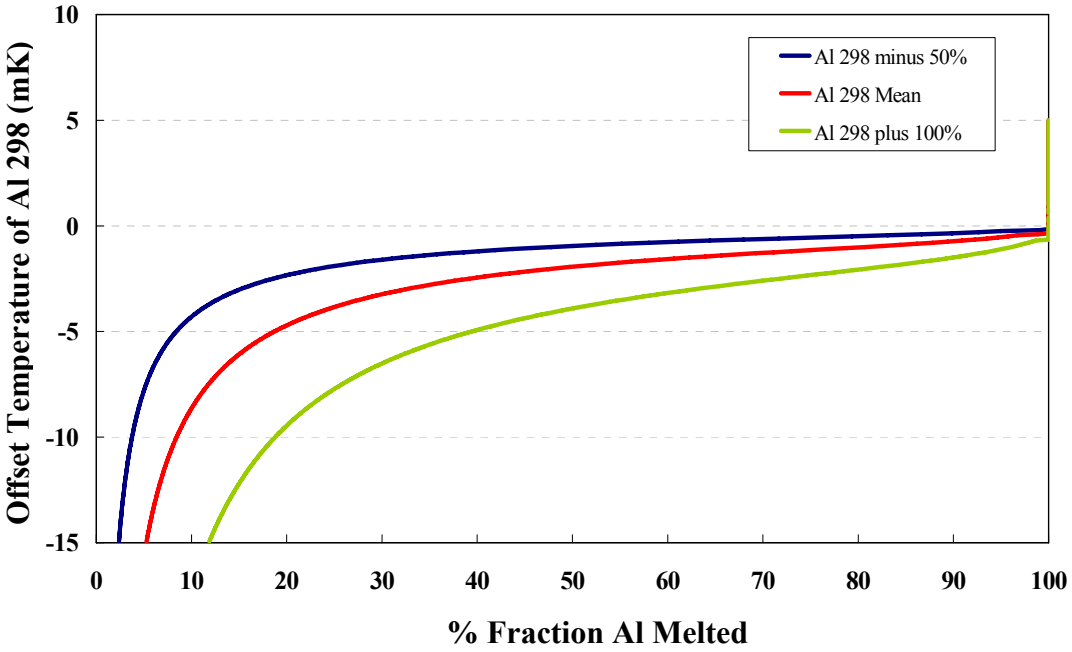

Figure 7.19 Melting curves of pure Al 298 fixed point obtained from MTDATA calculation analysis. The red line shows the curve calculated using the GD-MS result (impurity effect on the curve), the blue and the green lines show the calculated bounds (based on the quoted uncertainty of the GD-MS analysis i.e. factor of 2 which translates to –50% and +100% of reported value)

The melting of the initial undoped Al 298 curve compared to MTDATA experiments show much more rounding, which are not agreement very well with MTDATA analysis. Further the decrease in liquidus temperature seems very small compared to that measured when comparing with the reference cell. See comment above at section 7.1.1.2.

MTDATA of reference Al 1205 cell

NPL reports that the aluminium “shot” used in the manufacture of Al 1205 came from a batch used for another NPL cell and another made at Isotech. The shot had been sent by Isotech to NRC for GD-MS analysis, a copy of which was kindly supplied to NPL. This analysis was used to perform an MTDATA calculation. However initial calculations suggested a much larger temperature depression than was experimentally found. It has been postulated that the (relatively) large amount of

nitrogen found in the shot sample did not actually remain in the actual ingot – or that it was not chemically active – and consequently the MTDATA calculation gives abnormally high depressions for the pure cell. The MTDATA staff confirmed that there had been no accidental switching of data, and that a visual inspection of the GD-MS results would suggest that the shot was worse than the Al 174 and Al 298 samples, though in fact the ingot made from that shot related well to other standard ingots.

7.2.2 Influence of Titanium on High Purity Aluminium (298) Fixed Point

7.2.2.1 Al 298 doped with 0.9 ppmw of Titanium

Before the melting and the freezing curves of Al 298 after doping titanium were displayed, the instability of the PRT 261198 was checked by measurement in the reference Al 1205 cell as shown in Table 7.20.

Table 7.20 Stability of the PRT 261198, which was checked in the peak of the reference Al cell (Al 1205) at 1 mA.

Checking Time	**Date**	**Resistance Values (R_T, Ω)**	**Average R_T Values (Ω)**
Checked when Al 1205 Compared with undoped Al 298	18/09/07	84.997009	84.996905
	18/01/08	84.996800	
Checked when Al 1205 Compared with Al 298 doped Ti 0.9 ppmw	12/02/08	84.996536	84.996466
	27/02/08	84.996396	
The shift of PRT 261198 during the calibration = - 0.44 m **Ω**			

In Table 7.20, the shift of PRT 261198 during the thermal cycling checked against the reference Al cell decreased by 0.44 mΩ. It is equivalent to 5.5 mK approximately. Therefore, the resistance values would be added with this numerical shift for the freezing and melting curves of Al 298 fixed point after doping with titanium 0.9 ppmw.

A set of melting curves of Al 298 after doping with titanium at 0.9 ppmw is presented in Figure 7.20. All freezing curves are presented in Figure 7.21.

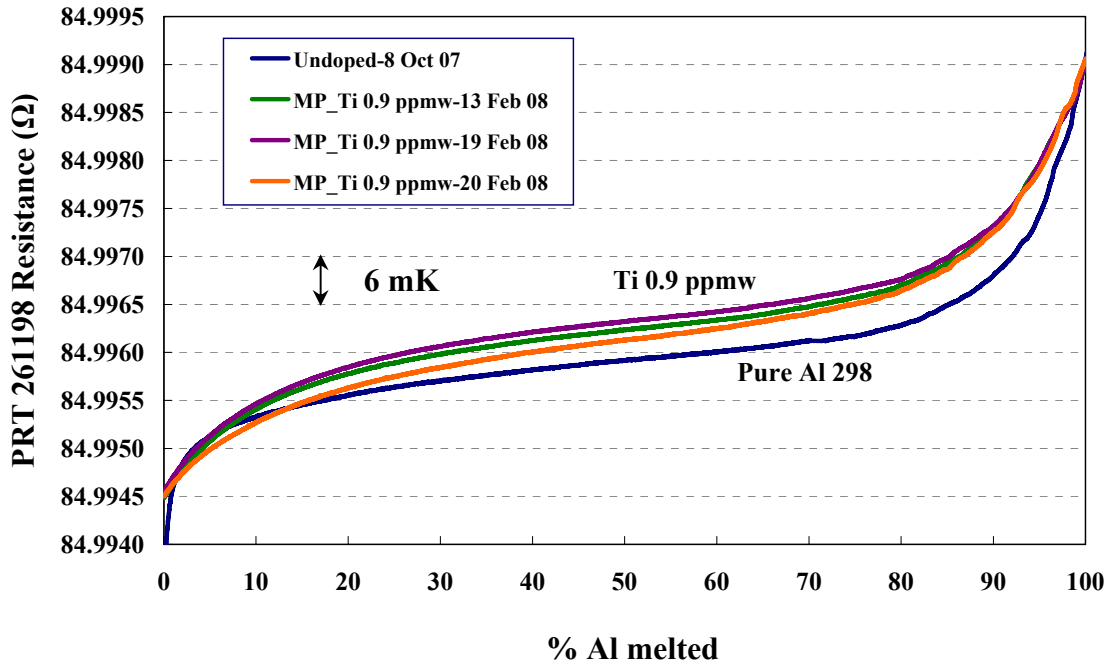

Figure 7.20 PRT resistance value at the melting temperature for "Al 298" after doping with 0.9 ppmw of titanium as a function of the approximate percentage melted. All curves were melted at different temperature settings. (All temperatures are nominal settings of the controller).

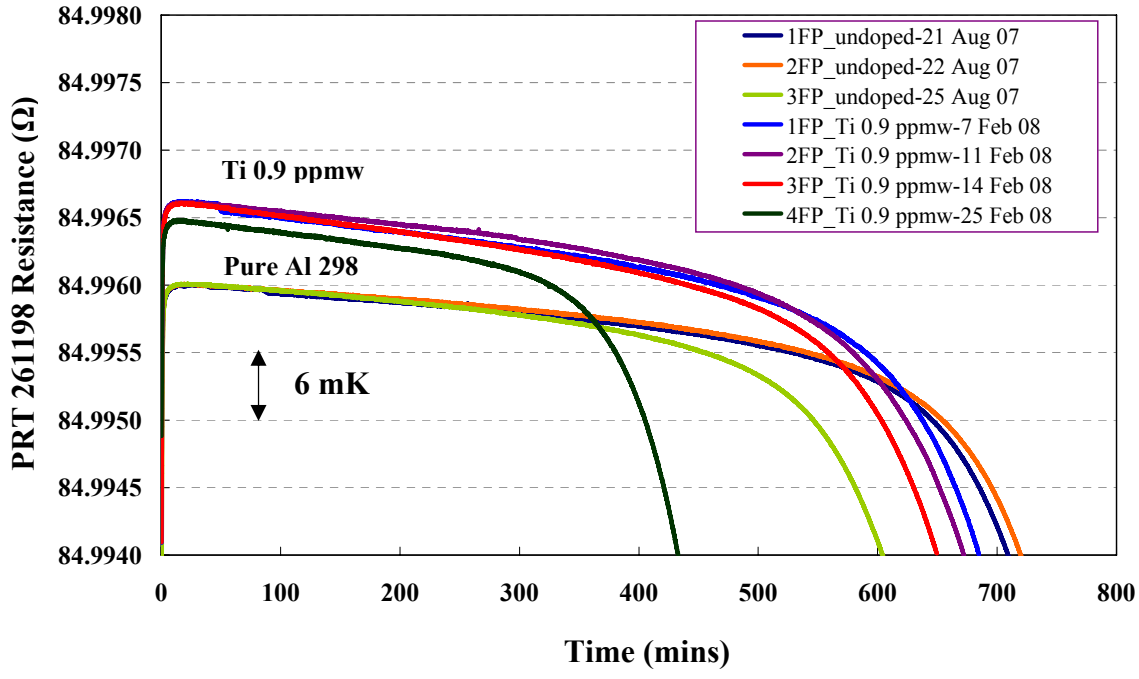

Figure 7.21 Three freezing curves of high purity undoped "Al 298" aluminium fixed-point the shift of these curves after doping with increasing concentrations of titanium, plotted as a function of time. The furnace setting point for all three measurements is set at the same temperature (nominally half a degree below the freezing point).

In Figure 7.20, the resistance values of melting temperature were increased after adding with Ti 0.9 ppmw. Figure 7.21 shows the Ti effect on aluminium fixed-point temperature. The temperatures at the freeze peak of Al 298 after adding 0.9 ppmw of Ti were elevated. The increased amount would be confirmed by the comparison with the reference Al cell, which will be discussed in Table 7.21. (The values of the undoped freezing curves in Figure 7.2 have been reduced (shifted down) to take account of the PRT shift.) The correction was obtained by measuring the shift shown by the thermometer in the undoped melting curves (see Figure 7.17) and the shift shown from the measurements in the reference cell. (The initial undoped freezing curves are presented in Figure 7.18.)

For this Al-Ti system, the sample with titanium at 0.9 ppmw presents an increase of the freeze peak. It is about 4.63 ± 5.45 mK higher than the undoped aluminium Al 298. The temperature change of the freezing and melting curves of the aluminium fixed-point obtained from this experiment was affected by the amount of titanium (+5.14 mK/ppmw). The results of this work confirmed the influence of very low-level impurities on the freezing/melting curves of the aluminium (Al 298) fixed point.

Table 7.21 Summary of the average resistance values (R_{Al}) in the comparison measurements at the peak freezing curves of aluminium fixed point between Al 298 after doping silicon at 0.9 ppmw and reference (Al 1205) cells with two PRTs (serial number 250329 and 261198).

PRTs serial number	**Date**	**R_T Al 298 doped Ti 0.9 ppmw (1 mA)**	**R_T NPL standard Al 1205 (1 mA)**	**Equivalent Temperature difference between Al 298 doped Ti 0.9 ppmw and Al 1205 cells** $[\Delta T = 12.5 * \Delta R_T]^+$ [Rusby, 2008]
261198	18/01/08*	-	(84.996830)	-
261198	07/02/08	84.996190	-	- 4.33 mK
261198	11/02/08	84.996135	-	- 5.01 mK
261198	12/02/08	-	84.996536	-
261198	25/02/08	84.995818	-	-
261198	27/02/08	-	84.996391	-
Average	-	-	84.996464	- 8.07 mK
261198	28/02/08	84.995743	-	-
261198	06/03/08	-	84.996285	-
Average	-	-	84.996338	- 7.44 mK
250329	18/01/08	-	84.093791	-
250329	05/02/08	84.093111	-	-8.50 mK
Overall Mean	-			**- 6.67 mK**
∴ Standard deviation (2s) = ± 3.76 mK				
∴ Mean of Temperature difference Al 298 doped Ti 0.9 ppmw – NPL standard fixed-point = - 6.67 mK				
∴ Mean of Temperature difference between Al 298 doped Ti 0.9 ppmw - undoped Al 298 = (-6.67) - (-11.30) = + 4.63 mK				
∴ Standard deviation (2s) Difference: Temperature difference between Al 298 doped Ti 0.9 ppmw - undoped Al 298 (by quadrature addition) ± 5.45 mK				

*shows an exceptional number result, which cannot be used to compare with other numbers. The colour presents the matching values used to calculate the temperature difference between Al 298 doped Ti 0.9 ppmw and Al 1205 cells. +12.5 (mK/mΩ) is the appropriate conversion factor for the sensitivity of $R(T_{90})$ at Al fixed-point temperature [Rusby, 2008].

7.2.2.2 Al 298 doped with 1.8 ppmw of Titanium

Considering the instability of the PRT 261198, this PRT was calibrated to check its resistance values in the reference Al cell as shown in Table 7.22.

Table 7.22 Stability of the PRT 261198, which was checked in the peak of the reference Al cell (Al 1205) at 1 mA.

Checking Time	Date	Resistance Values (R_T, Ω)	Average R_T Values (Ω)
Checked when Al 1205 Compared with Al 298 doped Ti 0.9 ppmw	12/02/08	84.996536	84.996405
	27/02/08	84.996396	
	06/03/08	84.996283	
Checked when Al 1205 Compared with Al 298 doped Ti 1.8 ppmw	07/03/08	84.996290	84.9960795
	20/03/08	84.996000	
	25/03/08	84.996048	
	01/04/08	84.995980	
The shift of PRT 261198 during the calibration = - 0.33 m Ω			

In Table 7.22, the shift of PRT 261198 during the thermal cycling checked against the reference Al cell decreased by 0.33 mΩ. It is equivalent to 4.13 mK approximately. A set of melting curves of Al 298 after doping with titanium at 1.8 ppmw is presented in Figure 7.22. All freezing curves are presented in Figure 7.23.

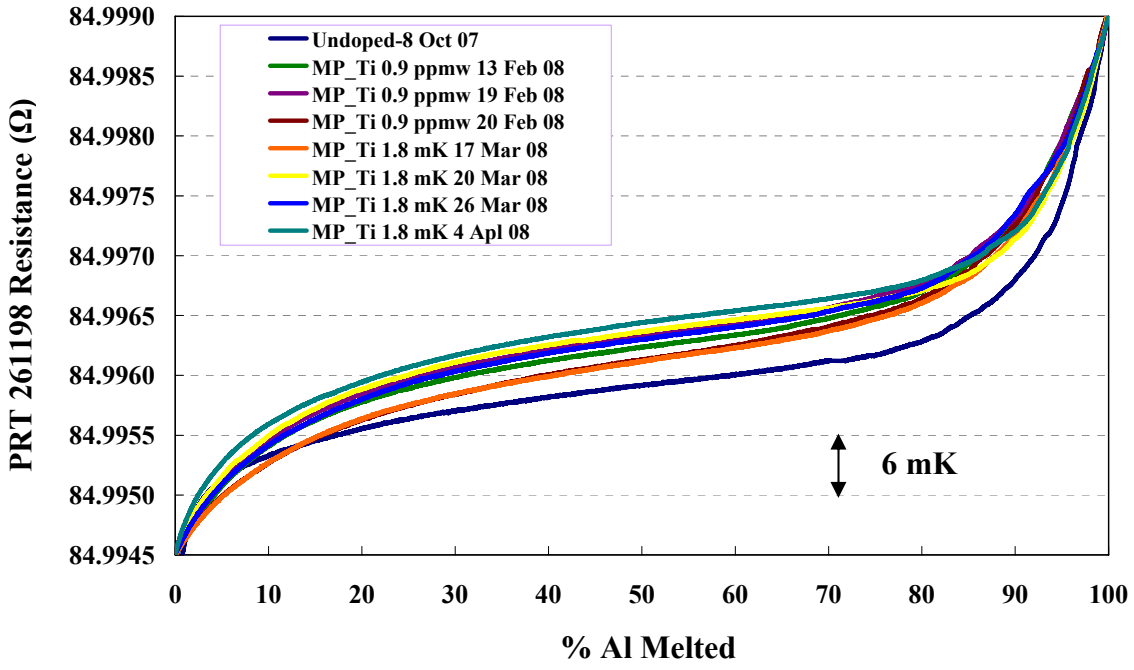

Figure 7.22 PRT resistance value at the melting temperature for "Al 298" after doping with increasing titanium impurity as a function of the approximate aluminium percentage melted. All curves were melted at different temperature settings. (All temperatures are nominal settings of the controller).

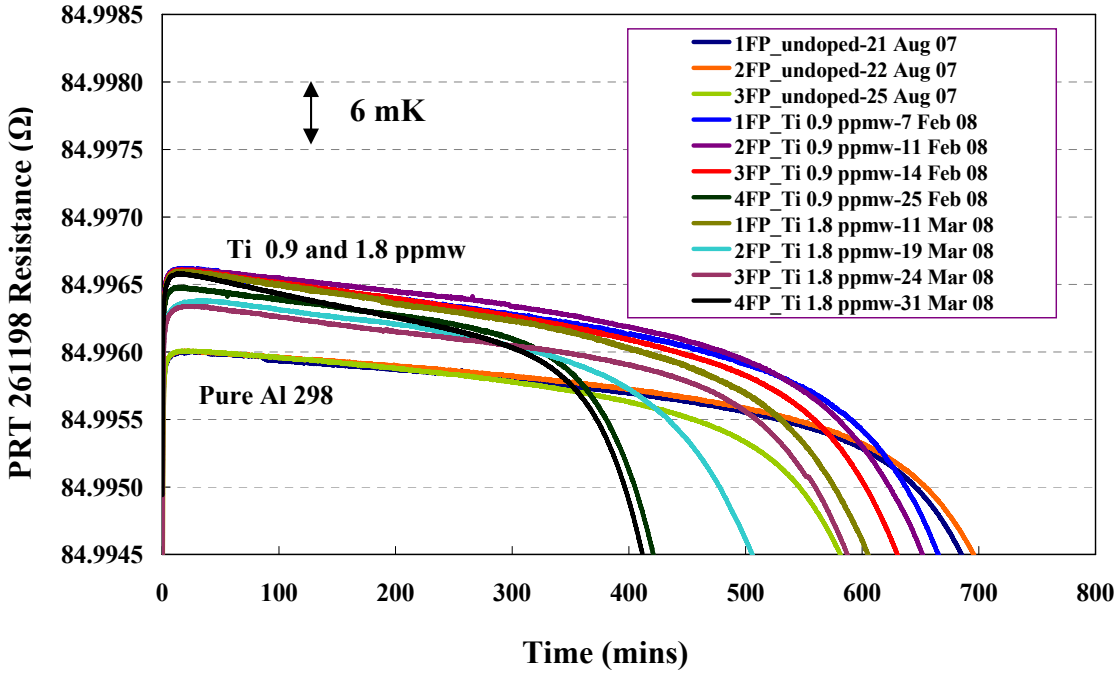

Figure 7.23 Three freezing curves of high purity undoped "Al 298" aluminium fixed-point showing the shift of these curves after doping with increasing concentrations of titanium, plotted as a function of time. The furnace set point for all three measurements is set at the same temperature (nominally half a degree below the freezing point).

The melting and freezing curves as shown in Figure 7.22 and 7.23 indicate that the temperatures were increased by adding the Ti 0.9 ppmw while the unchanged temperatures occurred after doping 1.8 ppmw of Ti are unexpected. However, the instability of the PRT on cycling appears on the curves. The offsets of the melting curves need to be corrected following "re-calibration" of the PRTs by comparison of the peak of the freezing curves against the reference Al cell. Therefore, it is summarised that the titanium impurity increases the Al 298 temperature by +5.14 mK/ppmw (based on the 1st measurement).

From the freeze peak comparison as shown in Table 7.22, it found that the temperature difference between Al 298 doped Ti 1.8 ppmw and "undoped" Al 298 measured at the freeze peak is 4.68 ± 4.30 mK. The additional concentration of Ti added at 1.8 ppmw had no effect on the melting and the freezing Al 298 temperatures when compared with the freeze peak value at Ti 0.9 ppmw, which is 4.63 ± 5.45 mK higher than the undoped as shown in Table 7.21.

Table 7.23 Summary of the average resistance values (R_{Al}) in the comparison measurements at the peak freezing curves of aluminium fixed point between Al 298 after doping with titanium at 1.8 ppmw and National standard (Al 1205) cells with two PRTs (serial number 250329 and 261198). All results are corrected for the hydrostatic head pressure from both Al cells.

PRTs serial number	**Date**	**R_T Al 298 doped Ti 1.8 ppmw (1 mA)**	**R_T NPL standard Al 1205 (1 mA)**	**Equivalent Temperature difference between Al 298 doped Ti 1.8 ppmw and Al 1205 cells** $[\Delta T = 12.5 * \Delta R_T]^+$ [Rusby, 2008]
261198	06/03/08	-	84.996285	-
261198	11/03/08	84.995786	-	- 6.24 mK
261198	19/03/08	84.995479	-	- 6.51 mK
261198	20/03/08	-	84.996000	-
261198	25/03/08	84.995425	84.996048	- 7.79 mK
261198	31/03/08	84.995541	-	- 5.49 mK
261198	01/04/08	-	84.995980	-
250329	04/03/08	84.093176	-	-7.05 mK
250329	05/03/08	-	84.093740	-
Overall Mean	-	-	-	**- 6.62 mK**
∴ Standard deviation (2s) = ± 1.73 mK				
∴ Mean of Temperature difference Al 298 doped Ti 1.8 ppmw – NPL standard fixed-point = - 6.62 mK				
∴ Mean of Temperature difference between Al 298 doped Ti 1.8 ppmw - "undoped" Al 298 = (-6.62) - (-11.30) = + 4.68 mK				
∴ Standard deviation (2s) Difference -Temperature difference between Al 298 doped Ti 1.8 ppmw - undoped Al 298 (by quadrature addition) ± 4.30 mK				

+12.5 (mK/mΩ) is the appropriate conversion factor for the sensitivity of $R(T_{90})$ at Al fixed-point temperature [Rusby, 2008].

7.2.3 Impurity Analysis of High Purity Aluminium (298) after Doping with Titanium

Glow Discharge Mass Spectrometry (GD-MS) Characteristics after Doping with Titanium

Table 7.24 lists the impurity elements detected in the Al 298 metal ingot. The uncertainty of this GD-MS analysis is considered to be accurate within a factor of two of the values obtained, at a confidence level of 95% though there is anecdotal evidence that the results are more accurate than quoted.

Considering the GD-MS measurement in the Al 298 ingot, which is the same method as the Al 174 ingot, four samples were also cut from the Al 298 before deliberate doping; three samples from three areas were tested soon after while the other one was tested a ~year later at the same time as the doped sample. Four similar samples were tested by GD-MS at different times, i.e. the first three undoped sample were checked a year ago, while the other undoped sample was detected as the same time as the doping sample.

C, N and O show large amounts when compared with other background impurities even though GDMS, which is not expected to be so accurate with these elements. Also, the date of measurement of the GD-MS technique indicates that it affects the detected amounts of the impurities in this metal ingot, e.g. Na, Zr, and Ag. These results can show some evidence of the uncertainty of the GD-MS technique.

Considering Titanium (Ti) impurity in Table 7.24, the amounts of Ti concentration of Al 298 ingot before doping when were checked at different times shows the slightly changed amount of Ti from 0.2 to 0.26 ppmw. After Al 298 adding with Ti 1.8 ppmw, the amount of Ti shows 1.6 ppmw. That means the increased total amount of Ti impurity is about 1.4 ppmw from the “pure” Al 298.

Table 7.24 GD-MS analysis results of the impurity concentrations of the Al 298 before and after doping [NRC report number: Al30337R1 (checked on 14/12/07) & Al30817 (checked on 22/08/08)]. These elements were detected in term of mass fraction (in parts per million by weight, ppmw). The uncertainty is quoted as a "factor of 2", though this is probably a conservative overestimate.

Element	Al 298 Before Doping (Average from three areas)	Al 298 Before doping (Kept a year until time of doped analysis)	Al 298 After Doping	Element	Al 298 Before Doping (Average from three areas)	Al 298 Before doping (Kept a year until time of doped analysis)	Al 298 After Doping
	ppmw				ppmw		
Li	<0.003	<0.001	< 0.002	**Br**	<0.02	<0.035	<0.05
Be	<0.001	<0.0005	<0.0008	**Rb**	<0.002	<0.0008	<0.001
B	<0.006	0.016	<0.001	**Sr**	<0.001	<0.0004	<0.002
C	4	50	50	**Y**	<0.001	<0.0006	<0.0007
N	0.47	1.4	1.7	**Zr**	0.02	0.038	0.037
O	30	130	220	**Nb**	<0.001	<0.0005	<0.001
F	<0.01	<0.007	<0.045	**Mo**	<0.003	<0.001	<0.002
Na	0.003	0.012	0.015	**Pd**	-	-	-
Mg	0.09	0.12	0.078	**Ag**	0.03	0.044	0.04
Al	Matrix	Matrix	Matrix	**Cd**	<0.02	<0.007	<0.012
Si	0.7	1.1	0.9	**In**	<0.003	<0.001	<0.002
P	<0.002	<0.002	0.004	**Sn**	<0.03	<0.012	<0.02
S	0.01	0.11	0.007	**Sb**	<0.007	<0.003	<0.005
Cl	0.04	0.32	<0.006	**Te**	<0.008	<0.003	<0.005
K	<0.02	<0.07	<0.065	**I**	<0.003	<0.001	<0.002
Ca	0.06	0.24	0.056	**Cs**	<0.001	<0.0005	<0.0007
Sc	0.07	0.073	0.067	**Ba**	<0.001	<0.0005	<0.0009
Ti	**0.2**	**0.26**	**1.6**	**La**	<0.0008	<0.0005	<0.0006
V	0.07	0.1	0.11	**Ce**	<0.0007	<0.0003	<0.0006
Cr	0.1	0.11	0.13	**Hf**	<0.003	<0.002	<0.003
Mn	0.1	0.09	0.08	**Ta**	-	-	-
Fe	0.1	0.34	0.2	**W**	0.04	0.04	0.05
Co	<0.0007	<0.0005	<0.0005	**Pt**	<0.01	<0.005	<0.008
Ni	<0.005	<0.002	<0.003	**Au**	<0.2	<1.3	1.8
Cu	0.07	0.085	0.23	**Hg**	<0.03	<0.015	<0.025
Zn	0.08	0.076	0.12	**Tl**	<0.008	<0.003	<0.006
Ga	0.006	<0.004	<0.006	**Pb**	<0.003	<0.001	<0.002
Ge	<0.01	<0.012	<0.02	**Bi**	<0.004	<0.002	<0.003
As	<0.004	<0.003	<0.004	**Th**	<0.001	<0.0005	<0.0008
Se	<0.05	<0.035	<0.05	**U**	<0.001	<0.0005	<0.0008

From the phase diagram calculation [Hansen, 1958], the fixed-point temperature of aluminium was interpolated to be elevated by 3.31 mK/ppmw of titanium impurity. Therefore, at Ti 1.4 ppmw in Al 298 ingot would be increased the freezing and the melting temperatures to 4.63 mK. This is the same amount obtained from the experiment of comparison. There appears to be less Ti in the sample than what we put in, based or both the temperature shift and the GD-MS. Perhaps some of the Ti has not been absorbed into the sample, and perhaps the GD-MS correctly measures what is really in the sample – or are the results of the total shift and the GD-MS value an agreement by chance?.

7.2.4 Photograph of Al 298 Fixed-Point Cell

The picture of Al 298 ingot before doping has already shown across in chapter 5 in Figure 5.20. The surface colour looks shiny, it is similar to that of Al 174 see Figure 7.13 (though Al 174 may look “rougher”). Unfortunately, we do not have the picture of Al 298 ingot after doping with titanium impurity as it is still being used in the laboratory at the time of writing.

7.2.5 Additional Data on Titanium in Aluminium

Following completion of the main body of work, the aluminium cell doped with titanium was used in a separate study on the degree of electrical noise picked up by an ASL resistance measurement bridge measuring a PRT in a real ingot/furnace environment where the electrical power was derived from different sources e.g. mains or different “ups” (uninterruptible power supplies – i.e. battery powered).

During these measurements (which were for noise detection only) it was noticed that an interesting shape could be seen on some of the freeze traces. As these measurements were for noise detection the aluminium was being slowly melted and slowly re-frozen without the usual intervening fast freeze and melt and often without a prolonged period at several degrees above the melting point (“over-melt”). It is therefore possible that some segregation was occurring that concentrated the effect of titanium on the cell trace. We are indebted to Dr Radka Veltcheva of the NPL Temperature Section for making her interesting results available to us. The comments on these remain our responsibility.

From the results of Veltcheva's work it would seem that the Ti in Al freezes show evidence of a "concave up" shape at the start of the freezing plateau following recallescence. This supports (at least the first part) of the theoretical curve calculated by MTDATA for Ti impurity in Aluminium [Head *et al*., 2008] but not seen in previous experiments made using adiabatic melting [Ancsin, 2003].

As an example of this recent measurement: Figure 7.24 shows the initial part of a 24 hour plateau trace that has evidence of a "concave up" shape, similarly to that calculated by MTDATA; see Figure 3.19. (Plateau traces on other occasions showed similar effects).

Figure 7.25 shows a longer trace with a concave up section but this was followed by a bump, which has not been predicted. It may be a sign of further impurity segregation. (Again there are measurements on other days that show a similar effect).The small oscillation at the end is probably due to the furnace oscillation. As the temperature drops further to that of the furnace the usual 30 mK oscillation in the control of this type of furnace would become visible, but this would be at a much lower temperature in order to provide the necessary offset to produce the freeze itself.

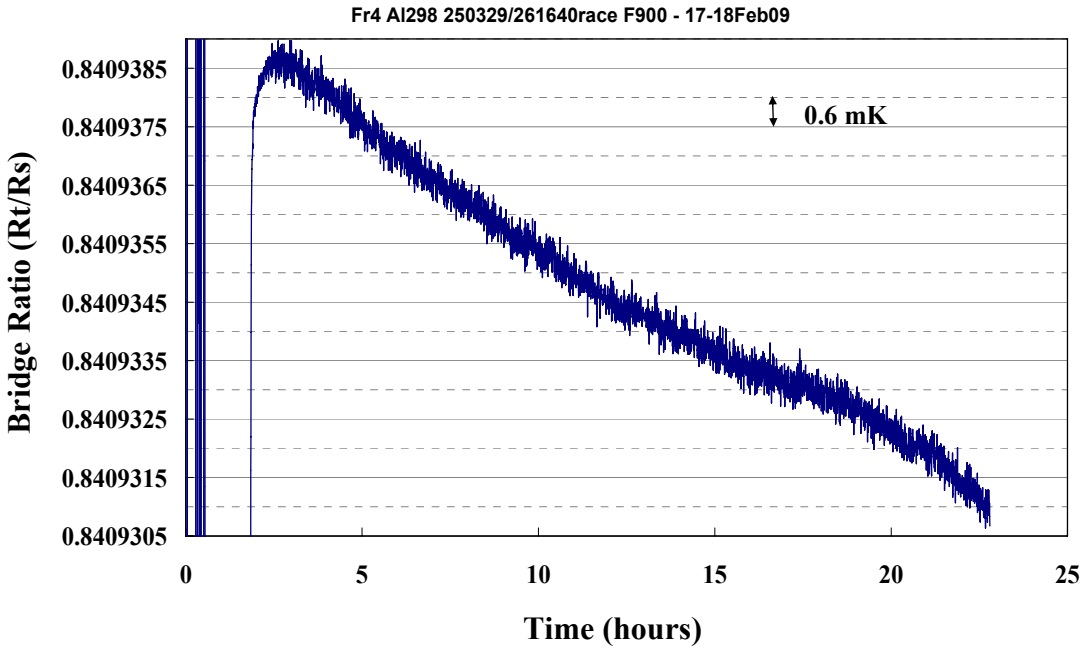

Figure 7.24 Example Freezing curve showing the initial concavity in the plateau, which lasted over 24 h.

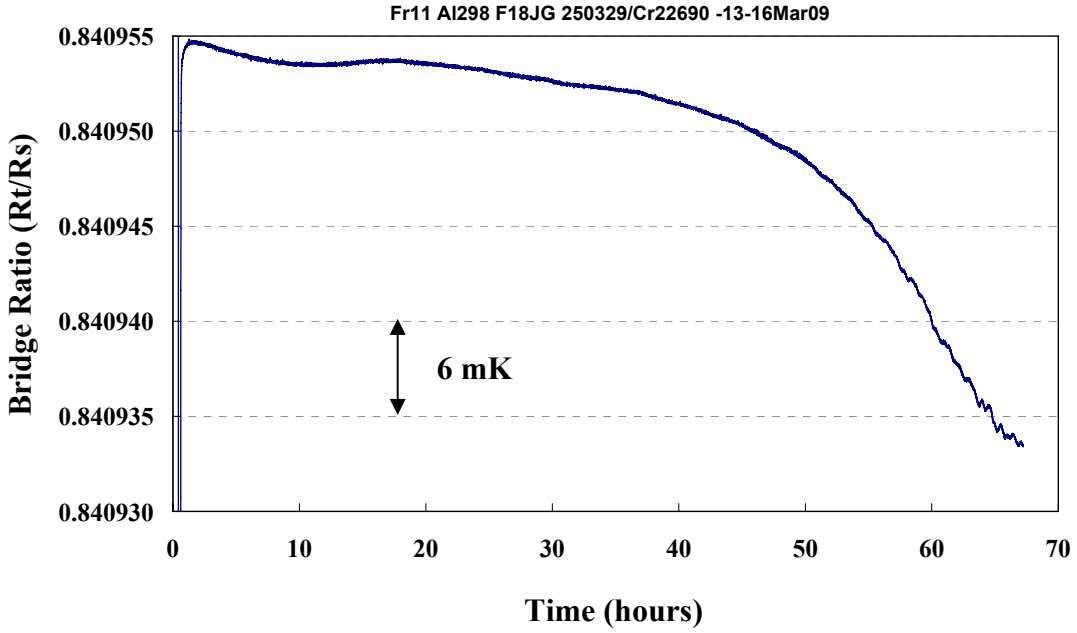

Figure 7.25 Example of a concavity at the start of a plateau followed by a "bump" and then a more normal freezing curve (See text re. little oscillations at end of trace).

Whether these results really do represent experimental evidence of what MTDATA calculated is of course debatable, but they do offer a tantalising piece of evidence. However it should be noted that abnormal conditions were necessary to show this. A closer look at the original curves shown in Chapter 7 of this thesis, and also those of the reference cell can show some repeatable concavity when the plateaus are extended to tens of hours, closer to the thermodynamic limit. (Ti is not the only positive impurity that can be detected in the reference cell – but these impurities are, of course, in low concentration).

(As an older furnace was used for these noise measurements (rather than the Hart furnace) therefore it is possible that weaker temperature control might cause some unwanted effects on the trace. However once the freeze was finished, prolonged temperature oscillations of amplitude 30 mK were seen – which is normal for this furnace. Further some of the more unusual plateau shapes have repeated on different days where the plateaux have lasted up to 60 h – the latter suggesting that the furnace is stable within its control oscillation, and therefore the effects are most likely to be real and due to the distribution of material within the ingot).

It is interesting to note that prolonged melts and freezes (without the intervening “over-melt” and fast freeze) have had interesting effects on both the positive impurities i.e. Sb in Sn and Ti in Al. However the manifestation has been quite different. For Sb in Sn the effects were seen in melts following long freezes; however for Ti in Al the effects seen (as long as they are real) are in FREEZES after multiple melt/freezes. (Nothing “unusual” was seen in Sn-Sb freezes or Al-Ti melts though the latter were very broad).

7.2.6 Mass of Aluminium (Al 298) Fixed-Point Ingot

The weight of the ingot was also calculated from the physical dimensions, which were measured from the real aluminium cell. The mass of Al 298 was estimated by two methods. Based on the dimensions of the Al 298 ingot and the graphite re-entrance well, the volume of the tin and the graphite was calculated. (Using standard densities this was converted to mass). As well as directly calculating the mass of aluminium, the calculated mass of graphite was subtracted from actually measured mass of graphite and aluminium together. (It is not possible to remove the graphite re-entrance-well as the tin clamps onto it during the freezing process.) This procedure was checked before the high purity Al 298 ingot was constructed in the new system and also was measured at the end of the experimental measurements.

Table 7.25 Mass of Al 298 fixed-point ingot as calculated based on a mass measurement (of the aluminium and central graphite) before doping the impurities.

Component(s) of Al 298 Cell	Mass (g)
Calculated Mass of Al 298 metal (Originally)	232.00
Measured Mass {Al 298 metal and graphite re-entrance well} (Originally) less the calculated mass of graphite	231.70
Measured Mass of Al 298 metal (Samples cut off) less the calculated mass of graphite	229.39

The measured mass of metal after cutting off the samples for the undoped GD-MS testing was used in calculation of the doping concentrations (in ppmw).

Chapter 8

Conclusions and Future Work

8.1 The Quantitative Effect of Low Level Impurities on Tin and Aluminium Temperatures

A summary of the influence of low level impurities on tin and aluminium fixed-point temperatures is shown in Table 8.1.

Table 8.1 The influence of low level impurities on tin and aluminium fixed points. The calculated deflections of impurity effect are based on Hansen's book [1958].

Fixed point doped with impurities	Total amount put in (ppmw)	Calculated deflection (mK)	GD-MS measurement (ppmw)	Calculated GD-MS deflection (mK)	Experimental deflection (mK)	Calculated impurity from experimental deflection (ppmw)
Sn-Co	7.4	**-4.44**	-	-	**-5.68**	9.46
Sn-Pb	**31.4**	**-4.18**	**23**	-3.06	**-6.51**	48.95
Sn-Sb	**23.2**	+2.97	**3.16**	**+0.45**	**+0.78**	6.10
Al-Cu	**16.2**	-5.99	**5.24**	**-1.99**	**-1.70**	4.60
Al-Si	**9.8**	-6.96	**1.51**	-1.07	-3.03	4.27
Al-Ti	**1.8**	+5.96	**1.37**	**+4.53**	**+4.68**	1.41

The results as presented in Table 8.1 show the calculated GD-MS deflection is in better agreement with the measured deflection for Sn-Sb; Al-Cu and Al-Ti. Also, the measured results suggest that the impurity one puts in does not always get into the active metal as seen the significantly different amount between the total amount put in and the GD-MS measurement for Sn-Sb; Al-Cu; and Al-Si. From the GD-MS results, it confirms that Co cannot be detected from this technique. For the Sn with negative addition (Co and Pb), there is better agreement between the calculated deflection and experimental deflection than the calculated GD-MS deflection. From the experimental results, they confirm that the standard non-adiabatic temperature measurements as used in the most laboratories can be used to determine temperature offsets and the shapes of the curves.

The repeatability of the freeze peak of tin and aluminium freezing curves is presented in Figure 8.1 and 8.2, respectively (the error bars are considered at a confidence level of 95%). The results of this work are compared with the results from Hansen [1958].

8.1.1 Tin Fixed-Point Temperature

Excepting Sb, the equilibrium curves of the tin fixed-point decreased roughly in line with expectations derived from interpolation of previous experiments as increasing amounts of impurities were introduced; the average measured rates are as follows: Co -0.73 ± 0.09; Pb -0.21 ± 0.01; and Sb +0.06 ± 0.03 in units of mK/ppmw.

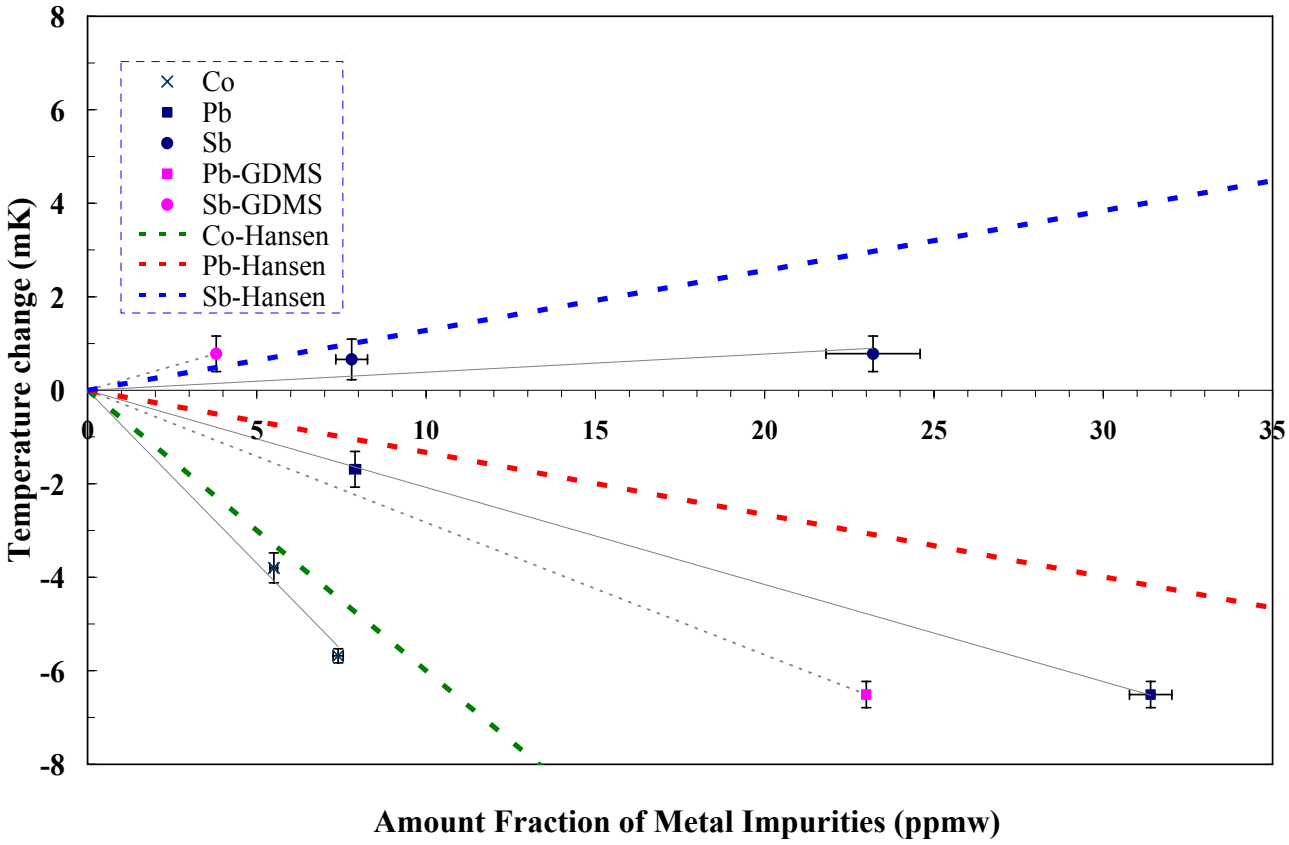

Figure 8.1 Temperature changes of freezing curves after doping tin with increasing concentrations of cobalt, lead, and antimony impurities.

8.1.2 Aluminium Fixed-Point Temperature

The temperature change of the freezing and melting curves of the aluminium fixed-point was affected by the amount of copper (-0.38 ± 0.10 mK/ppmw), silicon (-0.27 ± 0.16 mK/ppmw), and titanium (+5.14 ± 2.97 mK/ppmw) doping.

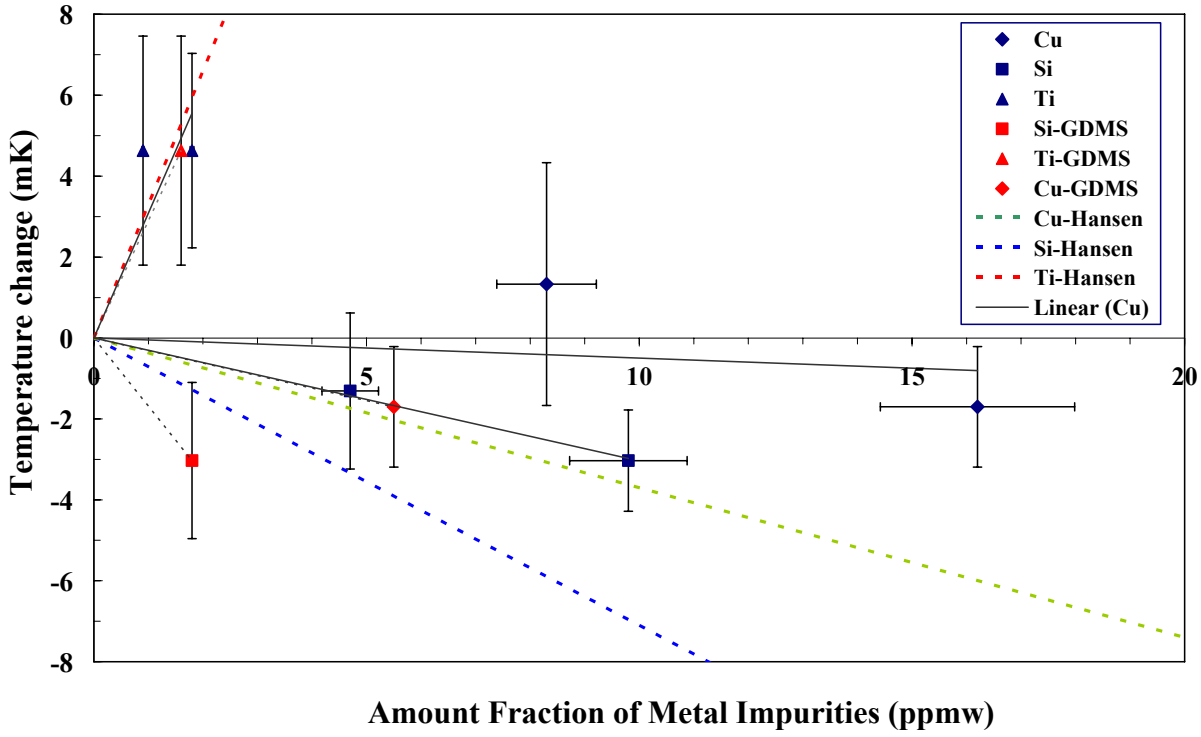

Figure 8.2 Temperature changes of freezing curves after doping aluminium with increasing concentrations of copper, silicon, and titanium impurities.

8.1.3 MTDATA Calculation based on Pre-doped GD-MS Result

In fact there are big differences between our pre-dope cell depression and that calculated by MTDATA based on GD-MS. Al is more depressed than what was calculated. This possibly suggests another contaminant not being picked up by GD-MS and/or not calculated for in MTDATA. The actual measured results must be accurate before comparing to MTDATA. More accurate thermometers need to be used to realise the temperature to get the better fit.

While the initial offset discrepancy for tin was much less, both tin and aluminium showed much more rounding than MTDATA would predict. Apart from additional impurity this might be due to the some segregation if the "fast" freezes were not fast enough.

After allowing for the uncertainties we have no evidence to change standard values for depression/elevation of temperature due to impurities. Interpolation from values obtained from larger doping quantities appears satisfactory (but noting our "mK level" uncertainties).

8.2 Summary of Contributions

The contributions of knowledge in this thesis are shown in the following list:

It has been shown practical to:

- Re-use normal fixed point ingots for controlled doping and to re-assemble the ingot many times and to use non-adiabatic furnace systems.
- Get dopants into the main mass of the ingot
- Take the ingot out and cut off samples without noticeable additional contamination (and GD-MS can see contamination if it did occur).
- Take repeat GD-MS analysis to give a trusted result for its uncertainty at low levels and dependence on "time of analysis".
- Get repeatable melts/freezes to overlay (melts shapes overlay to 1st order even though different times of melting).
- Extend melts and freezes to tens of hours (up to 70h)
- Have a means to compare (measure offset) of doped samples using 3 plateau peaks compared as against one plateau compare by 3 thermometers.

The experiments have:

- Compared GD-MS at low level doping with measured masses, which suggests GD-MS may be the best determinant, so far, of impurity concentration.
- Shown that impurities do mix throughout the cell after prolonged melting periods as seen in the GD-MS samples taken from three parts of an ingot.
- Confirmed the freeze as the most useful phase transition for calibration (as expected).
- Discovered thermal evidence in melts of impurity segregation during (slow) freezes.
- Presented a lot of data for others to use for comparison with more sophisticated chemical/thermal models of phase transitions.
- Shown calculating W value does not always help when using thermometers to compare between cells (W still ok for longer term thermometer calibration).
- It appears even "fast" freezes maintain a memory (i.e. cause segregation) for the next melt

8.3 Recommendation for Future Research

Experimental work in this thesis has been carried out and the results show the reproducibility of the melting and freezing temperatures after doping with impurities. However, there are still some related questions that should be investigated for the future.

8.3.1 Uncertainty Budgets

The reducing the uncertainty budget of the realisation of the tin and aluminium temperatures through the correction for impurities effect is still in investigation. The work suggests that GD-MS and MTDATA type models provide useful additional information to improve an impurity correction. However it also shows that other factors e.g. undetected impurity and impurity distribution (segregation) will start, which cause a contribution to the budget. This work is a step in the process of understanding the effect of impurities, a better understanding of which will further improve the impurity correction and reduce the term in the uncertainty budget.

8.3.2 Thermometers

This work has shown the limitation of our PRTs. Although we had expected PRT drift and included reference back to reference cells in the initial plan, the uncertainty change to the ongoing changes remained significant, particularly for Aluminium.

We had assumed the GD-MS uncertainty of a factor of two would be the dominant effect but the uncertainty of the thermometer drift, for the initial dopant quantities remained significant. The limited number of comparisons between cells has meant that proper statistics on the uncertainty of the difference has not been possible, though assuming the uncertainty in the mean is less than that of the sample (as quoted throughout this work)

8.3.3 GD-MS Technique

Because of the cobalt problem, which cannot be detected from GD-MS technique; therefore for future work it would be useful to get NRC to make a table of all the impurity combinations that mask each other in ITS-90 fixed point materials. Alternate analysis techniques – even of inferior resolution – may give bounds on impurities masked in the GD-MS technique and the best alternates should be investigated for the specific masking combinations.

8.3.4 Surface Chemical Analysis

Other types of the impurities in the metal fixed-point ingot can be also investigated by use the surface analysis. This is to reveal what the process is that is making the change to the surface colour of the ingot. This could lead to better handling of ingots and one wonders if one could segregate impurities on the surface whether one could "purify" old ingots. (Though in practice it would probably be cheaper to make a new one).

8.3.5 Impurity Modelling

A numerical model [Hunt, 2008] used by Professor John Hunt (Department of Materials, University of Oxford) is one type of impurity model, which has been used to estimate the affect of residual impurities in the low level contents on the actual measured equilibrium temperature curves. This model goes beyond the "simple" thermodynamic equilibrium model of MTDATA and incorporates the thermal conditions and history. This type of model is expected to use in an investigation of the future prospects for providing the predicted curve to fit and compare to our experimental curves in the future. While calibration will continue to use the freeze after prolonged melting as the main source of a "fixed point" in temperature, developing models that can explain both the melt and freeze under segregated conditions will give the model greater respectability when calculating the very important initial depression of the freeze.

8.4 Final Word

Correction of ingots temperature by impurity analysis remains a valid aim either rather than, or alongside, attempts to obtain more pure metal. This work has shown that the affect of small impurities can be detected, but much work remains to be done if some impurities are apparently not detectable by GD-MS alone. Further progress on modelling the interaction of both thermal and chemical interactions including their time history will greatly improve the reliability of this method and give more confidence in the application of the method of Sum of Individual Estimates as a means to correct ingot temperatures and thereby reduce the uncertainty in the temperature scale.

REFERENCES

Ancsin J. and Mendez-Lango E., 1999. *The reproducibility of some thermometric fixed points and the accuracy of temperature measurements using platinum resistance thermometers.* Metrologia, **36**, pp. 117-139.

Ancsin J., 2001a. *Equilibrium melting curves of relatively pure and doped silver samples*. Metrologia*,* **38,** pp. 229-235.

Ancsin J., 2001b. *Equilibrium melting curves of silver using high temperature calorimeter.* Metrologia, **38**, pp. 1-7.

Ancsin J., 2003. *Impurity dependence of the aluminium point*. Metrologia, **40,** pp. 36-41.

Ancsin J., 2007. *Impurity dependence of the Zn point*. Metrologia, **44**, pp. 303-307.

Ancsin J., 2008. *Impurity dependence of the Sn-point and the properties of the Sn–Fe 'eutectic'.* Metrologia, **45,** pp. 16-20.

Baker H., 1992. *ASM Handbook, Volume 3: Alloy Phase Diagrams*. Materials Park Ohio: ASM Int.

Batagelj V., Bojkovski J., and Drnovsek J., 2003. *Methods of reducing the uncertainty of the self-heating correction of a standard platinum resistance thermometer in temperature measurements of the highest accuracy.* Meas. Sci. Technol., **14,** pp. 2151-2158.

Betti M, Aldave de las Heras L., 2003. *Glow discharge mass spectrometry in nuclear research*. Spectroscopy Europe, **15/3,** pp. 15-24.

Bongiovanni G., Crovini L. and Marcarino P., 1975. *Effects of Dissolved Oxygen and Freezing Techniques on the Silver Freezing Point*. Metrologia, **11**, pp. 125 – 132.

Bonnier G., Elqourdou M., Renaot E., and Zvizdic D., 2002. *About the Influence of Chemical Impurities on the Gallium Temperature Fixed Point.* Proceedings of Tempmeko 2001, edited by Fellmuth B., Siedel J. and Scholz G., VDE-Verlag, Berlin, pp. 483-488.

Brice J.C., 1965. *The Growth of Crystals from the Melt*. Amsterdam: North-Holland Publishing Company, pp. 82.

Bureau International des Poids et Mesures (BIPM). 2004a. *"What is metrology"*, [Online] Available at: http://www.bipm.org/en/bipm/metrology/ [Accessed on 10 March 2008].

Bureau International des Poids et Mesures (BIPM). 2004b. *The Metre Convention*, [Online] Available at: http://www.bipm.org/en/convention/. [Accessed on 12 March 2008].

Bureau International des Poids et Mesures (BIPM). 2008. *CIPM Mutual Recognition Arrangement,* [Online] Available at: http://www.bipm.org/en/cipm-mra/. [Accessed on 12 March 2008].

Clark J., 2005. *Raoult's Law and Ideal Mixtures of Liquids*

Connolly J.J. and McAllan J.V., 1980. *Limitations on Metal Fixed Points Caused by Trace Impurities.* Metrologia, **16**, pp. 127-132.

Davies R.H., Dinsdale A.T., Gisby J.A., Robinson J.A.J. and Martin. S.M., 2002. *MTDATA - thermodynamic and phase equilibrium software from the national physical laboratory.* CALPHAD, **26(2)**, pp. 229-271.

EURAMET e.V., 2008. *EURAMET Technical Committee Projects*. [Online] Available at: http://www.euramet.org/index.php?id=tc-projects&no_cache=1&ctcp_projects[sword][title]=&ctcp_projects[sword][refid]=732&ctcp_projects[sword][subject_uid]=none&ctcp_projects[sword][collaboration]=none&ctcp_projects[sword][institute_uid]=none&ctcp_projects[sword][status]=none&ctcp_projects[sword][country_uid]=none&ctcp_projects[cmd]=search&ctcp_projects[cmd]=details&ctcp_projects[uid]=611, [Accessed on 5 October 2008].

Fellmuth B., 2001. *Influence of Impurities on the realisation of defining fixed points of the ITS-90*. Workshop of CCT WG3 and Euromet, Berlin.

Fellmuth B., Fischer J. and Tegeler E., 2001. *Uncertainty budgets for characteristics of SPRTs calibrated according to the ITS-90.* BIPM publication Document, CCT/01-02.

Fellmuth B., 2003. *Comments on the underestimation of the change of fixed-point temperatures by impurities due to a non-justified application of Raoult's law*. BIPM publication Document CCT/03-12.

Fellmuth B. and Hill D.K., 2006. *Estimating the influence of impurities on the freezing point of tin*. Metrologia**, 43,** pp. 71-83.

Furukawa G. T. and Bigge W. R., 1982. *Reproducibility of some triple point of water cells. Temperature Its Measurement and Control in Science and Industry.* American Institute of Physics, New York, **5**, pp. 291-297.

Furukawa G.T., Mangum B.W., and Strouse G.F., 1997. *Effects of different methods of preparation of ice mantles of triple point of water cells on the temporal behaviour of the triple-point temperatures.* Metrologia, **34**, pp. 215-233.

Gilman J. J., 1963. *The Art and Science of Glowing Crystals*. New York: John Wiley & Sons, Inc., pp. 8-10.

Hansen M., 1958. *"Constitution of Binary Alloys"*, 2nd ed, New York: McGraw-Hill.

Hart Scientific Inc., 2006. 9114 Freeze Point Furnaces User's Guide. [Online] Available at: ftp://ftp.hartscientific.com/manuals/9114.pdf. [Accessed on 15 May 09].

Head D.I., 2009. National Physical Laboratory (NPL), private communication.

Head D.I., Davies, Gray J., and Quested P., 2008. *The Comparison of MTDATA with the Melting/Freezing Point Curves of ITS-90 Metal Fixed Points.* Int. J. Thermophys., **29**, pp. 1796-1807.

Helden A.V., 1995. *The Galileo Project, Santorio Santorio*, 1995 [Online] Available at: http://galileo.rice.edu/sci/santorio.html. [Accessed on 20 June 08].

Hill K.D. and Rudtsch S., 2005. *Thermometry's dependence on chemical metrology: a needs-based assessment.* Metrologia, **42**, Short Communication, pp. L1-L4.

Hunt J., 2008. Internal Report, London: National Physical Laboratory (NPL).

Hunt J., Lowe D., and Zohaib M., 2008. *Imperial, Oxford and NPL project on modelling the affect of residual impurities on the determination of fixed points.* Internal Report, London: National Physical Laboratory (NPL).

ISO/IEC Guide 98, 1995. *Guide to the Expression of Uncertainty in Measurement;* International Organisation for Standardisation. Genéve, Switzerland, ISBN 92-67-10188-9.

Jimeno-Largo P., Bloembergen P., Ancsin J., 2004. *And Experimental and Theoretical Analysis of the Effect of Impurities on the Adiabatic Melting Curve of Silver.* In Proceedings of TEMPMEKO 2004, 9th International Symposium on Temperature and Thermal Measurements in Industry and Science. Cavtat - Dubrovnik Croatia, 22 - 25 June 2004, ed. by Zvizdic D., Bermanec L.G., Stasic T., Veliki T. (LPM/FSB, Zagreb, Croatia, 2005), pp. 233-238.

Jung H.J., 1997. *On the determination of the thermodynamic temperature of high temperature blackbodies via ITS-90 or alternative methods.* Proceedings of TEMPMEKO '96, edited by P. Marcarino, Levrotto & Bella, Torino, pp. 235-244.

King F. L., Teng J., Steiner R. E., 1995. *Special feature: Tutorial. Glow discharge mass spectrometry: Trace element determinations in solid samples.* Journal of Mass Spectrometry., **30(8)**, pp. 1061-1075.

Lowe D., Mingard K., Zohaib M. and Quested P., 2007. The Dependence of the Melting Temperature of Cobalt-Carbon Eutectic on the Morphology of its Microstructure. Int. J. Thermophys, **28**, pp. 2019-2027.

LGC setting standards in analytical science., 2009. About LGC [Online] Available at: http://www.lgc.co.uk/about_lgc.aspx [Access on 24 February 2009].

Mangum B. W., Bloembergen P., Chattle M. V. (NPL), Fellmuth B. (PTB), Marcarino P., and Pokhodun. A. I., 1997. *On the International Temperature Scale of 1990 (ITS-90) Part I: Some definitions. Metrologia*, 34, pp. 427-429.

Mangum B. W., Bloembergen P., Fellmuth B., Marcarino P. and Pokhodun A.I., 2000. *On the influence of impurities on fixed-point temperatures.* BIPM publication Document, CCT/99-11.

Mangum B.W., Strouse G.F., Guthrie W.F., Pello R., Stock M., Renaot E., Hermier Y., Bonnier G, Marcarino P, Gam K.S., Kang K.H., Kim Y-G, Nicholas J.V., White D.R., Dransfield T.D., Duan Y., Qu Y., Connolly J., Rusby R.L., Gray J., Sutton G.J., D I Head D.I., Hill K.D., Steele A., Nara K., Tegeler E., Noatsch U., Heyer D., Fellmuth B., Thiele-Krivoj B., Duris S., Pokhodun A.I., Moiseeva N.P., Ivanova A.G., de Groot M.J. and Dubbeldam J.F., 2002, *Summary of comparison of realizations of the ITS-90 over the range 83.8058 K to 933.473 K: CCT key comparison CCT-K3,* Metrologia, **39**, pp.179-205.

Massalski T.B., Okamoto H., Subramanian P.R. and Kacprzak L., 1990. *Binary Alloy Phase Diagrams*. 2nd ed. Materials Park Ohio: ASM Int.

Mendez-Lango E., 2002. *A Non-Destructive Method to Evaluate the Impurity Content in Triple Point of Water Cells.* Proceedings of Tempmeko 2001, edited by Fellmuth B., Siedel J. and Scholz G., VDE-Verlag, Berlin, 2002.

Michalski L., Eckersdof K., Kucharski J. and Mcghee J., 2001a. Temperature Measurement, 2nd Edition, Wiley Publishers, pp. 1.

Michalski L., Eckersdof K., Kucharski J. and Mcghee J., 2001b. Temperature Measurement, 2nd Edition, Wiley Publishers, pp.2-4.

Middleton W. E. K., 1966. *A History of the Thermometer and its Use in Meteorology*. Baltimore: Johns Hopkins University Press

National Physical Laboratory (NPL), 2003a. *"Temperature Measurement and Calibration"*, Teddington: Crown, pp. 1.1.

National Physical Laboratory (NPL), 2003b. *"Temperature Measurement and Calibration"*, Teddington: Crown, pp. 2.7-2.9.

National Physical Laboratory (NPL), 2003c. *"Temperature Measurement and Calibration"*, Teddington: Crown, pp. 3.1.

National Physical Laboratory (NPL), 2003d. *"Temperature Measurement and Calibration"*, Teddington: Crown, pp. 3.2.

National Physical Laboratory (NPL), 2003e. *"Temperature Measurement and Calibration"*, Teddington: Crown, pp. 3.2-3.7.

National Physical Laboratory (NPL), 2003f. *"Temperature Measurement and Calibration"*, Teddington: Crown, pp. 6.2-6.4.

National Physical Laboratory (NPL), 2003g. *"Temperature Measurement and Calibration"*, Teddington: Crown, pp. 6.7-6.8.

National Physical Laboratory (NPL), 2003h. *"Temperature Measurement and Calibration"*, Teddington: Crown, pp. 6.13.

Nicholas J.V. and White D.R., 2001a. *Traceable Temperatures - An Introduction to Temperature Measurement and Calibration*. 2nd ed. England: John Wiley & Sons Ltd., pp. 14-16.

Nicholas J.V. and White D.R., 2001b. *Traceable Temperatures - An Introduction to Temperature Measurement and Calibration*. 2nd ed. England: John Wiley & Sons Ltd., pp. 3-4.

Nicholas J.V. and White D.R., 2001c. *Traceable Temperatures - An Introduction to Temperature Measurement and Calibration*. 2nd ed. England: John Wiley & Sons Ltd., pp. 16.

Nicholas J. V. and White D. R., 2001d. Traceable Temperatures: An introduction to temperature measurement and calibration. 2nd ed., England: John Wiley & Sons Ltd., pp. 13-21.

Nicholas J. V. and White D. R., 2001e. Traceable Temperatures: An introduction to temperature measurement and calibration. 2nd ed., England: John Wiley & Sons Ltd., pp. 107.

Nicholas J. V. and White D. R., 2001f. Traceable Temperatures: An introduction to temperature measurement and calibration. 2nd ed., England: John Wiley & Sons Ltd., pp. 114-115.

Nicholas J. V. and White D. R., 2001g. Traceable Temperatures: An introduction to temperature measurement and calibration. 2nd ed., England: John Wiley & Sons Ltd., pp. 56-65.

Nicholas J. V. and White D. R., 2001h. Traceable Temperatures: An introduction to temperature measurement and calibration. 2nd ed., England: John Wiley & Sons Ltd., pp. 21-24.

Nicholas J. V. and White D. R., 2001i. Traceable Temperatures: An introduction to temperature measurement and calibration. 2nd ed., England: John Wiley & Sons Ltd., pp. 110.

Nicholas J.V. and White D.R., 2001j. *Traceable Temperatures: An Introduction to Temperature Measurement and Calibration.* John Wiley & Sons, LTD. 2nd ed. Chichester: John Wiley & Sons Ltd., pp. 100.

Nicholas J.V. and White D.R., 2001k. *Traceable Temperatures: An Introduction to Temperature Measurement and Calibration.* John Wiley & Sons, LTD. 2nd ed. Chichester: John Wiley & Sons Ltd., pp. 108.

NRC GD-MS services, 2009. National Research Council Canada (NRC), private communicate.

Nubbemeyer H.G. and Fischer J., 2002, *Final report on key comparison CCT-K4 of local realizations of aluminium and silver freezing-point temperatures*, Metrologia, **39,** Tech. Suppl., pp. 03001.

Peng L. and Besley L.M., 1993. *The properties of Chinese standard rhodium iron resistance thermometers.* Meas. Sci. Technol., **4**, pp. 1357-1362.

Pfann W. G., 1958a. *Zone Melting*. New York: John Wiley & Sons Inc., pp. 1.
Pfann W. G., 1958b. *Zone Melting*. New York: John Wiley & Sons Inc., pp.2.
Pfann W. G., 1958c. *Zone Melting*. New York: John Wiley & Sons Inc., pp.1-10.
Pfann W. G., 1958d. *Zone Melting*. New York: John Wiley & Sons Inc., pp.9.
Pfann W. G., 1958e. *Zone Melting*. New York: John Wiley & Sons Inc., pp.8-9.

Preston-Thomas H., 1990. *The International Temperature Scale of 1990 (ITS-90).* Metrologia, **27**, pp. 3-10.
Preston-Thomas H., 1990. *The International Temperature Scale of 1990 (ITS-90).* Metrologia, **27,** pp. 107 (Erratum)

Preston-Thomas H., Bloembergen B. and Quinn T. J., "Supplementary Information for the International Temperature Scale of 1990" , Monograph CCT/WG1, BIPM, Sèvres, France 1990, 29-78.

Qiu P, Sun J., Zhang J., Zhijun J., 2008. Tempbeijing, ACTA METROLOGICA SINICA., **29(4A).**

Ripple D., Fellmuth B., Groot M. de, Hermier Y., Hill K.D., Steur P.P.M., Pokhodun A., Matveyev M. and Bloembergen P., 2005. *Methodologies for the estimation of the uncertainties and the correction of fixed-point temperatures attributable to the influence of chemical impurities,* BIPM publication Document, CCT/05-08.

Renaot E., Valin M.H., and Elgourdou M., 2008. *Influence of Impurities and Filling Protocol on the Aluminium Fixed Point.* Int. J. Thermophys, **29**, pp. 852-860.

Rusby R. L., 2008. National Physical Laboratory (NPL), private communication.

Rusby R.L., 1987. *The basis of temperature measurement.* Meas. And Cont., **21**, pp. 40.

Rudtsch S., Fahr M., Fischer J., Gusarova T., Kipphardt H. and Matschat R., 2008. *High-purity Fixed-Points of the ITS-90 with Traceable Analysis of Impurity Content.,* in Proceedings of TEMPMEKO 2007, Int. J. Thermophys., **29**, pp. 139-150.

Stolen S. and Gronvold F., 1999. *J. Chem. Thermodynamics***, 31,** pp. 379 –398.

Strouse G.F., 1995. S*tandard Reference Material 1744: Aluminium Freezing Point Standard.* NIST Special Publication, **39**, pp. 260-124.

Strouse G., 2003. *NIST Methods of Estimating the Impurity Uncertainty Component for ITS-90 Fixed-Point Cells from the Ar TP to the Ag FP,* BIPM publication Document CCT/03-19.

"Thermodynamic Temperature". [Online] Available at: http://en.wikipedia.org/wiki/Thermodynamic_temperature [Accessed on 7 July 2007]

Thurmond C.D., 1959. *Semiconductors*, New York: Rheinhold.

Tiller W.A., Jackson K.A., Rutter J.W. and Chalmers B., 1953. *The redistribution of solute atoms during the solidification of metals.* Acta Metall., **1**, pp. 428 – 437.

Weinberg F. And McLaren E.H., 1961. *Zn:Tl Phase Diagram at very Low Thallium Concentrations.* Can. J. Phys., **39(4)**, pp. 588-595.

Weinberg F. And McLaren E.H., 1963. *The Solidification of Dilute Binay Alloys*. Transactions Of The Metallurgical Society Of AMIE, **277**, pp. 112 – 124.

Widiatmo J.V., Harada K., Kishimoto I. and Arai M., 2003. Development of a New Aluminium Point cell. SICE Annual Conference in Fukui, Japan, August 4-6, pp. 2607-2610.

Widiatmo J.V., Harada K., and Arai M., 2004. *Analyzing Metal Fixed-Point Cells from Their Plateaus.* SICE Annual Conference: International Conference on

Instrumentation Control and Information Technology, Sapporo - Japan, 4-6 August 2004, pp. 1936-1939. Society of Instrument and Control Engineers: Tokyo.

Widiatmo J.V., Harada K., Yamazawa K. and Arai M., 2006. Metrologia, **43**, pp. 561-572.

White D.R., Ballico M., Campo D. del, Duris S., Filipe E., Ivanova A., Kartal Dogan A., Mendez-Lango E., Meyer C.W., Pavese F., Peruzzi A., Renaot E., Rudtsch S. and Yamazawa K., 2007. *Uncertainty in the Realisation of the SPRT Sub-ranges of the ITS-90.* Int. J. Thermophys., **28**, pp. 1868-1881.

Villars P., Prince A. and Okamoto H., 1995. *Handbook of Ternary Alloy Phase Diagrams.* Materials Park Ohio: ASM Int.

Zhang J.T., Rudtsch S., Fahr M., 2008. *The Influence of Antimony of the Tin Point.* Int. J. Thermophys., **29**, pp. 151-157.

Zohaib M., 2009. 1st year transfer report, London: Imperial College.

.

Appendix A

Published Papers

IOP PUBLISHING METROLOGIA
Metrologia **44** (2007) L73–L75 doi:10.1088/0026-1394/44/6/L01

LETTER TO THE EDITOR

Argon pressure is maintained in an aluminium thermometric fixed-point cell

Patchariya Petchpong[1] **and David I Head**[2]

[1] Advanced Manufacturing and Enterprise Engineering Group, Brunel University, Uxbridge, Middlesex UB8 3PH, UK
[2] National Physical Laboratory, Teddington, Middlesex TW11 0LW, UK

E-mail: David.Head@npl.co.uk

Received 31 August 2007
Published 21 November 2007
Online at stacks.iop.org/Met/44/L73

Abstract
The argon and helium pressure in two types of temperature fixed-point cell enclosure has been measured for over two weeks. It was found that there was no significant change in the argon pressure over this time, in contrast to the report of Ancsin (2003 *Metrologia* **40** 232–4). Helium was found to diffuse out of the cell as expected. We conclude that argon is a suitable 'back-fill' gas for fixed-point cells.

1. Introduction

The freezing point of aluminium at one standard atmosphere (at 660.323 °C) is one of the fixed-points specified for use in the definition of the International Temperature Scale of 1990 (ITS-90) [2].

The optimal realization of the fixed-point to obtain a precise calibration relies on many factors including the materials of the cell components. The high-purity metal is contained in a pure graphite crucible and this is held in a gas-tight container made from quartz (silica). An inert gas filling is an important part of a fixed-point cell to assist thermal exchange inside the cell, to protect the graphite from oxidation and to prevent metal vaporization. To obtain the specified condition, the pressure must be adjusted or corrected to one standard atmosphere, 101.325 kPa. In the 'Supplementary Information for the ITS-90' [3], it is suggested that argon should be used as the internal pure gas in high temperature fixed-point cells.

Recently, however, Ancsin [1] has observed the diffusion of Ar gas out of a quartz housing at high temperature. In his experiments, five different gases (air, He, Ar, CO_2, N_2) were used to back-fill the Al cell. Each of them showed a drop in pressure over time from the initial value of 1 atm, except nitrogen. Ancsin wondered if the gases, including argon, were being absorbed by graphite or aluminium. After further experiment, he concluded that the greater part of the pressure decreases were due to the permeability of the walls of the quartz tubes at high temperatures, and the best choice among the five gases tested, for use in sealed quartz cells, is nitrogen.

However, although nitrogen is basically non-reactive, it may form nitrides in fixed-point cells at high temperatures. Also data, such as used in thermodynamic calculation programs, show that freezing curves can be depressed due to the solution of nitrogen as an impurity [4]. Consequently, nitrogen should be avoided and it is therefore important to check whether the reported problem with argon is repeatable.

This study investigates the effects of argon and helium being used for back-filling an Al fixed-point cell. Our results show that the argon filling gas did not significantly change its pressure, when used in both a translucent silica tube containing a graphite crucible and in an empty quartz enclosing tube. On the other hand, with helium the pressure did drop, as expected.

2. Experimental apparatus

An NPL design of an open Al cell was used for this experiment. The Al sample was contained in a graphite crucible of length 250 mm, which was put into a translucent silica tube of length 530 mm. A single zone Carbolite furnace was used in conjunction with a potassium heat

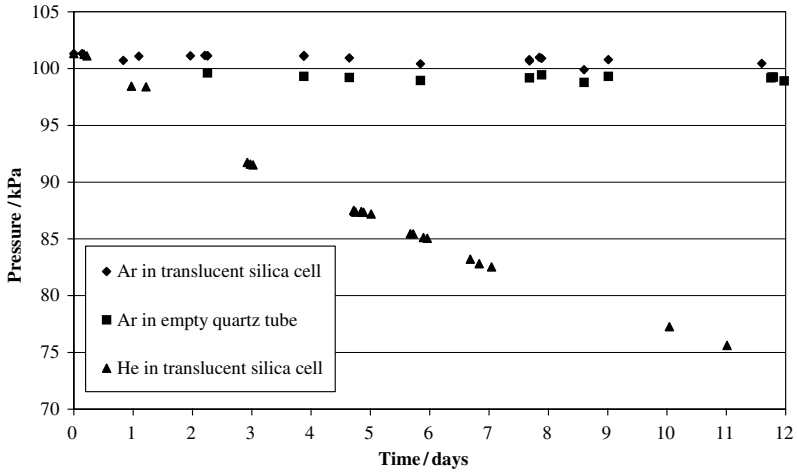

Figure 1. Graph of pressure over an Al fixed-point cell and in a separate empty quartz tube as a function of time in days.

pipe for maintaining a uniform temperature above or below 660 °C. A thyristor controller was used to control the furnace temperature, which applied only 120 V (through a transformer) to reduce the electrical noise. The resistance ratios of the platinum resistance thermometer (PRT) measurement were recorded from an ASL F18 resistance bridge, confirming the temperature stability of the fixed-point cell.

A gas handling system was used to set the pressure in the cell to approximately 101.3 kPa. The cell was connected via a copper tube to the system, which was connected by reinforced plastic tube to the vacuum pump (Edwards XDS10 scroll pump) and a Wallace and Tiernan precision pressure gauge. Before the experiments, the whole system was tested using a Leybold Vacuum PhoeniXL 300 helium leak detector.

Argon and helium were the gases used to back-fill the cell in two separate experiments as both gases were conveniently available in the laboratory and both can provide an inert atmosphere for the Al fixed-point cell.

The fixed-point cell was maintained at the operating temperature, either −0.5 °C or +0.5 °C of the equilibrium temperature, which were the settings for the cell to be frozen and molten, respectively, for almost two weeks and the internal pressure was monitored during this time. The results are shown in figure 1.

Starting on day 2, in a separate experiment the permeability of argon through the wall of a clear close-ended quartz tube was investigated. Thus, a quartz tube, without an Al cell, was inserted into a three-zone Hart Scientific furnace and was connected to a duplicate gas handling system. This system was also leak tested. Then, the empty cell was back-filled with gas, sealed up and left to observe if any decrease in pressure occurred at the Al fixed-point temperature. The initial pressure was set at about 99.6 kPa, which was slightly below 101.325 kPa, to ensure that if there was any air leak then it would increase the tube pressure. These results are also shown in figure 1. When air was let into the empty cell at the end of the experiment, then the pressure increased to 1 atm. (In fact, the silica broke on cooling between 660 °C and room temperature.)

3. Results

As observed in figure 1, the pressure of argon gas was virtually unchanged during the time at high temperature. After 12 days, the pressure was about 100.3 kPa, only 1 kPa lower, or reduced approximately 1% from the initial pressure. For practical thermometric purposes, this is negligible. It may be due to some argon diffusing out or being absorbed by the graphite or Al, but it might also be a limitation of the pressure measurement system. In any case, the amount of pressure reduction is much less than that reported by Ancsin (approximately 25 kPa over 10 days) [1].

These results indicate that argon gas did not significantly diffuse out of the translucent tube or become absorbed into the aluminium or graphite.

For helium, figure 1 shows that the pressure kept decreasing with time. At the end of the measurement period, the pressure was about 75.6 kPa, i.e. it had dropped by about 25% below its initial value over 12 days, while Ancsin's report showed an 80% reduction within 4 days. That the pressure of the helium should drop is not a surprise, as it is well known [5] that a quartz tube is permeable to helium. The result confirms the ability of our system to detect a pressure drop and that there is no long-term leak from the outside.

The results for the empty quartz tube filled with argon gas, also shown in figure 1, indicate that the pressure had dropped by about 0.87 kPa, which is 1% reduced, over the period. This is similar to the result for the translucent silica cell and indicates that argon does not diffuse significantly through clear quartz at this temperature.

From these results, we surmise that Ancsin may have been using an unusually permeable quartz tube. We wonder if the nitrogen appeared not to diffuse due to back diffusion of nitrogen from the surrounding air. However, we are not able to confirm this hypothesis.

4. Conclusions

The changes in pressure in our experiments suggest that argon is not absorbed or lost within the Al cell, in contradiction to the results of Ancsin. Our results showed at most a very

small permeation of argon, though the small pressure decrease may have been due to other effects such as limitations of the measurement system. This applies for both the translucent silica and the quartz tubes at the Al fixed-point temperature. Therefore, we conclude that argon is a suitable gas to use to back-fill the Al fixed-point cell.

Acknowledgments

One of us (P Petchpong) gratefully acknowledges the help of the staff of the Temperature Section of the UK National Physical Laboratory (NPL), which kindly supplied the aluminium cell, the fabrication support and advice for experimentation. We would also like to thank Isothermal Technology Ltd for the supply of a standard open cell tube. This work was financially supported by a scholarship from the Royal Thai Government and the UK Department of Trade and Industry (DTI).

References

[1] Ancsin J 2003 ITS-90: the instability of the Al point *Metrologia* **40** 232–4

[2] Preston-Thomas H 1990 The International Temperature Scale of 1990 (ITS-90) *Metrologia* **27** 3–10
Preston-Thomas H 1990 The International Temperature Scale of 1990 (ITS-90) *Metrologia* **27** 107 (Erratum)

[3] Consultative Committee on Thermometry (CCT) 1990 *Supplementary Information for the International Temperature Scale of 1990* (Sèvres: Bureau International des Poids et Mesures) pp 36–7

[4] Head D I, Davies H, Gray J and Quested P 2007 The comparison of MTDATA with the melting/freezing point traces of ITS-90 metal fixed points *Proc. Tempmeko 2007* (*Int. J. Thermophys.* to be published)

[5] Rayleigh Lord 1936 Studies on the passage of helium at ordinary temperature through glasses, crystals, and organic materials *Proc. R. Soc. Lond. A: Math. Phys. Sci.* **156** 350–7

Effects of Impurities on the Melting Curve of the Aluminium Fixed Point

David I Head[2], Patchariya Petchpong[1], Joe Y. H. Au[1]

(1. Advanced Manufacturing and Enterprise Engineering Group, Brunel University, Uxbridge, Middlesex UB8 3PH, UK;
2. National Physical Laboratory, Hampton Road, Teddington, Middlesex TW11 0LW, UK)

Abstract: This work describes the influences of trace impurities on the freezing and melting temperatures of high purity (99.9999%) aluminium (660.323 °C), specified for use in the International Temperature Scale of 1990 (ITS-90) [1]. The offsets and shapes of melting and freezing plateaus of high purity aluminium are investigated as a function of very low level dopants (mass fraction of ~1-20 parts per million by weight (ppmw)) of copper, silicon, and titanium pure metals. The freezing curves of the aluminium fixed-point decreased and increased in line with expectations derived from interpolation of previous experiments [2] as increased amounts of impurities were introduced; the rates are as follows: Cu -0.43; Si -0.85; and Ti +3.2 in units of mK/ppmw.

Key words: Aluminium fixed point; ITS-90; Temperature measurement; Impurity doping
CLC number: TB94 Document code: A Article ID: 1000-1158(2008)04A-0000-00

1. Introduction

The freezing point of aluminium (660.323 °C) is one of the metallic fixed-points specified for use in the definition of the International Temperature Scale of 1990 (ITS-90) [1]. Standard platinum resistance thermometers (SPRTs) are used for disseminating the precise reference temperatures provided by the fixed-points to define an agreed temperature scale accurate to around 1 mK (2s). The temperature offsets and shapes of melting and freezing plateaus of high purity aluminium are investigated as a function of the deliberately added impurities (concentrations of order ~1-20 ppmw) of copper, silicon, and titanium pure metals. In prior experiments on these binary alloy systems, using higher levels of impurities [2], the fixed-point temperature of aluminium was interpolated to be depressed by 0.37 mK/ppmw of copper and 0.71 mK/ppmw of silicon impurity. Conversely the aluminium transition temperature is increased by 3.31 mK/ppmw of titanium impurity. Therefore, we experimentally investigated the effects of very low levels of impurities on the aluminium transition temperature in order to check the temperature offset values interpolated from the experiments using relatively high levels of impurities. The realisation of the aluminium temperature fixed-point has an uncertainty budget of many parts or “components”. An improved understanding of the effects of low-level impurities would allow one to reduce the magnitude of the “impurity” component, which is a significant part of the budget.

Measurement of impurity effects has already been done using a special adiabatic furnace and a specialised cells design [3]. In this paper we try to produce such measurements using standard NPL equipment, under standard conditions, used in most national measurement institutes around the world.

Received: 2008-00-00
Corresponding e-mail address: david.head@npl.co.uk

2. Experimental procedure

Two nominally 99.9999% pure aluminium fixed-point cells, according to the NPL design, were used in this study to realise the reference standard temperature. The two cells were designated after the year they were fabricated in 1974 (Al 174) and 1998 (Al 298). Each cell assembly was connected to a gas control system including a vacuum pump (Edwards XDS10 scroll pump) and a Wallace & Tiernan precision pressure gauge. Before the experiments, the whole system was tested using a Leybold Vacuum PhoeniXL 300 helium leak detector to confirm a seal adequate for prohibiting any contamination from the surrounding. Afterwards, the two aluminium cells, made as "Open" cells, were filled with argon gas and the pressure in the cell was set at about 101.3 kPa at the fixed-point transition to assist thermal exchange inside the cell, to protect the graphite from oxidation and to prevent metal vaporization.

A single zone Carbolite furnace was used in conjunction with a potassium heat pipe for maintaining a uniform temperature above or below the phase transition temperature of the Al 174 cell. The Al 298 cell assembly was heated inside a three-zone Hart furnace. As the phase transition is powered by an offset in the furnace temperature, it means that the conditions are only quasi-adiabatic, but this was the desired way to carry out the tests, as these are the "normal" conditions for the realisation of fixed-points.

The resistance ratios of the measuring platinum resistance thermometer (PRT) were recorded on an Automatic Systems Laboratories Model ASL F18 ac resistance bridge.

The furnaces were maintained at an operating temperature, either –0.5 ^{o}C or + 0.5 ^{o}C of the transition temperature, which were the settings for the cell to be frozen and melted respectively. The freezing and melting curves of the two initially "pure" aluminium cells were measured at least three times. The stability of PRTs was determined at the water triple point in between the realisations. Thereafter small samples of the aluminium ingots were cut from the top, middle, and bottom. These pieces were sent for chemical analysis to determine the distribution of the impurity elements within the "pure" aluminium, before deliberate doping, by using glow discharge mass spectrometry (GD-MS) at the National Research Council of Canada (NRC). Subsequently the impurity levels in the aluminium samples after doping will be measured again by GD-MS. The initial freezing temperature of these "high purity" aluminium cells were calibrated several times against a standard aluminium cell by comparison of the thermometers readings in the two cells.

After the initial measurements of the two aluminium cells, three impurities; namely copper, silicon and titanium were used for doping. Each impurity was placed on the top, the middle and the bottom of the originally pure aluminium samples increasing the concentrations as follows (in ppmw); Cu: ~8.3 and ~16.2, Si: ~4.7 and ~9.8 in Al 174, with Ti: ~0.9 and ~1.8 in Al 298. After doping, each ingot was held at 5 ^{o}C above the aluminium melting temperature for several days to ensure a good mixing of the trace impurities within the aluminium. The temperature changes during freezing and melting of the aluminium after doping were measured and compared with the original curves to find out how much the trace impurities affected the temperatures of the aluminium fixed-points. As thermometers drift, a comparison between the doped and reference aluminium cells was carried out to investigate how much the trace impurities affected the temperatures of the initially pure aluminium fixed-point cells.

3. Results and Discussions

A set of three freezing curves of the "Al 174" aluminium fixed-point cell, before the doping process, is shown in Figure 1. All freezing measurements are determined at the furnace same setting. Examples of Al 174 melting curves, before doping, are shown in Figure 2.

The melting and freezing curves of high purity Al 174 aluminium confirm the reproducibility of the temperature measurements over a short time scale, and intercomparison with the reference fixed-point cell, ensures longer-term measurement accuracy.

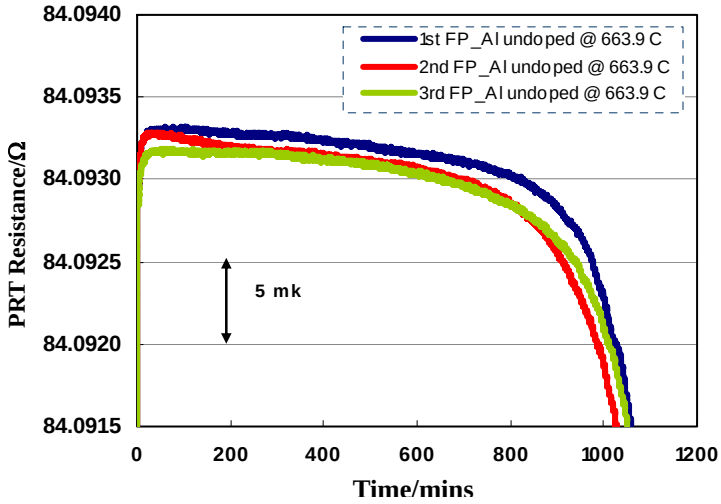

Figure 1 Three freezing curves of high purity Undoped "Al 174" aluminium fixed-point plotted as a function of time. The furnace setting point for all three measurements is set at the same temperature (nominally half a degree above the melting point).

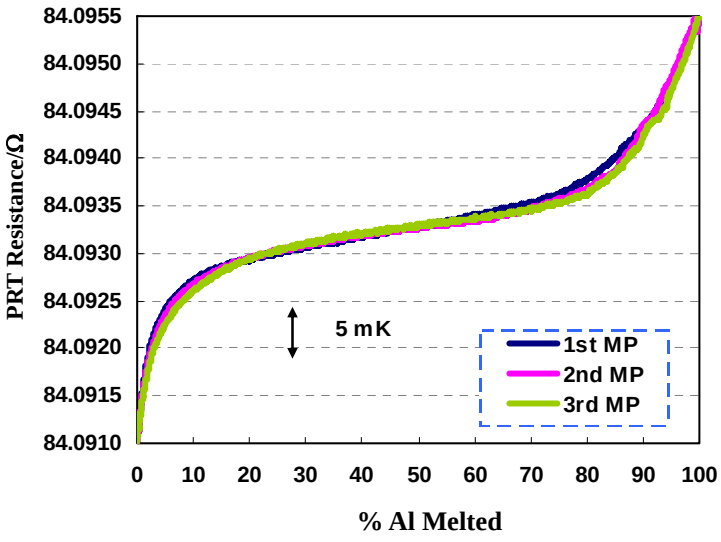

Figure 2 Melting curves of high purity Undoped "Al 174" aluminium fixed-point plotted as a function of aluminium percentage melted. The curves have been normalised to an approximate percentage melted (the best means for this normalisation is still under study).

Because segregation at the initial freeze front tends to make the first layer of frozen Al purer than the rest, it gives a better representation of the fixed point temperature. Thus, the best estimate of the liquidus point in a freeze is the maximum point of the freezing curve. Also, according to Physikalisch-Technische Bundesanstalt (PTB) - the German national metrology measurement institute - the peak of the freeze is the most reproducible part of the freezing curve, from which good results can be obtained. The reason is that the maximum temperature does not strongly depend on the homogeneity and stability of the furnace temperature [4]. Therefore, the temperature comparison between the Al 174 or Al 298 and the NPL national standard aluminium cell in this work was realised by using the peak of the freezing point curve.

Prior to doping, the initial freezing temperature of cell Al 174 was found to be 9 mK lower than the reference cell. That means the Al 174 ingot probably contained some initial impurities affecting its freezing and melting temperatures (this is as expected as it is an old cell retired due to some previous contamination). Also, the shape of the curves is no longer flat when compared with the reference cell. For an ideal pure aluminium fixed point, a purer metal usually shows a flatter plateau on the freezing and melting curves.

As these were existing impurities, it was necessary to carry out an elemental analysis of this aluminium fixed-point cell using the GD-MS technique, before doping the aluminium cell with any impurity elements in the next step of the procedure.

An example result of the impurity determination for the "high purity" aluminium (Al 174) fixed point by GD-MS analysis is reported in Table 1. This shows the impurity content measured in three areas of the aluminium ingot. This GD-MS analysis is considered to be accurate within a factor of two of the values obtained, at a confidence level of 95%. From the results we see that the impurity levels are the same throughout the cell (within the uncertainty quoted). This shows that the aluminium is sufficiently well mixed and that only one sample will need to be cut out for analysis after doping. (Cutting out of samples is a risky procedure).

Table 1. An example of the GD-MS analysis results of the initial "high purity" (6N) aluminium fixed point (Al 174) (NRC report number: 30337R1). The aluminium samples were cut from the three areas of the ingot, which are the top, the middle, and the bottom. These elements were detected in term of mass fraction (in parts per million by weight, ppmw). The uncertainty is quoted as a "factor of 2", though this is probably a conservative overestimate.

Element	Top	Middle	Bottom	Element	Top	Middle	Bottom
	ppmw				ppmw		
Li	<0.004	<0.003	<0.003	Br	<0.02	<0.02	<0.02
Be	<0.001	<0.001	<0.001	Rb	<0.001	<0.001	<0.002
B	0.01	0.007	0.003	Sr	<0.001	<0.001	<0.001
C	6	6	5	Y	<0.001	<0.001	<0.001
N	1	1	0.3	Zr	0.005	0.006	0.009
O	12	8	3	Nb	<0.001	<0.001	<0.001
F	<0.02	<0.01	<0.01	Mo	<0.003	<0.003	<0.003
Na	<0.002	<0.001	<0.002	Pd	-	-	-
Mg	<0.003	<0.003	<0.002	Ag	<0.009	<0.007	<0.008
Al	Matrix	Matrix	Matrix	Cd	<0.02	<0.01	<0.02
Si	0.2	0.1	0.2	In	<0.005	<0.01	<0.003
P	<0.003	<0.002	<0.002	Sn	<0.03	<0.02	<0.03
S	<0.003	<0.003	<0.003	Sb	<0.009	<0.006	<0.007
Cl	0.006	0.004	0.003	Te	<0.009	<0.007	<0.008
K	<0.02	<0.02	<0.02	I	<0.004	<0.003	<0.003
Ca	<0.03	<0.03	<0.03	Cs	<0.001	<0.001	<0.001
Sc	0.05	0.05	0.05	Ba	<0.007	<0.001	<0.001
Ti	0.09	0.1	0.07	La	<0.001	<0.0007	<0.001
V	0.08	0.09	0.07	Ce	<0.001	<0.0007	<0.0009
Cr	0.02	0.02	0.03	Hf	<0.003	<0.002	<0.003
Mn	0.04	0.05	0.05	Ta	-	-	-
Fe	0.2	0.2	0.3	W	<0.004	<0.003	<0.003
Co	<0.001	<0.0006	<0.0007	Pt	<0.01	<0.01	<0.01
Ni	0.01	0.007	0.03	Au	<0.2	<0.2	<0.2
Cu	0.1	0.1	0.1	Hg	<0.04	<0.03	<0.03
Zn	0.1	0.09	0.1	Tl	<0.01	<0.008	<0.008
Ga	<0.007	<0.005	<0.006	Pb	<0.004	<0.003	<0.004
Ge	<0.01	<0.01	,0.01	Bi	<0.005	<0.004	<0.004
As	<0.007	<0.003	<0.004	Th	<0.001	<0.001	<0.001
Se	<0.1	<0.1	<0.05	U	<0.001	<0.001	<0.001

The Al 174 was initially doped with copper impurity; the shifts and shapes of the freezing and melting curves were investigated as the copper concentration was increased. This cell was regularly cross-compared, using platinum resistance thermometers, to the reference aluminium cell at the freeze peak. This ensures the reliable measurement of the small temperature shift due to the trace impurities, and not from any instability in the PRTs. A comparison of the melting curves, before and after doping with increasing copper concentration, is shown in Figure 3.

From comparison of the freeze peaks, at 8.3 ppmw of copper, the initial freezing point value did not change from the original aluminium temperature (which was slightly surprising – perhaps some unexpected segregation of the impurity had occurred). However, as shown in Figure 3, the offsets at the estimated liquidus point of the melting curves were decreased (subsequent melting /freezing may have provided sufficient dispersion of the impurity as that it produced an effect). For the Al 174 with the copper at 16.2 ppmw concentration, depressing of the freezing temperature was observed to be 2.9 mK (expected decrease was ~3 mK). The latter results are in reasonable agreement with the previous data [2].

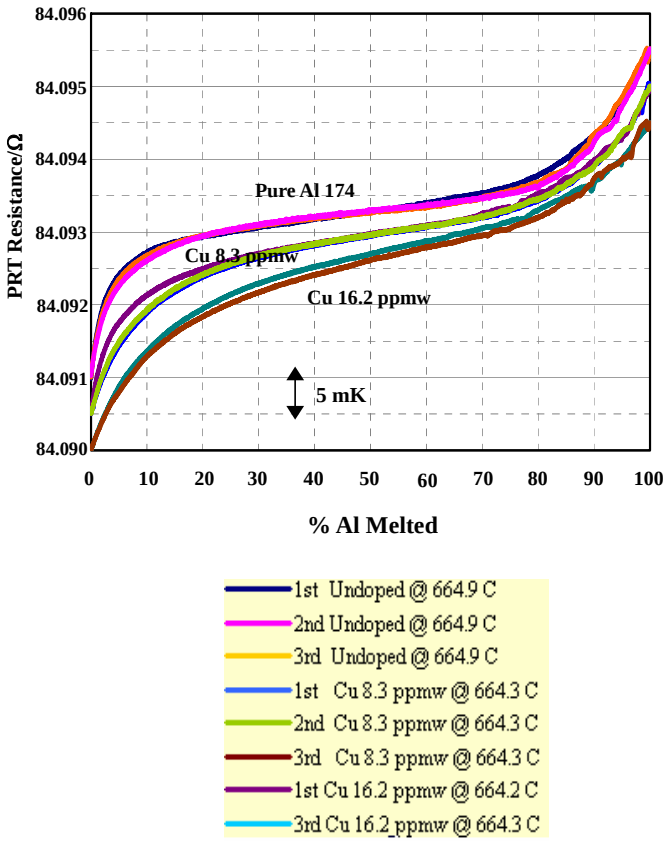

Figure 3 Melting curves of "Al 174" high purity aluminium fixed-point and the shift of these curves after doping the aluminium with increasing concentrations of copper, plotted as a function of aluminium percentage melted. The curves have been normalised to an approximate percentage melted (the best means for this normalisation is still under study).

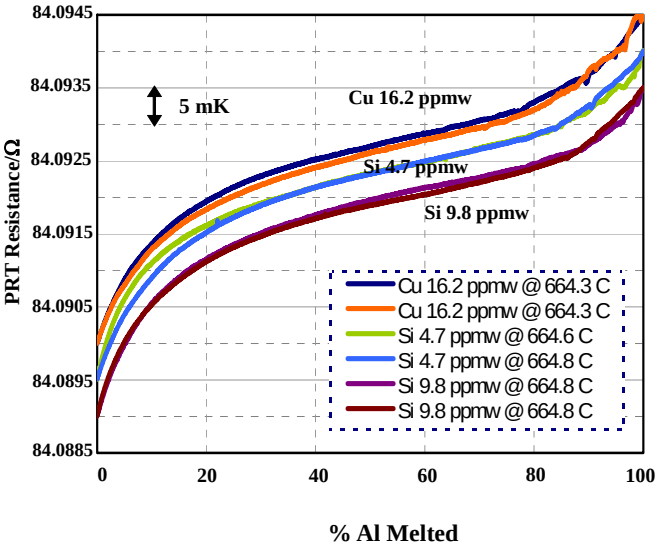

Figure 4 Melting curves of "Al 174" aluminium fixed-point (after further doping with increased amounts of Si) plotted as a function of aluminium percentage melted. The curves have been normalised to an approximate percentage melted (the best means for this normalisation is still under study).

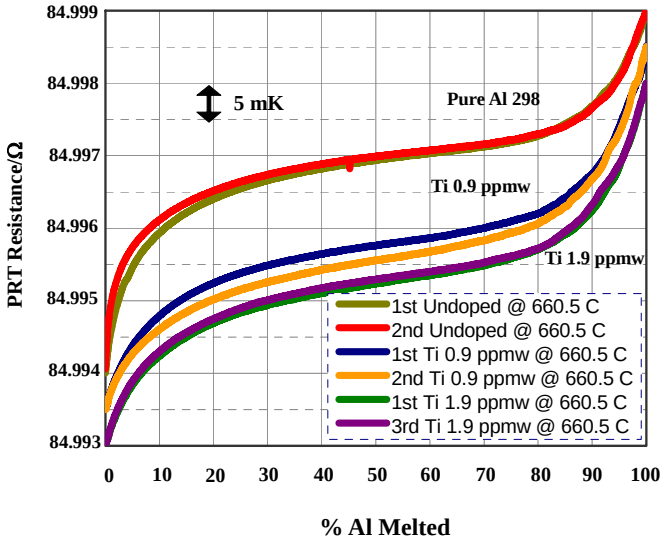

Figure 5 Melting curves of "Al 298" aluminium fixed-point (after doping with increasing Ti content) plotted as a function of aluminium percentage melted. The offsets of the curves have not been corrected for thermometer shifts – so only the shape is relevant. Separate corrections have been applied to calculate the offsets – see text.

The results obtained for doping the Al 174 cell with silicon impurity are presented in Figure 4. For this Al-Si system, the sample with silicon at 4.7 ppmw shows a decrease for the whole of the melting curve. From the freeze peak, it is about 3.2 mK lower than the previous aluminium doped with the copper impurity. Although the results of the first silicon doping (4.7 ppmw) agreed with the previous data [2] at the freeze peak, the outcome of Al 174 doped with the silicon at 9.8 ppmw did not give the results as expected at the freeze peak. However, the offsets and shapes of the melting curves showed the depression of the temperature for the whole curve. It seems freezes may not always show up impurities. (Although that complicates these experiments it does at least confirm the choice of freezes for use in ITS-90).

A similar experimental procedure was followed for the other Al 298 cell, but using titanium as an impurity. This is expected to elevate the transition temperature. The melting and freezing curves, before and after doping Al 298 with the impurity, are presented in Figure 5.

The shapes of the melting curve are repeatable, suggesting the thermometer and ingot are stable during the phase transition. However, between transitions the resistance values of the PRT, as shown in Figure 5, have dropped. We attribute this to PRT instabilities on cycling to high temperatures. Because measurements of the PRTs at the water triple point did not shift in proportion, the W values obtained from the experiment also moved. (W is the ratio of the thermometer resistance at the fixed point to the resistance at the water triple point). It was found that the resistance values were more reproducible than W values. (Hence the reason why resistance values were selected to show on all figures) The offsets of the melting curves need to be corrected following "re-calibration" of the PRTs by comparison of the peak of the freezing curves against the NPL reference Al cell. All freezing values increased following the introduction of the impurities, as expected. Considering the sample doped with 0.9 ppmw titanium, the freeze peak was elevated by about 3.3 mK from initial curve. The next freeze peak at 1.9 ppmw titanium increased to a total of 5.2 mK. Therefore, it is summarised that the titanium impurity increases the Al 298 temperature by 3.2 mK/ppmw.

4. Conclusion

The results of this work confirmed the influence of very low-level impurities on the freezing/melting curves of the aluminium fixed point. The temperature change of the freezing and melting curves of the aluminium fixed-point was affected by the amount of copper (-0.43 mK/ppmw), silicon (-0.85 mK/ppmw), and titanium (+3.2 mK/ppmw) doping. From the experiment, the melting/freezing curves of the aluminium fixed point decreased and increased in temperature in line with expectation as increasing amounts of trace impurity dopants were introduced. (The results are within 20% or better of the extrapolated values). This experiment shows that standard non-adiabatic temperature measurements can be used to determine temperature offsets. Standard procedures appear to mix pre-existing impurities uniformly. However, stability of thermometers remains a problem at this temperature and as comparison of the peak of the doped fixed point is only possible with one thermometer over a short time, then correcting for this is very time consuming.

5. Future Work

In the future, the aluminium sample will be re-analysed by GD-MS after doping to measure the detected concentration of the impurity elements. This analysis will be compared with the GD-MS results before doping, to confirm the increased impurity concentration in the aluminium cells. Thereafter, the GD-MS results will be used to calculate the theoretical temperature offset predicted by a special thermodynamic impurity model, i.e. the “MTDATA” program [5] developed by the materials-science department of NPL. From the MTDATA analysis, the theoretical and actual measured melting curve shapes, of the aluminium fixed point, before and after doping will be compared.

6. Acknowledgements

One of the authors (P Petchpong) would like to thank the Temperature section of the UK National Physical Laboratory (NPL) for providing all equipment and the Mass section of the NPL for supplying the mass measurements of both the aluminium metal ingots and also the trace impurities for doping. This work was financially supported by the UK Department for Innovation, Universities, and Skills (DIUS) and through a scholarship (for P Petchpong) from the Royal Thai Government.

REFERENCES

1. H. Preston-Thomas. The International Temperature Scale of 1990 (ITS-90). *Metrologia.* 1990, 27: 3–10.
   H. Preston-Thomas. The International Temperature Scale of 1990 (ITS-90). *Metrologia.* 1990, 27: 107(Erratum).
2. M. Hansen. Constitution of Binary Alloys. 2nd edition, New York: McGraw-Hill, 1958.
3. J. Ancsin. Impurity dependence of the aluminium point. *Metrologia.* 2003, 40: 36.
4. S. Rudtsch, M. Fahr, J. Fischer, T. Gusarova, H. Kipphardt and R. Matschat. High-Purity Fixed Points of the ITS-90 with Traceable Analysis of Impurity Contents. *International Journal of Thermophysics* 2008, 29: 139-150.
5. R.H. Davies, A.T. Dinsdale, J.A. Gisby, J.A.J. Robinson and S.M. Martin. MTDATA - thermodynamic and phase equilibrium software from the national physical laboratory. *CALPHAD.* 2002, 26(2): 229 – 27.

Impurity Effects on the Tin Fixed-Point Temperature

Patchariya Petchpong[1], David I Head[2], Joe Y. H. Au[1]

(1. Advanced Manufacturing and Enterprise Engineering Group, Brunel University, Uxbridge, Middlesex UB8 3PH, UK;
2. National Physical Laboratory, Hampton Road, Teddington, Middlesex TW11 0LW, UK)

Abstract: The purpose of this work is to study the effect of trace impurities on the temperature realised by a high purity (99.9999%) tin fixed-point. This is to improve the measurement of the temperature shift caused by low level impurity dopants, to test the interpolation of previous tin binary alloy systems [1] obtained using relatively high levels of impurities and to realise the change in shape of the melting transition for subsequent comparison with theory. The experiments and results revealed the shift of the melting and freezing curves of the initially "pure" tin cell by -0.71 mK/ppmw of cobalt, -0.18 mK/ppmw of lead and +0.06 mK/ppmw of antimony. It also confirmed the reproducibility of the temperature measurements and melting transition shape in this fixed-point.

Key words: Tin Fixed-Point Temperature; Impurity; Doping; Melting/Freezing Curves; International Temperature Scale of 1990 (ITS-90)

CLC number: TB94 Document code: A Article ID: 1000-1158(2008)04A-0000-00

1. Introduction

The freezing point of high purity tin (231.928 °C) is one of a series of fixed-points in the International Temperature Scale of 1990 (ITS-90) [1]. The accurate realisation of the tin fixed-point temperature, which plays an important role in the provision and dissemination of standard temperature values, strongly depends on the purity level of the tin material used. In this work, high purity (99.9999%) tin fixed-point cells were doped with a variety of impurities in order to study the offsets of their freezing temperatures and changes in the melting shape caused by those impurities. The trace impurities (of order ~1-20 parts per million by weight (ppmw)) of cobalt, lead, and antimony metals were selected for addition to the high purity tin samples. In previous work the Sn-X binary alloy system was studied at larger fractions of impurity X [2], and the tin temperature was interpolated to be depressed by 0.60 mK/ppmw and 0.133 mK/ppmw for cobalt and lead impurity, respectively. Conversely, the tin transition plateau was raised by 0.128 mK/ppmw of antimony impurity. Antimony is the only impurity that is known to elevate the liquidus temperature of tin. Our measurements using lower concentrations of dopants planned to test the interpolation of this previous data obtained using relatively high levels of impurities. A better understanding of low-level impurities would help reduce the uncertainty budget of the tin fixed-point realisation, where impurities are the biggest contribution to the uncertainty budget.

Several measurements of the effects of impurities on the tin fixed-point have already been done [3-7]. However, this more recent work (but using other dopants) has been done using special adiabatic furnaces and specially designed cells [6]. In this paper we produce such measurements using standard NPL equipment, under standard conditions, as used in most national measurement institutes around the world.

Received: 2008-00-00
Corresponding e-mail address: david.head@npl.co.uk

2. Experimental Details

In this study, two standard purity (nominally 99.9999%) tin fixed-point cells were used to study the influence of trace impurities on the equilibrium tin temperature. Both standard tin cells were named after their donors as "Spanish tin" and "Mini Isotech tin"; these tin ingots were donated by Centro Espanñol De Metrología (CEM), Spain, and the Isothermal Technology Company, respectively. For the Spanish tin cell, the ingot was contained in a graphite crucible of length 200 mm and diameter 45 mm, which was held in a new container made from silica of length 470 mm and diameter 49 mm. Cells like this, containing up to about 1 kg of pure metal, are used in most National Metrology Institutes (NMIs) around the world. For the second cell, named "Mini Isotech tin", the ingot was smaller than normal i.e. it is 110 mm in length, 26 mm in outer diameter, and had an inner diameter of 16 mm. The total mass of tin sample put in this cell was approximately 240 g. The Mini Isotech tin ingot was housed inside a high purity graphite crucible contained within a quartz tube. These two "open" tin fixed-point cells were filled with high purity argon gas at a pressure of 101.3 kPa at the fixed-point temperature.

Thereafter the two tin cells were installed in three-zone furnaces set for maintaining an even temperature distribution around the tin cell. The furnace temperature is set below or above the equilibrium tin fixed-point with settings for the cell to be frozen and melted, respectively. This means that the conditions are only quasi-adiabatic, but this was the desired way to carry out the tests, as these are the "normal" conditions for the realisation of fixed-points. The freezing and melting transitions of each initially "pure" tin cell were measured at least three times.

An Automatic Systems Laboratories (ASL) Model F18 ac resistance bridge was used to measure the resistance ratio values of 25 Ω platinum resistance thermometers in the two tin fixed-point cells, against 100 Ω standard resistors.

After completing the initial freezing and melting measurements using the high purity tin, a total of three small pieces were removed from three areas of the tin ingot; namely the top, the middle and the bottom, with a small cleaned hacksaw. These pieces were then analysed using glow discharge mass spectrometry (GD-MS) at the National Research Council of Canada (NRC) in order to investigate the quantity and distribution (or uniformity) of the impurity elements within the "pure" tin, before deliberate doping. Subsequently the impurity levels in the tin samples, after doping, will be re-measured by using GD-MS again.

After the resistance ratio of the PRT in pure tin was obtained, masses of pure cobalt (99.99+%), lead (99.99+%), and antimony (99.5%), employed as impurities for doping, were weighed by a microbalance (Mettler AT20). The originally pure tin ingots were doped with three types of impurities; namely cobalt and lead in the Spanish cell and antimony in the Mini cell; total concentrations as follows (in ppmw): Co ~5.5 and ~7.4, Pb ~7.9 and ~31.4, Sb ~7.8 and ~23.2. Each type of the impurity metals was put on the top, the middle, and the bottom of the ingots.

After each doping, the ingots were re-inserted back into the graphite crucibles and the silica containers. Then the assembled cells were put into the furnaces and set at 8 ^{o}C above the tin melting temperature for several days to ensure a good mixing of the impurities within the tin. Three freezing and melting plateaus after each doping were realised. During this time the doped cells were compared against a new sealed tin reference cell by cross-transfer of the PRTs. This allowed the measurement of how much the temperature of the doped cells dropped (increased) from the initial "pure" tin value. Cross comparison to a reference cell allows the removal of any shift due to any instability in the PRT itself, which is possible at this level of resolution.

3. Results and Discussions

A set of three melting curves from the high purity Spanish tin fixed-point cell, before the doping process, is shown in Fig.1. The melting curves take different lengths of time depending on the furnace offset temperature. (Examples of high purity tin freezing curves, before doping, are shown in Fig. 3).

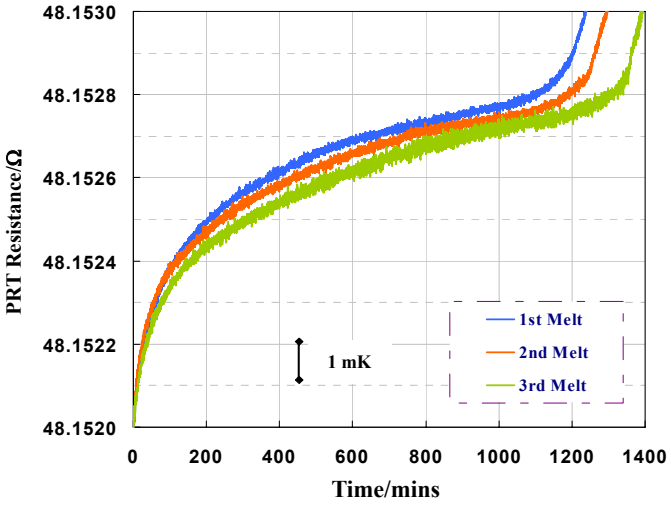

Fig. 1 Three melting curves of a high purity undoped "Spanish" tin fixed-point plotted as a function of time. The furnace setting point for all three measurements is set at the same temperature (nominally half a degree above the melting point).

All the melting and freezing curves of the undoped Spanish tin confirm the reproducibility of the measurements of this tin fixed-point cell.

After comparison with the reference tin cell, the initial freezing temperature of the Spanish cell was found to be 3 mK lower than the reference tin cell. That means the Spanish tin ingot contained some pre-existing contamination affecting its freezing and melting temperatures (this was expected, and part of the reason why it could be used for doping, which effectively destroys the value of the cell). We understand that the influence of each impurity in the host material remains independent of each other at low concentrations. The magnitude of each effect on the temperature depends on both the species type and the amount of that particular species and the total temperature change is the sum of the individual effects, taking account of any sign.

Elemental analysis of the Spanish tin fixed-point cell, using the GD-MS technique, was carried out before deliberate doping the tin cell with any impurity elements.

Tab. 1 GD-MS analysis results of the initial impurity concentration of the "Spanish" tin fixed point (NRC report number: 30337R1). Tin samples were cut from three areas of the ingot, which are the top, the middle, and the bottom. These elements were detected in term of mass fraction (in parts per billion by weight, ppbw). The uncertainty is quoted as a "factor of 2", though this is probably a conservative overestimate.

Element	Top	Middle	Bottom	Element	Top	Middle	Bottom
	ppbw				ppbw		
Li	<0.3	<0.4	<0.3	Br	<25	<20	<25
Be	<0.1	<0.2	<0.1	Rb	<0.3	0.9	<0.3
B	<0.3	<0.4	<0.2	Sr	<0.2	<0.3	<0.2
C	1500	2100	1300	Y	<0.2	<0.2	<0.2
N	85	500	170	Zr	<0.2	<0.2	<0.2
O	290	880	430	Nb	<0.2	<0.3	<0.2
F	<1	<1	<0.6	Mo	<1	<1	<1
Na	<0.3	<0.4	<0.2	Pd	-	-	-
Mg	<0.3	<0.3	<0.3	Ag	<2	<2	<2
Al	<0.2	<0.2	<0.2	Cd	<20	<30	<20
Si	0.8	0.3	0.3	In	3600	4200	4000
P	2	<0.3	0.8				
S	400	120	550	Sb	<45	<50	<35
Cl	0.8	3	<0.4	Te	<2	<3	<3
K	<45	<45	<45	I	<6	<6	<4
Ca	<5	<6	<5	Cs	<0.5	<0.5	<0.6
Sc	<0.2	<0.3	<0.2	Ba	<0.2	<0.3	<0.4
Ti	<0.1	<0.2	<0.2	La	<0.3	<0.2	<0.4
V	<0.1	<0.1	<0.1	Ce	<0.2	<0.2	<0.3
Cr	<0.4	<0.6	<0.4	Hf	<0.6	<0.8	<0.6
Mn	<0.2	<0.3	<0.3	Ta	-	-	-
Fe	<4	<4	<3	W	<0.6	<0.7	<0.5
Co	<100	<100	<100	Pt	<2	<2	<2
Ni	<16	<20	<17	Au	<10	<10	<10
Cu	<1	<1	<1	Hg	<8	<10	<7
Zn	<2	<2	<2	Tl	<1	<1	<1
Ga	<0.8	<1	<0.8	Pb	14	10	20
Ge	<2	<2	<2	Bi	<0.5	<0.7	<0.5
As	<10	<12	<13	Th	<0.2	<0.2	<0.2
Se	<80	<80	<40	U	<0.3	<0.3	<0.7

Tab. 1 lists the impurity elements detected in three areas of the tin metal ingot. The uncertainty of this GD-MS analysis is considered to be accurate within a factor of two of the values obtained, at a confidence level of 95% though there is anecdotal evidence that the results are more accurate than quoted. GD-MS is the best technique (most sensitive) available at present to determine the amount of the impurities. The pre-existing impurities would contribute to the initial 3 mK offset with respect to the reference cell. From the GD-MS results we see that the impurity levels are the same throughout the cell, which shows the homogeneity of the impurity concentration (within the uncertainty quoted). This indicates that the tin is sufficiently well mixed after properly melting of the sample. In future only one sample will need to be cut out for analysis after doping. (Cutting out of samples is a risky procedure).

The offsets and shapes of the melting and freezing curves for the undoped and doped samples of tin are shown in Fig. 2 and 3. Melting curves are dependent on the thermal history of the sample. This is a result of changes in impurity segregation during the former freezing process. If impurities are left molten for a long time we assume they will become uniformly distributed. However, if the freezing process takes a long period, there will be time for segregation to occur: this does not happen if the sample is frozen quickly. Therefore, all melting curves in this work were measured following a fast freeze. (approximately 1 hr).

The results as illustrated in Fig. 2 and 3 confirm that cobalt depresses the phase transition temperature as expected. The peak of the freezing curves after doping had dropped by ~3.7 mK and ~5.4 mK (based on our initial analysis) for concentrations of 5.5 ppmw and 7.4 ppmw of cobalt, respectively. According to Physikalisch-Technische Bundesanstalt (PTB) - the German national metrology measurement institute - the peak of the freeze is the most reproducible part of the freezing curve, from which good results can be obtained. The reason is that the maximum temperature does not strongly depend on the homogeneity and stability of the furnace temperature [8].

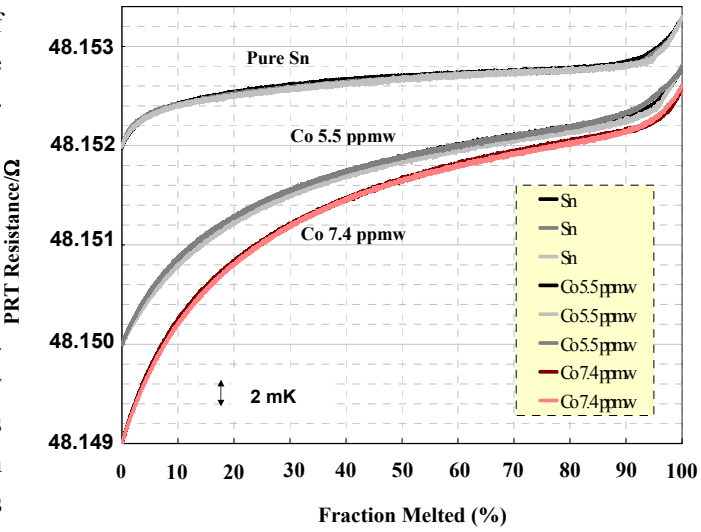

Fig. 2 Three melting curves of high purity "Spanish" tin and the shift of these curves after doping the tin with increasing concentration of cobalt impurities. The curves have been normalised to an approximate percentage melted (the best means for this normalisation is still under study).

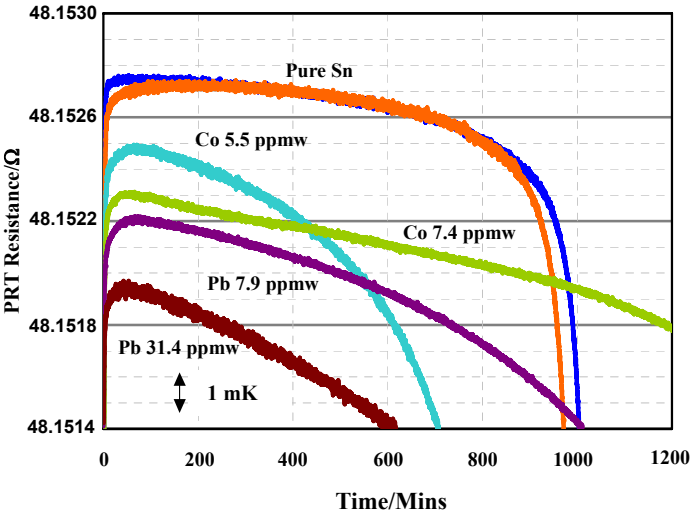

Fig. 3 Example of high purity tin freezing curves and the shift of these curves after doping the tin with increasing concentrations of cobalt and lead impurities, plotted as a function of time. The end of the curve tin doped with 7.4 ppmw cobalt continues off the graph due to the small furnace temperature offset.

Fig. 4 shows the significant impurity dependence of the tin melting point affected by a low concentration of lead. (At 7.9 ppmw lead in tin the freezing maximum temperature decreased by ~ 1.4 mK, while at 31.4 ppmw the curves had dropped by ~ 4.7 mK compared with the reference high purity tin cell).

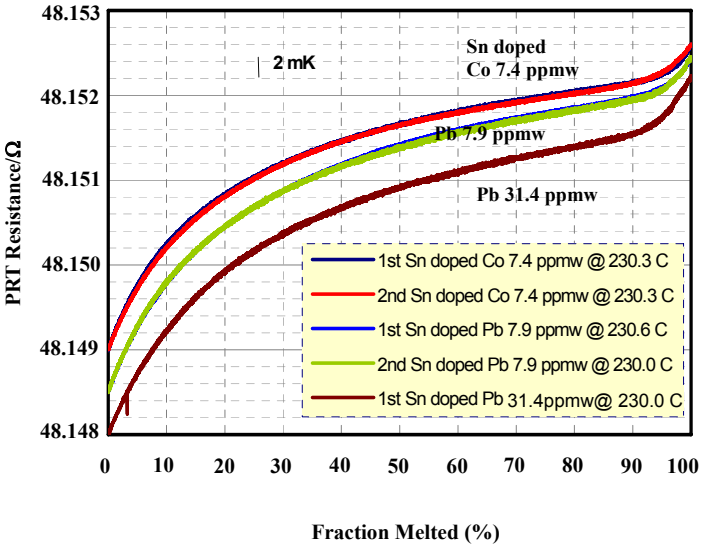

Fig. 4 Melting curves of "Spanish Tin" after doping with low level concentrations of lead. The curves are compared with the previous curves of Spanish tin doped with cobalt. The temperatures are nominal settings of the furnace.

The results obtained after doping with cobalt and lead support the previous data that the temperatures of the fixed point were affected at these low impurity levels. Moreover, their curves, before and after doping, confirm the reproducibility of the temperature measurements in these fixed-point cells.

In Fig. 5, the offset of the "Mini tin" fixed point, after doping with low levels of antimony, is presented. The melting temperature of the 7.8 ppmw antimony doped tin is higher than for the "pure" Mini tin. It indicates that at low levels, antimony elevates the melting and freezing temperatures although the temperature change is less than expected. After comparison with the reference tin cell, the peak of the freezing curves after doping had increased ~ 0.5 mK. However for the antimony doping very unusual melting traces have been produced – with a pronounced bump/ increase in the temperature for several hours at the start of the melt, before settling back (antimony is expected to increase the temperature of the whole plateau). PTB has also reported "bumps", but of a much shorter duration [5]. It may be the result of non-uniform distribution of the antimony, but how that would produce this curve shape, and why it is roughly reproducible remains unexplained.

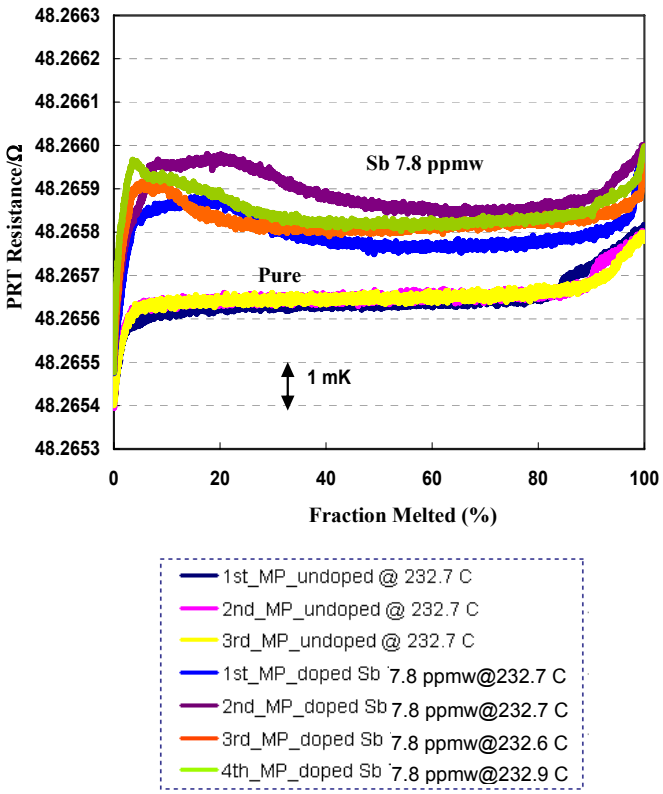

Fig. 5 PRT resistance value changing for "Mini Tin" after doping with antimony as a function of the approximate tin percentage melted.

4. Conclusions

Excepting Sb, the equilibrium curves of the tin fixed-point decreased roughly in line with expectations derived from interpolation of previous experiments as increasing amounts of impurities were introduced; the measured rates are as follows: Co -0.71; Pb -0.18; and Sb +0.06 in units of mK/ppmw. These are within 30% of the extrapolated values.

This experiment shows that standard non-adiabatic temperature measurements can be used to determine temperature offsets. Standard procedures appear to mix pre-existing impurities uniformly with the possible exception of antimony.

5. Future Work

In the future, the tin sample will be re-analysed by GD-MS after doping to detect the measured concentration of the impurity elements. This analysis will be compared with the GD-MS results before doping, to confirm the increasing cobalt, lead and antimony contents in the tin cells. Furthermore, the GD-MS results will be used to confirm or not the calculated impurity level based on mass measurements. Assuming this we will calculate the theoretical temperature offset, and melting shape predicted by a special thermodynamic impurity model, i.e. the "MTDATA" program [9] developed by the materials-science department of NPL. The theoretical and actual measured melting curve shapes, of the tin fixed point, before and after doping will be compared.

6. Acknowledgements

One of the authors (P Petchpong) would like to give special thanks to the Temperature section of the UK National Physical Laboratory (NPL) for providing all equipment and the Mass section of the NPL for supplying the mass measurements of both the tin metal ingots and the impurity dopants. We also gratefully acknowledge the Temperature division of Centro Espanñol De Metrología (CEM), Spain, and the company Isothermal Technology for the donation of the standard tin fixed-point cells. This work was financially supported by the UK Department for Innovation, Universities, and Skills (DIUS) and through a scholarship (for P Petchpong) from the Royal Thai Government.

REFERENCES

1. H. Preston-Thomas. The International Temperature Scale of 1990 (ITS-90). *Metrologia.* 1990, 27: 3–10.
   H. Preston-Thomas. The International Temperature Scale of 1990 (ITS-90). *Metrologia.* 1990, 27: 107(Erratum).
2. M. Hansen. Constitution of Binary Alloys. 2nd edition, New York: McGraw-Hill, 1958.
3. J.J. Connolly and J.V. McAllan. Limitations on Metal Fixed Points Caused by Trace Impurities. *Metrologia.* 1980, 16: 127.
4. S. Stolen and F. Gronvold. Effects of trace impurities on metal fixed points: antimony and bismuth in Tin. *J. Chem. Thermodyn*. 1999, 31: 379.
5. J. Zhang, S. Rudtsch and M. Fahr. The Influence of Antimony on the Tin Point. *International Journal of Thermophysics* 2008, 29: 151-157.
6. J. Ancsin. Impurity dependence of the Sn-point and the properties of the Sn–Fe 'eutectic'. *Metrologia.* 2008, 45: 16-20.
7. B. Fellmuth and K.D. Hill. Estimating the influence of impurities on the freezing point of tin. *Metrologia.* 2006, 43: 71-83.
8. S. Rudtsch, M. Fahr, J. Fischer, T. Gusarova, H. Kipphardt and R. Matschat. High-Purity Fixed Points of the ITS-90 with Traceable Analysis of Impurity Contents. *International Journal of Thermophysics* 2008, 29: 139-150.
9. R.H. Davies, A.T. Dinsdale, J.A. Gisby, J.A.J. Robinson and S.M. Martin. MTDATA - thermodynamic and phase equilibrium software from the national physical laboratory. *CALPHAD.* 2002, 26(2): 229 – 27.

SICE Annual Conference 2008
August 20-22, 2008, The University Electro-Communications, Japan

Influence of a Trace Impurity on Tin Fixed Point Plateaus

Patchariya Petchpong[1], David I. Head[2], Joe Y. H. Au[1]

[1]Advanced Manufacturing and Enterprise Engineering Group, Brunel University, Uxbridge, Middlesex UB8 3PH, UK

(E-mail: patchariya.petchpong@brunel.ac.uk)

[2]National Physical Laboratory, Hampton Road, Teddington, Middlesex, TW11 0LW, UK

(E-mail: david.head@npl.co.uk)

Abstract: The effect of trace cobalt impurity on the realisation of a high purity (99.9999%) tin fixed-point is presented. The aim is to improve the measurement of the temperature shift caused by low level impurity dopants, to test the interpolation of previous binary alloy systems [1] obtained using relatively high levels of impurities. The experiments and results, described below, revealed the shift of the melting and freezing curves of an initially "pure" tin cell by -0.71 mK/ppmw of cobalt, and confirmed the reproducibility of the temperature measurements in this fixed-point cell.

Keywords: Tin fixed-point temperature, International Temperature Scale of 1990 (ITS-90), Thermometry

1. INTRODUCTION

The International Temperature Scale of 1990 (ITS-90) defines a precise calibration procedure [2] using standard platinum resistance thermometers (SPRTs), measured at the reference temperature of metallic fixed-points, to define an agreed temperature scale accurate to better than 1 mK. The influence of chemical impurities on the fixed-point is one of most important contributions to the uncertainty budgets of the fixed-point measurements. If the impurities and their effects on the pure fixed-point metals were identified, the total impurity correction to the temperature of the metal fixed-point would be more precise and reliable.

In this work, the freezing point temperature of high purity tin (at 231.928 °C), one of a series of metallic fixed-points of the ITS-90, is investigated in order to study the offsets of the melting/freezing temperature of tin due to low levels of cobalt impurity content. In prior experiments on binary alloy systems [1], the fixed-point temperature of tin at very low impurity level is interpolated to be decreased by 0.60 mK/ppmw of cobalt.

Therefore, the aim of this work is to test the interpolation of previous data; all of which were obtained from relatively high impurity concentrations. Moreover, an improved understanding of low level impurities would allow one to reduce the uncertainty budget component, which is attributed to the influence of chemical impurities for the realisation of the tin temperature fixed-point. Several previous researchers have studied the effect of impurities on the equilibrium plateaus of the tin fixed-point temperature [3-6]. Furthermore, this type of work (but using other dopants) has already been done using special adiabatic furnaces [6]. In this paper we try to reproduce such measurements using standard NPL equipment, which provides a standard controlled condition, as used by national measurement institutes (NMIs) worldwide. This is important in ensuring the inter-changeability of temperature measurements around the world.

2. EXPERIMENTAL PROCEDURE

An original nominally 99.9999% pure tin fixed-point ingot was used to realise the reference standard temperature. Cells like this, containing up to about 1 kg of pure metal, are used in most NMIs around the world. This "open cell" was filled with argon gas with the pressure set at 101.3 kPa. A three-zone furnace was used for maintaining the temperatures at the equilibrium tin fixed-point, but the set point temperature was offset by different amounts for the ingot to be frozen or melted. This means that the conditions are only quasi-adiabatic, but this was the desired way to carry out the tests, as these are the "normal" conditions for the realisation of fixed-points. A 25 Ω platinum resistance thermometer (PRT) and a 100 Ω standard resistor were used to realise the measurements by reading their resistance ratio using an Automatic Systems Laboratories Model F18 ac resistance bridge. Each original freezing and melting temperature curve was repeated a couple of times. The initial freezing temperature of this "high purity" tin cell was calibrated several times against a "never doped" reference tin cell by direct comparison of the thermometers readings in two cells.

After completion of the initial freezing and melting measurements, but just before doping small samples of tin were cut from the top, the middle, and the bottom of the ingot. These pieces were sent for chemical analysis to detect the distribution of any background impurity elements by using glow discharge mass spectrometry (GD-MS) at the National Research Council of Canada (NRC). This is the "state-of-the-art" technique to measure any impurities in the "pure" metal fixed-point cell. The lower limit of detection is down to the ppb level.

After the equilibrium resistance ratio of the PRT in pure tin was obtained, the masses of cobalt (99.99+% pure) employed as impurities for doping were weighed

using a microbalance (Mettler AT20). The originally pure tin sample was doped with cobalt at the top, the middle, and the bottom by increasing the concentrations of cobalt (in ppmw) from ~5.5 to ~7.3. The whole sample was held at 8 °C above the tin melting temperature for several days to ensure a good mixture of tin and cobalt. Three freezing and melting plateaus at each doping were realised. Finally, the calibration by comparison between the doped tin and reference tin cells was carried out to investigate how much the fixed-point temperature dropped from the initial pure tin value.

3. DISCUSSION

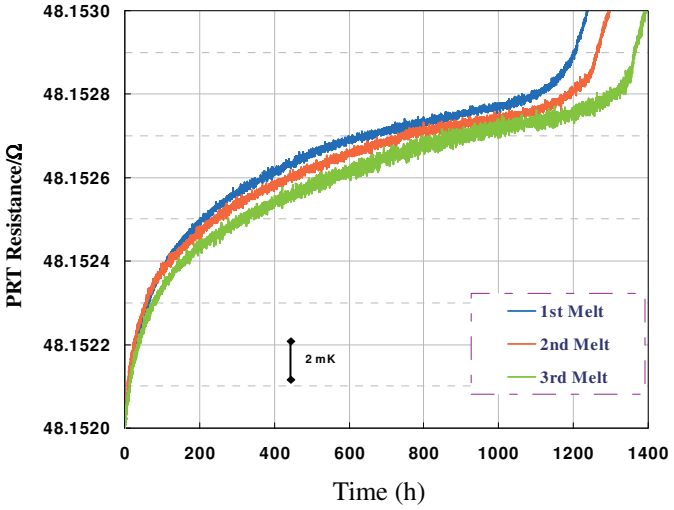

Figure 1 Three melting curves of a high purity tin fixed-point plotted as a function of time. The furnace setting point for all three measurements is set at the same temperature (nominally half a degree above the melting point).

A set of three melting curves of the high purity tin fixed-point cell, before the doping process, is shown in Figure 1. The melting curves take different lengths of time depending on the furnace offset temperature. (Examples of high purity tin freezing curves, before doping, are shown in Figure 3). All the melting and freezing curves of high purity tin confirm the reproducibility of the temperature measurements of this tin fixed-point cell. After calibration by comparison between two tin cells, namely this tin cell and a "never doped" reference tin cell, the initial freezing temperature of this cell was found to be 3 mK lower than the reference tin cell.

This result indicates that this tin cell already contains some impurities affecting its freezing temperature. We understand that the influence of each impurity in the host material remains independent of each other at low concentrations. The magnitude of each temperature effect depends on both the species type and the amount of that particular species and the total temperature change is the sum of the individual effects, taking account of any sign.

Therefore, it is necessary to carry out the elemental analysis of this tin fixed-point cell using the GD-MS technique, before doping the tin cell with any impurity elements in the next step of the procedure.

Table 1 The results of the GD-MS analysis of the initial "high purity" tin fixed point (NRC report number: 30337R1). The tin samples were cut from the three areas of the ingot, which are the top, the middle, and the bottom. These elements were detected in term of mass fraction (in parts per billion by weight, ppbw). The uncertainty is quoted as a "factor of 2", though this is probably a conservative overestimate.

Element	Top	Middle	Bottom	Element	Top	Middle	Bottom
Li	<0.3	<0.4	<0.3	Br	<25	<20	<25
Be	<0.1	<0.2	<0.1	Rb	<0.3	0.9	<0.3
B	<0.3	<0.4	<0.2	Sr	<0.2	<0.3	<0.2
C	1500	2100	1300	Y	<0.2	<0.2	<0.2
N	85	500	170	Zr	<0.2	<0.2	<0.2
O	290	880	430	Nb	<0.2	<0.3	<0.2
F	<1	<1	<0.6	Mo	<1	<1	<1
Na	<0.3	<0.4	<0.2	Pd	-	-	-
Mg	<0.3	<0.3	<0.3	Ag	<2	<2	<2
Al	<0.2	<0.2	<0.2	Cd	<20	<30	<20
Si	0.8	0.3	0.3	In	3600	4200	4000
P	2	<0.3	0.8				
S	400	120	550	Sb	<45	<50	<35
Cl	0.8	3	<0.4	Te	<2	<3	<3
K	<45	<45	<45	I	<6	<6	<4
Ca	<5	<6	<5	Cs	<0.5	<0.5	<0.6
Sc	<0.2	<0.3	<0.2	Ba	<0.2	<0.3	<0.4
Ti	<0.1	<0.2	<0.2	La	<0.3	<0.2	<0.4
V	<0.1	<0.1	<0.1	Ce	<0.2	<0.2	<0.3
Cr	<0.4	<0.6	<0.4	Hf	<0.6	<0.8	<0.6
Mn	<0.2	<0.3	<0.3	Ta	-	-	-
Fe	<4	<4	<3	W	<0.6	<0.7	<0.5
Co	<100	<100	<100	Pt	<2	<2	<2
Ni	<16	<20	<17	Au	<10	<10	<10
Cu	<1	<1	<1	Hg	<8	<10	<7
Zn	<2	<2	<2	Tl	<1	<1	<1
Ga	<0.8	<1	<0.8	Pb	14	10	20
Ge	<2	<2	<2	Bi	<0.5	<0.7	<0.5
As	<10	<12	<13	Th	<0.2	<0.2	<0.2
Se	<80	<80	<40	U	<0.3	<0.3	<0.7

The results of the impurity determination for the "high purity" tin by GD-MS analysis are reported in Table 1. This shows the impurity content measured in three areas of the tin ingot. This GD-MS analysis is considered to be accurate within a factor of two of the values obtained, at a confidence level of 95%. From the results we see that the impurity levels are the same throughout the cell (within the uncertainty quoted). This shows that the tin is sufficiently well mixed and that only one sample will need to be cut out for analysis after doping. (Cutting out of samples is a risky procedure).

Moreover, the indium impurity in the undoped "high

purity" tin ingot, as seen on Table 1, is the biggest component. In previous data [1], the tin melting/freezing temperature was shifted by –0.29 mK/ppmw of indium impurity content. It is therefore suggested that the shift of the initial freezing temperature of tin, compared with the reference tin cell, is partly caused by the amount of indium impurity. The other impurities found in the tin ingot (See Table 1) also contribute to the tin fixed-point temperature decrease (we have still to compare this with theoretical calculations using the "MTDATA" program [7].)

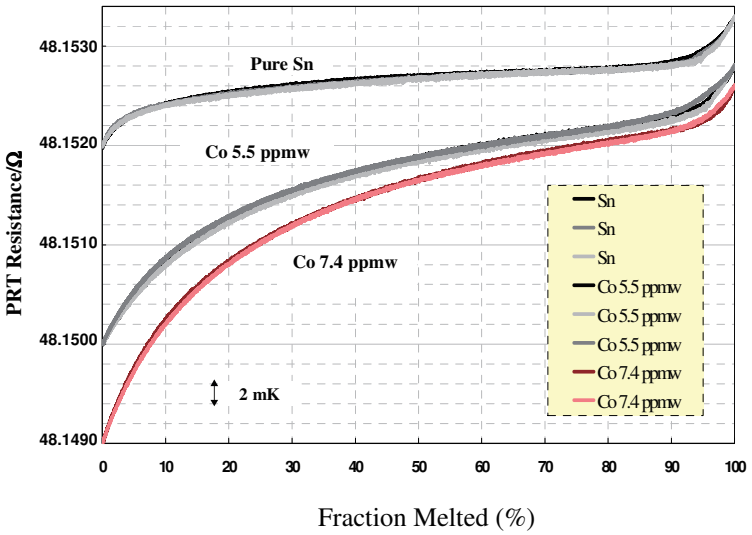

Figure 2 Melting curves of high purity tin and the shift of these curves after doping the tin with increasing concentration of the cobalt impurities. The curves have been normalised to an approximate percentage melted (the best means for this normalisation is still under study).

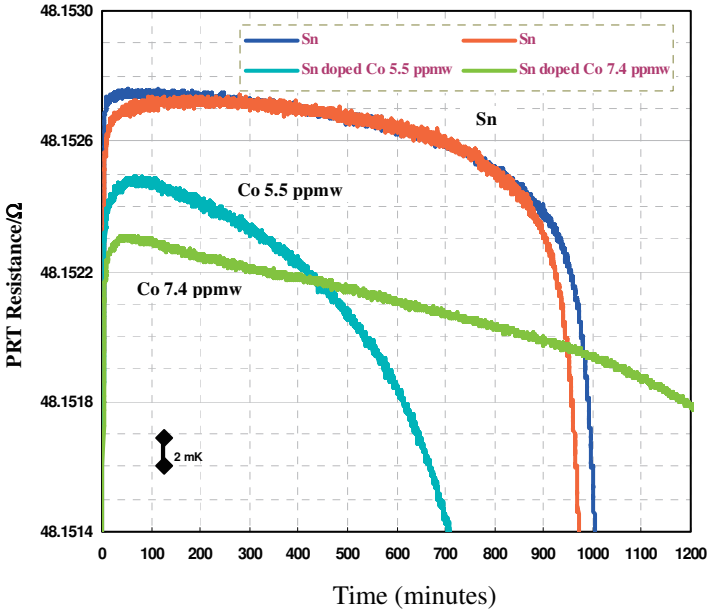

Figure 3 Example of high purity tin freezing curves and the shift of these curves after doping the tin with increasing concentrations of cobalt impurity, plotted as a function of time. The end of the curve tin doped with 7.4 ppmw cobalt continues off the graph due to the small furnace temperature offset.

The results as shown in Figure 2 and 3 confirm that cobalt depresses the phase transition temperature as expected. The peak of the freezing curves after doping had dropped by ~3.7 mK and ~5.4 mK (based on our initial analysis) for concentrations of 5.5 ppmw and 7.4 ppmw of cobalt, respectively. The equilibrium curves of the tin fixed point decreased in line with expectations derived from the interpolation of previous experiments [2]. As increasing amounts of impurities were introduced, the tin was shifted on average by -0.71 mK/ppmw of cobalt. The results obtained can be confused by shifts of the thermometer itself – to overcome this the PRT has to be checked in the reference cell. However this check is only practical periodically, so the timing of intervening thermometer shifts can affect the final analysis.

3. CONCLUSION

The temperature change of the freezing and melting curves of a tin fixed-point was affected by the amount of cobalt doping (-0.71 mK/ppmw). From the experiment, the melting/freezing curves of a tin fixed point decreased temperature in line with expectation as increasing amounts of cobalt were introduced. This experiment shows that standard non-adiabatic temperature measurements can be used to determine temperature offsets. Standard procedures appear to mix pre-existing impurities uniformly.

4. FUTURE WORK

In the future, the tin sample will be re-analysed by GD-MS after doping to detect the measured concentration of the impurity elements. This analysis will be compared with the GD-MS results before doping, to confirm the increasing cobalt content in the tin cell. Furthermore, the GD-MS results will be used to calculate the theoretical temperature offset predicted by a special thermodynamic impurity model, i.e. the "MTDATA" program [7] developed by the materials-science department of NPL. From the MTDATA analysis, the theoretical and actual measured melting curve shapes, of the tin fixed point, before and after doping will be compared.

5. ACKNOWLEDGEMENTS

One of the authors (P Petchpong) would like to special thanks to the Temperature section of the UK National Physical Laboratory (NPL) for providing all equipment and the Mass section of the NPL for supplying the mass measurements of both the metal ingot and cobalt impurity. We also gratefully acknowledge the Temperature division of Centro Espanñol De Metrología (CEM), Spain for the donation

of a standard tin fixed-point cell. This work was financially supported by the UK Department for Innovation, Universities, and Skills (DIUS) and through a scholarship (for P Petchpong) from the Royal Thai Government.

REFERENCES

[1] M. Hansen "Constitution of Binary Alloys", 2ed edition (New York: McGraw-Hill), 1958.

[2] H. Preston-Thomas "The International Temperature Scale of 1990 (ITS-90)", *Metrologia,* Vol. **27**, pp. 3-10, 1990.

H. Preston-Thomas "The International Temperature Scale of 1990 (ITS-90)", *Metrologia,* Vol. **27**, p. 107 (Erratum), 1990.

[3] J.J. Connolly and J.V. McAllan "Limitations on Metal Fixed Points Caused by Trace Impurities", *Metrologia,* Vol. **16**, pp. 127 - 132, 1980.

[4] S. Stolen and F. Gronvold "Effects of trace impurities on metal fixed points: antimony and bismuth in Tin", *J. Chem. Thermodyn,*Vol. **31**, pp. 379 - 398, 1999.

[5] J. Zhang, S. Rudtsch and M. Fahr "The Influence of Antimony on the Tin Point", *Int. J. Thermophys.*, Vol. **29**, pp. 151-157, 2008.

[6] J. Ancsin "Impurity dependence of the Sn-point and the properties of the Sn–Fe 'eutectic' ", *Metrologia,* Vol. **45**, pp. 16 - 20, 2008.

[7] R.H. Davies, A.T. Dinsdale, J.A. Gisby, J.A.J. Robinson and S.M. Martin, "MTDATA - thermodynamic and phase equilibrium software from the national physical laboratory"**,** *CALPHAD*, Vol. 26(2), pp. 229 – 271, 2002.

Appendix B
Uncertainty Budgets

The following data are taken from the document CCT/01-02 [Fellmuth et al., 2001].

Table B-1 PTB Uncertainty budgets, corresponding to the ISO guidelines, for the calibration of SPRTs at the defining fixed points

(Temperature equivalents in mK, *k*: coverage factor, 6N: 99.9999% etc.)

Fixed-point	e-H_2	Ne	O_2	Ar	Hg	H_20	Ga	In	Sn	Zn	Al	Ag
Highest purity	6N	5N	6N	6N	6N		7N	6N	6N	6N	6N	6N
Immersion depth / cm	2.5	2.5	2.5	2.5	2.5	19.0	26.0	16.0	15.0	16.0	16.8	18.5
Type B uncertainty components (mK)												
1. Chemical impurities, isotopes	0.17	0.16	0.19	0.14	0.06	0.031	0.06	0.25	0.31	0.54	0.40	0.65
2. Hydrostatic head correction	0.005	0.02	0.02	0.04	0.03	0.004	0.01	0.02	0.02	0.02	0.02	0.08
3. Error in gas pressure					0.01	0.005	0.01	0.10	0.08	0.12	0.30	0.30
4. Standard resistor	0.001	0.001	0.002	0.003	0.01	0.05	0.01	0.01	0.01	0.01	0.01	0.01
5. Bridge measurement	0.04	0.01	0.01	0.01	0.05	0.015	0.02	0.11	0.12	0.16	0.20	0.25
6. Uncertainty propagation from TPW	<0.001	0.001	0.01	0.02	0.05		0.08	0.09	0.11	0.15	0.20	0.28
7. Self-heating error	0.02	0.02	0.02	0.02	0.05	0.04	0.05	0.15	0.20	0.20	0.20	0.20
8. Heat-flux immersion error	0.02	0.02	0.02	0.02	0.02	0.01	0.01	0.20	0.10	0.10	0.10	0.10
9. Choice of fixed-point value	0.05	0.05	0.05	0.05	0.05	0.01	0.03	0.06	0.06	0.06	0.20	0.20
Type B combined (mK)	**0.18**	**0.17**	**0.20**	**0.16**	**0.12**	**0.074**	**0.12**	**0.40**	**0.43**	**0.64**	**0.65**	**0.87**
Type A uncertainty component (mK)	**0.05**	**0.05**	**0.05**	**0.05**	**0.05**	**0.03**	**0.05**	**0.20**	**0.15**	**0.15**	**0.30**	**0.30**
Standard combined uncertainty (mK)	**0.19**	**0.18**	**0.21**	**0.17**	**0.13**	**0.08**	**0.13**	**0.45**	**0.45**	**0.66**	**0.71**	**0.92**
Expanded combined uncertainty, $k = 2$ (mK)	**0.38**	**0.36**	**0.41**	**0.33**	**0.27**	**0.16**	**0.26**	**0.89**	**0.91**	**1.31**	**1.43**	**1.83**

Table B-2 Uncertainty budgets of the "normal category", corresponding to the ISO guidelines, for the calibration of SPRTs at the defining fixed points. The italic font style indicates that the values are different from those in Table B-1.

(Temperature equivalents in mK, *k*: coverage factor, 6N: 99.9999% etc.)

Fixed-point	e-H_2	Ne	O_2	Ar	Hg	H_20	Ga	In	Sn	Zn	Al	Ag
Highest purity	6N	5N	6N	6N	6N		7N	6N	6N	6N	6N	6N
Immersion depth / cm	2.5	2.5	2.5	2.5	2.5	19.0	26.0	16.0	15.0	16.0	16.8	18.5
Type B uncertainty components (mK)												
1. Chemical impurities, isotopes	*0.42*	*0.20*	*0.20*	*0.29*	*0.25*	*0.10*	*0.20*	*0.78*	*0.52*	*0.71*	*1.50*	*3.60*
2. Hydrostatic head correction	0.01	0.02	0.02	0.04	0.03	0.00	0.01	0.02	0.02	0.02	0.02	0.08
3. Error in gas pressure					0.01	*0.15*	0.01	*0.63*	*0.70*	*1.70*	*4.30*	*5.70*
4. Standard resistor	0.001	0.001	0.002	0.003	0.01	0.05	0.01	0.01	0.01	0.01	0.01	0.01
5. Bridge measurement	0.04	0.01	0.01	0.01	0.05	0.02	0.02	0.11	0.12	0.16	0.20	0.25
6. Uncertainty propagation from TPW	*<0.001*	*0.002*	*0.02*	*0.04*	*0.17*		*0.22*	*0.32*	*0.38*	*0.51*	*0.67*	*0.86*
7. Self-heating error	0.02	0.02	0.02	0.02	0.05	0.04	0.05	0.15	0.20	0.20	0.20	0.20
8. Heat-flux immersion error	0.02	0.02	0.02	0.02	0.02	0.01	0.01	0.20	0.10	0.10	0.10	0.10
9. Choice of fixed-point value	0.05	0.05	0.05	0.05	0.05	*0.05*	0.03	0.06	0.06	0.06	0.20	0.20
Type B combined (mK)	**0.43**	**0.20**	**0.21**	**0.30**	**0.32**	**0.20**	**0.30**	**1.09**	**0.99**	**1.93**	**4.62**	**6.81**
Type A uncertainty component (mK)	**0.05**	**0.05**	**0.05**	**0.05**	**0.05**	**0.03**	**0.05**	**0.20**	**0.15**	**0.15**	**0.30**	**0.30**
Standard combined uncertainty (mK)	**0.43**	**0.21**	**0.21**	**0.30**	**0.32**	**0.20**	**0.31**	**1.11**	**1.00**	**1.94**	**4.63**	**6.81**
Expanded combined uncertainty, $k = 2$ (mK)	**0.86**	**0.42**	**0.42**	**0.60**	**0.64**	**0.40**	**0.62**	**2.21**	**2.00**	**3.88**	**9.25**	**13.63**

Appendix C

Furnace Diagram

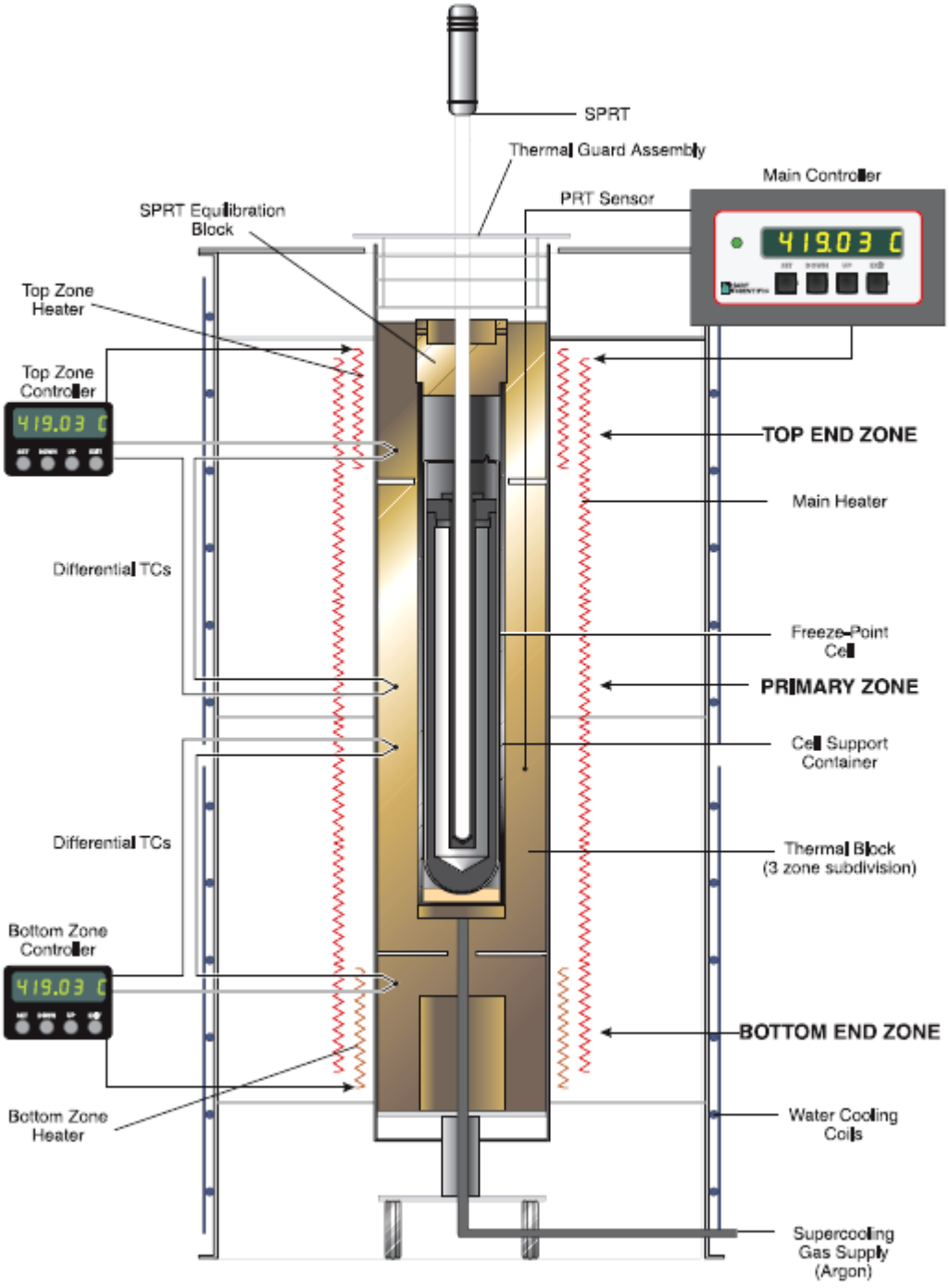

9114 Heater Block Assembly (Three zone Hart Furnace)

[Hart Scientific Inc., 2006]